

**ADAPTIVE BACKSTEPPING CONTROL
AND SAFETY ANALYSIS FOR
MODERN FIGHTER AIRCRAFT**

ISBN 978-90-8570-735-6

Printed by Wöhrmann Print Service, Zutphen, The Netherlands.

Copyright © 2011 by E.R. van Oort. All rights reserved. No part of the material protected by this copyright notice may be reproduced or utilized in any form or by any means, electronic or mechanical, including photocopying, recording or by any information storage and retrieval system, without the prior permission of the author.

ADAPTIVE BACKSTEPPING CONTROL AND SAFETY ANALYSIS FOR MODERN FIGHTER AIRCRAFT

PROEFSCHRIFT

ter verkrijging van de graad van doctor
aan de Technische Universiteit Delft,
op gezag van de Rector Magnificus prof. ir. K.C.A.M. Luyben,
voorzitter van het College voor Promoties
in het openbaar te verdedigen op dinsdag 5 april 2011 om 15.00 uur
door

Eduard Richard VAN OORT

ingenieur luchtvaart en ruimtevaart
geboren te Bilthoven.

Dit proefschrift is goedgekeurd door de promotor:

Prof. dr. ir. J.A. Mulder

Copromotor:

Dr. Q.P. Chu

Samenstelling promotiecommissie:

Rector Magnificus	voorzitter
Prof. dr. ir. J.A. Mulder	Technische Universiteit Delft, promotor
Dr. Q.P. Chu	Technische Universiteit Delft, copromotor
Prof. lt. gen. b.d. B.A.C. Droste	Technische Universiteit Delft
Prof. dr. ir. M. Verhaegen	Technische Universiteit Delft
Prof. Dr.-Ing. F. Holzapfel	Technische Universität München
ir. J.H. Breeman	Nationaal Lucht- en Ruimtevaartlaboratorium
M.A. Niestroy, Ph.D.	Lockheed Martin Aeronautics
Prof. dr. ir. M. Mulder	Technische Universiteit Delft, reservelid

The research presented in this dissertation has been financially supported by the Defence Material Organisation, Defence Research & Development, the Dutch Aerospace Laboratory NLR and the Delft University of Technology. A technical contribution has been made by Lockheed Martin Aeronautics and the NLR.



SUMMARY

There exist many examples of aircraft incidents in which the pilots have successfully used the remaining control authority over an aircraft to save the airframe and its passengers and cargo from apparently hopeless failure conditions. Unfortunately, the opposite is also true. Several accidents happened in which the crew was not able to save the aircraft, although post-flight analysis showed that it was possible with alternative, perhaps unconventional, control strategies. These aircraft accidents indicate that there is a potential benefit of fault tolerant flight control (FTFC) techniques, which are able to accommodate changes in the aircraft's dynamics due to damage to the aircraft and failures of its systems. From an aeronautical-technical point of view some accidents that happened over the last decades possibly could have been prevented with such FTFC control techniques.

Generally speaking FTFC can be classified into two types: *passive* and *active*. The passive methods result in fixed controllers that are designed to be robust against a class of presumed faults. However, any controller with a large enough robustness radius to encompass most failure situations will very likely be unnecessarily conservative in many cases, including the nominal case. Additionally, there is no guarantee that unanticipated and multiple simultaneous failures can be handled, or that such a controller even exists. In contrast to the passive methods, the active methods react to the system failures actively by reconfiguring the control actions such that stability and acceptable performance of the entire system can be maintained even in the presence damage and failures.

The current state of technology still indicates some remaining problems and limitations of fault tolerant flight control systems. The passive fault tolerant approaches are limited to restricted failure cases, and therefore an active approach has more potential when unknown failures and a large combination of possible and simultaneous failures has to be considered. Only a limited number of approaches yields control designs that are valid over a large operating range, and especially estimation of the dynamical model is very often only performed at or around the current flight condition. No globally valid model is built by these methods and estimated models are not stored for later re-use when the same flight condition is revisited. Direct adaptive control approaches tune the controller parameters to achieve the desired performance and do not estimate a model of the system. Many of the neural network based approaches suffer from convergence problems, and

simultaneously rely on a black-box structure which reduces the transparency of the aircraft models estimated through these designs. In this research an approach is taken based on the knowledge of flight dynamics and therefore all quantities and variables appearing in the estimated models have a physical meaning, leading to transparent models and additionally these models can be used for on-line failure diagnosis as well as reconfiguration.

Loss-of-control (LOC) incidents do not only happen to aircraft with failures. Some reports claim that LOC has contributed to more fatal commercial airliner accidents and related fatalities than any other factor during the last ten years of world-wide operations. At this point, the industry has not yet incorporated widespread LOC prevention. Flight envelope protection is a first and necessary step that is taken by aircraft designers towards LOC prevention. Knowledge of the safe flight envelope is very important to prevent LOC accidents and still allow aircraft to operate at the edges of their performance envelope. In post-failure flight conditions one would like to know the region of the envelope in which the aircraft can still maneuver safely, to continue the mission and make a safe (crash) landing possible. This area has not received a lot of attention yet by the aerospace research community, not even for aircraft without any faults or failures.

The research described in this dissertation therefore has the following objectives.

- Development of a control scheme which achieves the desired performance characteristics over the whole flight envelope of the aircraft, even in the presence of faults and failures.
- Since modern aircraft have many different and redundant control effectors, the desired control effect has to be distributed over the available effectors. This distribution is performed optimally with respect to a cost criterion and takes the individual control effector characteristics into account. Stability of the control law with control allocation can be shown.
- Aircraft failures or damage influence the dynamics of the system, which need to be identified on-line to allow active reconfiguration of the control design and restore control performance. Severe failures cause changes in the required structure, for example asymmetric damage contributes to the complexity of the required model structure. When the model structure and estimated parameters match the underlying physics of the system, the estimated model can be used for fault diagnosis and derivation of the post-failure safe flight envelope. Development of on-line model structure selection methods is required and the estimated model has to be stored efficiently onboard.
- Especially for highly maneuverable aircraft and aircraft with faults and failures the aircraft dynamics pose important constraints on the safe maneuvering space. In post-failure flight conditions knowledge of the safe envelope can be the difference between an inevitable accident or safe (crash) landing. Thus,

a method has to be developed which calculates the safe envelope, based on a available model of the aircraft, and takes input constraints and disturbances into account.

Adaptive backstepping is a recursive, Lyapunov-based, nonlinear design method which makes use of parameter update laws to deal with parametric uncertainties in the system. The main idea of backstepping is to design the control law recursively by considering some of the state variables as “virtual control inputs”, and designing stabilizing functions for these. With the inclusion of command filters, the backstepping design is applicable to non lower triangular systems and the whole design is simplified considerably as the need for analytic derivatives of the “virtual control inputs” is removed.

Different parameter update laws can be designed, resulting in the integrated, modular, and composite update law designs. The integrated design employs a Lyapunov based update law, while the modular update law allows the use of a recursive least squares identifier. However, nonlinear damping terms are required in the control law to achieve the modularity between the controller and identifier. The composite update law combines the integrated and modular designs, and has the best parameter convergence properties of all three designs.

In a comparison between the integrated and modular approaches, both resulted in an improvement of performance in post-failure flight conditions over a non-adaptive control design. The tracking performance and parameter estimation characteristics of the modular design were better than for the integrated design.

Control allocation can be integrated within the backstepping framework by designing update laws for the optimizing control effector signals from a Lyapunov perspective. In this design, the control effector commands continuously converge to the optimal solution instead of explicitly solving the control allocation problem exactly at each time instant.

The full envelope estimation problem is approached by partitioning the complete flight envelope into smaller regions called hyperboxes. In each hyperbox a locally valid linear in the parameters model is identified. The output of the local models is interpolated using B-splines to obtain the output over the full envelope. Since the B-splines have local support, only a limited amount of partitions is active for each flight condition, reducing the computational load.

The model structure required to model aerodynamic failures is not known a-priori, inclusion of too many regressors leads to over-fitting and decreases extrapolation capabilities. An on-line structure selection method based on orthogonal least squares is developed which can be used in combination with the adaptive backstepping control design. The structure selection procedure recursively selects a regressor from the set of candidates which achieves the largest reduction of the fit error until a stopping criterion is satisfied.

The adaptive backstepping control design with control allocation, flight envelope partitioning and structure selection is tested on the over-actuated, nonlinear ADMIRE aircraft model. The proposed control design shows excellent performance

for a variety of simulated fault and failure cases ranging from a simple change in the aerodynamic coefficients, to actuator failures and center of gravity shifts. When the failure is in the space spanned by the set of available regressor candidates, the correct model structure can be identified, and the correct parameter values are estimated if a persistency of excitation condition is satisfied. Even if the failure cannot be completely characterized by the available set of regressor candidates, tracking performance can be very good as long as the residual error between the estimated model and the true behavior is small.

Application of adaptive flight control techniques has shown that it may be possible to stabilize a damaged aircraft for a variety of faults and failures, it is still unclear what maneuvers are still possible and how much the performance of the aircraft has degraded due to these faults and failures.

Future research on fault tolerant flight control should include realistic aerodynamic failure models, and test-flights with UAV and research aircraft. The interaction between adaptive control designs and the pilot has to be investigated. Before application of FTFC in production aircraft is possible, guidelines and requirements for validation and verification have to be developed.

The safe flight envelope is defined as the region in the state space for which safe operation of the aircraft, and safety of its cargo and passengers, can be guaranteed while externally posed constraints are not violated. This region in the state space can be described by the intersection between the dynamical, structural and environmental envelopes. The safe dynamical envelope can be determined by evaluating the forwards and backwards reachable sets for a given set of safe states, for example trim conditions. These reachable sets are obtained through evolution of the initial or target set using a model of the system dynamics by the level set approach, for which different solution methods exist. Based on a comparison of simple examples the semi-Lagrangian approach was selected as the most promising for application to the safe flight envelope determination problem of nonlinear aircraft dynamics with control inputs and disturbances. The proposed method is applied to the longitudinal dynamics of an F-16 aircraft model. The shape of the forwards and backwards reachable sets matches with what is expected from flight dynamics. At higher altitude the aircraft becomes less maneuverable for the same airspeed due to reduction of dynamic pressure. When the center of gravity is shifted backwards in longitudinal direction, the aircraft becomes more unstable, resulting in greater maneuverability, but at the cost of greater difficulty to get the aircraft back to a trim condition. In the case of a loss in hydraulic pressure, resulting in more stringent constrained horizontal stabilizer deflections, the maneuvering capabilities of the aircraft severely degrade at low airspeeds.

Further research on this subject is required, for example by splitting the full envelope problem into slow and fast dynamics by means of time-scale separation arguments. Furthermore, if the solution speed can be improved, on-line applications can be attempted.

CONTENTS

Summary	v
1 Introduction	1
1.1 Background	1
1.2 Fault Tolerant Flight Control	3
1.2.1 Types of Fault-Tolerant Control Systems	4
1.2.2 Objectives and Structure of Active FTCS	4
1.2.3 Overview of Reconfigurable Flight Control	6
1.2.4 Reconfigurable Flight Control in Practice	8
1.3 Research Goals and Approach	8
1.4 Contributions	10
1.5 Outline	11
Bibliography	13
I Backstepping and Model Identification Theory	19
2 Introduction to Adaptive Nonlinear Control	21
2.1 What is Feedback Control	21
2.2 Flight Control Approaches	22
2.2.1 Small-signal Linearization	23
2.2.2 Gain-scheduling	23
2.2.3 Feedback Linearization	24
2.2.4 Backstepping	25
2.3 Adaptive Control	26
2.3.1 Direct Adaptive Control	26
2.3.2 Indirect Adaptive Control	27
2.4 System Identification	27
2.4.1 Model Parameter Optimization	28
2.4.2 Model Structure Selection	29
2.5 Conclusions	30
3 Backstepping Control Design	31

3.1	Stability Concepts for Nonlinear Systems	31
3.1.1	Stability Properties	32
3.1.2	Lyapunov's Direct Method	33
3.2	Control Lyapunov Functions	35
3.3	Backstepping Design	38
3.3.1	Integrator Backstepping	38
3.3.2	Recursive Backstepping Design	41
3.3.3	Time-scale Separation NDI versus Backstepping	42
3.3.4	Missile Example	42
3.4	Backstepping with Uncertainty	45
3.4.1	Nonlinear Damping	46
3.4.2	Robust Backstepping	48
3.4.3	Robust Backstepping Example	49
3.5	Command Filtering	50
3.5.1	Command Filtering Backstepping	51
3.5.2	Missile Example	53
3.6	Non-affine in Control Backstepping	53
3.6.1	Singular Perturbation Theory	54
3.6.2	Non-affine Backstepping Design	56
3.6.3	Example	56
3.7	Conclusions	57
4	Adaptive Backstepping Control Design	59
4.1	Dynamic Feedback Control	59
4.2	Adaptive Backstepping	61
4.2.1	Adaptive Integrator Backstepping	61
4.2.2	Recursive Adaptive Backstepping	63
4.3	Command Filtered and Tuning Functions Design	64
4.3.1	Constrained Adaptive Backstepping (CABS)	64
4.3.2	CABS Missile Example	67
4.4	Modular Adaptive Backstepping	70
4.4.1	Weakness of Certainty Equivalence	70
4.4.2	ISS-Backstepping Design	72
4.4.3	Swapping Filters	74
4.4.4	Identifier Choice and Stability Proof	76
4.5	Command Filtered Modular ISS-Backstepping Design	77
4.5.1	Command Filtered Modular Design	77
4.5.2	Modular Backstepping Missile Example	79
4.6	Composite Adaptive Backstepping	80
4.7	Adaptive Backstepping of Pure Feedback Systems	82
4.8	Conclusions	82
	Bibliography	85

II	Modular Backstepping Flight Control	89
5	Aircraft Dynamics	91
5.1	Aircraft Dynamics	91
5.1.1	Coordinate Frames	91
5.1.2	Assumptions	93
5.1.3	Equations of Motion	94
5.1.4	Wind-Axis Equations of Motion	96
5.2	Atmospheric Model	96
5.3	Control Variables	97
5.4	Control Effectors	97
5.5	High Fidelity F-16 Model	98
5.5.1	Aircraft Geometry	98
5.5.2	Engine Model	98
5.5.3	Aerodynamic Model	99
5.6	ADMIRE Model	100
5.6.1	Aircraft Geometry	100
5.6.2	Engine Model	101
5.6.3	Aerodynamic Model	101
5.7	Conclusions	102
6	A Comparison of Adaptive Control Designs	103
6.1	Introduction	103
6.2	Aircraft Model	104
6.3	Control System Design	106
6.3.1	Static Backstepping Design	107
6.3.2	Filtered Integrated Adaptive Backstepping Design	108
6.3.3	Filtered Modular Adaptive Backstepping Design	109
6.3.4	Tuning Function Adaptive Backstepping Design	110
6.4	Control Allocation Methods	111
6.4.1	Weighted Pseudo-inverse Control Allocation	111
6.4.2	Quadratic Programming	112
6.5	Results	113
6.5.1	Simulation Scenarios	114
6.5.2	Nominal Performance	115
6.5.3	Failure Performance	116
6.5.4	Specific Failure Scenario Comparison	119
6.6	Conclusions	119
7	Adaptive Optimizing Nonlinear Control Design	125
7.1	Introduction	125
7.2	Problem Definition and Preliminaries	126
7.3	Non-adaptive Control Design	128
7.3.1	High-level Control Design	128

7.3.2	Control Allocation Design	128
7.4	Adaptive Control Design	130
7.4.1	Integrated Update Law	131
7.4.2	Modular Update Law	132
7.4.3	Composite Update Law	135
7.5	Fighter Aircraft Model Application	136
7.5.1	Controller Design	137
7.5.2	Nominal Simulation Results	137
7.5.3	Elevator Failure	139
7.5.4	Aileron Failure	139
7.6	Conclusions	141
8	Full Envelope Modular Adaptive Control	145
8.1	Introduction	145
8.2	Controller Design	146
8.2.1	System dynamics	147
8.2.2	Backstepping Control Law Design	148
8.2.3	Nonlinear Swapping Filters	151
8.3	Identifier Design	152
8.3.1	Local Model Update	152
8.3.2	Full Envelope Interpolation	154
8.3.3	Covariance Resetting	156
8.4	Application to the F-16 Model	157
8.4.1	F-16 Aircraft Model and Assumptions	157
8.4.2	Partition Model Structure	158
8.4.3	F-16 Control Law Design	158
8.5	Simulation Scenarios and Results	160
8.5.1	Controller Tuning	160
8.5.2	Simulation Scenarios	162
8.5.3	Simulation Results	163
8.6	Conclusions	170
9	Adaptive Control with Structure Selection	177
9.1	Introduction	177
9.2	Aircraft Dynamics and Problem Statement	178
9.3	Control Law Design	180
9.3.1	Vector Backstepping	180
9.3.2	Command Filtering	182
9.3.3	Optimizing Control Allocation	182
9.3.4	Adaptive Optimizing Control Allocation	183
9.3.5	Nonparameteric Robustness Modification	185
9.4	Model Structure Selection and Identification	186
9.4.1	Least Squares and Orthogonal Decompositions	186
9.4.2	Error Analysis	187

9.4.3	Model Structure Selection	188
9.4.4	Selection on the Cholesky and QR Factorizations	189
9.4.5	Updating the Decomposition	191
9.5	Full Envelope Aerodynamic Modeling	192
9.5.1	Local Model Structure	192
9.5.2	Local Model Updating and Resetting	193
9.6	ADMIRE Application and Simulation Results	193
9.6.1	Controller Tuning	193
9.6.2	Incremental Aerodynamic Model	194
9.6.3	Nominal Simulation Results	195
9.6.4	Changes in Aerodynamic Coefficients	195
9.6.5	Actuator Failures	196
9.6.6	Center of Gravity Shift	197
9.7	Conclusions	199
Bibliography		209
III Safe Flight Envelope		215
10 Flight Envelope Protection		217
10.1	Introduction	217
10.2	The Flight Envelope	219
10.3	Flight Envelope Protection Methods	221
10.4	Survey of (Safe) Flight Envelope Estimation	222
10.5	Conclusions	224
11 Level Set Methods		225
11.1	Forwards and Backwards Reachable Sets	225
11.2	The Flight Envelope and Reachable Set Analysis	226
11.3	Connection to Lyapunov Theory	227
11.4	Implicit Functions and Surfaces	228
11.5	Level Set Method	229
11.6	Reachable Sets and Differential Games	230
11.6.1	The Hamilton-Jacobi PDE	230
11.6.2	HJ PDE for the Backwards and Forwards Reachable Sets	232
11.7	HJ-PDE Solution Methods	233
11.7.1	Lagrangian-methods	233
11.7.2	Euler-methods	234
11.7.3	Semi-Lagrangian methods	235
11.7.4	Hybrid methods	236
11.8	Reachable Set Examples	237
11.8.1	Double Integrator	237
11.8.2	Acoustic Capture	238
11.8.3	Aircraft Collision Avoidance	240

11.8.4 Computational Load	242
11.9 Conclusions	243
12 F-16 Longitudinal Envelope	245
12.1 Aircraft Model and Assumptions	245
12.2 Trim Set	247
12.3 Level Set Problem and Solver Settings	247
12.4 Nominal Aircraft Results	249
12.4.1 Low Altitude Maneuverability	250
12.4.2 High Altitude Results Altitude Comparison	250
12.5 Center of Gravity Shift Comparison	250
12.6 Constrained Actuator Comparison	252
12.7 Conclusions	253
Bibliography	257
IV Conclusions and Recommendations	263
13 Conclusions and Recommendations	265
13.1 Conclusions	265
13.1.1 Damaged Aircraft Control	266
13.1.2 Control Allocation	267
13.1.3 Damaged Aircraft Identification	268
13.1.4 Flight Envelope Determination	268
13.1.5 Final Conclusions	269
13.2 Recommendations and Future Prospects	270
Appendices	273
A System and Stability Concepts	275
B F-18 Aerodynamic Model Data	277
C Semi-Lagrangian Level Set Implementation	279
C.1 kd-tree Grids	279
C.2 Spatial Derivative Approximation	279
C.3 Adaptive kd-tree CIR-scheme	280
Bibliography	283
Nomenclature	299
Samenvatting	303
Acknowledgments	309

CONTENTS

xv

Curriculum Vitae

311

INTRODUCTION

This chapter forms the introduction to the dissertation. First some exemplary accidents and incidents are described to provide a setting for the problems addressed by the research presented. Then, a brief overview of the research already performed in this field is given and the research goals are formulated. Finally, an overview of the contributions and contents of the dissertation is given.

1.1 Background

On the first of May, 1983, a simulated dogfight training took place between two F-15Ds, and four A-4N Skyhawks over the skies of the Negev desert. At some point one of the F-15Ds collided with one of the Skyhawks. The pilot did not realize it was a collision and afterwards explained that it felt like flying through the jet stream of one of the other aircraft. The A4 exploded upon collision and the pilot of the F-15 found himself trying to control a spinning aircraft with a thirty degrees nose down attitude. Instead of ejecting from the aircraft, he engaged the afterburner and the rolling motion of the aircraft stopped. Then, he was able to bring the nose up and establish level flight. When the pilot asked a wingman to come and inspect his aircraft, a large spray of fuel hid the true damage to the aircraft: the F-15 is so badly damaged in the collision that the aircraft is flying on just one wing. The pilot was able to prevent stalling and maintain control because of the lift generated by the large horizontal surface area of the fuselage, the stabilators and remaining wing area. The pilot approached the airfield at a speed roughly twice the normal landing speed, the emergency landing tailhook was torn off completely during the landing and the aircraft stopped just 20 ft before the end of the runway. The

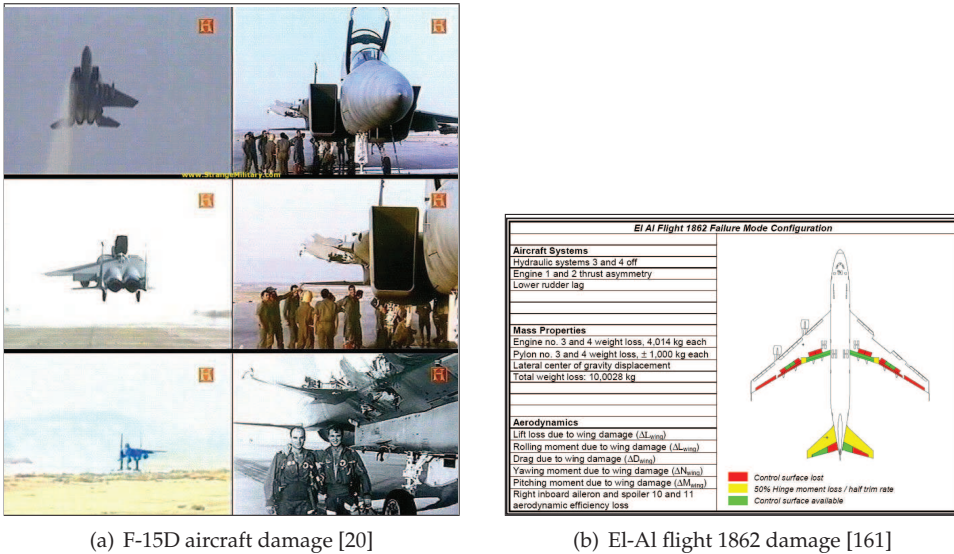
McDonnell Douglas company, designer of the aircraft, attributes saving the aircraft to the amount of lift generated by the engine intake and fuselage, and “a hell of a good pilot”.

Another example of a pilot saving a large part of his passengers and aircraft is United Airlines Flight UA-232. On July 19, 1989, the Douglas DC-10 suffered an uncontained engine failure of its tail mounted engine. Shrapnel was hurled from that engine with enough force to penetrate the hydraulic lines of all three of the aircraft’s hydraulic systems. The hydraulic fluid rapidly drained from all systems, and this resulted in none of the conventional flight controls working except the thrust levers of the two remaining engines. Using differential thrust, the pilot crew was able to control the aircraft to some extent and was able to make a crash landing on the runway.

There exist more examples of aircraft incidents in which the pilots have successfully used the available control authority over an aircraft to save an airframe, its passengers and cargo from apparently hopeless failure conditions. Unfortunately, the opposite is also true. Several accidents happened in which the crew was not able to save the aircraft, although post-flight analysis showed that it was possible with alternative or unconventional control strategies. A notable example of such an accident would be El Al Flight 1862. On October 4, 1992, a Boeing 747 cargo plane crashed into two apartment buildings in the Bijlmermeer neighborhood of Amsterdam, near Schiphol Airport. Engine number three separated from the right wing of the aircraft shortly after take-off, damaging the wing flaps, and struck engine number four which also separated. Analysis showed that the aircraft still had marginal controllability left in severely restricted flight envelope [161]. Simulator experiments using different fault tolerant flight control approaches have shown that landing the aircraft would have been possible [98, 178]. However, the aircraft did not have such a fault tolerant control system, and perhaps even more importantly, the pilots did not have any knowledge about the restricted flight envelope of the aircraft and when they tried to reduce the speed for landing the aircraft banked sharply to the right without any chance of recovery.

The described aircraft accidents show that there is a potential benefit of fault tolerant flight control techniques, which are able to accommodate large changes in the aircraft’s dynamics due to severe damage to the aircraft and failures of its systems. From an aeronautical-technical point of view these accidents and many more that happened over the last decades could possibly have been prevented [45].

Loss-of-control (LOC) incidents do not only happen to aircraft with failures. Some reports claim that LOC has contributed to more fatal commercial airliner accidents and related fatalities than any other factor during the last ten years of worldwide operations [15, 145]. At this point, the industry has not yet incorporated widespread LOC prevention. Flight envelope protection, whether by hard constraints (for example Airbus) or soft constraints (for example Boeing), is a first and necessary step taken by aircraft designers towards LOC prevention, trying to enhance safety. All aircraft have physical limits that should not be exceeded. For example, when the airspeed is too low, the aircraft may stall, if the airspeed is



(a) F-15D aircraft damage [20]

(b) El-Al flight 1862 damage [161]

Figure 1.1: Left wing missing after a mid-air collision of an F-15D aircraft 1.1(a). Indication of the damage to El-Al Flight 1862 sustained after separation of engines three and four in 1.1(b).

too high or a maneuver too demanding, excessive loads on the airframe can be generated with the risk of damaging the structure.

1.2 Fault Tolerant Flight Control

The work presented in this dissertation is by no means the only research that has been done on fault tolerant control for aircraft, nor does it try to address and solve *all* problems related to safe flight control. Related and overlapping approaches in research projects conducted at the Faculty of Aerospace Engineering of Delft University of Technology are Lombaerts [96], Sonneveldt [163].

Before discussing fault tolerant flight control, first the entities within the pilot-aircraft system are introduced. The cockpit is the interface between the pilot and the aircraft, through the displays the pilot obtains information about the aircraft and flight computer state. Sensors measure aircraft and environmental state variables such as airspeed, outside air temperature, and fuel flow to the engine. The flight computer uses this sensor information to translate the commands by the (auto)pilot to actuator commands, and sends processed information to the cockpit displays for interpretation by the pilot. The relations between the different elements of the pilot-aircraft system are shown in figure 1.2.

1.2.1 Types of Fault-Tolerant Control Systems

Generally speaking, Fault Tolerant Control Systems (FTCS) can be classified into two types: *passive* and *active*. The passive methods result in fixed controllers that are designed to be robust against a class of presumed faults [51]. The approach does not require fault-detection schemes nor controller reconfiguration and results in satisfactory performance if the faults fall within the robustness radius of the controller. However, any controller with a large enough robustness radius to encompass most failure situations will very likely be unnecessarily conservative in many cases. Additionally, there is no guarantee that unanticipated or multiple simultaneous failures can be handled, or that such a controller even exists.

In contrast to the passive methods, the active methods react to the system failures actively by reconfiguring the control actions such that stability and acceptable performance of the entire system can be maintained. Often, degraded performance may have to be accepted [13, 138, 174] since the system with faults cannot achieve the same levels as performance as the nominal system. To achieve a successful control system reconfiguration, the active approach relies heavily on real-time fault detection and diagnosis (FDD) schemes using measurements to provide information about the status of the system.

1.2.2 Objectives and Structure of Active FTCS

Typically, an active FTCS method is composed out of four sub-systems:

- a reconfigurable controller,
- an FDD scheme,
- a controller reconfiguration mechanism, and
- a command/reference governor,

which results in the general structure of active FTCS as shown in figure 1.3. First of all the information measured by the sensors is combined, processed and filtered to reconstruct the actual state of the aircraft. The anomaly detection scheme can use on-board models of the aircraft, sensors and actuators to detect and diagnose faults and failures. This information is sent to the reconfiguration mechanism and to the command governor units. The reconfiguration mechanism is able to handle (parametric) changes in the system dynamics and possibly restructure the control allocation scheme. The control laws in combination with the command and reference governor should compensate for the fault-induced changes in the system so that stability and acceptable performance can be maintained in an operational envelope which is as large as possible.

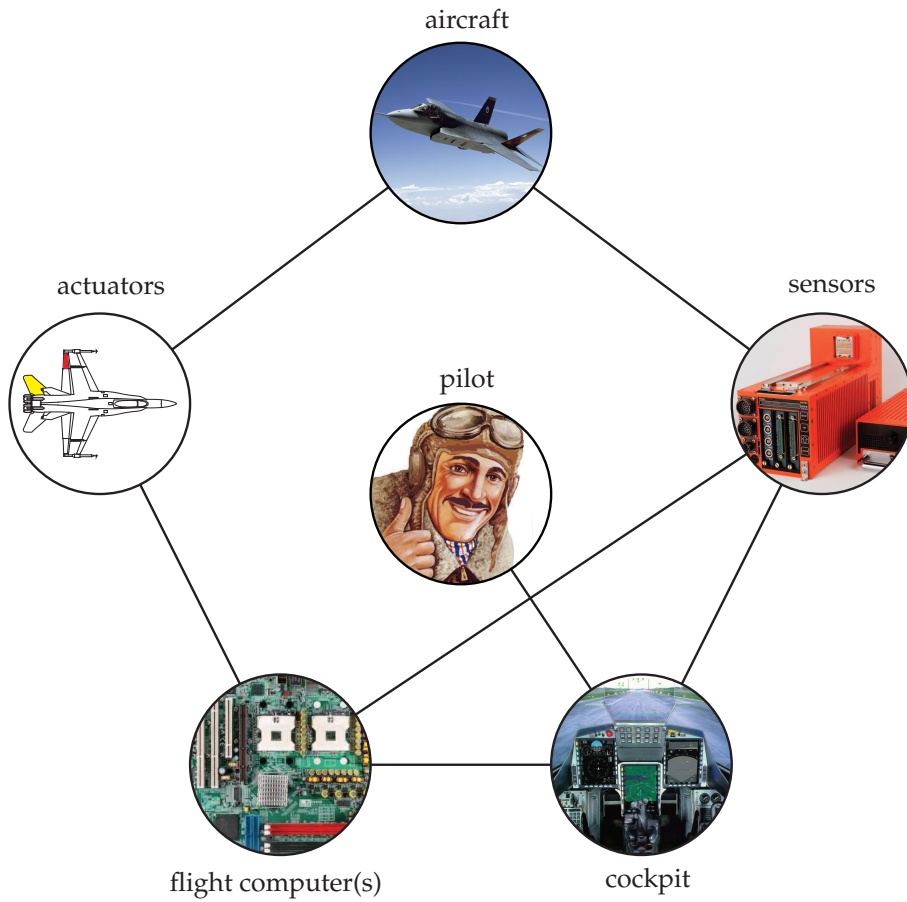


Figure 1.2: Overview of the interaction between the pilot, cockpit, flight control computer, actuators, sensors and the aircraft.

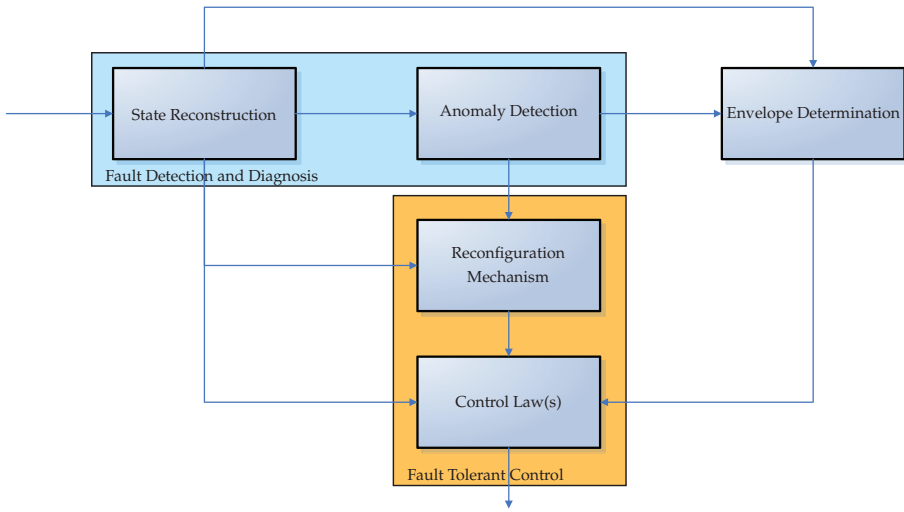


Figure 1.3: General structure of an active FTCS

1.2.3 Overview of Reconfigurable Flight Control

An extensive overview of active FTCS is given in an excellent bibliographical review by Zhang and Jiang [210], which includes over 300 references and different classifications of FTCS. In this section a condensed overview of active FTCS and research programs is given, with focus on flight control.

The idea of control reconfiguration can be traced back through the history of manned-flight in many cases where pilots have exploited the remaining control authority over aircraft with degraded control performance. Thus, man itself can be considered as the first RFC system. In the early days of automatic RFC most studies were based on backup flight control effectors, which would compensate for failure of a primary control surface. Many of these are still very relevant for control reconfiguration. The earliest detailed study showing the value of control reconfiguration was performed by the Grumman Aerospace Corporation for the United States Air Force [16] and was followed by a study for the United States Navy [65]. These studies demonstrated the importance of considering reconfiguration already during the design process.

Research in the area of reconfigurable flight control (RFC) really started in the 1980s, and has remained an important research topic since. Since then an enormous amount and variety of research has been published. This overview is limited to RFC methods which have been demonstrated in flight or high-fidelity simulation, methods that only handle sensor failures and/or switch between redundant hardware will be omitted. Most of the RFC methods developed in the 80s required a separate system for failure detection, isolation and estimation (FDIE). An important

example of this approach was developed by General Electric where an extended Kalman filter was used to perform FDIE. The information from the FDIE was subsequently used to generate the same accelerations of the degraded aircraft as the nominal aircraft. Quite a few research programs and benchmarks have since been performed. Below some of the important and large research programs are listed in chronological order.

Self-repairing flight control systems (1984 - 1990) The research focused on control reconfiguration after faults or failures of one of the actuators [50].

Automatic redesign for restructurable control systems (1984 - 1987) A fault tolerant approach using fault detection and optimal control design was developed and applied to a Boeing-737 aircraft simulation model [100].

Self-designing flight control (1993-1996) An indirect-adaptive control law using Modified Sequential Least Squares and a Receding Horizon Optimal Controller was designed to build a mathematical model of the aircraft dynamics in flight and then use this information to generate control gains in real time that compensate for the failure [118].

RESTORE by the US Air Force (1996-2000) An adaptive neural network was integrated with a dynamic inversion controller to accommodate actuator failures for the X-36 tailless aircraft [17]. The two test flights that were completed helped validation of simulation results.

ACTIVE and IFCS at NASA (1996-2004) The ACTIVE and later IFCS flight tests used on-board algorithms to identify changes in aerodynamic characteristics using Neural Networks and the flight control system used this information to generate additional open-loop commands [42].

Fault-tolerant control by GARTEUR (2004 - 2008) In this research project different FDI and RFC methods were tested on benchmark scenarios and in a piloted moving-base simulator experiment. This provided supporting information on the practical and operational implications of advanced flight control systems integration from a human factors perspective [45].

The increase in computational power in the 1990s led to an explosion in the number and types of approaches applied to the RFC problems [173]. This opened the door to experiment with more complex nonlinear design approaches. Furthermore, there had been considerable theoretical advances in the areas of adaptive and nonlinear control methods during the 1980s and early 1990s. Among the popular advanced control design methods are model-based control techniques such as Non-linear Dynamic Inversion (NDI) [78, 159], adaptive backstepping [88], Model Reference Adaptive Control (MRAC) [92, 93, 120] and variable structure control (VSC) [46, 83]. Some examples of such methods applied to full envelope flight control include NDI with Recursive Least Squares (RLS) estimation of aerodynamic derivatives of a linearized single flight condition model [97], NDI in combination with

Neural Networks (NN) [21, 110, 153, 156], backstepping using B-spline networks to approximate the aerodynamic derivatives [57, 164], backstepping in combination with NN approximation [137, 150, 151]. Hybrid combinations of these control techniques are possible, for example the combination of NDI and MRAC Nguyen, Krishnakumar, Kaneshige, and Nespeca [127], direct adaptive control with NN [82, 179], and variable structural control for single flight condition models [2, 154].

1.2.4 Reconfigurable Flight Control in Practice

In 1999 the Boeing F/A-18 E/F Super Hornet was the first military production aircraft delivered with a reconfigurable control law [47]. The aircraft uses reconfiguration only for a single stabilator failure mode, which is designed to fail in a locked neutral position. Excellent handling qualities are maintained following the failure. As can be seen, real-world applications are very limited. One explanation for this has been the difficulty in certifying these approaches for safe flight, especially since no requirements for adaptive flight control methods exist. There has been some progress in developing tools for analyzing RFC such as the use of linear matrix inequality techniques [25, 203]. Progress was made for more advanced control laws by Buffington, Tallant, Crum, et al. [18], describing some validation and verification techniques for adaptive and intelligent control approaches. A different approach would be to implement reconfigurable control laws that are easier to certify. An example would be an adaptive element that does not change the baseline control law and hence should be interpreted as an autopilot mode or stability augmentation system during certification [119, 204].

1.3 Research Goals and Approach

The overview of performed research in the previous section still shows some remaining problems and limitations of fault tolerant flight control systems. The passive fault tolerant approaches are limited to restricted failure cases, and therefore an active approach has more potential when unknown failures and a large combination of possible failures has to be considered. Only a limited number of approaches yields control designs that are valid over a large operating range, and especially estimation of the dynamical model is very often only performed at or around the current flight condition. No globally valid model is built by these methods and estimated models are not stored for later re-use when the same flight condition is revisited. Direct adaptive control approaches tune the controller parameters to achieve the desired performance and do not estimate a model of the system. Many of the neural network based approaches suffer from convergence problems, and simultaneously rely on a black-box structure which reduces the transparency of the aircraft models estimated through these designs. In this research an approach is taken based on the knowledge of flight dynamics and therefore all quantities and variables appearing in the estimated models have a physical meaning, leading to

transparent models and additionally these models can be used for on-line failure diagnosis as well as reconfiguration.

An area that has not received a lot of attention yet by the aerospace research community is the problem of safe flight envelope determination, not even for aircraft without any faults or failures. Knowledge of the safe flight envelope is very important to prevent loss-of-control accidents and still allow aircraft to operate at the edges of their performance envelope. In post-failure flight conditions one would like to know the region of the envelope in which the aircraft can still maneuver safely, and make a safe (crash) landing.

The research described in this dissertation therefore has the following objectives:

- *Damaged Aircraft Control* A control scheme has to be developed which achieves the desired performance characteristics over the whole flight envelope of the aircraft. Additionally, in the presence of faults and failures in the system, the control law has provable stability and state boundedness characteristics. Combined with on-line model identification the control design clearly enhances performance and survivability in post-failure flight conditions.
- *Control Allocation* Modern aircraft have many different control effectors. While this property allows on-line reconfiguration as it provides redundancy, it poses an additional problem in the control design since the desired control effect has to be distributed over the available control effectors. This distribution is performed optimally with respect to a cost criterion and takes the individual control effector characteristics into account. Stability of the control law with control allocation can be shown.
- *Damaged Aircraft Identification* Aircraft failures or damage influence the dynamics of the system, which need to be identified on-line to allow active reconfiguration of the control design and restore control performance. Severe failures cause changes in the required model structure, and additionally, asymmetric damage contributes to the complexity of the required model structure. When the model structure and estimated parameters match the underlying physics of the system, the estimated model can be used for fault diagnosis and derivation of the safe flight envelope post-failure. Therefore, development of on-line model structure selection methods is required and the estimated model has to be stored efficiently onboard.
- *Flight Envelope Determination* Especially for highly maneuverable aircraft and aircraft with faults and failures the aircraft dynamics pose important constraints on the safe maneuvering space. In post-failure flight conditions knowledge of the safe envelope can be the difference between an inevitable accident or safe (crash) landing. Thus, a method has to be developed which calculates the safe envelope, based on a available model of the aircraft, and takes input constraints and disturbances into account.

1.4 Contributions

A part of the work presented in this dissertation is taken from the following journal publications and conference papers, in chronological order:

E. R. van Oort, L. Sonneveldt, Q. P. Chu, and J. A. Mulder. “Modular Adaptive Input-to-state Stable Backstepping of a Nonlinear Missile Model”. In: *AIAA Guidance, Navigation, and Control Conference and Exhibit*. Hilton Head, South Carolina, USA, Aug. 2007

L. Sonneveldt, E. R. van Oort, Q. P. Chu, and J. A. Mulder. “Comparison of Inverse Optimal and Tuning Functions Designs for Adaptive Missile Control”. In: *Proceedings of the AIAA Guidance, Navigation, and Control Conference and Exhibit*. 2007

E. R. van Oort, L. Sonneveldt, Q. P. Chu, and J. A. Mulder. “A Comparison of Adaptive Nonlinear Control Designs for an Over-actuated Fighter Aircraft Model”. In: *AIAA Guidance, Navigation, and Control Conference and Exhibit*. Honolulu, Hawaii, USA, Aug. 2008

T. J. J. Lombaerts, E. R. van Oort, Q. P. Chu, J. A. Mulder, and D. A. Joosten. “Online Aerodynamic Model Structure Selection and Parameter Estimation for Fault Tolerant Control”. In: *Journal of Guidance, Control, and Dynamics* 33.3 (2010), pp. 707–723

E. R. van Oort, Q. P. Chu, and J. A. Mulder. “Safe Flight Envelope Determination by Reachability Analysis”. In: *Proceedings of the ICNPAA 2010 World Congress: 8th International Conference on Mathematical Problems in Engineering, Aerospace and Sciences*. São José dos Campos, Brazil, 2010

E. R. van Oort, L. Sonneveldt, Q. P. Chu, and J. A. Mulder. “Full Envelope Modular Adaptive Control of a Fighter Aircraft using Orthogonal Least Squares”. In: *Proceedings of the AIAA Guidance, Navigation, and Control Conference*. 2010-7857. AIAA. Toronto, Ontario, Canada, Aug. 2010

E. R. van Oort, L. Sonneveldt, Q. P. Chu, and J. A. Mulder. “Full Envelope Modular Adaptive Control of a Fighter Aircraft using Orthogonal Least Squares”. In: *Journal of Guidance, Navigation and Dynamics* 33.5 (2010), pp. 1461–1472

E. R. van Oort, Q. P. Chu, and J. A. Mulder. “Maneuver Envelope Determination through Reachability Analysis”. In: *Proceedings of the CEAS EURO GNC 2011 conference*. Accepted, to be presented. 2011

E. R. van Oort, Q. P. Chu, and J. A. Mulder. “Safe Dynamic Flight Envelope Determination with Application to an F-16 Model”. In: *Journal of Guidance, Control, and Dynamics* (2011). Under review.

E. R. van Oort, Q. P. Chu, and J. A. Mulder. “Adaptive Dynamic Control Allocation and Backstepping Design”. In: *Proceedings of the AIAA Guidance, Navigation, and Control Conference*. Under review. 2011

E. R. van Oort, L. Sonneveldt, Q. P. Chu, and J. A. Mulder. "Adaptive Dynamic Control Allocation and Backstepping Design". In: *Journal of Guidance, Control, and Dynamics* (2011). To be submitted.

1.5 Outline

The dissertation consists of four parts: *Part I: Backstepping and Model Identification Theory*, *Part II: Modular Backstepping Flight Control*, *Part III: Safe Flight Envelope*, and *Part IV: Conclusions and Recommendations*. Each of the first three starts with an introductory chapter which introduces the subject, important concepts and definitions used in the respective part, and relates the part to the dissertation as a whole. The structure of the individual parts is described below.

Part I: The first part of the dissertation contains theory on nonlinear control, and especially on the backstepping approach. Chapter 2 introduces the concept of feedback control and gives an overview of control methods that have been widely applied in aircraft control. In chapter 3 the theory related to backstepping for systems with known dynamics is introduced. This theory is extended in chapter 4 to systems with unknown, constant parameters. Using the theory in the adaptive backstepping chapter, control laws can be designed which achieve boundedness of the closed-loop system, placing the burden of tracking performance on the model identification part. The theory introduced in this part is applied to the tracking control design for a simple longitudinal missile model to illustrate the differences and improvements of the various control designs.

Part II: The second part applies the theory introduced in the first part to fault tolerant aircraft control. Chapter 5 introduces the reader to aircraft dynamics and important reference frames. It also includes a discussion of the variables that can be controlled. Chapter 6 compares three adaptive backstepping designs with different control allocation methods on a simple aircraft model with constant model parameters. The control allocation part is included in the Lyapunov design in chapter 7. In chapter 8 the modular backstepping approach is used for full flight envelope fault tolerant control of an F-16 aircraft model. Chapter 9 presents the results of a composite adaptive backstepping design together with full envelope parameter estimation, model structure selection and control allocation for fault tolerant control of the ADMIRE aircraft model.

Part III: In the third part, the safe flight envelope problem is addressed. Chapter 10 gives an introduction to the concept of flight envelope, and discusses why knowledge of this flight envelope is so valuable. Additionally, a survey of methods to analyze the behavior of nonlinear aircraft dynamics is given. Chapter 11 introduces the implicit surface description for sets, as well as the level set method. Then it discusses selected solution methods of the level set. At the end of this chapter some examples of reachability analysis for relatively

simple systems are presented. In chapter 12 the results of application of a semi-Lagrangian level set method to the safety analysis of the longitudinal F-16 model are presented.

Part IV: Chapter 13 presents and summarizes the conclusions drawn from the work presented in the dissertation. Finally recommendations and future research directions are formulated.

BIBLIOGRAPHY

- [2] H. Alwi, C. Edwards, O. Stroosma, and J. A. Mulder. "Fault Tolerant Sliding Mode Control Design with Piloted Simulator Evaluation". In: *Journal of Guidance, Control, and Dynamics* 31.5 (2008), pp. 1186–1201.
- [13] M. Blanke, M. Satorswiecki, and N. E. Wu. "Concepts and Methods in Fault-Tolerant Control". In: *Proceedings of the 2001 American Control Conference*. June 2001, pp. 2606–2620.
- [15] Boeing Company. *Statistical Summary of Commercial Jet Airplane Accidents: Worldwide Operations since 1959*. Tech. rep. Boeing Commercial Airplanes, 2009.
- [16] J. A. Boudreau and H. I. Berman. *Dispersed and Reconfigurable Digital Flight Control Systems*. Tech. rep. Grumman Aerospace Corporation, 1979.
- [17] J. S. Brinker and K. A. Wise. "Flight Testing of Reconfigurable Control Law on the X-36 Tailless Aircraft". In: *Journal of Guidance, Control, and Dynamics* 24 (May 2001), pp. 903–909.
- [18] J. Buffington, G. Tallant, V. Crum, et al. "Validation and Verification of Intelligent and Adaptive Control Systems". In: *Proceedings of the Second AIAA Unmanned Unlimited Conference*. AIAA-2003-6603. 2003.
- [20] R. C. *F-15 loses wing in mid-air collision - lands safely*. Accessed 2010-08-19. Aug. 19, 2010. URL: <http://www.strangemilitary.com/content/item/110099.html>.
- [21] A. Calise, S. Lee, and M. Sharma. "Development of a Reconfigurable Flight Control Law for the X-36 Tailless Aircraft". In: *Journal of Guidance, Control and Dynamics* 24.5 (2001), pp. 896–902.
- [25] J. Chen, R. J. Patton, and Z. Chen. "An LMI Approach to Fault-Tolerant Control of Uncertain Systems". In: *Proceedings of the 1998 IEEE/CIRA/ISAS Conference*. 1998, pp. 175–180.
- [42] B. Dunbar. *NASA - NASA Dryden Fact Sheet - Intelligent Flight Control System*. Apr. 28, 2010. URL: <http://www.nasa.gov/centers/dryden/news/FactSheets/FS-076-DFRC.html> (visited on 12/2009).

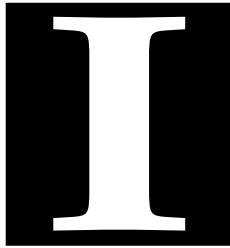
- [45] C. Edwards, T. J. J. Lombaerts, and H. Smaili, eds. *Fault Tolerant Flight Control - A Benchmark Challenge*. 1st ed. Lecture Notes in Control and Information Sciences 399. Springer, 2010.
- [46] C. Edwards and S. Spurgeon. *Sliding Mode Control: Theory and Applications*. Washington, D.C.: Taylor and Francis, 1998, pp. 31–34, 65.
- [47] L. Egbert and I. Halley. “Stabilator Reconfiguration Flight Testing on the F/A-18E/F”. In: *Proceedings of the SAE Control and Guidance Meeting*. Mar. 2001.
- [50] R. Eslinger and P. Chandler. “Self-repairing flight control system program overview”. In: *Proceedings of the IEEE 1988 National Aerospace and Electronics Conference*. Vol. 2. May 1988, pp. 504–511.
- [51] J. S. Eterno, J. L. Weiss, D. P. Looze, and A. S. Willsky. “Design issues for fault tolerant-restructurable aircraft control”. In: *Proceedings of the 24th IEEE Conference on Decision and Control*. Dec. 1985, pp. 900–905.
- [57] J. A. Farrell, M. Sharma, and M. Polycarpou. “Backstepping Based Flight Control with Adaptive Function Approximation”. In: *Journal of Guidance, Control and Dynamics* 28.6 (Jan. 2005), pp. 1089–1102.
- [65] K. D. Graham, T. B. Cunningham, and C. Shure. *Airframe Flight Control Survivability Through use of Computational Techniques*. Tech. rep. 77028-30. Naval Air Development Center, 1980.
- [78] A. Isidori. *Nonlinear Control Systems*. 3rd ed. Springer, 1995.
- [82] E. N. Johnson, A. J. Calise, and M. A. Turbe. “Fault Tolerance Through Direct Adaptive Control Using Neural Networks”. In: *Proceedings of the AIAA Guidance, Navigation, and Control Conference, San Francisco*. 2006.
- [83] H. K. Khalil. *Nonlinear Systems*. 3rd ed. Prentice Hall, 2002.
- [88] M. Krstić, I. Kanellakopoulos, and P. V. Kokotović. *Nonlinear and Adaptive Control Design*. John Wiley and Sons, 1995.
- [92] I. D. Landau. *Adaptive control: the model reference approach*. Ed. by M. Dekker. Dekker, New York, 1979.
- [93] I. D. Landau and B. Courtiol. “Design of multivariable adaptive model following control systems”. In: *Automatica* 10.5 (1974), pp. 483–494.
- [96] T. J. J. Lombaerts. “Fault Tolerant Flight Control, A Physical Model Approach”. PhD thesis. Delft University of Technology, Faculty of Aerospace Engineering, 2010.
- [97] T. J. J. Lombaerts, H. O. Huisman, Q. P. Chu, J. A. Mulder, and D. A. Joosten. “Nonlinear Reconfiguring Flight Control Based on Online Physical Model Identification”. In: *Journal of Guidance, Control, and Dynamics* 32.3 (2009), pp. 727–748.

- [98] T. J. J. Lombaerts, E. R. van Oort, Q. P. Chu, and J. A. Mulder. "On-line Aerodynamic Model Structure Selection and Parameter Estimation for Fault Tolerant Control". In: *AIAA Guidance, Navigation, and Control Conference*. AIAA-2009-5725. Chicago, Illinois, Aug. 2009.
- [99] T. J. J. Lombaerts, E. R. van Oort, Q. P. Chu, J. A. Mulder, and D. A. Joosten. "Online Aerodynamic Model Structure Selection and Parameter Estimation for Fault Tolerant Control". In: *Journal of Guidance, Control, and Dynamics* 33.3 (2010), pp. 707–723.
- [100] D. Looze, J. Weiss, J. Eterno, and N. Barrett. "An automatic redesign approach for restructurable control systems". In: *Control Systems Magazine, IEEE* 5.2 (May 1985), pp. 16–22.
- [110] M. B. McFarland and A. J. Calise. "Multilayer neural networks and adaptive nonlinear control of agile anti-air missiles". In: *Proceedings of the AIAA Guidance, Navigation, and Control Conference*. AIAA. Reston, VA, Aug. 1997, pp. 401–410.
- [118] J. F. Monaco, D. G. Ward, R. L. Barron, and R. A. Bird. "Implementation and Flight Test Assessment of an Adaptive, Reconfigurable Flight Control System". In: *Proceedings of the AIAA Guidance, Navigation, and Control Conference, New Orleans, Louisiana*. Aug. 1997, pp. 1443–1454.
- [119] J. F. Monaco, D. G. Ward, and A. J. Bateman. "A Retrofit Architecture for Model-Based Adaptive Flight Control". In: *Proceedings of the AIAA First Intelligent Systems Conference*. 2004.
- [120] R. V. Monopoli. "Model reference adaptive control with an augmented error signal". In: *Automatic Control, IEEE Transactions on* 19.5 (1974), pp. 474–484.
- [127] N. Nguyen, K. Krishnakumar, J. Kaneshige, and P. Nespeca. "Flight Dynamics and Hybrid Adaptive Control of Damaged Aircraft". In: *Journal of Guidance, Control, and Dynamics* 31.3 (2008), pp. 751–764.
- [137] A. A. Pashilkar, N. Sundararajan, and P. Saratchandran. "Adaptive Nonlinear Neural Controller for Aircraft Under Actuator Failures". In: *Journal of Guidance, Control, and Dynamics* 30 (2007), pp. 835–847.
- [138] R. J. Patton. "Fault-Tolerant Control: The 1997 situation". In: *Proceedings of the 3rd IFAC Symposium on Fault Detection, Supervision and Safety for Technical Processes*. Aug. 1997, pp. 1033–1055.
- [145] H. Ranter. *Airliner Accident Statistics 2006*. Tech. rep. Aviation Safety Network, 2007.
- [150] M. Sharma and D. G. Ward. "Flight-path angle control via neuro-adaptive backstepping". In: *Proceedings of the AIAA Guidance, Navigation, and Control Conference and Exhibit*. Monterey, California, USA, Aug. 2002.
- [151] D. H. Shin and Y. Kim. "Nonlinear Discrete-Time Reconfigurable Flight Control Law Using Neural Networks". In: *Control Systems Technology, IEEE Transaction on* 14.3 (May 2006), pp. 408–422.

- [153] Y. Shin, A. J. Calise, and M. D. Johnson. "Adaptive Control of Advanced Fighter Aircraft in Nonlinear Flight Regimes". In: *Journal of Guidance, Control, and Dynamics* 31.5 (2008), pp. 1464–1477.
- [154] Y. B. Shtessel and J. Buffington. "Multiple Time Scale Flight Control Using Reconfigurable Sliding Modes". In: *Journal on Guidance, Control and Dynamics* 22.6 (1999), pp. 873–883.
- [156] S. N. Singh and M. Steinberg. "Adaptive Control of Feedback Linearizable Nonlinear Systems With Application To Flight Control". In: *Proceedings of the AIAA Guidance, Navigation and Control Conference*. July 1996.
- [159] J. J. E. Slotine and W. Li. *Applied Nonlinear Control*. Prentice Hall, 1991.
- [161] M. H. Smaili and J. A. Mulder. "Flight data reconstruction and simulation of El Al Flight 1862". In: *AIAA Modeling and Simulation Technologies Conference and Exhibit*. AIAA-2000-4586. Washington, DC, 2000.
- [163] L. Sonneveldt. "Adaptive Backstepping Control for Modern Fighter Aircraft". PhD thesis. Delft University of Technology, Faculty of Aerospace Engineering, July 2010.
- [164] L. Sonneveldt, Q. P. Chu, and J. A. Mulder. "Nonlinear Flight Control Design using Constrained Adaptive Backstepping". In: *Journal of Guidance, Navigation, and Dynamics* 30.2 (2007), pp. 322–336.
- [165] L. Sonneveldt, E. R. van Oort, Q. P. Chu, and J. A. Mulder. "Comparison of Inverse Optimal and Tuning Functions Designs for Adaptive Missile Control". In: *Proceedings of the AIAA Guidance, Navigation, and Control Conference and Exhibit*. 2007.
- [173] M. Steinberg. "Historical Overview of Research in Reconfigurable Flight Control". In: *Proceedings of the Institution of Mechanical Engineers, Part G: Journal of Aerospace Engineering* 219.4 (2005), pp. 263–275.
- [174] R. F. Stengel. "Intelligent Failure-Tolerant Control". In: *IEEE Control Systems Magazine* 11.4 (1991), pp. 14–23.
- [178] O. Stroosma, M. H. Smaili, T. J. J. Lombaerts, and J. A. Mulder. "Piloted Simulator Evaluation of New Fault-Tolerant Flight Control Algorithms for Reconstructed Accident Scenarios". In: *AIAA Modeling and Simulation Technologies Conference and Exhibit, Honolulu, Hawaii, Aug 18 - 21*. AIAA 2008-6534. 2008.
- [179] S. Suresh, S. N. Omkar, and V. Mani. "Direct Adaptive Neural Flight Controller for F-8 Fighter Aircraft". In: *Journal of Guidance, Control, and Dynamics* 29.2 (2006), pp. 454–464.
- [190] E. R. van Oort, Q. P. Chu, and J. A. Mulder. "Adaptive Dynamic Control Allocation and Backstepping Design". In: *Proceedings of the AIAA Guidance, Navigation, and Control Conference*. Under review. 2011.

- [191] E. R. van Oort, Q. P. Chu, and J. A. Mulder. "Maneuver Envelope Determination through Reachability Analysis". In: *Proceedings of the CEAS EURO GNC 2011 conference*. Accepted, to be presented. 2011.
- [192] E. R. van Oort, Q. P. Chu, and J. A. Mulder. "Safe Dynamic Flight Envelope Determination with Application to an F-16 Model". In: *Journal of Guidance, Control, and Dynamics* (2011). Under review.
- [193] E. R. van Oort, Q. P. Chu, and J. A. Mulder. "Safe Flight Envelope Determination by Reachability Analysis". In: *Proceedings of the ICNPAA 2010 World Congress: 8th International Conference on Mathematical Problems in Engineering, Aerospace and Sciences*. São José dos Campos, Brazil, 2010.
- [194] E. R. van Oort, L. Sonneveldt, Q. P. Chu, and J. A. Mulder. "A Comparison of Adaptive Nonlinear Control Designs for an Over-actuated Fighter Aircraft Model". In: *AIAA Guidance, Navigation, and Control Conference and Exhibit*. Honolulu, Hawaii, USA, Aug. 2008.
- [195] E. R. van Oort, L. Sonneveldt, Q. P. Chu, and J. A. Mulder. "Adaptive Dynamic Control Allocation and Backstepping Design". In: *Journal of Guidance, Control, and Dynamics* (2011). To be submitted.
- [196] E. R. van Oort, L. Sonneveldt, Q. P. Chu, and J. A. Mulder. "Full Envelope Modular Adaptive Control of a Fighter Aircraft using Orthogonal Least Squares". In: *Proceedings of the AIAA Guidance, Navigation, and Control Conference*. 2010-7857. AIAA. Toronto, Ontario, Canada, Aug. 2010.
- [197] E. R. van Oort, L. Sonneveldt, Q. P. Chu, and J. A. Mulder. "Full Envelope Modular Adaptive Control of a Fighter Aircraft using Orthogonal Least Squares". In: *Journal of Guidance, Navigation and Dynamics* 33.5 (2010), pp. 1461–1472.
- [198] E. R. van Oort, L. Sonneveldt, Q. P. Chu, and J. A. Mulder. "Modular Adaptive Input-to-state Stable Backstepping of a Nonlinear Missile Model". In: *AIAA Guidance, Navigation, and Control Conference and Exhibit*. Hilton Head, South Carolina, USA, Aug. 2007.
- [203] K. A. Wise and J. L. Sedwick. "Stability Analysis of Reconfigurable and Gain Scheduled Flight Control Systems using LMIs". In: *Proceedings of the AIAA Guidance, Navigation, and Control Conference*. 1998, pp. 118–126.
- [204] J. M. Wohletz. "Retrofit Systems for Reconfiguration in Civil Aviation". PhD thesis. Massachusetts Institute of Technology, Cambridge, Massachusetts, 2000.
- [210] Y. Zhang and J. Jiang. "Bibliographical review on reconfigurable fault-tolerant control systems". In: *Annual Reviews in Control* 32.2 (Dec. 2008), pp. 229–252.

PART



**BACKSTEPPING
AND
MODEL IDENTIFICATION THEORY**

In this part of the dissertation theory is introduced to support the applications to aircraft fault tolerant control in Part II. First, a short introduction to control in general, and its applications in aviation is given. Then, one of the main subjects is introduced: backstepping. In the last chapter the backstepping method is extended to be applicable to systems with unknown parameters. A simple longitudinal missile model is used to illustrate the different approaches through the whole part.

INTRODUCTION TO ADAPTIVE NONLINEAR CONTROL

In this chapter first an introduction to the basic concepts of feedback and control is given. An overview of control methods used for flight control design is presented. Adaptive control methods extend the control concepts to systems with large uncertainties and unknown dynamics. An introduction to different modeling techniques is given.

2.1 What is Feedback Control

A *dynamical system* is a system whose behavior changes over time, often in response to external influence. The term *feedback* refers to a situation in which two or more dynamical systems are connected together such that each system influences the other, and their dynamics are therefore coupled. The term *control* has many meanings, and varies between different communities and its context. In this dissertation, control is defined as the theory and algorithms which deal with influencing the behavior of dynamical systems. Typically, control systems are designed such that the influenced system follows some desired reference input, while achieving some level of disturbance rejection. An example of control in this sense is the cruise control of a car: a control system designed to maintain a constant vehicle speed despite variations in road slope. Feedback control is also the mechanism that keeps homeostasis in the human body [201]. Alfred Wallace, the often omitted co-discoverer of the theory of evolution, and Charles Darwin suspected that feedback over longer time periods is responsible for the evolution of species [32]. The standard feedback control loop block diagram is shown in figure 2.1. This shows the interconnection

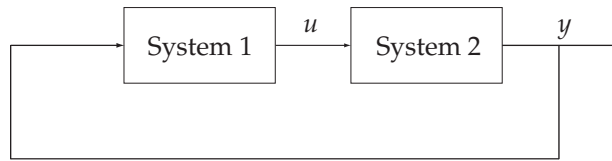


Figure 2.1: Standard feedback system block diagram.

between the outside world, the system itself, and the control system influencing the system.

Automatic control systems already date back to the ancient Greeks and Arabs who designed fluid-level regulators. The Industrial Revolution in Europe sparked the desire for self-driven machines, thereby introducing the requirement for automatic control systems. Control theory began to acquire its language by James Maxwell in 1868 through his work on automatic governors [109]. Other events resulting in large interest and developments in automatic control were the Second World War and the space-race between the United States and the Soviet Union. Nowadays, it is hard to imagine a life without automatic control: it can be found in nearly every system around us.

Most of the systems encountered in practice are inherently nonlinear meaning that the relation between the input and the output of the system is not simply a linear mapping but rather some nonlinear combination of the input and the system states. Linear control design methods can sometimes be applied to nonlinear systems over limited operating regions. However, problems with a sufficiently large operation region or highly nonlinear dynamics may require that the nonlinearities in the system are directly addressed in the control system design to achieve the desired level of performance. Modern fighter aircraft are notable examples of such systems; they are designed for large operating envelopes, inherently unstable and highly nonlinear. A wide range of methods exists in literature addressing various types of nonlinearity and the way the nonlinearity affects the system. In the next section some of these methods are discussed.

2.2 Flight Control Approaches

This section contains a brief overview of some methods which have been applied in aircraft control design, either in industry or academia. First of all the small-signal linearization and gain-scheduling approaches are discussed. Second, the feedback linearization and nonlinear dynamic inversion schemes are presented. Finally, a brief introduction to the backstepping design method is given.

2.2.1 Small-signal Linearization

The name *small-signal linearization* is used to characterize the fact that a linear model is a good representation of the true nonlinear system if the system trajectory $x(t)$ remains close to some equilibrium point x_e or to some nominal trajectory $x^*(t)$. Additionally, this name also distinguishes this type of linearization from the feedback linearization method discussed below.

If the nonlinear system is linearized around the equilibrium $(x, u) = (0, 0)$, then the resulting linear model is described by

$$\dot{x} = Ax + Bu \quad (2.1)$$

where the matrices $A \in \mathbb{R}^{n \times n}$ and $B \in \mathbb{R}^{n \times m}$ are given by

$$A = \left. \frac{\partial f}{\partial x}(x, u) \right|_{x=0, u=0} \quad B = \left. \frac{\partial f}{\partial u}(x, u) \right|_{x=0, u=0}. \quad (2.2)$$

Linear control design approaches can now be used to design a feedback controller for the system, for example proportional-integral-derivative controllers and \mathcal{H}_∞ -synthesis.

If a tracking controller is designed based on a linearization valid at some operating point, then as the reference moves away from the equilibrium point, the state $x(t)$ will try to follow it. As the distance between the actual state and the equilibrium increases, the linear approximation becomes increasingly less accurate. As the accuracy of the approximation decreases, the designed linear controller might become unsuitable causing a degradation of performance and stability. Instead of linearizing around a fixed equilibrium point, linearization around a reference trajectory $x_r(t)$ and associated nominal control signal u^* known a-priori is a possibility. This method yields similar results as linearizing around a single operating point. The main difference is that linearizing around a trajectory generally results in a time-varying linear model for which other linear control design methods exist.

2.2.2 Gain-scheduling

In the section above a linearization method suitable for systems which stay relatively close to a desired operating point or nominal trajectory has been described. The *gain-scheduling* approach is an extended version of the small signal linearization around *multiple operating points*. For each linear model a feedback controller is designed, creating a family of feedback control laws. Each of these control laws is applicable in the neighborhood of a specific operating point. The family is combined into a single control law whose parameters are varied by a *scheduling scheme* usually based on the system state and reference signal.

Intuitively, if for each linearization point the region of attraction with the control law is larger than the scheduled operating region corresponding to the point, the resulting gain-scheduled control system will be stable. Unfortunately, deriving

formal stability results is very complex for this approach (see e.g. [148, 149]). Another limitation of the method is that the designed controller is fixed, therefore any mismatch between the model and the true system due to disturbances and uncertainty will cause performance degradation. Additionally, the selection of the number of linearization points and the individual controller tuning is still a cumbersome and labor intensive process since each linearization point has to be handled individually, and afterwards the complete system performance has to be evaluated. However, it has been used successfully and very frequently in flight control, see for example [76, 111, 128, 171, 172, 176].

2.2.3 Feedback Linearization

Feedback linearization (FBL) can be described as an approach to transform a nonlinear system to an equivalent linear system through a combination of state or output feedback and a coordinate transformation. The technique is one of the most powerful and common techniques found in nonlinear control. Consider the n -th order system in companion form

$$\begin{aligned} \dot{x}_1 &= x_2 \\ &\vdots \\ \dot{x}_{n-1} &= x_n \\ \dot{x}_n &= f(x) + g(x)u. \end{aligned} \tag{2.3}$$

The nonlinearities $f(x)$ and $g(x)$ in this system can be canceled by designing a feedback linearizing control law of the form

$$u = g^{-1}(x) [v - f(x)]$$

which results in a chain of n integrators from the virtual control input v to the state x_1 . Not all systems are in this basic form. The class of systems which can be transformed into the companion form by a nonlinear coordinate transformation, called diffeomorphism, is called feedback linearizable. The diffeomorphism to transform the system into the companion form can be found systematically using Lie-derivatives.

The major drawback of feedback linearization is that it relies on exact cancellation of the nonlinearities in the system. If one of the functions, for example $f(x)$, is uncertain, exact cancellation of the nonlinearities becomes impossible. For uncertainties that are relatively small, robust control techniques can be used to design controllers with adequate performance. However, when the uncertainties become large, a different approach is required: adaptive control. Another problem of the feedback linearization method is that not all systems can be transformed to a linearizable form. The backstepping technique introduced in the following section can be applied to a class of systems which is larger than feedback linearizable systems, and allows for more flexibility in the design.

2.2.4 Backstepping

The name *backstepping* originates from the fact that it is a recursive design method which *steps back* toward the control inputs starting with the differential equations which are separated from them by the largest number of integrators [88]. The design procedure is in some ways very similar to feedback linearization and nonlinear dynamic inversion. However, instead of first transforming the system into the companion form directly, a stabilizing feedback is constructed for each subsystem by considering a combination of states appearing one integrator step later as a virtual control input. This process is repeated until a stabilizing control law for the actual control inputs can be defined.

The approach is best illustrated by giving a simple example, chapters 3 and 4 discuss the backstepping method in much more detail. Consider a second order system

$$\begin{aligned}\dot{x}_1 &= x_2 \\ \dot{x}_2 &= f(x_1, x_2) + g(x_1, x_2)u,\end{aligned}\tag{2.4}$$

with $g(x_1, x_2) \neq 0$ for some operating envelope. The control objective is to track a differentiable reference signal $x_r(t)$. The key idea of backstepping is that the tracking problem is solved if the control input u could force the state $x_2(t)$ to satisfy

$$x_2 = -c_1(x_1 - x_r) + \dot{x}_r, \quad c_1 > 0.\tag{2.5}$$

In that case, x_1 satisfies $\dot{x}_1 = -c_1(x_1 - x_r) + \dot{x}_r$, implying that $x_1(t)$ converges to $x_r(t)$ and then tracks the reference signal. This notion is equivalent to treating x_2 as a *virtual control input* for the x_1 subsystem. Thus, define an virtual control law $\alpha(x_1, x_r, \dot{x}_r)$, defined as

$$\alpha(x_1, x_r, \dot{x}_r) = -c_1(x_1 - x_r) + \dot{x}_r.$$

Now introduce a change of coordinates

$$\begin{aligned}z_1 &= x_1 - x_r \\ z_2 &= x_2 - \alpha(x_1, x_r, \dot{x}_r),\end{aligned}$$

which will be referred to as the error system. The dynamics of the error system become

$$\begin{aligned}\dot{z}_1 &= -c_1 z_1 + z_2 \\ \dot{z}_2 &= v = f(x_1, x_2) + g(x_1, x_2)u - \frac{\partial \alpha}{\partial x_1} \dot{x}_1 - \frac{\partial \alpha}{\partial x_r} \dot{x}_r - \frac{\partial \alpha}{\partial \dot{x}_r} \ddot{x}_r\end{aligned}$$

The control law for u can now be designed using a control Lyapunov function (CLF) defined as $V(z_1, z_2) = \frac{1}{2}(z_1^2 + z_2^2)$. The Lyapunov function can be considered as some measure of the energy in the error system. The derivative of the CLF is given by

$$\dot{V} = -c_1 z_1^2 + z_1 z_2 + z_2 v$$

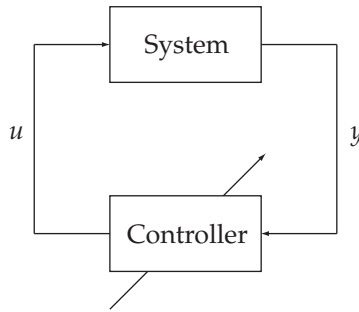


Figure 2.2: Direct adaptive control scheme.

from which we design the modified control input

$$u = g^{-1}(x_1, x_2) \left[-c_2 z_2 - f(x_1, x_2) - z_1 + \frac{\partial \alpha}{\partial x} \dot{x}_1 - \frac{\partial \alpha}{\partial x_r} \dot{x}_r - \frac{\partial \alpha}{\partial \dot{x}_r} \ddot{x}_r \right], \quad c_2 > 0$$

to render the CLF derivative negative definite

$$\dot{V} = -c_1 z_1^2 - c_2 z_2^2 \leq 0,$$

dissipating the “energy” in the error system.

2.3 Adaptive Control

There is a long and rich history of attempts to invent, design and build systems capable of controlling systems with uncertainties and/or unpredictable changes in their dynamics. It can be argued that this even dates back to the first feedback systems, since even the most elementary feedback loops can often tolerate significant uncertainties. Adaptive control can be interpreted as dynamic feedback: controllers with a higher order to be able to adapt themselves to changes in the controlled system. Mainly two types of adaptive control exists, distinguished by whether the tuning gains of the controller are adapted, or that the model of the system to be controlled is estimated. These control approaches are called *direct adaptive control* and *indirect adaptive control* respectively. This dissertation is focused on indirect adaptive control since this control approach can yield an accurate model of the system, which can be extremely valuable for failure diagnosis.

2.3.1 Direct Adaptive Control

In the *direct* adaptive control approach the identifier acts simultaneously as a controller. The adaptation mechanism is designed to adjust the identifier to match some unknown nonlinear controller that will stabilize the system, and make the

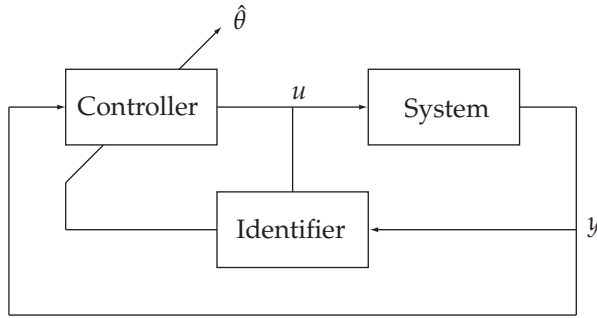


Figure 2.3: Indirect adaptive control scheme.

closed-loop system meet the desired performance objectives. The scheme is called direct since the system itself is not identified, but the parameters of the controller are directly updated. This controller architecture is shown in figure 2.2.

2.3.2 Indirect Adaptive Control

An *indirect* approach to adaptive control is made up of an identifier which is used to identify the unknown system dynamics by estimating some model parameters, and a *certainty equivalence* control scheme in which the system the controller is designed assuming that the parameter estimates are their true values. This adaptive control architecture is shown in figure 2.3. If the estimated model is a good approximation of the true system, then it is easier to meet the control objectives. If on the other hand the system does not react as expected or predicted, the estimated model is incorrect and therefore should be adjusted to match the true system behavior.

2.4 System Identification

The name system identification is a general term to describe the mathematical tools and algorithms to build dynamical models for systems from measured data. In technical terms, system identification is defined by Zadeh [208] as "the determination on the basis of input and output, of a system (model) within a specified class of systems (models), to which the system under test is equivalent (in terms of a criterion)". From this definition it follows that three entities are involved in system identification: measurement data, a set of models, and a criterion.

In this dissertation only models that are linear in their parameters are considered, that is, models of the form

$$\hat{y} = \varphi^T(x, u)\hat{\theta} \quad (2.6)$$

where \hat{y} is the estimated model output, x is the system state, u is the system input, $\varphi(x, u)$ defines the model structure and is often called the *regressor* function, and

$\hat{\theta}$ is the model *parameter estimate* or *parameter vector*. Note that the function φ can depend nonlinearly on the state and input variables of the system.

Many different methods of theoretical modeling ranging from first principles to empirical modeling based only on measurement data can be pursued. Basically, three different modeling approaches can be distinguished:

White-box models are fully derived by first principles, i.e. physical, chemical, biological, economical, etc. laws. All equations and parameters can be determined by theoretical modeling. Typically, models whose structure is completely derived from first principles are placed under white box models even when some parameters are estimated from data.

Black-box models are solely based on measurement data. Both the model structure and parameters are determined from experimental modeling. For building black box models, little or no prior knowledge is exploited, and the estimated model does not have a direct relationship to first principles.

Gray-box models are a combination of white and black box models. They are characterized by the integration of various kinds of information that is available about the system. Often, the model structure candidates rely on prior knowledge and the parameters are determined through measurement data. The model structure can also be determined from collected measurement data.

All three model types can be used in indirect adaptive control schemes. The model identification task for on-line system identification is composed out of two tasks:

1. selecting a model structure, and
2. determining the model parameters.

In black box modeling these two tasks can be tackled simultaneously, while for white box models only the second task has to be performed. Structure selection is especially important for gray box models to avoid over- and underfitting the measured data. These two tasks will be discussed in more detail below.

2.4.1 Model Parameter Optimization

If the cost criterion for a particular model structure is selected as the sum of squares of the output errors, and the model output is linear in the unknown parameter, a quadratic optimization problem is obtained. This type of optimization problem has the following properties

- a unique optimum exists,
- the surface of the cost function is a hyper-parabola,
- a recursive formulation is possible,

- the computational cost is low.

which makes it very attractive for on-line applications. When the parameter optimization problem to be solved is defined as

$$\min_{\theta(t)} \int_0^t \left(y(\tau) - \varphi^T(\tau)\theta(\tau) \right)^2 d\tau = \min_{\theta} \int_0^t \varepsilon(\tau)^2 d\tau \quad (2.7)$$

then the gradient descent algorithm

$$\dot{\hat{\theta}} = \gamma \varphi \varepsilon, \quad \gamma > 0 \quad (2.8)$$

updates the parameter estimate in the direction of the steepest descent direction of the cost function with respect to the error. The gradient update law (2.8) can be considered as a first-order approximation of the cost function.

Faster convergence of the estimate to the optimal value can be achieved by taking the second order derivative of the cost function into account (Newton's method). By introduction of the notation

$$\langle x, y^T \rangle = \int_0^t x(\tau) y^T(\tau) d\tau \quad (2.9)$$

and the *correlation matrix* $N = \langle \varphi, \varphi^T \rangle$, the problem (2.7) can be rewritten as

$$\min_{\hat{\theta}(t)} \langle y, y \rangle - 2 \langle y, \varphi^T \rangle \hat{\theta} + \hat{\theta}^T N \hat{\theta}.$$

After differentiation with respect to the parameter estimate the normal equation is obtained

$$N \hat{\theta}(t) = \langle \varphi, y \rangle.$$

where N can be interpreted as the second order derivative of the cost function with respect to the parameter estimate. The optimization problem can be solved recursively by tracking the inverse of $\Gamma = N^{-1}$ and the estimate $\hat{\theta}$ and the recursive least squares filter is obtained

$$\dot{\hat{\theta}} = \Gamma \varphi \varepsilon \quad (2.10a)$$

$$\dot{\Gamma} = -\Gamma \dot{N} \Gamma = -\Gamma \varphi \varphi^T \Gamma \quad (2.10b)$$

2.4.2 Model Structure Selection

Model structure selection deals with selecting an appropriate model structure such that the actual system can be approximated as good as possible within the set of allowable model structures. An over-parameterized model structure can lead to unnecessarily complicated computations for finding the parameter estimates and for using the estimated model. An under-parameterized model can be too

inaccurate. Therefore, often Occam's razor is often applied for model structure selection, stating that "the simplest solution is usually the correct one" or "the simplest explanation that covers all the facts is usually the best".

The matrix φ in (2.6) for gray and black box models can be defined in different ways, and combinations of the methods below are possible.

Taylor Expansion A Taylor expansion is taken around an operating point up to a certain order. The parameter vector then determines how the different contributions of the Taylor expansion terms are weighted. If a first order Taylor expansion model is made, the model will be at best a tangent hyperplane to the true system. It is fairly easy to extract information about the actual system from the Taylor expansion model structure. For example, in aircraft control the sign of the dependence of the pitch moment coefficient on the angle of attack determines the aircraft's static stability and in the Taylor model this is easily observed from the sign of parameter multiplying the angle of attack.

Basis Functions and Neural Networks These two techniques are more appropriate for the black-box approach, since no model structure is assumed a-priori. The coefficients multiplying the basis functions are estimated and depending on the number of basis-functions any function can be approximated accurately.

2.5 Conclusions

In this chapter a brief overview of important concepts in feedback control was given. Some approaches used in the flight control domain to handle the nonlinear behavior of aircraft were introduced. The concept of adaptive control and two of its flavors, indirect and direct, were discussed. One of the key aspects in indirect adaptive control is system identification which is composed out of model structure determination and parameter estimation. Since aircraft, and especially fighter aircraft, are nonlinear systems with large operating regimes, a nonlinear control method with a lot of flexibility is selected for further research: the backstepping approach.

BACKSTEPPING CONTROL DESIGN

Lyapunov theory is a very important tool for both linear as well as nonlinear control. One of the main difficulties in the early days of nonlinear control was the problem of finding a Lyapunov function for a given system. The invention of constructive control tools for nonlinear control design, like backstepping, has been well received in the control community. Along with a Lyapunov function to prove stability of the closed-loop system, a control law stabilizing the system is designed.

In this chapter first of all important design tools based on Lyapunov functions are introduced. These tools are then used to introduce the backstepping design procedure, starting with simple systems and extending to the class of block-strict feedback systems. Then, several extensions and modifications of the backstepping method are introduced which can handle a larger class of systems.

3.1 Stability Concepts for Nonlinear Systems

Stability plays a crucial role in system theory and control engineering, and has been researched quite extensively in the past century. Some of the most fundamental concepts of stability were introduced by the Russian mathematician and engineer Alexandr Lyapunov [107]. The work of Lyapunov was extended and brought to the attention of the control engineering and applied mathematics communities by LaSalle, Krasovskii and many others.

3.1.1 Stability Properties

Note that stability is a property of an equilibrium, not of a system as a whole. Often however, the system will be referred to as stable if all of its equilibrium points are stable. Consider the time-varying system

$$\dot{x} = f(x, t) \quad (3.1)$$

where $x \in \mathbb{R}^n$, and $f : \mathbb{R}^n \times \mathbb{R}_+ \rightarrow \mathbb{R}^n$ is a piecewise continuous function in t and locally Lipschitz in x . The solution of (3.1) which starts from the point x_0 at time $t_0 \geq 0$ is denoted as $x(t; x_0, t_0)$ with $x(t_0; x_0, t_0) = x_0$. Lyapunov concepts describe continuity properties of $x(t; x_0, t_0)$ with respect to x_0 . If the initial condition is perturbed to \tilde{x}_0 , then, for stability, the resulting perturbed solution $x(t; \tilde{x}_0, t_0)$ is required to stay close to $x(t; x_0, t_0)$ for all $t \geq 0$. In addition, for asymptotic stability, the error $x(t; \tilde{x}_0, t_0) - x(t; x_0, t_0)$ is required to vanish as $t \rightarrow \infty$. Summarizing, the solution $x(t; x_0, t_0)$ of (3.1) is

bounded if there exists a constant $B(x_0, t_0) > 0$ such that

$$|x(t; x_0, t_0)| < B(x_0, t_0), \quad \forall t \geq 0, \quad (3.2)$$

stable if for each $\epsilon > 0$ there exists a $\delta(\epsilon, t_0)$ such that

$$|\tilde{x}_0 - x_0| < \delta \Rightarrow |x(t; \tilde{x}_0, t_0) - x(t; x_0, t_0)| < \epsilon, \quad \forall t \geq 0, \quad (3.3)$$

attractive if there exists an $r(t_0) > 0$ and, for each $\epsilon > 0$, a $T(\epsilon, t_0)$ such that

$$|\tilde{x}_0 - x_0| < r \Rightarrow |x(t; \tilde{x}_0, t_0) - x(t; x_0, t_0)| < \epsilon, \quad \forall t \geq t_0 + T, \quad (3.4)$$

asymptotically stable if it is both stable and attractive, and,

unstable if it is not stable.

When the constants defined above are not dependent on t_0 , the corresponding properties are called *uniform*. Note that this is the case when the system itself is time invariant: $\dot{x} = f(x)$. For the adaptive control designs of the next chapter, *uniform stability* is more desirable than just stability. An even more desired property is *uniform asymptotic stability* (UAS). The solution $x(t; x_0, t_0)$ is UAS if it is uniformly stable and uniformly attractive. This interpretation of stability is illustrated in \mathbb{R}^2 in figure 3.1. All trajectories starting from the inner disc remain in the outer disc and are therefore bounded by the outer circle.

The set of initial conditions $\mathcal{D} = \{x_0 \in \mathbb{R}^n | x(t_0) = x_0 \text{ and } |x(t)| \rightarrow \infty \text{ as } t \rightarrow \infty\}$ is the domain of attraction of the origin. If \mathcal{D} is equal to \mathbb{R}^n , then the origin is said to be *globally asymptotically stable*. A globally stable equilibrium point implies that x_e is a unique equilibrium point, thus all solutions converge to this point independent of their starting point. In some cases it is not possible to prove stability of the equilibrium point x_e , yet it may still be possible to use Lyapunov analysis to show boundedness of the solution [83].

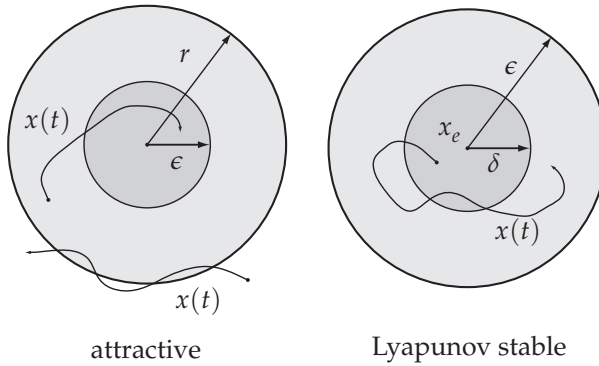


Figure 3.1: Lyapunov stability illustrated in \mathbb{R}^2

3.1.2 Lyapunov’s Direct Method

To be of practical interest, the stability condition should not require that the ordinary differential equation (3.1) is solved explicitly; in general it is not possible or not straightforward to find analytical solutions. A different method was introduced by Lyapunov [107] to prove stability: Lyapunov’s Direct Method. The method can be interpreted as a generalization of the idea that there exists some measure of the energy in a system. The rate of change of the energy in the system provides a way to investigate stability of an equilibrium point. Formally, let $B(r)$ be a ball of size r around the origin: $B(r) = \{x \in \mathbb{R}^n \mid |x| < r\}$.

A continuous function $V(x)$ is

positive definite on $B(r)$ if $V(0) = 0$ and $V(x) > 0, \forall x \in B(r)$ such that $x \neq 0$,

positive semi-definite on $B(r)$ if $V(0) = 0$ and $V(x) \geq 0, \forall x \in B(r)$ such that $x \neq 0$,

negative (semi-)definite on $B(r)$ if $-V(x)$ is positive (semi-)definite, and

radially unbounded if $V(0) = 0, V > 0$ on $\mathbb{R}^n / \{0\}$ and $V(x) \rightarrow \infty$ as $x \rightarrow \infty$.

A continuous function $V(x, t)$ is

positive definite on $B(r)\mathbb{R}$ if there exists a positive definite function $\alpha(x)$ on $B(r)$ such that

$$V(0, t) = 0, \forall t \geq 0 \text{ and } V(x, t) \geq \alpha(x), \forall t \geq 0, x \in B(r),$$

radially unbounded on $B(r)$ if $V(0) = 0$ and $V(x) \geq 0, \forall x \in B(r)$ such that $x \neq 0$,

$$V(0, t) = 0, \forall t \geq 0 \text{ and } V(x, t) \geq \alpha(x), \forall t \geq 0, x \in \mathbb{R}^n,$$

decescent on $B(r) \times \mathbb{R}$ if there exists a positive definite function $\alpha(x)$ on $B(r)$ such that

$$V(x, t) \leq \alpha(x), \quad \forall t \geq 0, x \in B(r)$$

Using these concepts, the following method can be used to determine the stability of an equilibrium point of a system by studying an appropriate Lyapunov function $V(x, t)$. The time derivative of $V(x, t)$ is taken along the trajectories of the system (3.1)

$$\dot{V}(x, t)|_{\dot{x}=f(x,t)} = \frac{\partial V}{\partial t} + \frac{\partial V}{\partial x} f(x, t)$$

Theorem 3.1 (Lyapunov's Direct Method). *Let $V(x, t) : \mathcal{D} \times \mathbb{R}_+ \rightarrow \mathbb{R}_+$ be a continuously differentiable and positive definite function, where \mathcal{D} is an open region containing the origin.*

- if $\dot{V}(x, t)|_{\dot{x}=f(x,t)}$ is negative semi-definite for $x \in \mathcal{D}$, then the equilibrium $x_e = 0$ is stable;
- if $V(x, t)$ is decrescent and $\dot{V}(x, t)|_{\dot{x}=f(x,t)}$ is negative semi-definite for $x \in \mathcal{D}$, then the equilibrium $x_e = 0$ is uniformly stable;
- if $\dot{V}(x, t)|_{\dot{x}=f(x,t)}$ is negative definite for $x \in \mathcal{D}$, then the equilibrium $x_e = 0$ is asymptotically stable;
- if $V(x, t)$ is decrescent and $\dot{V}(x, t)|_{\dot{x}=f(x,t)}$ is negative definite for $x \in \mathcal{D}$, then the equilibrium $x_e = 0$ is uniformly asymptotically stable;
- if there exist three positive constants c_1, c_2 and c_3 such that $c_1|x|^2 \leq V(x, t) \leq c_2|x|^2$ and $\dot{V}|_{\dot{x}=f(x,t)} \leq -c_3|x|^2$ for all $t \geq 0$ for all $x \in \mathcal{D}$, then the equilibrium x_e is exponentially stable.

Proof. The proof can be found in chapter 4 of Khalil [83]. □

The requirement that the time derivative of the Lyapunov function is negative definite is quite stringent. In some cases it is still possible to conclude asymptotic convergence when it is only negative semi-definite using LaSalle's invariance theorem, see Khalil [83]. This theorem is only valid for autonomous systems, for non-autonomous systems Barbalat's lemma can be applied to show convergence.

Lemma 3.2 (Barbalat's Lemma). *If the differentiable function $\phi(t)$ tends to a finite limit as $t \rightarrow \infty$ and if $\dot{\phi}$ is uniformly continuous (or $\ddot{\phi}$ is bounded), then*

$$\lim_{t \rightarrow \infty} \dot{\phi}(t) = 0.$$

Combination of this lemma with Lyapunov's direct method leads to the powerful theorem due to LaSalle and Yoshizawa

Theorem 3.3 (LaSalle-Yoshizawa). *Let $x_e = 0$ be an equilibrium point of (3.1) and suppose that f is locally Lipschitz in x and uniformly in t . Let $V : \mathbb{R}^n \times \mathbb{R}_+ \rightarrow \mathbb{R}_+$ be a continuously differentiable function $V(x, t)$ such that*

$$\gamma_1(|x|) \leq V(x, t) \leq \gamma_2(|x|) \quad (3.5)$$

$$\dot{V} = \frac{\partial V}{\partial x}(x)f(x, t) \leq -W(x) \leq 0 \quad (3.6)$$

$\forall t \geq 0, \forall x \in \mathbb{R}^n$, where γ_1, γ_2 are class \mathcal{K}_∞ functions, and W is a continuous function. Then, all solutions of (3.1) are globally uniformly bounded and satisfy

$$\lim_{t \rightarrow \infty} W(x(t)) = 0. \quad (3.7)$$

In addition, if $W(x)$ is positive definite, then the equilibrium point $x = 0$ is globally uniformly asymptotically stable (GUAS).

Proof. The proof is given in appendix A of Krstić, Kanellakopoulos, and Kokotović [88]. \square

The main feat of Lyapunov's direct method is that it can be applied without explicitly solving the differential equation (3.1). Unfortunately, theorem 3.3 does not provide any means of constructing the Lyapunov function $V(x, t)$. The theorem only gives sufficient conditions, and hence it can be difficult to find a Lyapunov function.

Another important stability concept used in this dissertation is that of input-to-state stability (ISS), introduced by Sontag [167].

Definition 3.4 (Input-to-State Stability). *The system $\dot{x} = f(t, x, u)$ where f is piecewise continuous in t and locally Lipschitz in x and u , is said to be ISS if there exists a class \mathcal{KL} function β and a class \mathcal{K} function γ , such that, for any $x(0)$ and for any input $u(\cdot)$ continuous and bounded on $[0, \infty)$ the solution exists for all $t \geq 0$ and satisfies*

$$|x(t)| \leq \beta(|x(t_0)|, t - t_0) + \gamma \left(\sup_{t_0 \leq \tau \leq t} |u(\tau)| \right)$$

for all t_0 and t such that $0 \leq t_0 \leq t$.

The function $\gamma(\cdot)$ is often referred to as an ISS-gain for the system. This definition implies that an ISS system is bounded-input bounded-state stable and has a GUAS equilibrium at $x = 0$ when $u(t) = 0$.

3.2 Control Lyapunov Functions

The objective of designing a control system is to create a closed-loop system with desirable stability properties, rather than just analyzing the properties of a given

system. Therefore, an extension of the Lyapunov function, introduced in the previous section, the control Lyapunov function (CLF) is used.

Consider a system

$$\dot{x} = f(x, u), \quad x \in \mathbb{R}^n, \quad u \in \mathbb{R}, \quad f(0, 0) = 0 \quad (3.8)$$

where the goal is to design a feedback control law $\alpha(x)$ for the control variable u such that the equilibrium $x = 0$ of the closed loop system

$$\dot{x} = f(x, \alpha(x)) \quad (3.9)$$

is globally asymptotically stable. It is possible to pick a $V(x)$ as a Lyapunov function candidate, and require that its derivative along the solutions of (3.9) satisfies $\dot{V}(x) \leq -W(x)$, where $W(x)$ is a positive definite function. Therefore, an $\alpha(x)$ has to be found which guarantees that for all $x \in \mathbb{R}^n$

$$\frac{\partial V(x)}{\partial x} f(x, \alpha(x)) \leq -W(x), \quad \forall x \in \mathbb{R}^n. \quad (3.10)$$

A stabilizing control law for the system (3.8) may exist, but due to a (poor) choice of $V(x)$ and $W(x)$ may fail to satisfy (3.10). A system for which a good choice of $V(x)$ and $W(x)$ exists is said to possess a CLF. More precisely, the definition of a CLF is given below.

Definition 3.5 (Control Lyapunov Function (CLF)). *A smooth positive definite and radially unbounded function $V : \mathbb{R}^n \rightarrow \mathbb{R}_+$ is called a CLF for (3.8) if*

$$\inf_{u \in \mathbb{R}} \left\{ \frac{\partial V(x)}{\partial x} f(x, u) \right\} < 0, \quad \forall x \neq 0. \quad (3.11)$$

The existence of a CLF is equivalent to global asymptotic stabilizability [4]. The use of CLFs in control design is illustrated by a very basic scalar example.

Example 3.1 (Scalar system example)

Consider a the system

$$\dot{x} = -x^3 + \cos(x) + u \quad (3.12)$$

for which the task is to design a feedback control law which creates and globally stabilizes the equilibrium at $x = 0$. Using the concept of nonlinear dynamic inversion and feedback linearization it is quite straightforward to design the control law

$$u = x^3 - \cos(x) - x \quad (3.13)$$

which cancels both the nonlinearities, and replaces them with $-x$, such that the resulting feedback system is linear: $\dot{x} = -x$. Taking

$$V(x) = \frac{1}{2}x^2 \quad (3.14)$$

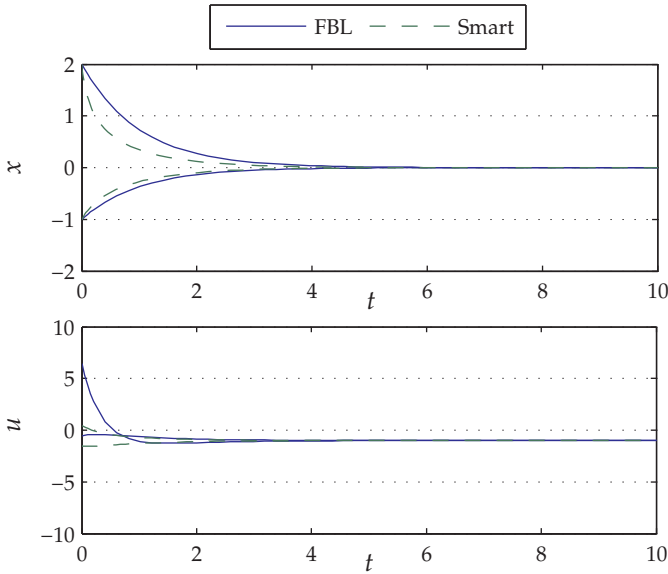


Figure 3.2: Comparison of the two CLF based designs. One based on feedback linearization, the other one “smart”.

as a CLF for (3.12), the control law satisfies the requirement (3.10) with $W(x) = x^2$.

It is possible to design a better control law which does not cancel the x^3 non-linearity. For stabilization at $x = 0$ the negative feedback term $-x^3$ is helpful, especially for large values of $|x|$. Simultaneously, the presence of x^3 in the control law is potentially harmful since it can lead to large control input signals u , and can easily cause destabilization when there is small uncertainty in the system. Thus, a new control law is designed which avoids cancellation of the x^3 term as

$$u = -\cos(x) - x \quad (3.15)$$

which meets the requirement (3.11) with $W(x) = x^2 + x^4$.

The example shows one of the strengths of constructive Lyapunov-based designs: they are very flexible in the choice of control law. The different control designs are compared in figure 3.2. Two initial conditions are shown $x = 2$ and $x = -1$. The control input for the smart controller is much lower for the first initial condition, as was expected. Additionally, the transient response of the smart controller design is faster than the FBL design. The major deficiency of the CLF concept as a design tool is that for most nonlinear systems a CLF is not known. The task of finding an appropriate CLF may be as complex as designing a stabilizing

feedback law. For some classes of nonlinear systems, these two tasks are solved simultaneously by the backstepping procedure.

An extension of the CLF for systems with uncertainties is the ISS-CLF. Existence of an ISS-CLF is a necessary and sufficient condition for input-to-state stabilizability.

Definition 3.6 (ISS-CLF). A smooth function $V : \mathbb{R}^n \times \mathbb{R}_+ \rightarrow \mathbb{R}_+$, positive definite and radially unbounded in x for each d , is called an ISS-control Lyapunov function for $\dot{x} = f(x, t) + w^T(x, t)d + g(x, t)u$ if there exists a class \mathcal{K}_∞ function ρ such that the following implication holds for all $x \neq 0$ and all d :

$$|x| \geq \rho(|d|) \Rightarrow \inf_{u \in \mathbb{R}} \left\{ \frac{\partial V}{\partial x} [f(x) + g(x, t)u] + \frac{\partial V}{\partial x} w(x)d \right\} < 0. \quad (3.16)$$

3.3 Backstepping Design

In this section the backstepping design is introduced. The previous section has shown how to use a CLF as a design tool. The backstepping approach extends this idea from scalar systems to systems with integrators. First, the backstepping procedure for scalar systems which are extended with a single integrator is given. Then, using this integrator backstepping approach, a recursive design procedure for strict feedback systems is defined.

3.3.1 Integrator Backstepping

Consider the system (3.12) extended with an integrator

$$\dot{x}_1 = -x_1^3 + \cos(x_1) + x_2 \quad (3.17a)$$

$$\dot{x}_2 = u. \quad (3.17b)$$

The design objective is the regulation of $x_1(t)$ to zero: $x_1(t) \rightarrow 0$ as $t \rightarrow \infty$, for all $x_1(0), x_2(0)$. Naturally, $x_2(t)$ must remain bounded. The only equilibrium of the system (3.17) with $x_1 = 0$ is at $(x_1, x_2) = (0, 1)$. To construct a CLF for the system (3.17) the fact that a CLF for the x_1 subsystem is already known, from the previous example, will be used. If x_2 really were the control input, then the corresponding CLF and control law would be $V(x_1) = \frac{1}{2}x_1^T x_1$ and $x_2 = -c_1 x_1 - \cos(x_1)$. However, x_2 is just a state variable and not a control input. In the backstepping design the variable x_2 is interpreted as an intermediate control input, and its desired value can be described by

$$x_{2,\text{des}} = -c_1 x_1 - \cos(x_1) \triangleq \alpha(x_1). \quad (3.18)$$

Now, introduce z as the deviation of x_2 from its desired value

$$z = x_2 - x_{2,\text{des}} = x_2 - \alpha(x_1) = x_2 + c_1 x_1 + \cos(x_1) \quad (3.19)$$

The state x_2 can be interpreted as a *virtual* control input, and its desired value $\alpha(x_1)$ as a *stabilizing function*. The variable z is the corresponding *error variable*. Now, apply a change of coordinates to (x_1, z) coordinates such that the system is in a more convenient form. In the new coordinates, the system dynamics can be expressed as

$$\begin{aligned}\dot{x}_1 &= -x_1^3 + \cos(x_1) + x_2 \\ &= -x_1^3 + \cos(x_1) + (z + x_{2,\text{des}}) \\ &= -c_1 x_1 - x_1^3 + z\end{aligned}\tag{3.20a}$$

$$\begin{aligned}\dot{z} &= \dot{x}_2 - \dot{\alpha}(x_1) = \dot{x}_2 + (c_1 - \sin(x_1))\dot{x}_1 \\ &= u + (c_1 - \sin(x_1)) (c_1 x_1 - x_1^3 + z).\end{aligned}\tag{3.20b}$$

Now a CLF for the system (3.17) has to be selected. First try constructing the CLF by augmenting $V(x_1)$ with a quadratic term in the error variable z

$$V_a(x_1, z) = \frac{1}{2}x_1^T x_1 + \frac{1}{2}z^T z.\tag{3.21}$$

The derivative of this CLF candidate along the solutions of the system (3.20) is

$$\begin{aligned}\dot{V}_a(x_1, z, u) &= x_1^T \left[-c_1 x_1 - x_1^3 + z \right] \\ &\quad + z^T \left[u + (c_1 - \sin(x_1)) (c_1 x_1 - x_1^3 + z) \right] \\ &= -c_1 x_1^2 - x_1^4 \\ &\quad + z^T \left[x_1 + u + (c_1 - \sin(x_1)) (-c_1 x_1 - x_1^3 + z) \right].\end{aligned}\tag{3.22}$$

Now, the control u can be chosen to make \dot{V}_a negative definite both in x_1 and z such that the CLF requirement (3.10) holds. For this reason, the cross term $x_1 z$ is grouped together with the control input. The simplest way to make \dot{V}_a negative definite is to set the bracketed part of (3.22) equal to $-c_2 z$, where $c_2 > 0$

$$u = -c_2 z - x_1 - (c_1 - \sin(x_1)) (-c_1 x_1 - x_1^3 + z)\tag{3.23}$$

This is just one way of achieving negative definiteness of the augmented CLF derivative, many more options are available. The design procedure used in this example is formalized by the integrator backstepping procedure.

Integrator backstepping as a design tool is based on the following assumption.

Assumption 3.7. Consider a system

$$\dot{x} = f(x) + g(x)u, \quad f(0) = 0,\tag{3.24}$$

where $x \in \mathbb{R}^n$ is the state, and $u \in \mathbb{R}$ is the control input. There exist a continuously differentiable feedback control law

$$u = \alpha(x), \alpha(0) = 0, \quad (3.25)$$

and a smooth, positive definite, radially unbounded function $V : \mathbb{R}^n \rightarrow \mathbb{R}_+$ such that

$$\frac{\partial V}{\partial x}(x) [f(x) + g(x)\alpha(x)] \leq -W(x) \leq 0, \forall x \in \mathbb{R}^n, \quad (3.26)$$

where $W : \mathbb{R}^n \rightarrow \mathbb{R}$ is positive semidefinite.

Under this assumption, the control (3.25) applied to the system (3.24) guarantees global boundedness of $x(t)$, and, via the LaSalle-Yoshizawa theorem, the regulation of $W(x(t))$ to zero.

Lemma 3.8 (Integrator Backstepping [88]). *Let the system (3.24) be augmented with an integrator*

$$\dot{x}_1 = f(x_1) + g(x_1)x_2 \quad (3.27a)$$

$$\dot{x}_2 = u, \quad (3.27b)$$

and suppose that (3.27a) satisfies assumption 3.7 with $x_2 \in \mathbb{R}$ as its control.

- If $W(x_1)$ is positive definite then

$$V_a(x_1, x_2) = V(x_1) + \frac{1}{2} [x_2 - \alpha(x_1)]^2 \quad (3.28)$$

is a CLF for the full system (3.27), that is, there exists a feedback control $u = \alpha_a(x_1, x_2)$ which renders $x_1 = 0, x_2 = 0$ the GAS equilibrium of (3.27). One such a control law is

$$u = -c(x_2 - \alpha(x_1)) + \frac{\partial \alpha}{\partial x_1}(x_1) [f(x_1) + g(x_1)x_2] - \frac{\partial V}{\partial x_1}(x_1)g(x_1) \quad (3.29)$$

with $c > 0$.

- If $W(x_1)$ is only semidefinite, then there exists a feedback control which renders $\dot{V}_a \leq -W_a(x_1, x_2) \leq 0$, such that $W_a(x_1, x_2) > 0$ whenever $W(x_1) > 0$ or $x_2 \neq \alpha(x_1)$. This guarantees global boundedness and convergence of the state to the largest invariant set M_a contained in the set

$$E_a = \left\{ \begin{bmatrix} x_1 \\ x_2 \end{bmatrix} \in \mathbb{R}^{n+1} \mid W(x_1) = 0, x_2 = \alpha(x_1) \right\}.$$

Proof. The proof is given in chapter 2 of Krstić, Kanellakopoulos, and Kokotović [88] □

3.3.2 Recursive Backstepping Design

The backstepping procedure has been demonstrated on a second order system with a simple integrator. The same procedure can be applied recursively to higher order systems. The only difference is that there are more “virtual states” to step through. The method starts with the state separated from the actual control input by the largest number of integrators, and each step of the backstepping technique can be divided into three parts.

1. Introduce a virtual control and error state variable. Rewrite the current state equation in terms of these variables,
2. Choose a CLF for the system, treating it as if it were the final stage,
3. Choose a stabilizing feedback term for the (virtual) control that makes the CLF stabilizable.

Nonlinear *strict-feedback* systems are of the form

$$\begin{aligned}
 \dot{x}_1 &= f_1(x_1) + g_1(x_1)x_2 \\
 \dot{x}_2 &= f_2(x_1, x_2) + g_2(x_1, x_2)x_3 \\
 &\vdots \\
 \dot{x}_i &= f_i(x_1, x_2, \dots, x_i) + g_i(x_1, x_2, \dots, x_i)x_{i+1} \\
 &\vdots \\
 \dot{x}_n &= f_n(x_1, x_2, \dots, x_n) + g_n(x_1, x_2, \dots, x_n)u
 \end{aligned} \tag{3.30}$$

where $x_j \in \mathbb{R}, u \in \mathbb{R}$ and $g_j \neq 0 \forall x$. The control objective is to let $y = x_1$ asymptotically track a reference signal $y_{\text{ref}}(t)$ whose first n derivatives are assumed known and bounded. The backstepping starts by defining the tracking errors

$$z_i = x_i - \alpha_{i-1} \tag{3.31}$$

where $\alpha_0 = y_{\text{ref}}$. and rewrite the dynamics of the error system as

$$\dot{z}_i = f_i(x_1, \dots, x_i) + g_i(x_1, \dots, x_i)x_{i+1} - \dot{\alpha}_{i-1} \tag{3.32}$$

where $x_{n+1} = u$. Then, for each subsystem a CLF function $V_i(z_1, \dots, z_i)$ is constructed as

$$V_i(z_1, \dots, z_i) = V_{i-1}(z_1, \dots, z_{i-1}) + \frac{1}{2}z_i^T z_i, \tag{3.33}$$

where α_i is a stabilizing feedback law that satisfies (3.26) for the x_{i-1} -subsystem. Such intermediate control laws are called *stabilizing functions* or *virtual control laws*. Now, the derivative of V_i with respect to time has to be made non-positive when $x_{i+1} = \alpha_i$. A possible feedback control that achieves this is

$$\alpha_i(x_1, \dots, x_i) = g_i^{-1} \left(-c_i z_i - f_i + \dot{\alpha}_{i-1} - g_{i-1}^T z_{i-1} \right) \tag{3.34}$$

with gains $c_i > 0$.

Theorem 3.9 (Recursive Backstepping Design for Tracking). *If V_n is radially unbounded and $g_i \neq 0$ holds globally, then the closed-loop system consisting of the tracking error dynamics (3.32) and the feedback control laws (3.34) has a globally asymptotic equilibrium at $(z_1, \dots, z_n) = 0$, and $z_i \rightarrow 0$ as $t \rightarrow \infty$. Since the tracking errors go to zero, this means that global asymptotic tracking is achieved:*

$$\lim_{t \rightarrow \infty} z_1 = \lim_{t \rightarrow \infty} (x_1 - y_{ref}) = 0. \quad (3.35)$$

Proof. The time derivative of V_n along the solutions of (3.32) is

$$\dot{V}_n = - \sum_{i=1}^n z_i^T c_i z_i$$

which shows that the equilibrium $(z_1, \dots, z_n) = 0$ is globally, uniformly stable. Additionally, by theorem 3.3 it can be shown that indeed $z_i \rightarrow 0$ as $t \rightarrow \infty$. \square

3.3.3 Time-scale Separation NDI versus Backstepping

A control law derived through time-scale separation (TSS) NDI can be viewed as “poor man’s” version of backstepping [184], since the TSS-NDI control law can be obtained from the backstepping design by dropping terms in each step. In the first step of the design, the control law is defined identical to the backstepping design. In the second and subsequent steps, the time derivatives of the preceding virtual control laws are neglected. The missing time derivative terms are important for stability and performance of the closed-loop. When there is sufficient time separation between the different loops, the subsystems of the system, the time derivative terms are small compared to the the other terms in the virtual control laws, and stability of the closed-loop system can be shown.

3.3.4 Missile Example

In this section the backstepping design will be applied to a simplified model of a surface-to-air missile. A second order nonlinear pitch-dynamics model was obtained from [74, 84]. The approximations are valid for the flight envelope $-10^\circ \leq \alpha \leq 10^\circ$ and $1.8 \leq M \leq 2.6$. The nonlinear equations of motion in the pitch plane are given by

$$\begin{aligned} \dot{\alpha} &= q + \frac{\bar{q}S}{mV_T} [C_z(\alpha, M) + b_z(M)\delta] \\ \dot{q} &= \frac{\bar{q}Sd}{I_{yy}} [C_m(\alpha, M) + b_m(M)\delta] \end{aligned} \quad (3.36)$$

where d is a reference length. The aerodynamic coefficients of the model are approximated by

$$\begin{aligned} C_z(\alpha, M) &= \varphi_{11}^T(\alpha, M)\theta \\ C_m(\alpha, M) &= \varphi_{21}^T(\alpha, M)\theta \\ b_z(M) &= \varphi_{12}^T(M)\theta \\ b_m(M) &= \varphi_{22}^T(M)\theta \end{aligned}$$

where

$$\begin{aligned} \varphi_{11}^T(\alpha, M) &= \left[\alpha^3 \quad \alpha|\alpha| \quad \alpha \quad \alpha|\alpha|M \quad \alpha M \quad 0^{1 \times 9} \right], \\ \varphi_{21}^T(\alpha, M) &= \left[0^{1 \times 7} \quad \alpha^3 \quad \alpha|\alpha| \quad \alpha \quad \alpha|\alpha|M \quad \alpha M \quad 0^{1 \times 2} \right], \\ \varphi_{12}^T(\alpha, M) &= \left[0^{1 \times 5} \quad M \quad 1 \quad 0^{1 \times 7} \right], \\ \varphi_{22}^T(\alpha, M) &= \left[0^{1 \times 12} \quad M \quad 1 \right], \end{aligned}$$

and $\theta \in \mathbb{R}^{14}$ is a vector of constant parameters.

Before the backstepping procedure can be started, it has to be noted that the missile model is not in lower triangular form. Therefore, the assumption is made that the control surface δ is a pure moment generator. This assumption is often made in flight control design, e.g. in Etkin and Reid [52], and Härkegård [68].

First the dynamics are rewritten in a more convenient form

$$\begin{aligned} \dot{x}_1 &= x_2 + f_1(x_1, M) + g_1(M)u \\ \dot{x}_2 &= f_2(x_1, M) + g_2(M)u \end{aligned} \tag{3.37}$$

with

$$\begin{aligned} x_1 &= \alpha, & x_2 &= q, \\ f_1(x_1, M) &= C_1 \varphi_{11}^T(x_1, M)\theta, & f_2(x_1, M) &= C_2 \varphi_{21}^T(x_1, M)\theta, \\ g_1(M) &= C_1 \varphi_{12}^T(M)\theta, & g_2(M) &= C_2 \varphi_{22}^T(M)\theta, \\ C_1 &= \frac{\bar{q}S}{mV_T}, & C_2 &= \frac{\bar{q}Sd}{I_{yy}}. \end{aligned}$$

Define the tracking errors

$$\begin{aligned} z_1 &= x_1 - y_{\text{ref}} \\ z_2 &= x_2 - \alpha_1 \end{aligned}$$

where y_{ref} is the reference signal, and α_1 is the virtual control to be designed in the first design step. *Step 1:* the z_1 dynamics satisfy

$$\dot{z}_1 = x_2 + f_1 - \dot{y}_{\text{ref}} = z_2 + \alpha_1 + f_1 - \dot{y}_{\text{ref}}. \tag{3.38}$$

Consider the CLF candidate V_1 for the z_1 -subsystem

$$V_1(z_1) = \frac{1}{2} z_1^T z_1.$$

The derivative of V_1 along the solution of (3.38) is given by

$$\dot{V}_1 = z_1^T \dot{z}_1 = z_1^T [z_2 + \alpha_1 + f_1 - \dot{y}_{\text{ref}} + g_1 u].$$

The virtual control law α_1 is selected as

$$\alpha_1 = -c_1 z_1 - f_1 + \dot{y}_{\text{ref}}, \quad c_1 = c_1^T > 0 \quad (3.39)$$

which renders the derivative \dot{V}_1 negative definite if $z_2 = 0$ and $g_1 u$ is ignored. The remaining cross-term will be dealt with in the second design step.

Step 2: the z_2 -dynamics are defined by

$$\dot{z}_2 = f_2 + g_2 u - \dot{\alpha}_1 \quad (3.40)$$

where

$$\begin{aligned} \dot{\alpha}_1 &= \frac{\partial \alpha_1}{\partial z_1} \dot{z}_1 + \frac{\partial \alpha_1}{\partial \dot{y}_{\text{ref}}} \ddot{y}_{\text{ref}} \\ &= -c_1 (x_2 + f_1 - \dot{y}_{\text{ref}}) - \frac{\partial f_1}{\partial x_1} (x_2 + f_1) + \dot{y}_{\text{ref}}. \end{aligned}$$

The CLF V_1 is augmented with an additional term to penalize the tracking error z_2 as

$$V_2(z_1, z_2) = V_1(z_1) + \frac{1}{2} z_2^T z_2.$$

The derivative of V_2 along the solutions of (3.38) and (3.40) satisfies

$$\begin{aligned} \dot{V}_2 &= -z_1^T c_1 z_1 + z_1^T g_1 u + z_1^T z_2 + z_2^T [f_2 + g_2 u - \dot{\alpha}_1] \\ &= -z_1^T c_1 z_1 + z_1^T g_1 u + z_2^T [z_1 + f_2 + g_2 u - \dot{\alpha}_1]. \end{aligned}$$

A control law for u can now be defined to cancel all the indefinite terms

$$u = g_2^{-1} [-c_2 z_2 - z_1 - f_2 + \dot{\alpha}_1], \quad c_2 = c_2^T > 0. \quad (3.41)$$

If $g_1 u = 0$, by theorem 3.3 the tracking errors $z_1, z_2 \rightarrow \infty$ as $t \rightarrow \infty$, meaning that the reference signal y_{ref} is asymptotically tracked. If $g_1 u \neq 0$ the derivative \dot{V}_2 becomes

$$\dot{V}_2 = -z_1^T c_1 z_1 - z_2^T c_2 z_2 + z_1^T g_1 u.$$

If $g_1 u$ is bounded then \dot{V}_2 is negative outside a compact ball around the origin of the tracking error system. The size of this ball can be reduced by increasing the gains c_1, c_2 . In this example, the presence of g_1 results in a closed-loop system with a steady state offset. An approach common in linear control design to reduce the size of this ball, or reduce the steady state offset, is by introducing integral action in the control law. Introduce a state variable that integrates the z_1 error

$$\lambda_1 = \int_0^t z_1 dt$$

and augment the first intermediate control

$$\alpha_1 = -c_1 z_1 - k_1 \lambda_1 - f_1 + \dot{y}_{\text{ref}} \quad (3.42)$$

where $k_1 = k_1^T > 0$ is the integral action gain matrix. The resulting closed loop (λ, z_1) -subsystem dynamics become

$$\begin{aligned} \dot{\lambda}_1 &= z_1 \\ \dot{z}_1 &= -c_1 z_1 - k_1 \lambda_1 + g_1 u \end{aligned}$$

which show an equilibrium at $(k_1 \lambda_1 = g_1 u, z_1 = 0)$. Define an augmented CLF candidate

$$V_{1,\text{int}}(z_1, \lambda_1) = \frac{1}{2} z_1^T z_1 + \frac{1}{2} \left(\lambda_1 - k_1^{-1} g_1 u \right)^T k_1 \left(\lambda_1 - k_1^{-1} g_1 u \right)$$

Assuming that $g_1 u$ is constant, the time derivative of this augmented CLF candidate along the solution (3.38) becomes

$$\begin{aligned} \dot{V}_{1,\text{int}} &= -z_1^T c_1 z_1 + z_1^T g_1 u - z_1^T k_1 \lambda_1 + \left(\lambda_1 - k_1^{-1} g_1 u \right)^T k_1 z_1 \\ &= -z_1^T c_1 z_1 \end{aligned}$$

which is only negative *semi*-definite. By means of Barbalat's lemma it can be shown that the equilibrium of the closed-loop system for the controller with integrator is asymptotically stable.

Numerical simulations for both the designed controllers have been performed using MATLAB/Simulink[®]. Figure 3.3 shows these simulation results for different settings of the gains. The simulations labeled *simple* have no integral actions, and relatively low gains $c_1 = 1$, $c_2 = 2$. These simulation clearly show the effect of neglecting the $g_1 u$ term in the control design. The *high gain* simulations have (very) high settings for the proportional control part, $c_1 = 10$, $c_2 = 20$. Finally, the lines labeled *PI* shows the results of the controller with normal proportional gain settings, and integral control, $c_1 = 1$, $c_2 = 2$, $k_1 = 5$. The last two controllers clearly reduce or counteract the effect of the neglected dynamics. However, the first approach does this using "brute-force", while the second approach can be interpreted as a simple form of adaptive control. This missile example system will be used throughout the remaining part of the dissertation to illustrate the modifications and extensions of the backstepping method.

3.4 Backstepping with Uncertainty

The full power of backstepping only emerges when systems with uncertain nonlinearities or unknown parameters are considered. First, the concept of nonlinear damping will be introduced which is used as a tool to counteract uncertainty. Then robust backstepping for systems with uncertainties is discussed.

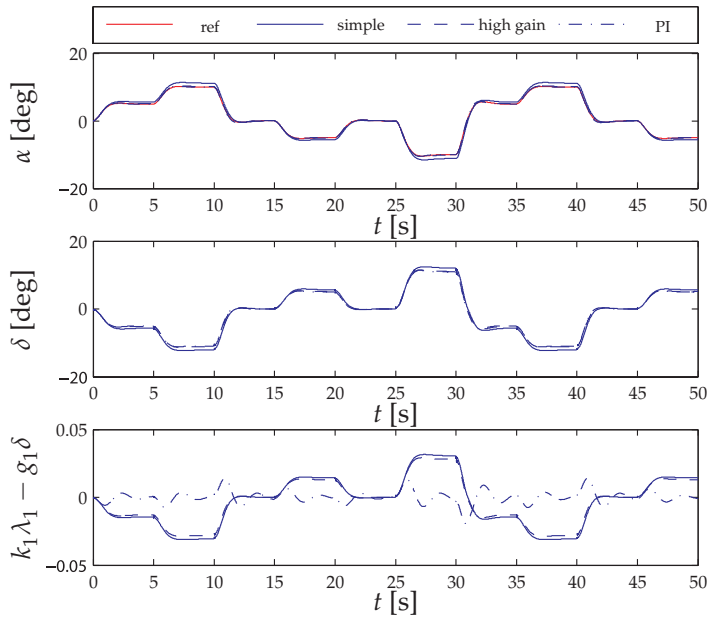


Figure 3.3: Angle of attack response (top), control surface deflection (middle), and bias dynamics (bottom) for the missile example for three backstepping controllers with different gains.

3.4.1 Nonlinear Damping

The concept of nonlinear damping is introduced using a very simple, scalar example. Consider a system

$$\dot{x} = u + \varphi(x)\Delta(t) \quad (3.43)$$

where $\varphi(x)$ is a smooth, known, nonlinearity and $\Delta(t)$ is a bounded, unknown function of t . Ignoring this uncertainty in the control design can have disastrous consequences. A linear controller is designed as $u = -cx$ which results in the closed loop system

$$\dot{x} = -cx + \varphi(x)\Delta(t)$$

Suppose that the uncertainty is an exponentially decaying function in time $\Delta(t) = \Delta(0)e^{-kt}$, and that $\varphi(x)$ is a smooth nonlinear function with faster than linear growth, for example $\varphi(x) = x^2$. Then, it is easily shown that the system will escape in finite time for certain combinations of initial conditions $x(0)$ and $\Delta(0)$ independently of the chosen gain c and the decay rate k .

By adding a *nonlinear damping* term to the control law this problem can be overcome, and boundedness of $x(t)$ for all bounded $\Delta(t)$ can be guaranteed

$$u = -cx - s(x)x \quad (3.44)$$

where the damping function $s(x)$ is left to be designed. Assume a quadratic function $V(x) = \frac{1}{2}x^2$ whose derivative is

$$\begin{aligned} \dot{V} &= xu + x\varphi(x)\Delta(t) \\ &= -cx^2 - x^2s(x) + x\varphi(x)\Delta(t) \end{aligned} \quad (3.45)$$

The objective of guaranteeing boundedness of the solutions can be expressed as rendering \dot{V} negative outside a compact region. This can for example be achieved with the choice

$$s(x) = \kappa\varphi^2(x), \quad \kappa > 0, \quad (3.46)$$

yielding the control law

$$u = -cx - \kappa x\varphi^2(x) \quad (3.47)$$

and the derivative

$$\begin{aligned} \dot{V} &= -cx^2 - \kappa x^2\varphi^2(x) + x\varphi(x)\Delta(t) \\ &= -cx^2 - \kappa \left[x\varphi(x) - \frac{\Delta(t)}{2\kappa} \right]^2 + \frac{\Delta^2(t)}{4\kappa} \\ &\leq -cx^2 + \frac{\Delta^2(t)}{4\kappa}. \end{aligned} \quad (3.48)$$

From this derivative it is easy to see that \dot{V} is negative whenever $|x(t)| > \frac{|\Delta(t)|}{2\sqrt{\kappa c}}$.

Lemma 3.10 (Nonlinear Damping [88]). *Let the system (3.24) be perturbed as in*

$$\dot{x} = f(x) + g(x) \left[u + \varphi^T(x)\Delta(x, u, t) \right] \quad (3.49)$$

where $\varphi(x)$ is a $(p \times 1)$ vector of known, smooth, nonlinear functions, and $\Delta(x, u, t)$ is a $(p \times 1)$ vector of uncertain nonlinearities which are uniformly bounded for all values of x, u, t . If Assumption 3.7 is satisfied with $W(x)$ positive definite and radially unbounded, then the control

$$u = \alpha(x) - \kappa \frac{\partial V(x)}{\partial x} g(x) |\varphi(x)|^2, \quad \kappa > 0, \quad (3.50)$$

when applied to (3.49), renders the closed-loop system ISS with respect to the disturbance input $\Delta(x, u, t)$ and hence guarantees global uniform boundedness of $x(t)$ and convergence to the residual set

$$\mathcal{R} = \left\{ x : |x| \leq \gamma_1^{-1} \circ \gamma_2 \circ \gamma_3^{-1} \left(\frac{\|\Delta\|_\infty^2}{4\kappa} \right) \right\}, \quad (3.51)$$

where $\gamma_1, \gamma_2, \gamma_3$ are class \mathcal{K}_∞ functions such that

$$\gamma_1(|x|) \leq V(x) \leq \gamma_2(|x|) \quad (3.52)$$

$$\gamma_3(|x|) \leq W(x). \quad (3.53)$$

Proof. See Krstić, Kanellakopoulos, and Kokotović [88, Ch. 2] \square

3.4.2 Robust Backstepping

The concept of nonlinear damping can be used recursively in the backstepping design, yielding the robust backstepping procedure. First of all the formal extension of backstepping for systems with uncertainty is given. Then, the procedure is generalized.

Lemma 3.11 (Boundedness via Backstepping). *Suppose that there exists a stabilizing feedback law $u = \alpha_1(x)$ for the system (3.49) that renders $x(t)$ globally uniformly bounded. Now consider the augmented system*

$$\begin{aligned} \dot{x}_1 &= f_1(x_1) + g_1(x_1)x_2 + \varphi_1^T(x_1)\Delta_1(x_1, u, t) \\ \dot{x}_2 &= u + \varphi_2^T(x_1, x_2)\Delta_2(x_1, x_2, u, t), \end{aligned} \quad (3.54)$$

where $\varphi_1(x_1)$ and $\varphi_2(x_1, x_2)$ are vectors of known, smooth nonlinear functions, $\Delta_1(x_1, u, t)$ and $\Delta_2(x_1, x_2, u, t)$ are vectors of uncertain nonlinearities which are uniformly bounded for all values x_1, x_2, u, t . For this system, the feedback control

$$\begin{aligned} u &= -c_2(x_2 - \alpha_1) + \frac{\partial \alpha_1}{\partial x_1}(f_1 + g_1 x_2) - g_1^T \frac{\partial V}{\partial x_1} \\ &\quad - \left(\varphi_2^T \kappa_2 \varphi_2 + \left(\frac{\partial \alpha_1}{\partial x_1} \varphi_1 \right)^T \mu_2 \frac{\partial \alpha_1}{\partial x_1} \varphi_1 \right) (x_2 - \alpha_1) \end{aligned} \quad (3.55)$$

guarantees global uniform boundedness of $x_1(t)$ and $x_2(t)$ with any $c_2 > 0$, and $\kappa_2 > 0$, $\mu_2 > 0$.

Now consider the class of robust-strict-feedback systems

$$\begin{aligned} \dot{x}_1 &= f_1(x_1) + g_1(x_1)x_2 + \varphi_1^T(x_1)\Delta_1(x, u, t) \\ &\vdots \\ \dot{x}_n &= f_n(x_1, \dots, x_n) + g_n(x_1, \dots, x_n)u + \varphi_n^T(x_1, \dots, x_n)\Delta(x, u, t) \end{aligned} \quad (3.56)$$

where $g_i \neq 0$, $\forall x \in \mathbb{R}^n$, and $\varphi(x_1, \dots, x_i)$ is a $(p \times 1)$ vector of known smooth nonlinear functions, and $\Delta(x, u, t)$ is a $(p \times 1)$ vector of uncertain nonlinearities

which are uniformly bounded for all values x, u, t . Then state $x(t)$ of the system (3.56) is globally, uniformly bounded if the control is chosen as

$$\begin{aligned}
 z_i &= x_1 - \alpha_{i-1} \\
 \alpha_i &= g_i^{-1} \left(-c_i z_i - f_i + \sum_{k=1}^{i-1} \frac{\partial \alpha_{i-1}}{\partial x_k} (f_k + g_k x_{k+1}) - g_{i-1}^T z_{i-1} \right. \\
 &\quad + \sum_{k=1}^{i-1} \frac{\partial \alpha_{i-1}}{\partial y_{\text{ref}}^{(k-1)}} y_{\text{ref}}^{(k)} - \varphi_i^T \kappa_i \varphi_i z_i \\
 &\quad \left. - \left(\sum_{j=1}^{i-1} \frac{\partial \alpha_{i-1}}{\partial x_j} \varphi_j \right)^T \mu_i \left(\sum_{j=1}^{i-1} \frac{\partial \alpha_{i-1}}{\partial x_j} \varphi_j \right) \right)
 \end{aligned} \tag{3.57}$$

with $\alpha_0 = y_{\text{ref}}$, $u = \alpha_n$, $x_{n+1} = u$ and c_i, κ_i, μ_i positive definite design matrices. Using the derivative of the Lyapunov function it can be shown that $z(t)$ is globally uniformly bounded, and that the tracking errors z converge to the compact set

$$\sum_{i=1}^n z_i^T c_i z_i \leq \frac{1}{4} \sum_{i=1}^n \Delta^T \kappa_i^{-1} \Delta + \frac{1}{4} \sum_{i=1}^n \Delta^T \mu_i^{-1} \Delta \tag{3.58}$$

3.4.3 Robust Backstepping Example

In this section the missile example is revisited to illustrate robust backstepping. In this case, the term $g_1 \delta$ is taken into account in the control design, by designing a control law which counteracts the disturbance by means of nonlinear damping. To cast the missile model into the form handled by the robust backstepping procedure, the assumption is made that δ can be bounded. This is a realistic assumption since the real control surface is mechanically constrained to certain deflection limits.

The missile dynamics are rewritten as

$$\begin{aligned}
 \dot{x}_1 &= x_2 + f_1(x_1) + w^T(x_1) \Delta_1(u) \\
 \dot{x}_2 &= f_2(x_1) + g_2(x_1) u
 \end{aligned} \tag{3.59}$$

where $w(x_1) = g_1$ and $\Delta_1(u) = u$. Using the robust backstepping design procedure (3.57) the following (intermediate) control laws are designed

$$\begin{aligned}
 \alpha_1 &= -c_1 z_1 - f_1 + \dot{y}_{\text{ref}} - w_1^T \kappa_1 w_1 z_1 \\
 u &= g_2^{-1} \left(-c_2 z_2 - f_2 + \frac{\partial \alpha_1}{\partial x_1} (x_2 + f_1) + \frac{\partial \alpha_1}{\partial \dot{y}_{\text{ref}}} \dot{y}_{\text{ref}} \right. \\
 &\quad \left. - \left(\frac{\partial \alpha_1}{\partial x_1} w_1 \right)^T \mu_2 \left(\frac{\partial \alpha_1}{\partial x_1} w_1 \right) z_2 \right)
 \end{aligned} \tag{3.60}$$

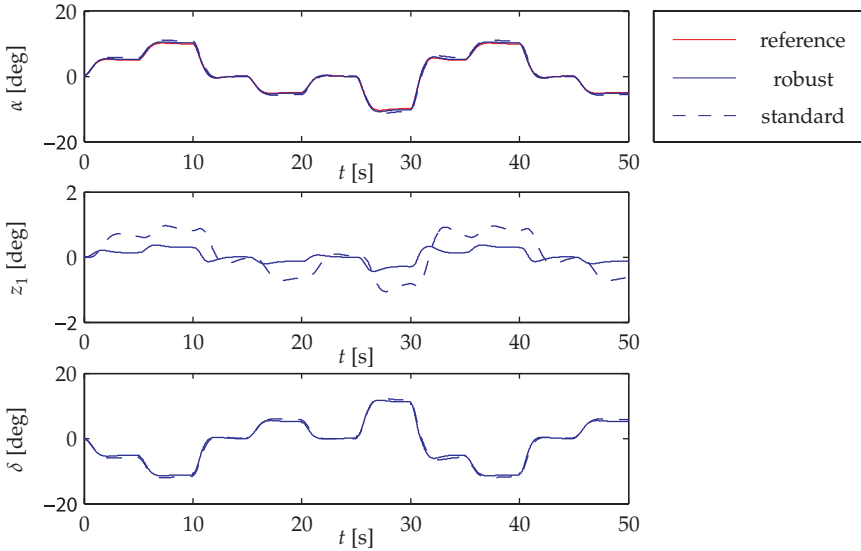


Figure 3.4: Response (top), tracking error (middle) and commanded control input (bottom) for the robust and standard backstepping designs applied to the missile example.

where $c_1, c_2, \kappa_1, \mu_2 > 0$ are design constants. Suppose that the control surface deflection δ is limited to 15° to either side, hence $|\Delta(t)| \leq 15^\circ$. The performance requirements are that the angle of attack response is kept within 1° of the reference command. Using (3.58) and the gains for the normal backstepping controller c_1 and c_2 the required nonlinear damping gains can be calculated by solving

$$z^T c_0 z^T \leq \frac{1}{4} \Delta^T \kappa_0 \Delta$$

for $\kappa_0^{-1} = \kappa_1^{-1} + \mu_2^{-1}$, $c_0 = \min(c_1, c_2) = 1$ and the given bound on the tracking error and disturbance. This results in the choice $\kappa_1 = \mu_2 = 450$. In figure 3.4 the response for the robust design with these nonlinear damping gains is compared to the standard backstepping controller as designed earlier in section 3.3.4. From the figure it can be observed that the robust control design indeed keeps the tracking error well within the prescribed limits.

3.5 Command Filtering

The backstepping method requires the derivatives of the intermediate stabilizing functions α . These derivatives can be derived analytically easily for simple systems.

When the order of the system increases, or the complexity of the system itself, analytic derivation becomes a tedious process. This becomes even more so for adaptive control systems. Command filters, often referred to as dynamic surface control [206, 207], can be introduced in the backstepping method to reduce the complexity. An additional advantage of these command filters is that the backstepping procedure can be applied to systems that are not in triangular form, such as for example aircraft dynamics. Finally, the command filters can be used to incorporate magnitude and rate constraints on the control input and intermediate states [55, 57, 58, 140], and remove the effect of these constraints from the tracking errors. In this section the command filtered backstepping approach is presented and the missile example is revisited.

3.5.1 Command Filtering Backstepping

Consider a non-triangular, feedback passive system

$$\begin{aligned}\dot{x}_1 &= f_1(x) + g_1(x)x_2 \\ \dot{x}_2 &= f_2(x) + g_2(x)u,\end{aligned}\tag{3.61}$$

where $x = (x_1, x_2) \in \mathbb{R}^2$. The control objective is to track a reference signal y_{ref} with derivative \dot{y}_{ref} . The functions $g_i \neq 0 \forall x$. First define the tracking errors

$$\begin{aligned}z_1 &= x_1 - y_{\text{ref}} \\ z_2 &= x_2 - x_{2,c}\end{aligned}\tag{3.62}$$

where $x_{2,c}$ will be defined through the backstepping design. Let

$$\alpha_1(z_1, \dot{y}_{\text{ref}}) = g_1^{-1} [-f_1 - c_1 z_1 + \dot{y}_{\text{ref}}]\tag{3.63}$$

with $c_1 > 0$ be a smooth feedback control, and define a positive definite function $V_1(z_1) = \frac{1}{2}z_1^T z_1$ such that

$$\frac{\partial V_1}{\partial z_1} [f_1 + g_1 \alpha_1 - \dot{y}_{\text{ref}}] = -W(z_1)\tag{3.64}$$

where $W(z_1) = z^T c_1 z_1$ is positive definite in z_1 . The tracking problem is now solved by first defining

$$\begin{aligned}x_{2,c}^0 &= \alpha_1(z_1, \dot{y}_{\text{ref}}) - \tilde{\zeta}_2 \\ \dot{\tilde{\zeta}}_1 &= -c_1 \tilde{\zeta}_1 + g_1 (x_{2,c} - x_{2,c}^0)\end{aligned}\tag{3.65}$$

where $\tilde{\zeta}_2$ will be defined later in the design. The signal $x_{2,c}^0$ is filtered to produce the command signal $x_{2,c}$ and its derivative $\dot{x}_{2,c}$. By design of the filter, the signal $(x_{2,c} - x_{2,c}^0)$ is bounded and small. Therefore, as long as g_1 is bounded, then $\tilde{\zeta}_1$

is bounded since it is the output of a stable linear filter. Define the compensated tracking errors

$$\bar{z}_i = z_i - \tilde{\zeta}_i. \quad (3.66)$$

and define

$$\begin{aligned} u_c^0 &= g_2^{-1} \left(-c_2 z_2 + \dot{x}_{2,c} - f_2 - g_1^T \bar{z}_1 \right) \\ \dot{\tilde{\zeta}}_2 &= -c_2 \tilde{\zeta}_2 + g_2 \left(u_c - u_c^0 \right) \end{aligned} \quad (3.67)$$

with $c_2 > 0$, u_c^0 is filtered to produce u_c and \dot{u}_c . The actual control signal applied to the system is $u = u_c$. Again, by design the signal $(u_c^0 - u_c)$ is small and bounded; therefore, if g_2 is bounded, then $\tilde{\zeta}_2$ is bounded because it is the output of a stable linear filter. The variables \bar{z}_i represent compensated tracking errors, obtained after removing the corresponding unachieved portion of $x_{2,c}^0$ and u_c^0

The tracking error system dynamics can be written as

$$\begin{aligned} \dot{z}_1 &= f_1 + g_1 x_{2,c}^0 - \dot{y}_{\text{ref}} + g_1 (x_{2,c} - x_{2,c}^0) + (g_1 x_2 - g_1 x_{2,c}) \\ &= f_1 + g_1 \alpha_1 - \dot{y}_{\text{ref}} - g_1 \tilde{\zeta}_2 + g_1 (x_{2,c} - x_{2,c}^0) + (g_1 x_2 - g_1 x_{2,c}) \\ &= -c_1 z_1 - g_1 \tilde{\zeta}_2 + g_1 (x_{2,c} - x_{2,c}^0) + g_1 (x_2 - x_{2,c}) \\ &= -c_1 z_1 + g_1 \bar{z}_2 + g_1 (x_{2,c} - x_{2,c}^0) \end{aligned} \quad (3.68)$$

$$\begin{aligned} \dot{z}_2 &= f_2 + g_2 u_c^0 - \dot{x}_{2,c} + g_2 (u_c - u_c^0) \\ &= -c_2 z_2 - g_1^T \bar{z}_1 + g_2 (u_c - u_c^0) \end{aligned}$$

and the augmented tracking error dynamics are

$$\begin{aligned} \dot{\bar{z}}_1 &= \dot{z}_1 - \dot{\tilde{\zeta}}_1 \\ &= -c_1 \bar{z}_1 + g_1 \bar{z}_2 \\ \dot{\bar{z}}_2 &= -c_2 \bar{z}_2 - g_1^T \bar{z}_1 \end{aligned} \quad (3.69)$$

Consider the Lyapunov function candidate

$$V(\bar{z}_1, \bar{z}_2) = \frac{1}{2} \left(\bar{z}_1^T \bar{z}_1 + \bar{z}_2^T \bar{z}_2 \right). \quad (3.70)$$

The time derivative of this CLF along the solution of (3.69) becomes

$$\begin{aligned} \dot{V} &= \bar{z}_1^T \left(-c_1 \bar{z}_1 + g_1 \bar{z}_2 \right) + \bar{z}_2^T \left(-c_2 \bar{z}_2 - g_1^T \bar{z}_1 \right) \\ &= -\bar{z}_1^T c_1 \bar{z}_1 - \bar{z}_2^T c_2 \bar{z}_2 \end{aligned} \quad (3.71)$$

which shows that the origin of the compensated tracking error system (\bar{z}_1, \bar{z}_2) is exponentially stable. Intuitively it follows that if χ_1, χ_2 are small, then the origin of the tracking error system (z_1, z_2) is attractive.

3.5.2 Missile Example

The introduction of the non-adaptive backstepping method is concluded with another visit of the missile example. Instead of using the analytic derivative of the first control law with respect to time, now the filtered versions will be used. Additionally, the use of the filters allows addressing the $g_1\delta$ term appearing in the α subsystem directly.

The control design is very similar to the standard backstepping design with integrator action. The tracking errors are defined as

$$\begin{aligned} z_1 &= x_1 - y_{\text{ref}} \\ z_2 &= x_2 - x_{2,c} \end{aligned}$$

where $x_{2,c}$ is the output of a command filter. The virtual control laws are defined as

$$\begin{aligned} \alpha_1 &= -c_1 z_1 - k_1 \lambda_1 - f_1 - g_1 u_c + \dot{y}_{\text{ref}} \\ \alpha_2 &= g_2^{-1} (-c_2 z_2 - \bar{z}_1 - f_2 + \dot{x}_{2,c}) \end{aligned} \quad (3.72)$$

where the compensated tracking errors are defined as

$$\bar{z}_i = z_i - \bar{\zeta}_i.$$

The signals

$$x_{2,c}^0 = \alpha_1 - \bar{\zeta}_2 \quad (3.73)$$

$$u_c^0 = \alpha_2 \quad (3.74)$$

are filtered by the command filters to produce $x_{2,c}$, $\dot{x}_{2,c}$ and u_c . The effect of these command filters is measured by

$$\dot{\bar{\zeta}}_1 = -c_1 \bar{\zeta}_1 + (x_{2,c} - x_{2,c}^0) \quad (3.75)$$

$$\dot{\bar{\zeta}}_2 = -c_2 \bar{\zeta}_2 + g_2 (u - u^0). \quad (3.76)$$

In this example second order filters were applied. Using the filters, the command surface deflection is limited to $[-15, 10]$ degrees to show the effect of constraining the input on the filters and the closed-loop response. The bandwidth and damping of the filters were chosen as $\omega_{\alpha_1} = 80$ rad/s, $\zeta_{\alpha_1} = 0.7$, $\omega_u = 100$ rad / s, and $\zeta_u = 0.7$. Figure 3.5 shows the response of the closed-loop system with the command filtered backstepping design with $c_1 = 1$, $c_2 = 2$. No integral action has been used in the controller, $k_1 = 0$.

3.6 Non-affine in Control Backstepping

A final modification of the backstepping method is done to be able to handle systems which are non-affine in the control variable. These systems occur very frequently in practice, aircraft are notable examples.

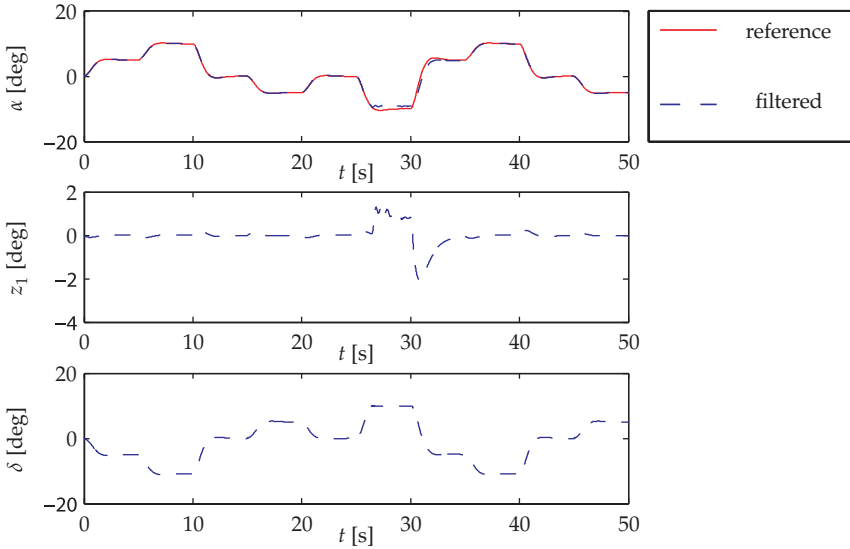


Figure 3.5: Response (top), tracking error (middle) and commanded control input (bottom) for the command filtered backstepping design applied to the missile example.

3.6.1 Singular Perturbation Theory

Instead of the analytical approach taken by Krstić, Kanellakopoulos, and Kokotović [88] to handle non-affine systems, a different route will be taken by using singular perturbation theory. This approach results in slightly worse tracking characteristics, however it is able to design controllers for systems which do not be inverted analytically. Consider a singularly perturbed nonlinear system with the following state space description:

$$\Sigma_0 : \begin{cases} \dot{x} &= f(t, x, u, \varepsilon) & x(0) &= \zeta(\varepsilon) \\ \varepsilon \dot{u} &= g(t, x, u, \varepsilon) & u(0) &= \eta(\varepsilon) \end{cases} \quad (3.77)$$

where ε is a small positive parameter, $\zeta : \varepsilon \rightarrow \zeta(\varepsilon)$ and $\eta : \varepsilon \rightarrow \eta(\varepsilon)$ are smooth. Assume that f and g are continuously differentiable in their arguments for $(t, x, u, \varepsilon) \in [0, \infty) \times D_x \times D_u \times [0, \varepsilon_0]$, where $D_x \subset \mathbb{R}^n$, $D_u \subset \mathbb{R}^m$ are domains, $\varepsilon_0 > 0$. In addition, let Σ_0 be in *standard form*, i.e. $0 = g(t, x, u, 0)$ has $k \geq 1$ isolated real roots $u = h_i(t, x)$, $i \in \{1, \dots, k\}$ for each $(t, x) \in [0, \infty) \times D_x$. Pick one particular i , which is fixed. Let $v(t, x) = u - h(t, x)$. In singular perturbation theory, the system given by

$$\Sigma_{00} : \dot{x}(t) = f(t, x, h(t, x), 0), \quad x(0) = \zeta(0), \quad (3.78)$$

is called the *reduced system*, the system given by

$$\Sigma_b : \frac{dv}{d\tau} = g(t, x, v + h(t, x), 0), \quad v(0) = \eta_0 - h(0, \xi_0) \quad (3.79)$$

is the *boundary layer system*, where $\eta_0 = \eta(0)$ and $\xi_0 = \xi(0)$, $(t, x) \in [0, \infty) \times D_x$ are treated as fixed parameters. The new time scale τ is related to the original time t via the relationship $\tau = \frac{t}{\epsilon}$. Then the following result is due to Tikhonov [83, p. 434].

Theorem 3.12 (Tikhonov's Theorem). *Consider the singular perturbation system Σ_0 given in (3.77) and let $u = h(t, x)$ be an isolated root of $g(t, x, u, 0)$. Assume that the following conditions hold for all $(t, x, u - h(t, x), \epsilon) \in [0, \infty) \times D_x \times D_v \times [0, \epsilon_0]$ for some domains $D_x \in \mathbb{R}^n$ and $D_u \in \mathbb{R}^m$, which contain the corresponding origins.*

1. *On any compact subset of $D_x \times D_v$ the function f, g , their first partial derivatives with respect to (x, u, ϵ) , and the first partial derivative of g with respect to t are continuous and bounded, $h(t, x)$ and $\frac{\partial g}{\partial u}(t, x, u, 0)$ have bounded first derivatives with respect to their arguments, $\frac{\partial f}{\partial x}(t, x, h(x))$ is Lipschitz in x uniformly in t , and the initial conditions for ξ and η are smooth functions of ϵ .*
2. *The origin is an exponentially stable equilibrium point of the reduced system Σ_{00} (3.78). There exists a Lyapunov function $V : [0, \infty) \times D_x \rightarrow [0, \infty)$ that satisfies*

$$\begin{aligned} W_1(x) &\leq V(t, x) \leq W_2(x), \\ \frac{\partial V(t, x)}{\partial t} + \frac{\partial V(t, x)}{\partial x} f(t, x, h(t, x), 0) &\leq -W_3(x) \end{aligned}$$

for all $(t, x) \in [0, \infty) \times D_x$, where W_1, W_2 , and W_3 are continuous positive definite functions on D_x . Let c be a nonnegative number such that $\{x \in D_x | W_1(x) \leq c\}$ is a compact subset of D_x .

3. *The origin is an equilibrium point of the boundary layer system (3.79), which is exponentially stable uniformly in (t, x) .*

Let $R_v \in D_v$ denote the region of attraction of the autonomous system

$$\frac{dv}{d\tau} = g(0, \xi_0, v + h(0, \xi_0), 0)$$

and let Ω_v be a compact subset of R_v . Then for each compact set $\Omega_x \subset \{x \in D_x | W_2(x) \leq \rho c, 0 < \rho < 1\}$, there exists a positive constant ϵ_* such that for all $t \geq 0$, $\xi_0 \in \Omega_x$, $\eta_0 - h(0, \xi_0) \in \Omega_v$ and $0 < \epsilon < \epsilon_*$, Σ_0 has a unique solution x_ϵ on $[0, \infty)$ and

$$x_\epsilon(t) - x_{00}(t) = O(\epsilon)$$

holds uniformly for $t \in [0, \infty)$, where $x_{00}(t)$ denotes the solution of the reduced system (3.78).

3.6.2 Non-affine Backstepping Design

Suppose that a stabilizing feedback control law for the final step has to be designed for the system

$$\begin{aligned}\dot{z}_1 &= z_2 \\ \dot{z}_2 &= z_3 \\ &\dots \\ \dot{x}_n &= f(x_1, \dots, x_n, u)\end{aligned}\tag{3.80}$$

and a desired value $\alpha_n(z_1, \dots, z_n)$ is known for f . Then the following equation has to be solved

$$f(x_1, \dots, x_n, u) = \alpha_n(z_1, \dots, z_n)$$

to obtain the desired properties of the closed-loop system. Since this equation cannot (in general) be solved explicitly for u , an approximation of the dynamic inversion controller is constructed by introducing the following fast dynamics

$$\epsilon \dot{u} = -\operatorname{sgn}\left(\frac{\partial f}{\partial u}\right) q(t, z, u), \quad u(0) = u_0\tag{3.81}$$

where

$$q(t, x, u) = f(t, x, u) - \alpha_n.$$

Then, application of Tikhonov's theorem 3.12 shows exponential stability of the origin of (3.81). Additionally, it shows that for each compact subset $\Omega_z \in D_z$ there exist a positive constant ϵ_* and $T > 0$ such that for all $t > 0$, $z_0 \in \Omega_z$, $u_0 - h(0, z_0) \in \Omega_v$, and $0 < \epsilon < \epsilon_*$, the system (3.80), (3.81) has a unique solution $x_\epsilon(t)$ on $[0, \infty)$ and

$$x_\epsilon(t) = y_{\text{ref}}(t) + O(\epsilon)$$

holds uniformly for $t \in [T, \infty)$.

3.6.3 Example

Consider the system

$$\begin{aligned}\dot{x}_1 &= x_1 + x_2 + \frac{x_2^2}{5} \\ \dot{x}_2 &= x_1 x_2 + u + \frac{u^3}{7},\end{aligned}\tag{3.82}$$

for which the control objective is to let x_1 track a smooth reference signal y_{ref} . First the system needs to be transformed by means of a nonlinear mapping to feedback linearizable form. A straightforward diffeomorphism to apply is

$$\begin{aligned}\eta_1 &= x_1 \\ \eta_2 &= x_1 + x_2 + \frac{x_2^2}{5}\end{aligned}\tag{3.83}$$

which transforms the system into the desired form

$$\begin{aligned}
 \dot{\eta}_1 &= \dot{x}_1 = \eta_2 \\
 \dot{\eta}_2 &= \dot{x}_1 + \dot{x}_2 \left(1 + \frac{3x_2^2}{5} \right) \\
 &= x_1 + x_2 + \frac{x_2^3}{5} + \left(x_1 x_2 + u + \frac{u^3}{7} \right) \left(1 + \frac{3x_2^2}{5} \right) \\
 &= f(x, u).
 \end{aligned} \tag{3.84}$$

The tracking errors are defined as

$$\begin{aligned}
 z_1 &= \eta_1 - y_{\text{ref}} \\
 z_2 &= \eta_2 - \alpha_1
 \end{aligned}$$

and the virtual control law α_1 as

$$\alpha_1 = -c_1 z_1 + \dot{y}_{\text{ref}}.$$

The control law for u has to be found using dynamic inversion. The desired value of $f(x, u)$ is the result of applying the standard backstepping procedure to the (z_1, z_2) subsystem

$$\alpha_2 = -c_2 z_2 - z_1 + \dot{\alpha}_1.$$

In this case it is possible to analytically invert the equation $f(x, u) = \alpha_2$ to obtain u , and the result will be used to show that the approximate controller yields approximately the same tracking performance as claimed by theorem 3.12. The approximate inverse controller is defined by

$$\epsilon \dot{u} = -\text{sgn} \left(\frac{\partial f}{\partial u} \right) (f(x, u) - \alpha_2)$$

where ϵ is the time-scale constant. In figure 3.6 the response, tracking error and control input for the approximate inverse controller and the analytical controller are shown. The designed controllers are able to achieve excellent tracking performance when the time-scale constant is sufficiently small.

3.7 Conclusions

In this chapter the theory for designing backstepping controllers which can achieve global asymptotical stability of the origin of the error system when the dynamics of the system are known or achieve input-to-state stability of systems with bounded uncertainties. Extensions and tools for the design and analysis of robust designs which can handle uncertainty in the system to be controlled to a certain extent

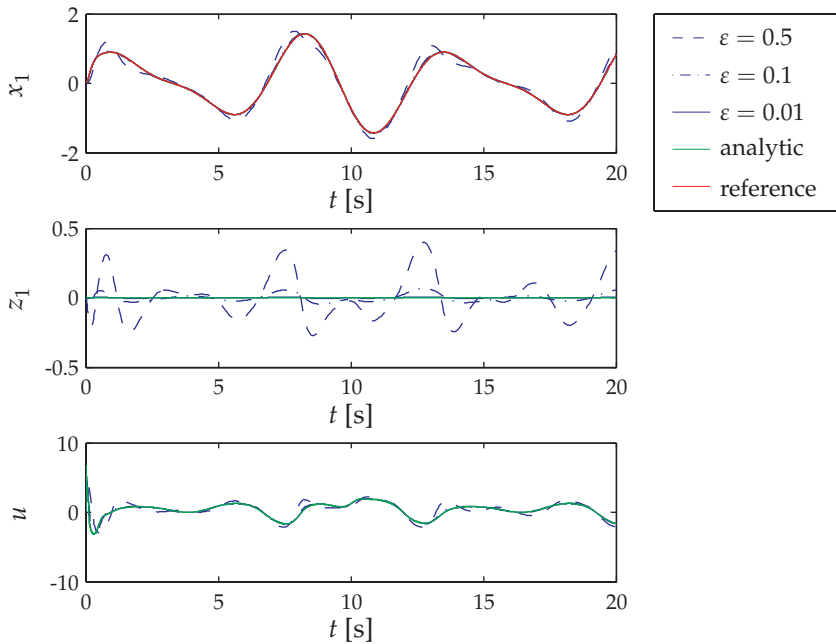


Figure 3.6: Output (top), tracking error (middle), and control input (bottom) for backstepping controllers with different time-scale-gain.

are presented. A method to avoid the tedious computation of virtual control law time derivatives was introduced by using command filters. An additional benefit of these filters is the backstepping method now can handle non-triangular system and can incorporate constraints in the control design. Finally, an extension of backstepping to non-affine in control systems has been presented.

In this chapter only systems with known dynamics or with relatively small uncertainties have been considered. The control designs presented in this chapter achieve good performance for such systems. However, when the uncertainties in the system become larger, the closed-loop performance will degrade and possibly can result in an unstable closed-loop system. In the next chapter control designs are presented which extend the backstepping approach such that systems with unknown constant parameters can be controlled.

ADAPTIVE BACKSTEPPING CONTROL DESIGN

In the preceding chapter control designs were presented which guarantee that in the presence of unknown bounded nonlinearities the closed-loop states remain bounded. In this chapter, and in the remainder of the dissertation, these uncertainties are more specific: they are constant parameters which appear linearly in the system equations. In the presence of such parametric uncertainties, both boundedness of the closed-loop system states and convergence of the tracking error to zero is achieved by means of the adaptive backstepping approach.

4.1 Dynamic Feedback Control

The main difference between static and dynamic (adaptive) feedback designs is illustrated by means of a simple nonlinear system. The scalar system from example 3.1 is revisited.

Example 4.1 (Unknown scalar system)

Consider the system

$$\dot{x} = \theta x^3 + \cos(x) + u \quad (4.1)$$

where $\theta \in \mathbb{R}$ is an unknown, constant parameter. If a bound on θ is known, a control law can be designed which guarantees global boundedness of $x(t)$ using the robust backstepping design. The interval to which $x(t)$ converges can be made arbitrarily small by increasing the gains of this controller. However, this approach increases the system bandwidth which is undesirable. Therefore, a control design

is made which achieves asymptotic convergence of $x(t) \rightarrow 0$ as $t \rightarrow \infty$ without increasing the controller gains. A dynamic feedback controller is designed. Suppose that θ were known, then the control

$$u = -\theta x^3 - \cos(x) - c_1 x \quad (4.2)$$

would render the derivative of $V_0(x) = \frac{1}{2}x^2$ negative definite. Since θ is not known, the *certainty-equivalence* form can be used, which replaces θ by its estimate $\hat{\theta}$

$$u = -\hat{\theta} x^3 - \cos(x) - c_1 x. \quad (4.3)$$

Substitution of the control law (4.3) into the dynamics (4.1) gives

$$\dot{x} = \tilde{\theta} x^3 - c_1 x \quad (4.4)$$

where $\tilde{\theta}$ is the *parameter estimation error*, defined as

$$\tilde{\theta} = \theta - \hat{\theta}. \quad (4.5)$$

The derivative of $V_0(x)$ now satisfies

$$\dot{V}_0 = -c_1 x^2 + \tilde{\theta} x^4.$$

Since the second term is indefinite due to the presence of $\tilde{\theta}$, no conclusions can be drawn about the stability of (4.4). The idea now is to extend the control law with an update law for $\hat{\theta}$, making the controller dynamic. To design this update law, V_0 is augmented with a quadratic term in the parameter estimation error $\tilde{\theta}$,

$$V_1(x, \tilde{\theta}) = \frac{1}{2}x^2 + \frac{1}{2\gamma}\tilde{\theta}^2, \quad (4.6)$$

where $\gamma > 0$ is the adaptation gain. The derivative of this function is

$$\begin{aligned} \dot{V}_1 &= x\dot{x} + \frac{1}{\gamma}\tilde{\theta}\dot{\tilde{\theta}} \\ &= -c_1 x^2 + \tilde{\theta} x^4 + \frac{1}{\gamma}\tilde{\theta}\dot{\tilde{\theta}} \\ &= -c_1 x^2 + \tilde{\theta} \left[x^4 + \frac{1}{\gamma}\dot{\tilde{\theta}} \right]. \end{aligned} \quad (4.7)$$

The second part is still indefinite and contains $\tilde{\theta}$ as a factor. However, the dynamics $\dot{\tilde{\theta}} = -\dot{\hat{\theta}}$ are available to cancel the indefinite part. Choose the update law

$$\dot{\hat{\theta}} = \gamma x^4 \quad (4.8)$$

which yields

$$\dot{V}_1 = -c_1 x^2 \leq 0.$$

Since $\dot{V}_1 \leq 0$, the equilibrium $x = 0$, $\tilde{\theta} = 0$ of the resulting closed loop system is globally stable. Additionally, by theorem 3.3, the desired regulation property $x \rightarrow 0$ as $t \rightarrow \infty$ holds.

The resulting adaptive control system consists of the parameter update law (4.8) and the control law (4.3). Note that this is a dynamic controller. It may seem that the adaptive design for the example is so simple because it is a first order system. In fact, it is due to the *matching* condition: the terms containing the unknown parameters in (4.1) can be directly canceled by u when θ is known.

4.2 Adaptive Backstepping

In the previous section the parametric uncertainty was in the span of the control. A more general case is *extended matching*, where the parametric uncertainty enters the system one integrator step before the control does. This approach will yield the adaptive integrator backstepping method. Recursive application of adaptive integrator backstepping results in the adaptive backstepping method.

4.2.1 Adaptive Integrator Backstepping

Consider the second order system

$$\begin{aligned}\dot{x}_1 &= x_2 + \varphi^T(x_1)\theta \\ \dot{x}_2 &= u.\end{aligned}\tag{4.9}$$

where $\varphi_1(x_1)$ is a vector function, $\theta \in \mathbb{R}^p$ a vector of p unknown constant parameters. If θ were known, integrator backstepping can be used to design a stabilizing function for x_2

$$\alpha_1(x_1, \theta) = -c_1 x_1 - \varphi_1^T(x_1)\theta.\tag{4.10}$$

Consider the Lyapunov function

$$V_0(x_1, x_2, \theta) = \frac{1}{2}z_1^T z_1 + \frac{1}{2}z_2^T z_2$$

where $z_1 = x_1$, $z_2 = x_2 - \alpha_1$, the CLF derivative is rendered negative definite by the control design

$$u = -c_2 z - x_1 + \frac{\partial \alpha_1}{\partial x_1} \left(x_2 + \varphi_1^T(x_1)\theta \right).$$

Since θ is unknown, the integrator backstepping design cannot be applied because of the dependence of α_1 and u on this unknown parameter. However, the main idea of integrator backstepping can still be used. *Step 1.* If x_2 were the control, an adaptive controller for the x_1 subsystem is given by

$$\begin{aligned}\alpha_1(x_1, \theta_1) &= -c_1 x_1 - \varphi_1^T(x_1)\hat{\theta}_1 \\ \dot{\hat{\theta}}_1 &= \Gamma_1 \varphi_1(x_1)x_1\end{aligned}\tag{4.11}$$

where $\hat{\theta}_1$ is the first estimate of θ . The derivative of the Lyapunov function

$$V_1(z_1, \hat{\theta}_1) = \frac{1}{2} z_1^T z_1 + \frac{1}{2} (\theta - \hat{\theta}_1)^T \Gamma_1^{-1} (\theta - \hat{\theta}_1) \quad (4.12)$$

along the solutions of (4.11) is

$$\begin{aligned} \dot{V}_1 &= z_1^T \dot{z}_1 - (\theta - \hat{\theta}_1)^T \Gamma_1^{-1} \dot{\hat{\theta}}_1 \\ &= z_1^T z_2 - z_1^T c_1 z_1 + (\theta - \hat{\theta}_1)^T (\varphi_1 z_1 - \Gamma_1^{-1} \dot{\hat{\theta}}_1) \\ &= z_1^T z_2 - z_1^T c_1 z_1. \end{aligned}$$

Step 2. The derivative of z_2 is now expressed as

$$\dot{z}_2 = \dot{x}_2 - \dot{a}_1 = u - \frac{\partial \alpha_1}{\partial x_1} \dot{x}_1 - \frac{\partial \alpha_1}{\partial \hat{\theta}_1} \dot{\hat{\theta}}_1.$$

Now an augmented Lyapunov function can be constructed

$$V_2(z_1, z_2, \theta_1) = V_1(z_1, \theta_1) + \frac{1}{2} z_2^T z_2$$

with derivative

$$\dot{V}_2 = -z_1^T c_1 z_1 + z_2^T \left[z_1 + u - \frac{\partial \alpha_1}{\partial x_1} x_2 - \frac{\partial \alpha_1}{\partial x_1} \varphi_1^T \theta - \frac{\partial \alpha_1}{\partial \theta_1} \Gamma_1 \varphi_1 z_1 \right]$$

for which a control u should be designed. However, it is clear that there is no design freedom left to cancel the term depending on θ . Therefore, a new estimate $\hat{\theta}_2$ of θ is introduced, and the Lyapunov function is augmented to

$$V_2(z_1, z_2, \hat{\theta}_1, \hat{\theta}_2) = V_1(z_1, \hat{\theta}_1) + \frac{1}{2} z_2^T z_2 + \frac{1}{2} (\theta - \hat{\theta}_2)^T \Gamma_2^{-1} (\theta - \hat{\theta}_2). \quad (4.13)$$

The derivative of V_2 is

$$\begin{aligned} \dot{V}_2 &= \dot{V}_1 + z_2^T \dot{z}_2 - (\theta - \hat{\theta}_2)^T \Gamma_2^{-1} \dot{\hat{\theta}}_2 \\ &= -z_1^T c_1 z_1 + z_2^T \left[z_1 + u - \frac{\partial \alpha_1}{\partial x_1} x_2 - \frac{\partial \alpha_1}{\partial \hat{\theta}_1} \Gamma_1 \varphi_1 z_1 \right] \\ &\quad - (\theta - \hat{\theta}_2)^T \Gamma_2^{-1} \left(\Gamma_2 \varphi_1 \frac{\partial \alpha_1^T}{\partial x_1} z_2 + \dot{\hat{\theta}}_2 \right) \end{aligned} \quad (4.14)$$

for which the control law and update law

$$\begin{aligned} u &= -z_1 - c_2 z_2 + \frac{\partial \alpha_1}{\partial x_1} x_2 + \frac{\partial \alpha_1}{\partial \theta_1} \Gamma_1 z_1 \varphi_1 + \frac{\partial \alpha_1}{\partial x_1} \varphi_1^T \hat{\theta}_2 \\ \dot{\hat{\theta}}_2 &= -\Gamma_2 \varphi_1 \frac{\partial \alpha_1^T}{\partial x_1} z_2 \end{aligned} \quad (4.15)$$

yields

$$\dot{V}_2 = -c_1 z_1^2 - c_2 z_2^2 \leq 0.$$

4.2.2 Recursive Adaptive Backstepping

Repeated application of adaptive integrator backstepping generalizes the approach to nonlinear systems which can be transformed through a diffeomorphism into *parametric strict-feedback form*

$$\begin{aligned}
 \dot{x}_1 &= x_2 + f_1(x_1) + \varphi_1^T(x_1)\theta \\
 \dot{x}_2 &= x_3 + f_2(x_1, x_2) + \varphi_2^T(x_1, x_2)\theta \\
 &\vdots \\
 \dot{x}_{n-1} &= x_n + f_{n-1}(x_1, \dots, x_{n-1}) + \varphi_{n-1}^T(x_1, \dots, x_{n-1})\theta \\
 \dot{x}_n &= f_n(x) + g(x)u + \varphi_n^T(x_1, \dots, x_n)\theta,
 \end{aligned} \tag{4.16}$$

where $g(x) \neq 0$ for all $x \in \mathbb{R}^n$, f represents the known dynamics, and $\theta \in \mathbb{R}^p$ is a vector of unknown constant parameters. For these systems, n design steps are required which is equal to the relative degree of the system. At each step, an error variable z_i , a stabilizing function α_i , and a parameter estimate $\hat{\theta}_i$ are generated. Therefore, if a system has p unknown parameters, the controller has to estimate $p \times n$ parameter estimates.

A controller for the system (4.16) can be designed which achieves tracking of a differentiable reference signal y_{ref} . Introduce the tracking errors

$$z_i = x_i - \alpha_{i-1}(x_1, \dots, x_{i-1}, y_{\text{ref}}, \dots, y_{\text{ref}}^{(i-1)}, \hat{\theta}_1, \dots, \hat{\theta}_{i-1}) \tag{4.17}$$

with $\alpha_0 = y_{\text{ref}}$, $z_0 = 0$. Then, the stabilizing functions α_i are defined by

$$\begin{aligned}
 \alpha_i &= -c_i z_i - z_{i-1} - f_i - \left(\varphi_i - \sum_{j=1}^{i-1} \frac{\partial \alpha_{i-1}}{\partial x_j} \varphi_j \right)^T \hat{\theta}_i \\
 &+ \sum_{j=1}^{i-1} \left[\frac{\partial \alpha_{i-1}}{\partial x_j} (x_{j+1} + f_{j+1}) + \frac{\partial \alpha_{i-1}}{\partial \hat{\theta}_j} \Gamma_j \left(\varphi_j - \sum_{k=1}^{j-1} \frac{\partial \alpha_{j-1}}{\partial x_k} \varphi_k \right) z_j \right].
 \end{aligned} \tag{4.18}$$

The control law for u and parameter update laws for each $\hat{\theta}_i$ are defined by

$$u = g^{-1}(x) \alpha_n(x, y_{\text{ref}}, \dots, y_{\text{ref}}^{(n)}, \hat{\theta}_1, \dots, \hat{\theta}_n) \tag{4.19}$$

$$\dot{\hat{\theta}}_i = \Gamma_i \left(\varphi_i - \sum_{j=1}^{i-1} \frac{\partial \alpha_{i-1}}{\partial x_j} \varphi_j \right) z_i \tag{4.20}$$

where $\Gamma_i = \Gamma_i^T > 0$ is the adaptation gain matrix, $c_i > 0$ are the controller gains. The controller design (4.18)-(4.20) guarantees global boundedness of $x(t)$, $\hat{\theta}_1(t)$, \dots , $\hat{\theta}_n(t)$, and regulation of $z(t)$ to zero. Consider then simple quadratic Lyapunov

function

$$V_n(z_1, \dots, z_n, \hat{\theta}_1, \dots, \hat{\theta}_n) = \frac{1}{2} \sum_{i=1}^n \left[z_i^2 + (\theta - \theta_i)^T \Gamma_i^{-1} (\theta - \theta_i) \right] \quad (4.21)$$

to prove this. Its derivative using the adaptive backstepping control design is

$$\dot{V}_n = - \sum_{i=1}^n z_i^T c_i z_i. \quad (4.22)$$

Convergence of the parameter estimates $\hat{\theta}_i$ is guaranteed, yet they do not necessarily converge to the true value θ .

4.3 Command Filtered and Tuning Functions Design

The overparameterization in the adaptive backstepping design can be solved in two different methods. The design of the parameter update law can be delayed to the final step, resulting in the tuning function adaptive backstepping design [88, Ch. 4]. The tuning function design requires the analytic derivative of the stabilizing function, resulting in a rather complex design process. The command filters introduced in section 3.5 can also be used to reduce the complexity of the adaptive backstepping design and remove the overparameterization. Additionally, in this section the adaptive backstepping design is extended to systems with unknown (virtual) control gains.

4.3.1 Constrained Adaptive Backstepping (CABS)

Consider a non-triangular, feedback passive system

$$\begin{aligned} \dot{x}_i &= f_i(x) + g_i(x)x_{i+1}, \quad i = 1, \dots, n-1 \\ \dot{x}_n &= f_n(x) + g_n(x)u \end{aligned} \quad (4.23)$$

where $x = (x_1, \dots, x_n)$ is the state, and u the control signal. The functions f_i, g_i are (partly) unknown. The sign of all $g_i(x)$ is known, and $g_i(x) \neq 0$ for all $x \in D_x$. The assumption is made that these unknown functions can be split into a known and unknown part as

$$\begin{aligned} f_i(x) &= f_i^0(x) + \varphi_{f_i}^T(x)\theta, \\ g_i(x) &= g_i^0(x) + \varphi_{g_i}^T(x)\theta. \end{aligned} \quad (4.24)$$

The tracking errors are defined as

$$z_i = x_i - x_{i,c} \quad (4.25)$$

where $x_{i,c}$ will be defined by the backstepping control method.

Step 1. This step is identical to the standard adaptive backstepping procedure. The first stabilizing function α_1 is defined as

$$\alpha_1 = \left(g_1^0 + \varphi_{g_1}^T \hat{\theta} \right)^{-1} \left(-c_1 z_1 - f_1^0 - \varphi_{f_1}^T \hat{\theta} + \dot{x}_{1,c} \right), \quad c_1 > 0. \quad (4.26)$$

Instead of using this stabilizing function directly, a new signal $x_{2,c}^0$ is defined as

$$x_{2,c}^0 = \alpha_1 - \zeta_2 \quad (4.27)$$

where ζ_2 will be defined in the next step. The signal $x_{2,c}^0$ is filtered to produce $x_{2,c}$ and its derivative $\dot{x}_{2,c}$. Magnitude and rate constraints can be incorporated in this filter. The effect of filtering on the tracking error z_1 is estimated by the stable, linear filter

$$\dot{\zeta}_1 = -c_1 \zeta_1 + \left(g_1^0 + \varphi_{g_1}^T \hat{\theta} \right) \left(x_{2,c} - x_{2,c}^0 \right). \quad (4.28)$$

Introduce the *compensated* tracking errors which remove the effect of filtering the stabilizing functions from the tracking error

$$\bar{z}_i = z_i - \zeta_1. \quad (4.29)$$

Select the first CLF V_1 as a quadratic function of the compensated tracking error \bar{z}_1 and the estimation error

$$V_1 = \frac{1}{2} \bar{z}_1^T z_1 + \frac{1}{2} \tilde{\theta}^T \Gamma^{-1} \tilde{\theta} \quad (4.30)$$

whose derivative is

$$\begin{aligned} \dot{V}_1 &= \bar{z}_1^T \left[f_1^0 + \varphi_{f_1}^T \theta + \left(g_1^0 + \varphi_{g_1}^T \theta \right) x_2 - \dot{x}_{1,c} - \dot{\zeta}_1 \right] + \tilde{\theta}^T \Gamma^{-1} \dot{\tilde{\theta}} \\ &= \bar{z}_1^T \left[f_1^0 + \varphi_{f_1}^T \theta + \left(g_1^0 + \varphi_{g_1}^T \hat{\theta} \right) \left(z_2 + x_{2,c} \right) - \dot{x}_{1,c} + c_1 \zeta_1 \right. \\ &\quad \left. - \left(g_1^0 + \varphi_{g_1}^T \hat{\theta} \right) \left(x_{2,c} - x_{2,c}^0 \right) + \varphi_{g_1}^T \tilde{\theta} x_2 \right] + \tilde{\theta}^T \Gamma^{-1} \dot{\tilde{\theta}} \\ &= \bar{z}_1^T \left[f_1^0 + \varphi_{f_1}^T \hat{\theta} + \left(g_1^0 + \varphi_{g_1}^T \hat{\theta} \right) \alpha_1 - \dot{x}_{1,c} + c_1 \zeta_1 \right. \\ &\quad \left. \left(g_1^0 + \varphi_{g_1}^T \hat{\theta} \right) \bar{z}_2 \right] - \tilde{\theta}^T \Gamma^{-1} \left(\dot{\tilde{\theta}} - \Gamma \varphi_{f_1} \bar{z}_1 - \Gamma \varphi_{g_1} x_2 \bar{z}_1 \right) \\ &= -\bar{z}_1^T c_1 \bar{z}_1 + \bar{z}_2^T \left(g_1^0 + \varphi_{g_1}^T \hat{\theta} \right) z_1 - \tilde{\theta}^T \Gamma^{-1} \left(\dot{\tilde{\theta}} - \Gamma \varphi_{f_1} \bar{z}_1 - \Gamma \varphi_{g_1} x_2 \bar{z}_1 \right) \end{aligned} \quad (4.31)$$

where the actual design of the parameter update law is postponed until the final step.

Step $i = 2, \dots, n - 1$. These steps are very similar to the first step. The stabilizing functions are defined as

$$\alpha_i = \left(g_i^0 + \varphi_{g_i}^T \hat{\theta} \right)^{-1} \left(-c_i z_i - \left(g_{i-1}^0 + \varphi_{g_{i-1}}^T \hat{\theta} \right)^T \bar{z}_{i-1} - f_i^0 - \varphi_{f_i}^T \hat{\theta} + \dot{x}_{i,c} \right), \quad c_i > 0. \quad (4.32)$$

The command filter inputs are defined similarly as before

$$x_{i,c}^0 = \alpha_{i-1} - \zeta_i \quad (4.33)$$

and the effect of filtering the stabilizing functions on the tracking errors is estimated by the linear filter

$$\dot{\zeta}_i = -c_i \zeta_i + \left(g_i^0 + \varphi_{g_i}^T \hat{\theta} \right) \left(x_{i+1,c} - x_{i+1,c}^0 \right). \quad (4.34)$$

The derivative of the CLF $V_i = V_{i-1} + \frac{1}{2} \bar{z}_i^T \bar{z}_i$ becomes

$$\begin{aligned} \dot{V}_i = & - \sum_{k=1}^i \bar{z}_k^T c_k \bar{z}_k + \bar{z}_{i+1}^T \left(g_i^0 + \varphi_{g_i}^T \hat{\theta} \right)^T \bar{z}_i \\ & + \tilde{\theta}^T \Gamma^{-1} \left(\dot{\hat{\theta}} - \sum_{k=1}^i \Gamma \varphi_{f_k} \bar{z}_k + \Gamma \varphi_{g_k} x_{k+1} \bar{z}_k \right) \end{aligned} \quad (4.35)$$

Step n . The final step yields the actual control signal u by filtering

$$u^0 = \alpha_n = \left(g_n^0 + \varphi_{g_n}^T \hat{\theta} \right)^{-1} \left(-c_n z_n - \left(g_{n-1}^0 + \varphi_{g_{n-1}}^T \hat{\theta} \right)^T \bar{z}_{n-1} - f_n^0 - \varphi_n^T \hat{\theta} + \dot{x}_{n,c} \right) \quad (4.36)$$

where the effect of filtering the commanded signal on the tracking error z_n is estimated by

$$\dot{\zeta}_n = -c_n \zeta_n + \left(g_n^0 + \varphi_{g_n}^T \hat{\theta} \right) \left(u - u^0 \right). \quad (4.37)$$

Consider the final stage Lyapunov function quadratic in the compensated tracking error and the parameter estimation error

$$V_n = \frac{1}{2} \sum_{i=1}^n \bar{z}_i^T \bar{z}_i + \tilde{\theta}^T \Gamma^{-1} \tilde{\theta} \quad (4.38)$$

whose derivative along the closed-loop solutions becomes

$$\dot{V}_n = - \sum_{i=1}^n \bar{z}_i^T c_i \bar{z}_i - \tilde{\theta}^T \Gamma^{-1} \left(\dot{\hat{\theta}} - \sum_{i=1}^n \Gamma \varphi_{f_i} \bar{z}_i + \Gamma \varphi_{g_i} x_{i+1} \bar{z}_i \right) \quad (4.39)$$

where $x_{n+1} = u$. The only design freedom left to cancel the indefinite terms is the parameter update law $\dot{\hat{\theta}}$. The parameter update law additionally has to be chosen such that $g_i \neq 0$ for all x . This can be guaranteed by applying parameter projection. Suppose that a convex region Π defined as

$$\Pi = \{ \hat{\theta} \in \mathbb{R}^p \mid \mathcal{P}(\hat{\theta}) \leq 0 \} \quad (4.40)$$

where \mathcal{P} is a smooth, convex function. The projection operator is defined as

$$\text{Proj}(\tau) = \begin{cases} \tau, & \hat{\theta} \in \Pi^0 \text{ or } \nabla_{\hat{\theta}} \mathcal{P}^T \tau \leq 0 \\ \left(I - \gamma \frac{\nabla_{\hat{\theta}} \mathcal{P} \nabla_{\hat{\theta}} \mathcal{P}^T}{\nabla_{\hat{\theta}} \mathcal{P}^T \gamma \nabla_{\hat{\theta}} \mathcal{P}} \right) \tau & \hat{\theta} \in \partial \Pi \text{ and } \nabla_{\hat{\theta}} \mathcal{P}^T \tau > 0 \end{cases} \quad (4.41)$$

where Π^0 is the interior of Π , $\partial \Pi$ is the boundary of Π , and γ is a positive definite matrix. If the parameter estimate $\hat{\theta}$ is inside the desired region Π , then the adaptation law is implemented directly. If $\hat{\theta}$ is on the boundary of Π and the update is directed outwards of the region, then the update is projected onto the hyperplane tangent to the boundary. Therefore, the projection keeps the parameter estimate within the desired region Π for all time. Thus, the parameter update law is defined using the projection operator as

$$\dot{\hat{\theta}} = \text{Proj} \left(\sum_{i=1}^n \Gamma \varphi_{f_i} \bar{z}_i + \Gamma \varphi_{g_i} x_{i+1} \bar{z}_i \right) \quad (4.42)$$

to cancel the indefinite terms in the CLF derivative (4.39). The resulting derivative is

$$\dot{V}_n = - \sum_{k=1}^n \bar{z}_k c_k \bar{z}_k \quad (4.43)$$

which shows that the origin of the compensated tracking error is globally asymptotically stable when the parameter estimate and its update are within the specified convex region. Additionally, since \bar{z} is bounded and ξ is small when the filter settings are chosen appropriately, the real tracking error z will converge to zero, resulting in global asymptotic tracking of the reference signal y_{ref} . A rigorous proof based on singular perturbations and Tikhonov's theorem 3.12 is given by Farrell, Polycarpou, Sharma, and Dong [56].

4.3.2 CABS Missile Example

To illustrate the benefits of adaptive backstepping for systems with parametric uncertainties, the missile example is revisited once more. The aerodynamic coefficients appearing the missile dynamics are considered to be unknown. The assumption is made that the sign of the function g_2 is known. Since the command filtered backstepping approach is chosen, the $g_1 \delta$ term in the missile dynamics can be taken into account in the design.

Recalling (3.36), the system is defined as

$$\dot{\alpha} = q + \frac{\bar{q} S}{m V_T} [C_z(\alpha, M) + b_z(M) \delta]$$

$$\dot{q} = \frac{\bar{q} S d}{I_{yy}} [C_m(\alpha, M) + b_m(M) \delta]$$

which is rewritten in the form used by the CABS backstepping procedure as

$$\begin{aligned}\dot{x}_1 &= x_2 + f_1^0(x_1, x_2, u, M) + \varphi_{f_1}^T(x_1, x_2, u)\theta \\ \dot{x}_2 &= f_2^0(x_1, x_2, M) + \varphi_{f_2}^T(x_1, x_2) + \left(g_2^0(x_1, x_2) + \varphi_{g_2}^T(x_1, x_2)\theta\right)u.\end{aligned}\quad (4.44)$$

where the unknown constant parameter vector $\theta \in \mathbb{R}^8$ for a given Mach number. The regressor functions are defined as

$$\begin{aligned}\varphi_{f_1}^T(x_1, x_2, u) &= C_1 \begin{bmatrix} x_1^3 & x_1|x_1| & x_1 & u & 0^{1 \times 4} \end{bmatrix} \\ \varphi_{f_2}^T(x_1, x_2) &= C_2 \begin{bmatrix} 0^{1 \times 4} & x_1^3 & x_1|x_1| & x_1 & 0 \end{bmatrix} \\ \varphi_{g_2}^T(x_1, x_2) &= C_2 \begin{bmatrix} 0^{1 \times 7} & 1 \end{bmatrix}\end{aligned}$$

with

$$C_1 = \frac{\bar{q}S}{mV_T}, \quad C_2 = \frac{\bar{q}Sd}{I_{yy}}.$$

The known, or a-priori model part of the missile dynamics (for example through wind-tunnel experiments) referred to as the on-board model is defined by f_1^0 , f_2^0 , and g_2^0 . Effectively, the controller should estimate a deviation from the a-priori missile model through an incremental model parameter $\theta \in \mathbb{R}^8$. The control task is to let the angle of attack track a reference signal y_{ref} . The tracking errors are defined as

$$\begin{aligned}z_1 &= x_1 - y_{\text{ref}} \\ z_2 &= x_2 - x_{2,c}\end{aligned}$$

where $x_{2,c}$ is the filtered virtual control. The stabilizing functions are defined as

$$\alpha_1 = -c_1 z_1 - f_1^0 - \varphi_{f_1}^T \hat{\theta} + \dot{y}_{\text{ref}}, \quad c_1 > 0 \quad (4.45)$$

$$\alpha_2 = \left(g_2^0 + \varphi_{g_2}^T \hat{\theta}\right)^{-1} \left(-c_2 z_2 - \dot{z}_1 - f_2^0 - \varphi_{f_2}^T \hat{\theta} + \dot{x}_{2,c}\right), \quad c_2 > 0. \quad (4.46)$$

Finally, the update laws follow from the CABS procedure and are

$$\dot{\hat{\theta}} = \text{Proj} \left(\Gamma \left(\varphi_{f_1} \bar{z}_1 + \varphi_{f_2} \bar{z}_2 + \varphi_{g_2} u \bar{z}_2 \right) \right) \quad (4.47)$$

where $\Gamma = \Gamma^T > 0$. The projection operator is applied to keep $g_2^0 + \varphi_{g_2}^T \hat{\theta}$ from changing sign. Therefore, it effectively keeps $|\varphi_{g_2}^T \hat{\theta}| \leq |g_2^0| - b$, where b is a constant design parameter. This choice of stabilizing functions and update laws renders the derivative of the CLF

$$V = \frac{1}{2} \left(\bar{z}_1^T \bar{z}_1 + \bar{z}_2^T \bar{z}_2 + \bar{\theta}^T \Gamma^{-1} \bar{\theta} \right)$$

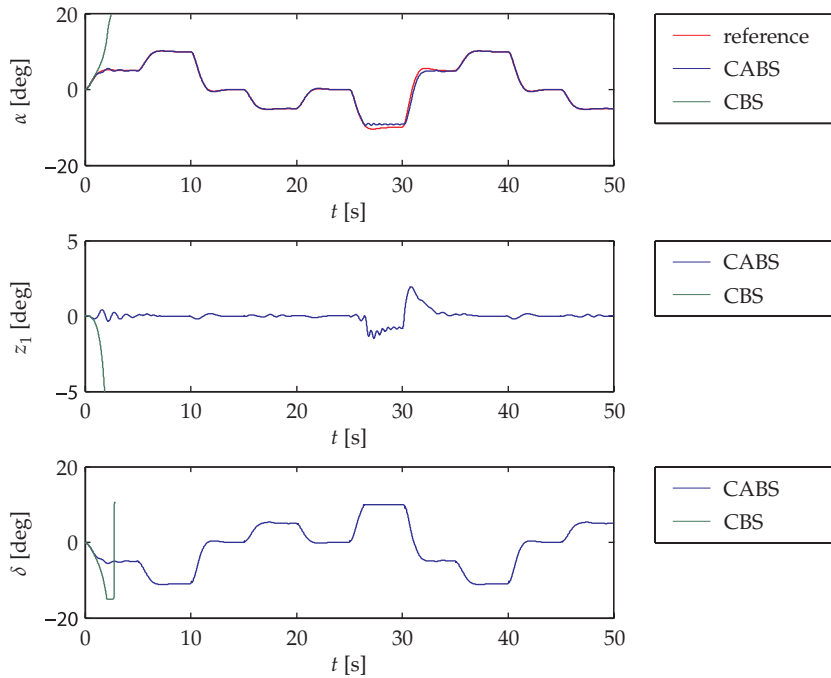


Figure 4.1: Response (top), tracking error (middle), and control input (bottom) for the CABS and CBS control designs applied to the missile example.

negative semi-definite. Hence, theorem 3.3 can be used to show that the equilibrium $(\bar{z}, \bar{\theta}) = 0$ is globally stable, and that the compensated tracking errors \bar{z} converge to zero asymptotically.

The adaptive design is applied to the missile model, a mismatch between the true model and the on-board model is simulated by a mismatch in Mach number between the on-board model and the true model. The missile actually flies at $M = 2.0$, while the controller gets $M = 1.8$ as an input. This results in highly unstable dynamics if the estimation is switched off as illustrated in figure 4.1 by the CBS design. The controller gains have been selected equal as in the non-adaptive command-filtered backstepping design in section 3.5.2, and the adaptation gain $\Gamma = 2000I$. The response of the missile and the parameter estimates are shown in figure 4.1 and 4.2 respectively. Note that the parameter estimates are not converging to their true values, but rather to arbitrary constants when no change occurs to the system. The oscillatory behavior in this case is due to the tuning of the command filters.

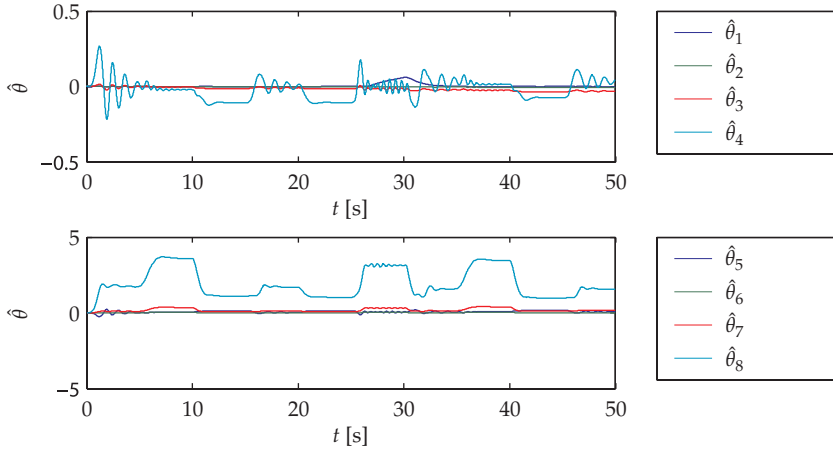


Figure 4.2: Parameter estimates for the CABS control design.

4.4 Modular Adaptive Backstepping

So far, the design of the control law has been integrated with the design of the parameter update laws. In this section an alternative approach to adaptive control of uncertain systems using backstepping is taken. The preceding designs are limited to Lyapunov based update laws, and hence the estimation is driven by the tracking error. For linear control designs, this restriction can be removed by estimation based designs which achieve *modularity* of the controller and identifier: any stabilizing controller can be combined with any identifier. The controller is capable of stabilizing the system when the parameters are known: this is called the *certainty equivalence principle*. The identifier on the other hand guarantees certain boundedness properties independently of the controller. This modularity makes this approach more versatile than the Lyapunov based identifier design.

4.4.1 Weakness of Certainty Equivalence

In this section the weakness of certainty equivalence principle when applied naively to nonlinear systems is illustrated. As observed in chapter 3 there is a fundamental difference between instability phenomena in linear and nonlinear systems. This will be illustrated using a simple example which has been visited earlier when discussing the robust backstepping design. Applying the certainty equivalence principle results in an unbounded closed-loop system for certain combinations of initial conditions.

Consider a scalar system

$$\dot{x} = u + \varphi^T(x)\theta \quad (4.48)$$

where $\varphi(x)$ is a vector of smooth nonlinear functions, and θ is a vector of unknown constant parameters. For this system, the simplest and most obvious certainty equivalence controller is

$$u = -x - \varphi^T(x)\hat{\theta} \quad (4.49)$$

where $\hat{\theta}$ is the estimate of θ . With this controller, the resulting equivalence feedback system is

$$\dot{x} = -x + \varphi^T(x)\tilde{\theta} \quad (4.50)$$

where $\tilde{\theta} = \theta - \hat{\theta}$. Earlier in this chapter update laws $\dot{\hat{\theta}}$ were designed using Lyapunov designs. In this design, a standard identifier is used to give an estimate to the controller instead: two modules are connected that are designed independently. In this case, consider a normalized gradient identifier

$$\dot{\chi} = -\chi + \varphi(x), \quad \chi(0) = 0 \quad (4.51)$$

$$\dot{\zeta} = -\zeta - \varphi^T(x)\hat{\theta}, \quad \zeta(0) = x(0) \quad (4.52)$$

$$\dot{\hat{\theta}} = \frac{\chi\chi^T}{1 + \chi^T\chi} (x - \chi^T\hat{\theta} - \zeta). \quad (4.53)$$

It is easy to check that $x - \chi^T\hat{\theta} - \zeta = \chi^T\tilde{\theta}$ such that

$$\dot{\tilde{\theta}} = -\frac{\chi\chi^T}{1 + \chi^T\chi}\tilde{\theta}. \quad (4.54)$$

Using the inequality $\tilde{\theta}^T\chi\chi^T\tilde{\theta} \leq \tilde{\theta}^T\chi^T\chi\tilde{\theta}$, note that

$$\begin{aligned} \frac{d}{dt} \left(\frac{1}{2}\tilde{\theta}^T\tilde{\theta} \right) &= -\tilde{\theta}^T \frac{\chi\chi^T}{1 + \chi^T\chi} \tilde{\theta} \geq -\tilde{\theta}^T \frac{\chi^T\chi}{1 + \chi^T\chi} \tilde{\theta} \\ &\geq -\tilde{\theta}^T\tilde{\theta}, \end{aligned} \quad (4.55)$$

which implies that

$$|\tilde{\theta}(t)| \geq |\tilde{\theta}(0)|e^{-t}. \quad (4.56)$$

Therefore, the convergence of the identifier can at best be exponential. Connecting this identifier with the certainty equivalence controller (4.49) for the case that

$$\varphi(x) = x^2, \quad \tilde{\theta} = \tilde{\theta}(0)e^{-t} \quad (4.57)$$

yields the following certainty equivalence feedback system

$$\dot{x} = -x + x^2\tilde{\theta}(0)e^{-t}. \quad (4.58)$$

In this case, an analytical solution is available

$$x(t) = \frac{2x(0)}{x(0)\tilde{\theta}(0)e^{-t} + (2 - x(0)\tilde{\theta}(0))e^t} \quad (4.59)$$

for which is it easy to see that whenever

$$x(0)\tilde{\theta}(0) > 2 \quad (4.60)$$

the solution of the closed loop system escapes to infinity in finite time as the denominator tends to zero. This instability is caused by the nonlinearity $\varphi(x) = x^2$. If the nonlinearity would have been bounded by linear growth, $|\varphi(x)| \leq k|x|$, the above instability would not have occurred. This example shows that there are two options: either design a much faster identifier, as used in the CABS design, or a stronger controller with a bigger stability margin against disturbances such as $\tilde{\theta}$; a more robust design. In the next section a control is designed which guarantees boundedness of all closed-loop system states when the estimation error is bounded, and its derivative is either bounded or square-integrable.

4.4.2 ISS-Backstepping Design

The modular scheme is based on the robust backstepping scheme introduced in section 3.4 and the ISS-CLF concept from section 3.2. The parameter estimation error and its derivative are considered as external disturbance inputs, and the controller is required to achieve boundedness of the system state whenever these inputs are bounded. The controller design for nonlinear systems in parametric strict-feedback form (4.16) is very similar to that of the over-parametrized backstepping design as given in section 4.2, with the addition of nonlinear damping terms.

Step 1. The design procedure starts by introducing the tracking errors

$$\begin{aligned} z_1 &= x_1 - y_{\text{ref}} \\ z_2 &= x_2 - \alpha_1 \end{aligned}$$

which have the dynamics

$$\begin{aligned} \dot{z}_1 &= \dot{x}_1 - \dot{y}_{\text{ref}} = x_2 + f_1 + \varphi_1^T \theta - \dot{y}_{\text{ref}} \\ &= z_2 + \alpha_1 + f_1(x_1) + w_1^T \theta - \dot{y}_{\text{ref}} \end{aligned}$$

where $w_1 = \varphi_1$. A stabilizing function α_1 is designed which damps the effect the parameter estimation error has on the tracking error z_1

$$\alpha_1 = -c_1 z_1 - s_1 z_1 - f_1 - w_1^T \hat{\theta} + \dot{y}_{\text{ref}} \quad (4.61)$$

where the nonlinear damping gain s_1 is given by

$$s_1 = w_1^T \kappa_1 w_1, \quad \kappa_1 = \kappa_1^T > 0.$$

Step $i = 2, \dots, n - 1$. The design continues by introducing more tracking errors

$$z_i = x_i - \alpha_{i-1}$$

whose dynamics are

$$\begin{aligned} \dot{z}_i &= \dot{x}_i - \dot{\alpha}_{i-1} \\ &= x_{i+1} + f_i + \varphi_i^T \theta - \sum_{k=1}^{i-1} \frac{\partial \alpha_{i-1}}{\partial x_k} (x_{k+1} + f_k + \varphi_k^T \theta) \\ &\quad - \sum_{k=1}^{i-1} \frac{\partial \alpha_{i-1}}{\partial y_{\text{ref}}^{(k-1)}} y_{\text{ref}}^{(k)} - \frac{\partial \alpha_{i-1}}{\partial \hat{\theta}} \dot{\hat{\theta}} \\ &= z_{i+1} + f_i + \alpha_i + w_i^T \theta \\ &\quad - \sum_{k=1}^{i-1} \left(\frac{\partial \alpha_{i-1}}{\partial x_k} (x_{k+1} + f_k) + \frac{\partial \alpha_{i-1}}{\partial y_{\text{ref}}^{(k-1)}} y_{\text{ref}}^{(k)} \right) - \frac{\partial \alpha_{i-1}}{\partial \hat{\theta}} \dot{\hat{\theta}} \end{aligned}$$

where

$$w_i = \varphi_i - \sum_{k=1}^{i-1} \frac{\partial \alpha_{i-1}}{\partial x_k} \varphi_k.$$

A stabilizing function for the system can be designed which damps the effect of the estimation error, and the effect of its derivative on the error dynamics. A possible stabilizing function is

$$\alpha_i = -z_{i-1} - (c_i + s_i)z_i - f_i - w_i^T \hat{\theta} + \sum_{k=1}^{i-1} \left(\frac{\partial \alpha_{i-1}}{\partial x_k} (x_{k+1} + f_k) + \frac{\partial \alpha_{i-1}}{\partial y_{\text{ref}}^{(k-1)}} y_{\text{ref}}^{(k)} \right) \quad (4.62)$$

where

$$s_i = w_i^T \kappa_i w_i + \left(\frac{\partial \alpha_{i-1}}{\partial \hat{\theta}} \right)^T \mu_i \left(\frac{\partial \alpha_{i-1}}{\partial \hat{\theta}} \right), \quad \kappa_i = \kappa_i^T > 0, \quad \mu_i = \mu_i^T > 0.$$

Step n . Finally, the last step yields the control law for u . The tracking error dynamics are given by

$$\dot{z}_n = gu + f_n + w_n^T \theta - \sum_{k=1}^{i-1} \left(\frac{\partial \alpha_{n-1}}{\partial x_k} (x_{k+1} + f_k) + \frac{\partial \alpha_{n-1}}{\partial y_{\text{ref}}^{(k-1)}} y_{\text{ref}}^{(k)} \right) - \frac{\partial \alpha_{n-1}}{\partial \hat{\theta}} \dot{\hat{\theta}}$$

where

$$w_n = \varphi_n - \sum_{k=1}^{n-1} \frac{\partial \alpha_{n-1}}{\partial x_k} \varphi_k.$$

The control law

$$\begin{aligned} u &= g^{-1} \left[-z_{n-1} - (c_n + s_n)z_n - f_n - w_n^T \hat{\theta} \right. \\ &\quad \left. + \sum_{k=1}^{n-1} \left(\frac{\partial \alpha_{i-1}}{\partial x_k} (x_{k+1} + f_k) + \frac{\partial \alpha_{i-1}}{\partial y_{\text{ref}}^{(k-1)}} y_{\text{ref}}^{(k)} \right) \right] \end{aligned} \quad (4.63)$$

damps out the effect of the estimation error and its derivative on the tracking error dynamics using the nonlinear damping gain

$$s_n = w_n^T \kappa_n w_n + \left(\frac{\partial \alpha_{n-1}}{\partial \hat{\theta}} \right)^T \mu_n \left(\frac{\partial \alpha_{n-1}}{\partial \hat{\theta}} \right).$$

The input-to-state properties of the error system can be shown by introducing the following constants

$$c_0 = \min_{1 \leq i \leq n} \lambda(c_i), \quad \kappa_0 = \left(\sum_{i=1}^n \kappa_i^{-1} \right)^{-1}, \quad \mu_0 = \left(\sum_{i=1}^n \mu_i^{-1} \right)^{-1}. \quad (4.64)$$

Consider the following CLF

$$V = \frac{1}{2} z^T z$$

whose derivative along the solutions of the tracking error system is given by

$$\begin{aligned} \dot{V} &= - \sum_{i=1}^n z_i^T c_i z_i - \sum_{i=1}^n z_i^T \left(w_i^T \kappa_i w_i + \frac{\partial \alpha_{i-1}^T}{\partial \hat{\theta}} \mu_i \frac{\partial \alpha_{i-1}}{\partial \hat{\theta}} \right) z_i \\ &\quad + \sum_{i=1}^n z_i^T \left(w_i^T \tilde{\theta} - \frac{\partial \alpha_{i-1}}{\partial \hat{\theta}} \hat{\dot{\theta}} \right) \\ &\leq - \sum_{i=1}^n z_i^T c_0 z_i - \sum_{i=1}^n \left(w_i z_i - \frac{1}{2} \kappa_i^{-1} \tilde{\theta} \right)^T \kappa_i \left(w_i z_i - \frac{1}{2} \kappa_i^{-1} \tilde{\theta} \right) + \frac{1}{4} \tilde{\theta}^T \kappa_0^{-1} \tilde{\theta} \\ &\quad - \sum_{i=1}^n \left(\frac{\partial \alpha_{i-1}}{\partial \hat{\theta}} - \frac{1}{2} \mu_i^{-1} \hat{\dot{\theta}} \right)^T \mu_i \left(\frac{\partial \alpha_{i-1}}{\partial \hat{\theta}} - \frac{1}{2} \mu_i^{-1} \hat{\dot{\theta}} \right) + \frac{1}{4} \hat{\dot{\theta}}^T \mu_0^{-1} \hat{\dot{\theta}} \\ &\leq - \sum_{i=1}^n z_i^T c_0 z_i + \frac{1}{4} \tilde{\theta}^T \kappa_0^{-1} \tilde{\theta} + \frac{1}{4} \hat{\dot{\theta}}^T \mu_0^{-1} \hat{\dot{\theta}}. \end{aligned} \quad (4.65)$$

which shows that the ISS property of z with respect to $\tilde{\theta}$ and $\hat{\dot{\theta}}$.

4.4.3 Swapping Filters

The goal of a swapping filter, for example (4.52), is to transform a dynamic parametric model into static form, such that standard parameter estimation algorithms can be used. These normal parameter estimation algorithms are not directly applicable since measurements of \dot{x} are often not available. The term *swapping* describes the fact that the order of the transfer function describing the dynamics and the time-varying parameter error $\tilde{\theta}$ is exchanged.

Two different swapping schemes are presented, one using a *z-swapping* derived from the tracking error model, and the other called *x-swapping* derived from the state dynamics. Each of these two schemes allows application of gradient and least squares update laws.

z-Swapping

Consider the parametric z -model

$$\dot{z} = A_z(z, \hat{\theta}, t)z + W^T(z, \hat{\theta}, t)\tilde{\theta} + Q^T(z, \hat{\theta}, t)\hat{\theta}. \quad (4.66)$$

By applying the filters

$$\dot{\Omega}^T = A_z(z, \hat{\theta}, t)\Omega^T + W^T(z, \hat{\theta}, t), \quad \Omega \in \mathbb{R}^{p \times n}, \quad (4.67)$$

$$\dot{\psi} = A_z(z, \hat{\theta}, t)\psi - \Omega^T\hat{\theta} - Q^T(z, \hat{\theta}, t)\hat{\theta}, \quad \psi \in \mathbb{R}^n \quad (4.68)$$

the linear parametric model

$$z + \psi = \Omega^T\tilde{\theta} + \tilde{\epsilon} \quad (4.69)$$

is obtained. The signals z , ψ , and Ω are available, and $\tilde{\epsilon}$ is an exponentially decaying signal due to initial conditions of the filter, and is governed by

$$\dot{\tilde{\epsilon}} = A_z(z, \hat{\theta}, t)\tilde{\epsilon}, \quad \tilde{\epsilon} \in \mathbb{R}^n. \quad (4.70)$$

Define the estimation error ϵ as

$$\epsilon = z + \psi. \quad (4.71)$$

Then, introduce an additional filter such that the swapping terms explicitly appear in the estimation error

$$\dot{\Omega}_0 = A_z(z, \hat{\theta}, t)\Omega_0 + W^T(z, \hat{\theta}, t)\hat{\theta} - Q^T(z, \hat{\theta}, t)\hat{\theta}, \quad \Omega_0 \in \mathbb{R}^n \quad (4.72)$$

and replace $\psi = \Omega_0 - \Omega^T\hat{\theta}$ the estimation error can be written as

$$\epsilon = z + \Omega_0 - \Omega^T\hat{\theta} = \Omega^T\tilde{\theta} + \tilde{\epsilon}. \quad (4.73)$$

This results in an estimation error that is linear in the parameter estimation error, allowing application of either a gradient or least squares update laws.

x-Swapping

Instead of the parametric z -model, consider the parametric x -model

$$\dot{x} = f(x, u) + F^T(x, u)\theta \quad (4.74)$$

which includes the class of parametric-strict feedback systems (4.16) with the particular choices

$$f(x, u) = \begin{bmatrix} x_2 + f_1(x_1) \\ \vdots \\ x_n + f_{n-1}(x_1, \dots, x_{n-1}) \\ f_n(x) + g_n(x)u \end{bmatrix}, \quad F^T(x, u) = \begin{bmatrix} \varphi_1^T(x_1) \\ \vdots \\ \varphi_{n-1}^T(x_1, \dots, x_{n-1}) \\ \varphi_n^T(x) \end{bmatrix}.$$

Then, introduce two filters

$$\dot{\Omega}_0 = A(x, t)(\Omega_0 + x) - f(x, u), \quad \Omega_0 \in \mathbb{R}^n \quad (4.75)$$

$$\dot{\Omega}^T = A(x, t)\Omega^T + F^T(x, u), \quad \Omega \in \mathbb{R}^{p \times n} \quad (4.76)$$

where $A(x, t)$ is a negative definite matrix for each x continuous in t . Again, the prediction error can be written in similar form as for the z -swapping scheme

$$\epsilon = \Omega^T \tilde{\theta} + \tilde{\epsilon}. \quad (4.77)$$

To guarantee boundedness of Ω when $F(x, u)$ grows unbounded, a particular choice of $A(x, t)$ is made

$$A(x, t) = A_0 - \rho F^T(x, u)F(x, u)P \quad (4.78)$$

where $\rho > 0$ and A_0 is an arbitrary constant negative definite matrix such that

$$PA_0 + A_0^T P + I = 0, \quad P = P^T > 0.$$

Then, the dynamics of $\tilde{\epsilon}$ are governed by

$$\dot{\tilde{\epsilon}} = A(x, t)\tilde{\epsilon} \quad (4.79)$$

4.4.4 Identifier Choice and Stability Proof

The signals from the z - and x -swapping filters can be used to drive the parameter update laws. The simplest update for $\hat{\theta}$ is the gradient update law

$$\dot{\hat{\theta}} = \Gamma \frac{\Omega \epsilon}{1 + \nu \text{tr}(\Omega^T \Omega)}, \quad \Gamma = \Gamma^T > 0, \quad \nu \geq 0. \quad (4.80)$$

The constant matrix Γ is the update gain, similar to the gain used in the over-parametrized and CABS designs. The constant ν is a parameter which can be used to normalize the update law. The least squares update law is very similar to the gradient update law, with time-varying update gain Γ

$$\begin{aligned} \dot{\hat{\theta}} &= \Gamma \frac{\Omega \epsilon}{1 + \nu \text{tr}(\Omega^T \Gamma \Omega)} \\ \dot{\Gamma} &= -\Gamma \frac{\Omega \epsilon}{1 + \nu \text{tr}(\Omega^T \Gamma \Omega)} \Gamma, \quad \Gamma(0) = \Gamma^T(0) \geq 0, \quad \nu \geq 0. \end{aligned} \quad (4.81)$$

Especially for the least squares update law a lot of variations and modification exist in literature.

For both the update law choices, the following lemma determines the properties of the identifier desired by the modular control design for either swapping scheme.

Lemma 4.1 (Identifier Properties). *Let the maximal interval of existence of solutions of be (4.16), the z -swapping filters (4.67) and (4.72) or the x -swapping filters (4.75) and (4.76), either the gradient (4.80) or least squares (4.81) update laws be $\left[0, t_f\right)$. Then for $v \geq 0$ the following properties hold:*

$$(i) \quad \tilde{\theta} \in \mathcal{L}_\infty[0, t_f)$$

$$(ii) \quad \epsilon \in \mathcal{L}_2[0, t_f) \cap \mathcal{L}_\infty[0, t_f)$$

$$(iii) \quad \dot{\hat{\theta}} \in \mathcal{L}_2[0, t_f) \cap \mathcal{L}_\infty[0, t_f).$$

Proof. The complete proof can be found in Krstić, Kanellakopoulos, and Kokotović [88, Ch. 6]. The proof is based on analyzing three Lyapunov functions $V_1(\Omega)$, $V_2(\tilde{\epsilon})$ and $V_3(\tilde{\theta}, \tilde{\epsilon})$. \square

Additionally, it is possible to establish additional properties of the least squares algorithm. Namely that $\hat{\theta}(t)$ converges to a constant vector, and $\dot{\hat{\theta}} \in \mathcal{L}_1$.

Using lemma 4.1, the following theorem states the properties of the closed-loop system for any combination of swapping scheme and update law choice of the modular backstepping design.

Theorem 4.2. *All the signals in the closed-loop adaptive system consisting of the system dynamics (4.16), modular control design, the z -swapping filters (4.67) and (4.72) or the x -swapping filters (4.75) and (4.76), either the gradient (4.80) or least squares (4.81), are globally uniformly bounded, and $(z, \epsilon) \rightarrow 0$ as $t \rightarrow \infty$. This means that global asymptotic tracking is achieved*

$$\lim_{t \rightarrow \infty} \left[y(t) - y_{ref}(t) \right] = 0. \quad (4.82)$$

4.5 Command Filtered Modular ISS-Backstepping Design

The modular backstepping design can be simplified by using command filters to produce the derivatives of the stabilizing functions. Additionally, in this section the modular backstepping design is extended to systems with unknown control gains.

4.5.1 Command Filtered Modular Design

Consider a non-triangular, feedback passive system

$$\begin{aligned} \dot{x}_i &= f_i(x) + g_i(x)x_{i+1}, \quad i = 1, \dots, n-1 \\ \dot{x}_n &= f_n(x) + g_n(x)u \end{aligned} \quad (4.83)$$

where $x = (x_1, \dots, x_n)$ is the state, u is the control input. The functions f_i and g_n are (partly) unknown. Note that in this case the assumption is made that the functions g_i are known for $i = 1, \dots, n-1$. The sign of g_n is known, and $g_n(x) \neq 0$ for all $x \in \mathcal{D}_x$. Assume that the unknown functions can be split into a known and an unknown part as

$$\begin{aligned} f_i(x) &= f_i^0(x) + \varphi_{f_i}^T(x)\theta, \\ g_n(x)u &= g_n^0(x)u + \varphi_{g_n}^T(x, u)\theta. \end{aligned} \quad (4.84)$$

The design of the command filtered modular backstepping design is actually nearly identical to the CABS design, with the addition of nonlinear damping terms. The design can be summarized as

$$z_i = x_i - x_{i,c} \quad (4.85)$$

$$\bar{z}_i = z_i - \zeta_i \quad (4.86)$$

$$x_{i,c}^0 = \alpha_{i-1} - \zeta_i \quad (4.87)$$

$$\alpha_i = g_i^{-1} \left(-c_i z_i - s_i \bar{z}_i - g_{i-1}^T \bar{z}_i - f_i^0 - \varphi_{f_i}^T \hat{\theta} + \dot{x}_{i,c} \right) \quad (4.88)$$

$$s_i = \begin{cases} \varphi_{f_i}^T \kappa_i \varphi_{f_i} & i = 1, \dots, n-1 \\ \left(\varphi_{f_i}^T \kappa_i \varphi_{f_i} + \varphi_{g_i}^T \kappa_i \varphi_{g_i} \right) & i = n \end{cases} \quad (4.89)$$

$$\dot{\chi}_i = -c_i \chi_i + g_i \left(x_{i+1,c} - x_{i+1,c}^0 \right) \quad (4.90)$$

where $c_i > 0, \kappa_i > 0$ are constants and $z_0 \equiv 0, \alpha_0 \equiv y_{\text{ref}}, x_{n,c} \equiv u_c$. Furthermore, the signals $x_{i,c}^0$ are filtered by stable filters to produce $x_{i,c}$ and its derivative. Parameter projection is applied to keep the sign of $g_n(x)$ from changing due to the parameter estimate

$$\dot{\hat{\theta}} = \text{Proj} \left(\Gamma \frac{\Omega \epsilon}{1 + \nu \text{tr}(\Omega^T \Gamma \Omega)} \right). \quad (4.91)$$

The derivative of the CLF $V(\bar{z}) = \frac{1}{2} \bar{z}^T \bar{z}$ when the projection operator is not effect using the filtered modular control design becomes

$$\begin{aligned} \dot{V} &= \sum_{i=1}^n \bar{z}_i^T \dot{\bar{z}}_i \\ &= - \sum_{i=1}^n \bar{z}_i^T c_i \bar{z}_i - \sum_{i=1}^n \bar{z}_i^T \varphi_{f_i}^T \kappa_i \varphi_{f_i} \bar{z}_i + \sum_{i=1}^n \bar{z}_i^T \varphi_{f_i}^T \tilde{\theta} - \bar{z}_n^T \varphi_{g_n}^T \kappa_n \varphi_{g_n} \bar{z}_n + \bar{z}_n^T \varphi_{g_n}^T \tilde{\theta} \\ &\leq - \sum_{i=1}^n \bar{z}_i^T c_0 \bar{z}_i - \sum_{i=1}^n \left(\varphi_{f_i} \bar{z}_i - \frac{1}{2} \kappa_i^{-1} \tilde{\theta} \right)^T \kappa_i \left(\varphi_{f_i} \bar{z}_i - \frac{1}{2} \kappa_i^{-1} \tilde{\theta} \right)^T \\ &\quad - \left(\varphi_{g_n} \bar{z}_n - \frac{1}{2} \kappa_n^{-1} \tilde{\theta} \right)^T \kappa_n \left(\varphi_{g_n} \bar{z}_n - \frac{1}{2} \kappa_n^{-1} \tilde{\theta} \right) + \frac{1}{4} \tilde{\theta}^T \kappa_0^{-1} \tilde{\theta} \end{aligned}$$

$$\leq - \sum_{i=1}^n \bar{z}_i^T c_0 \bar{z}_i + \frac{1}{4} \bar{\theta}^T \kappa_0^{-1} \bar{\theta}$$

where $c_0 = \min_{1 \leq i \leq n} \lambda_{\min} c_i$, $\kappa_0 = \left(\sum_{i=1}^n \kappa_i^{-1} \right)^{-1}$. This shows that the Lyapunov functions is negative definite outside a compact ball around the origin. If the command filter settings are chosen appropriately, the signals ζ_i are small, and hence z_i will be small.

Theorem 4.3. *All the signals in the closed-loop adaptive system consisting of the system dynamics (4.16), the filtered modular control design, the z -swapping filters (4.67) and (4.72) or the x -swapping filters (4.75) and (4.76), either the gradient (4.80) or least squares (4.81), are globally uniformly bounded, and $(z, e) \rightarrow 0$ as $t \rightarrow \infty$. This means that global asymptotic tracking is achieved*

$$\lim_{t \rightarrow \infty} \bar{z}_1 = 0. \quad (4.92)$$

and $z_1 \rightarrow 0$ if the effect of the command filters is negligible.

4.5.2 Modular Backstepping Missile Example

The filtered modular backstepping design illustrated by means of application on the missile example. The same parameterization as for the missile CABS example, section 4.3.2, is used. The control design is very similar to the CABS design with the addition of nonlinear damping terms in the stabilizing functions. The stabilizing functions are defined as

$$\alpha_1 = -c_1 z_1 - s_1 \bar{z}_1 - f_1^0 - \varphi_{f_1}^T \hat{\theta} + \dot{y}_{\text{ref}} \quad (4.93)$$

$$\alpha_2 = \left(g_2^0 + \varphi_{g_2}^T \hat{\theta} \right)^{-1} \left(-c_2 z_2 - \bar{z}_1 - s_1 \bar{z}_1 - f_2^0 - \varphi_{f_2}^T \hat{\theta} + \dot{x}_{1,c} \right) \quad (4.94)$$

where

$$s_1 = \varphi_{f_1}^T \kappa_1 \varphi_{f_1}, \quad s_2 = \left(\varphi_{f_2} + \varphi_{g_2} \right)^T \kappa_2 \left(\varphi_{f_2} + \varphi_{g_2} \right)$$

and $u_c^0 = \alpha_2$. A least squares type update law is used in combination with the x -swapping scheme. Projection of the parameter estimate is required such that the sign of $g_2^0 + \varphi_{g_2}^T \hat{\theta}$ remains constant. The resulting control design has a 6 command filter states, 72 recursive least squares filter states, 18 swapping filter states, for a total of 96 states which significantly more than required for the CABS controller design. A mismatch between the true dynamics of the missile and the model is simulated by a mismatch in the measured Mach number which serves as an input to the controller. The controller measures Mach 1.8 while the missile actually flies at Mach 2.0, resulting in a destabilizing disturbance in the closed-loop dynamics. The modular controller rapidly estimates this destabilizing dynamics as seen in figures 4.3 and 4.4. In this case the true parameters are not estimated over this relatively short time span, this can be explained by the fact that the regressor functions are

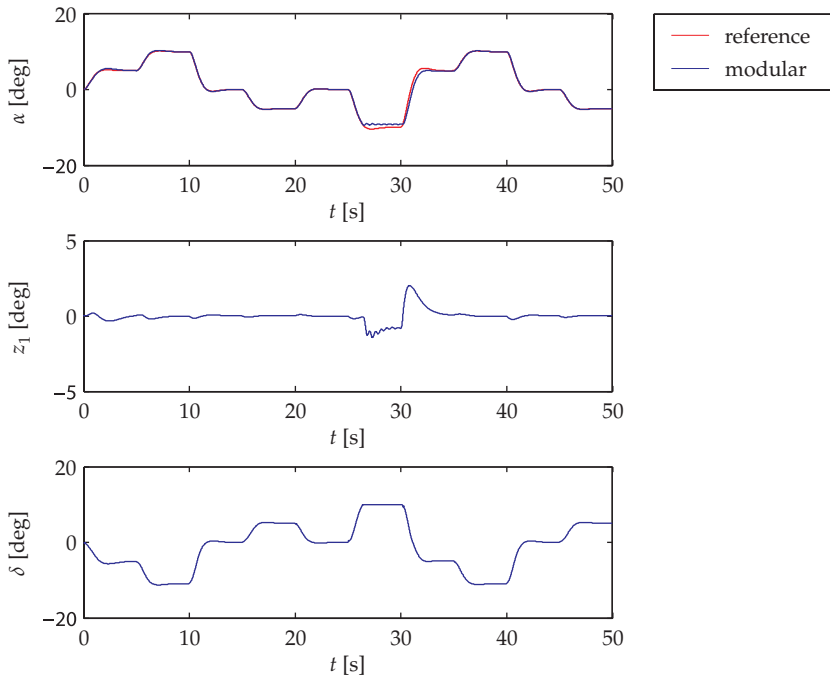


Figure 4.3: Response (top), tracking error (middle), and control input (bottom) for the modular backstepping design applied to the missile example.

almost linearly dependent. Although the parameter estimates do not converge to their true values, tracking of the desired reference signal is achieved.

4.6 Composite Adaptive Backstepping

Since the parameter uncertainty is reflected in both the tracking error and the prediction error, it is desirable to extract information from both these sources. This type of parameter updating is called composite adaptation [160], and can be seen as an extension of the integrated backstepping approach. The design can also be interpreted as a hybrid combination of the integrated and the modular design. The biggest drawback of the modular approach is the use of nonlinear damping terms in the stabilizing functions and control law to counteract the effect of the estimation error and its derivative. A weak point of the integrated approach was its sensitivity to tuning and convergence properties. The composite design eliminates the need for the nonlinear damping terms, and improves the convergence characteristics of the integrated design.

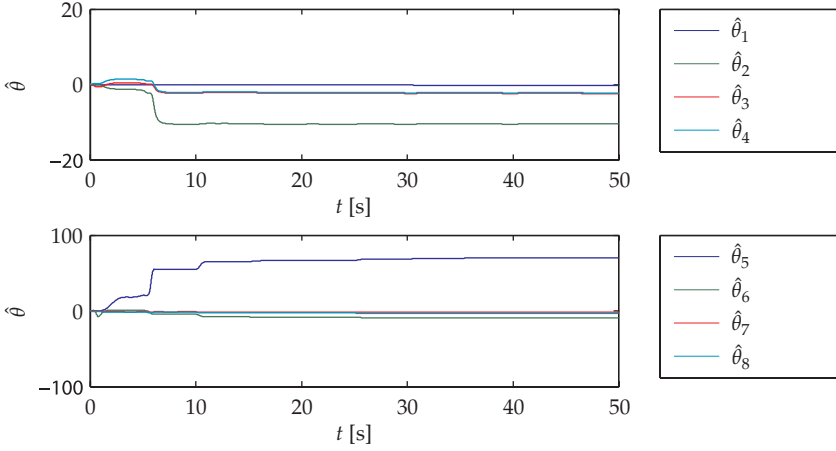


Figure 4.4: Parameter estimates for the modular backstepping control design with recursive least squares identifier.

The composite update law is composed as

$$\begin{aligned} \dot{\hat{\theta}} &= \text{Proj} \left(\Gamma \left(\Phi \bar{z} + \frac{\Omega \Psi \epsilon}{1 + \nu \text{tr}(\Omega^T \Gamma \Omega)} \right) \right) \\ \dot{\Gamma} &= -\Gamma \frac{\Omega \Psi \Omega^T}{1 + \nu \text{tr}(\Omega^T \Gamma \Omega)} \Gamma \end{aligned} \quad (4.95)$$

where $\Psi = \Psi^T \geq 0$ is a weight matrix to control how the adaptation law should weigh the information from the tracking error with respect to the information from the estimation error. This matrix can also be interpreted as a scaling factor in the least squares update law and setting the matrix to zero yields the CABS design. Consider the following CLF

$$V = \frac{1}{2} \left[\bar{z}^T \bar{z} + \tilde{\theta}^T \Gamma^{-1} \tilde{\theta} + \tilde{\epsilon}^T P \Psi \tilde{\epsilon} \right]. \quad (4.96)$$

Upon examination of the unnormalized update law, $\nu = 0$,

$$\begin{aligned} \frac{d}{dt} \left(\Gamma^{-1} \tilde{\theta} \right) &= -\Gamma^{-1} \dot{\Gamma} \Gamma^{-1} \tilde{\theta} - \Gamma^{-1} \dot{\hat{\theta}} \\ &= \Omega \Psi \Omega^T \tilde{\theta} - \Omega R \epsilon - \Gamma^{-1} \Phi \bar{z} \\ &= -\Omega \Psi \tilde{\epsilon} - \Gamma^{-1} \Phi \bar{z}. \end{aligned}$$

This, combined with the fact that the $\tilde{\epsilon}$ dynamics are governed by (4.70) or (4.79), yields the following time-derivative for the CABS control design with composite update law (4.95)

$$\begin{aligned}
\dot{V} &= -\bar{z}^T \dot{\bar{z}} - \frac{1}{2} \dot{\hat{\theta}}^T \Gamma^{-1} \tilde{\theta} + \frac{1}{2} \tilde{\theta}^T \frac{d}{dt} (\Gamma^{-1} \tilde{\theta}) + \frac{1}{2} \tilde{\epsilon}^T P \Psi \dot{\tilde{\epsilon}} + \frac{1}{2} \dot{\tilde{\epsilon}}^T \Psi P \tilde{\epsilon} \\
&\leq -\sum_{i=1}^n \bar{z}_i^T c_i \bar{z}_i - \frac{1}{2} \epsilon^T \Psi \Omega^T \tilde{\theta} - \frac{1}{2} \tilde{\theta}^T \Omega \Psi \tilde{\epsilon} - \frac{1}{2} \tilde{\epsilon}^T \Psi \tilde{\epsilon} \\
&\leq -\sum_{i=1}^n \bar{z}_i^T c_i \bar{z}_i - \frac{1}{2} \epsilon^T \Psi \epsilon + \frac{1}{2} \epsilon^T \Psi \tilde{\epsilon} - \frac{1}{2} \tilde{\epsilon}^T \Psi \epsilon + \frac{1}{2} \tilde{\epsilon}^T \Psi \tilde{\epsilon} - \frac{1}{2} \tilde{\epsilon}^T \Psi \tilde{\epsilon} \\
&\leq -\sum_{i=1}^n \bar{z}_i^T c_i \bar{z}_i - \frac{1}{2} \epsilon^T \Psi \epsilon
\end{aligned}$$

with $\Gamma > 0$ and $P > 0$. The CLF derivative shows convergence of both the compensated tracking error and the estimation error to zero. If the command filter tuning is chosen appropriately, the signals ζ are small and hence the tracking error z will be small, resulting in asymptotic tracking of the reference signal.

4.7 Adaptive Backstepping of Pure Feedback Systems

The pure-feedback design from section 3.6 can be extended quite easily to uncertain non-affine in control systems. However, care must be taken that the sign of the derivative of the control gain function with respect to the control input is strictly positive or negative. This can be achieved by either parameter projection alone, which would become a very complex and tedious task, or a special choice of regressor functions with parameter projection. An example of such functions are integrated Gaussians

$$\varphi_i(x, u) = \int_0^u e^{-(x-c_i)^T(x-c_i)/\sigma_i^2} d\zeta \quad (4.97)$$

where ζ is the integration variable, c_i is vector defining the center, σ_i is the width of the Gaussian. Note that $\frac{\partial \varphi(x, u)}{\partial u} > 0$, and therefore by applying simple parameter projection the sign of the control gain function can be preserved.

4.8 Conclusions

In this chapter several adaptive backstepping design approaches were introduced. Using these approaches stabilizing control laws can be designed which achieve convergence of the tracking error to zero and boundedness of the closed-loop system states in the presence of parametric uncertainties in the system. The use of

command filters greatly simplifies the designs and for the integrated adaptive back-stepping designs even avoids over-parameterization. The modular adaptive back-stepping design allows application of non-Lyapunov based update laws for the unknown parameter such as gradient based and least squares update laws. It achieves this modularity by including nonlinear damping terms. The composite adaptive update law eliminates the need for these nonlinear damping terms by using information from both the tracking error and the estimation error in the update law. In the next part these control approaches are used for aircraft control.

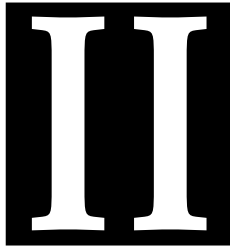
BIBLIOGRAPHY

- [4] Z. Artstein. “Stabilization with relaxed controls”. In: *Nonlinear Analysis* 7.11 (1983), pp. 1163–1173.
- [32] C. G. Darwin and A. R. Wallace. “On the tendency of species to form varieties; and on the perpetuation of varieties and species by natural means of selection”. In: *Journal of the Proceedings of the Linnean Society of London. Zoology* 3 (1858), pp. 45–62.
- [52] B. Etkin and L. D. Reid. *Dynamics of Flight: Stability and Control*. 3rd. John Wiley & Sons, 1996.
- [55] J. Farrell, M. Polycarpou, and M. Sharma. “Adaptive Backstepping with Magnitude, Rate, and Bandwidth Constraints: Aircraft Longitude Control”. In: *American Control Conference*. Denver, CO, June 2003, pp. 3898–3903.
- [56] J. A. Farrell, M. Polycarpou, M. Sharma, and W. Dong. “Command Filtered Backstepping”. In: *Automatic Control, IEEE Transactions on* 54.6 (June 2009), pp. 1391–1395.
- [57] J. A. Farrell, M. Sharma, and M. Polycarpou. “Backstepping Based Flight Control with Adaptive Function Approximation”. In: *Journal of Guidance, Control and Dynamics* 28.6 (Jan. 2005), pp. 1089–1102.
- [58] J. Farrell, M. Sharma, and M. Polycarpou. “On-line Approximation Based Aircraft Longitudinal Control”. In: *American Control Conference, Denver, CO*. Denver, CO, June 2003, pp. 1011–1015.
- [68] O. Härkegård. “Backstepping and Control Allocation with Applications to Flight Control”. PhD thesis. Linköping, Sweden: Linköping University, 2003.
- [74] R. A. Hull, D. Schumacher, and Z. Qu. “Design and Evaluation of Robust Nonlinear Missile Autopilots from a Performance Perspective”. In: *Proc. of the American Control Conference, Washington*. June 1995.
- [76] R. A. Hyde and K. Glover. “The application of scheduled \mathcal{H}_∞ controllers to a VSTOL aircraft”. In: *Automatic Control, IEEE Transactions on* 38.7 (1993), pp. 1021–1039.
- [83] H. K. Khalil. *Nonlinear Systems*. 3rd ed. Prentice Hall, 2002.

- [84] S. H. Kim, Y. S. Kim, and C. Song. "A Robust Adaptive Nonlinear Control Approach to Missile Autopilot Design". In: *Control Engineering Practice* 12.2 (2004), pp. 149–154.
- [88] M. Krstić, I. Kanellakopoulos, and P. V. Kokotović. *Nonlinear and Adaptive Control Design*. John Wiley and Sons, 1995.
- [107] A. M. Lyapunov. *The general problem of the stability of motion*. Ed. by A. T. Fuller. Taylor and Francis Ltd., 1992.
- [109] J. C. Maxwell. "On Governors". In: *Proceedings of the Royal Society of London* 16 (1867), pp. 270–283.
- [111] D. McRuer, I. Ashkenas, and D. Graham. *Aircraft Dynamics and Automatic Control*. Princeton University Press, 1973.
- [128] R. A. Nichols, R. T. Reichert, and W. J. Rugh. "Gain scheduling for \mathcal{H}_∞ controllers: a flight control example". In: *Control Systems Technology, IEEE Transactions on* 1 (1993), pp. 69–75.
- [140] M. M. Polycarpou, J. A. Farrell, and M. Sharma. "Robust On-line Approximation Control of Uncertain Nonlinear Systems Subject to Constraints". In: *9th IEEE International Conference on Engineering of Complex Computer Systems*. 2004, pp. 66–74.
- [148] J. Shamma and M. Athans. "Analysis of gain scheduled control for nonlinear plants". In: *Automatic Control, IEEE Transactions on* 35.8 (Aug. 1990), pp. 898–907.
- [149] J. Shamma and M. Athans. "Gain scheduling: potential hazards and possible remedies". In: *Control Systems Magazine, IEEE* 12.3 (June 1992), pp. 101–107.
- [160] J. J. E. Slotine and W. Li. "Composite Adaptive Control of Robot Manipulators". In: *Automatica* 25 (1989), pp. 509–519.
- [167] E. D. Sontag. "Smooth stabilization implies coprime factorization". In: *IEEE Transactions on Automatic Control* 34 (1989), pp. 435–443.
- [171] G. Stein. "Applications of Adaptive Control". In: ed. by K. S. Narendra and R. V. Monopoli. Academic Press, New York, 1980. Chap. Adaptive flight control - a pragmatic view.
- [172] G. Stein, G. Hartmann, and R. Hendrick. "Adaptive Control Laws for F-8 Flight Test". In: *Automatic Control, IEEE Transactions on* 22 (1977), pp. 758–767.
- [176] B. L. Stevens and F. L. Lewis. *Aircraft Control and Simulation*. 2nd ed. Wiley Interscience, New York, 2003.
- [184] J. Thunberg and J. W. C. Robinson. "Block Backstepping, NDI, and Related Cascade Designs for Efficient Development of Nonlinear Flight Control Laws". In: *Proceedings of the AIAA Guidance, Navigation, and Control Conference and Exhibit*. AIAA 2008-6960. AIAA. Honolulu, HI, USA, 2008.

- [201] N. Wiener. *Cybernetics or Control and Communication in the Animal and the Machine*. New York: Wiley & Sons, Inc., 1948.
- [206] P.-C. P. Yip. "Robust and Adaptive Nonlinear Control using Dynamic Surface Controller with Applications to Intelligent Vehicle Highway Systems". PhD thesis. University of California, 1997.
- [207] P.-C. P. Yip and J. K. Hedrick. "Adaptive dynamic surface control: a simplified algorithm form adaptive backstepping control of nonlinear systems". In: *International Journal of Control* 71.5 (1998), pp. 959–979.
- [208] L. A. Zadeh. "From Circuit Theory to System Theory". In: *Proceedings of the IRE*. Vol. 50. 5. May 1962, pp. 856–865.

PART



MODULAR BACKSTEPPING FLIGHT CONTROL

In this part of the dissertation the theory introduced in the first part is applied on different aircraft models, ranging from a relatively simple single flight condition over-actuated model of an F-18-like aircraft to full envelope nonlinear models of the F-16 and ADMIRE. The adaptive backstepping approaches introduced in chapter 4 are extended with different control allocation methods as well as full envelope model identification.

AIRCRAFT DYNAMICS

This chapter forms an introduction to flight dynamics for the reader not familiar with the subject. It defines important reference frames and derives the equations of motion for a rigid symmetric aircraft. Finally, two different non-linear aircraft models are introduced.

5.1 Aircraft Dynamics

In this chapter the equations of motion for symmetric aircraft flying over a flat Earth are derived. First of all, some coordinate frames and the relevant aircraft states are introduced. Then, the assumptions made to derive the equations of motion are stated. The external forces and moments acting on the aircraft are discussed and the equations of motion are derived. Then, the most common control variables and available control effectors are discussed. The chapter is concluded with an overview of a high-fidelity F-16 model and the ADMIRE model to which the methods developed in this dissertation are applied.

5.1.1 Coordinate Frames

Before deriving the equations of motion for aircraft several coordinate frames are required

Earth-Fixed Reference Frame F_E : This coordinate system has its origin fixed to an arbitrary point on the surface of the Earth. The z_E -axis points toward the center of the Earth, and $x_E y_E$ defines a tangent plane to the Earth's surface. Normally, x_E points to the North and y_E points East.

Body-Fixed Reference System F_B : The origin and axes of the coordinate system are fixed with respect to the geometry of the aircraft. If the aircraft has a plane of symmetry, then x_B and z_B lie in that plane of symmetry. Normally, x_B points towards the nose of the aircraft, z_B down, and y_B over the right wing.

Stability-Axis Reference Frame F_S : In this dissertation, the stability-axes are defined as a body-carried coordinate system where the x_S -axis is the projection of the velocity vector onto the plane of symmetry of the aircraft.

Wind-Axis Reference Frame F_W : This reference frame is body carried in which the x_W -axis points in the direction of the velocity vector of the aircraft relative to the air mass. The z_W -axis is in the plane of symmetry of the aircraft, and the y_W -axis points to the right.

The coordinate systems are shown in figure 5.1. The position of the aircraft is defined in the F_E reference frame. The attitude of the aircraft is the rotation from F_E to F_B . The rotation sequence from F_E to F_B is defined by the angles of yaw, pitch, and roll. The yaw angle ψ is the rotation around the z_E axis, followed by the pitch angle θ around the new y -axis, and finally the roll angle ϕ around the new x -axis. This representation of attitude has a singularity at ± 90 degrees of pitch which for military aircraft is a potential problem. Therefore, a quaternion representation of the aircraft's attitude is used which avoids this singularity. The transformation matrix from F_E to F_B is defined as

$$T_{E \rightarrow B} = \begin{bmatrix} (q_0^2 + q_1^2 - q_2^2 - q_3^2) & 2(q_1q_2 + q_0q_3) & 2(q_1q_3 - q_0q_2) \\ 2(q_1q_2 - q_0q_3) & (q_0^2 - q_1^2 + q_2^2 - q_3^2) & 2(q_2q_3 + q_0q_1) \\ 2(q_1q_3 + q_0q_2) & 2(q_2q_3 - q_0q_1) & (q_0^2 - q_1^2 - q_2^2 + q_3^2) \end{bmatrix},$$

where the transformation from the Euler, or Tait-Bryan, angles to quaternion representation is defined as

$$\mathbf{q} = \begin{bmatrix} q_0 \\ q_1 \\ q_2 \\ q_3 \end{bmatrix} = \pm \begin{bmatrix} \cos \frac{\phi}{2} \cos \frac{\theta}{2} \cos \frac{\psi}{2} + \sin \frac{\phi}{2} \sin \frac{\theta}{2} \sin \frac{\psi}{2} \\ \sin \frac{\phi}{2} \cos \frac{\theta}{2} \cos \frac{\psi}{2} + \cos \frac{\phi}{2} \sin \frac{\theta}{2} \sin \frac{\psi}{2} \\ \cos \frac{\phi}{2} \sin \frac{\theta}{2} \cos \frac{\psi}{2} + \sin \frac{\phi}{2} \cos \frac{\theta}{2} \sin \frac{\psi}{2} \\ \cos \frac{\phi}{2} \cos \frac{\theta}{2} \sin \frac{\psi}{2} + \sin \frac{\phi}{2} \sin \frac{\theta}{2} \cos \frac{\psi}{2} \end{bmatrix}.$$

When the F_B is rotated around the y_B axis by the angle of attack α the F_S reference frame is obtained. Finally, rotation around the z_S -axis by the sideslip angle yields

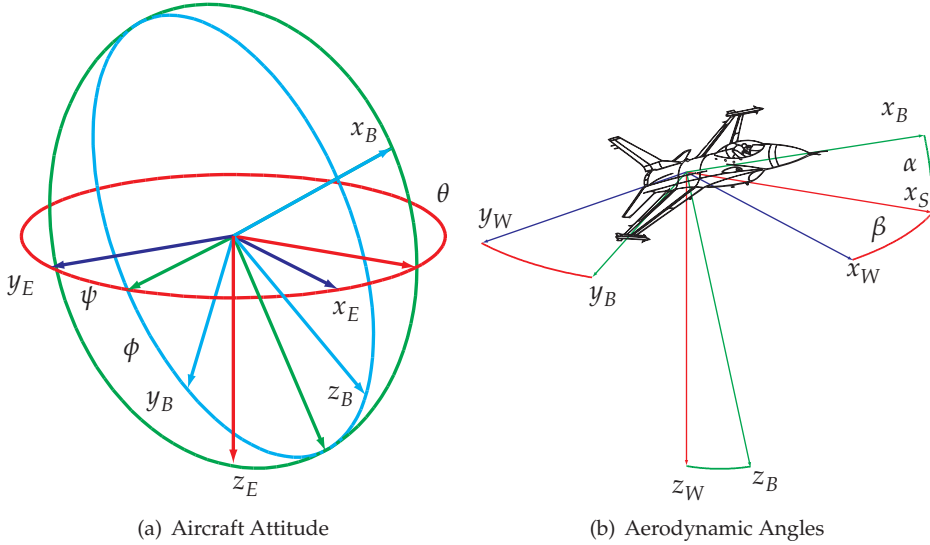


Figure 5.1: Coordinate systems and aircraft attitude representation.

F_W . This results in two additional rotation matrices defined as

$$T_{B \rightarrow S} = \begin{bmatrix} \cos \alpha & 0 & \sin \alpha \\ 0 & 1 & 0 \\ -\sin \alpha & 0 & \cos \alpha \end{bmatrix} \quad (5.1)$$

$$T_{B \rightarrow W} = \begin{bmatrix} \cos \beta & \sin \beta & 0 \\ -\sin \beta & \cos \beta & 0 \\ 0 & 0 & 1 \end{bmatrix} T_{B \rightarrow S} \quad (5.2)$$

5.1.2 Assumptions

Before proceeding to the derivation of the equations of motion, the following assumptions are made

1. The aircraft is a rigid body (as opposed to flexible) and has constant mass over the duration of the considered motion. The equations of motion simplify considerably due to this assumption, and it is quite valid. The decrease in mass of an F-16 aircraft flying at maximum dry thrust for 1 minute is less than 1% of the aircraft's total mass.
2. The aircraft's mass distribution is symmetric with respect to the $X_b O Z_b$ plane, such that the cross-products of inertia I_{xy} and I_{yz} are zero.

3. Earth is considered flat and non-rotating, and regarded as an inertial reference frame. This assumption is valid when dealing with control design of aircraft, but does not hold when designing guidance or navigation systems for flight over larger portions of Earth.
4. The air in front of the aircraft's trajectory is considered to be at rest relative to the Earth's surface.
5. The force, or thrust, produced by the engine is assumed to be in the X_bOZ_b plane and to act parallel to the X_b -axis. The gyroscopic effect caused by the angular momentum of the rotating turbine is considered constant.

Note that assumptions requiring symmetry of the aircraft are most likely violated when the aircraft sustains damage to the airframe. The aerodynamic effects resulting from the damage are however larger than the influence of the center of gravity shift and miss-aligned principle moment of inertia axes. A derivation of the equations of motions without this assumption can be found in Bacon and Gregory [7], Lombaerts [96].

5.1.3 Equations of Motion

Under the above assumptions, the aircraft has six degrees of freedom, three translations and three rotations. The aircraft's motion can thus be described by its position, attitude, linear velocity, and angular velocity over time. The aircraft dynamics can be described by a state space model with 13 states consisting of

- $\mathbf{p} = [x_E \ y_E \ z_E]^T$ the aircraft position in F_E ,
- $\mathbf{V} = [u_B \ v_B \ w_B]^T$ the velocity vector expressed in F_B ,
- \mathbf{q} is a quaternion vector describing the orientation of F_B relative to F_E ,
- $\boldsymbol{\omega} = [p_B \ q_B \ r_B]^T$ the angular velocity of the aircraft in F_B .

The equations governing these state vectors can be compactly written as

$$\dot{\mathbf{p}} = T_{E \rightarrow B}^T(\mathbf{q})\mathbf{V} \quad (5.3)$$

$$\mathbf{F} = m(\dot{\mathbf{V}} + \boldsymbol{\omega} \times \mathbf{V}) \quad (5.4)$$

$$\dot{\mathbf{q}} = \Omega(\boldsymbol{\omega})\mathbf{q} \quad (5.5)$$

$$\mathbf{M} = \mathbf{J}\dot{\boldsymbol{\omega}} + \boldsymbol{\omega} \times \mathbf{J}\boldsymbol{\omega} \quad (5.6)$$

where \mathbf{F} is the sum of external forces on the aircraft's center of gravity, m is the aircraft's mass, Ω is an anti-symmetric matrix defined as

$$\Omega(\boldsymbol{\omega}) = \begin{bmatrix} 0 & -p_B & -q_B & -r_B \\ p_B & 0 & r_B & -q_B \\ q_B & -r_B & 0 & p_B \\ r_B & q_B & -p_B & 0 \end{bmatrix},$$

\mathbf{M} is the sum of external moments, and \mathbf{J} is the inertia tensor. The external forces and moments have three major sources: gravity, engine thrust, and aerodynamic efforts.

Gravity Contribution

The gravity contribution consists of only a force since it acts on the center of gravity. The gravitational force, mg , is directed along the positive z_E -axis. Therefore, in F_B the resulting external force due to gravity can be written as

$$\mathbf{F}_G = T_{E \rightarrow B}(\mathbf{q}) \begin{bmatrix} 0 & 0 & mg \end{bmatrix}^T.$$

Engine Contribution

The engine thrust only produces an external force in the x_B -axis direction due to assumption 5. Therefore,

$$\mathbf{F}_E = \begin{bmatrix} T & 0 & 0 \end{bmatrix}^T.$$

Additionally, due to the rotation of the turbine an gyroscopic moment is introduced when the aircraft rotates.

$$\mathbf{M}_E = \mathbf{H}_E \times \omega$$

Aerodynamic Contribution

The aerodynamic forces and moments are due to the interaction between the aircraft body and the airflow. Their magnitude and direction are determined by the amount of air diverted by the aircraft in different directions. The amount of air diverted is mainly decided by the velocity of the aircraft with respect to the surrounding air, the properties of the surrounding air, the geometry of the aircraft, the angular rotation rate and the aircraft's control surface deflections δ . A standard way of modeling the aerodynamic forces and moments is

$$\begin{aligned} \text{Force} &= \bar{q} S C_F(\alpha, \beta, \omega, \delta, M, \dots) \\ \text{Moment} &= \bar{q} S l C_M(\alpha, \beta, \omega, \delta, M, \dots) \end{aligned}$$

where $\bar{q} = \frac{1}{2} \rho V_T^2$ is the aerodynamic pressure, S is the aircraft wing area, and l is a reference length, normally chosen as the chord for the pitch moment and the wingspan for the lateral moments, C_F and C_M are aerodynamic coefficients. These aerodynamic coefficients are hard to model analytically and are usually obtained through (virtual) wind tunnel experiments and actual flight tests. The resulting aerodynamic force and moment expressions in F_B are

$$\mathbf{F}_A = \begin{bmatrix} \bar{X} \\ \bar{Y} \\ \bar{Z} \end{bmatrix} = \bar{q} S \begin{bmatrix} C_X \\ C_Y \\ C_Z \end{bmatrix}$$

and

$$\mathbf{M}_A = \begin{bmatrix} \bar{L} \\ \bar{M} \\ \bar{N} \end{bmatrix} = \bar{q}S \begin{bmatrix} C_l b \\ C_m \bar{c} \\ C_n b \end{bmatrix}$$

5.1.4 Wind-Axis Equations of Motion

For control design it is often more convenient to formulate the equations of motion related to the aircraft velocity in the F_W reference frame.

$$\dot{V}_T = \frac{1}{m} (-D + T \cos \alpha \cos \beta + mg_1) \quad (5.7a)$$

$$\dot{\alpha} = q_S - p_S \tan \beta + \frac{1}{mV_T \cos \beta} (-L - T \sin \alpha + mg_3) \quad (5.7b)$$

$$\dot{\beta} = -r_S + \frac{1}{mV_T} (Y - T \cos \alpha \sin \beta + mg_2) \quad (5.7c)$$

where the contributions due to gravity are generated by $T_{B \rightarrow W} T_{E \rightarrow B} \mathbf{g}$. The relationship between the aerodynamic forces expressed in the two coordinate systems is given by

$$\begin{bmatrix} D \\ Y \\ L \end{bmatrix} = T_{B \rightarrow W} \begin{bmatrix} \bar{X} \\ \bar{Y} \\ \bar{Z} \end{bmatrix}. \quad (5.8)$$

5.2 Atmospheric Model

The aerodynamic forces and moments are dependent on the atmospheric flight condition. Given the aircraft's altitude and airspeed the atmospheric conditions can be calculated using the ISA atmosphere model. For the troposphere, i.e. for altitudes below 11 km, this atmospheric model is given below. First of all the temperature is calculated by the following relation between temperature and altitude h

$$T_h = T_0 + \lambda h. \quad (5.9)$$

where λ is the temperature gradient. Using this temperature, the speed of sound and the Mach number can be calculated by

$$M = \frac{V_T}{a} = \frac{V_T}{\sqrt{\gamma R T_h}}. \quad (5.10)$$

where R is the specific gas constant of air, γ is the ratio of specific heats. The pressure is calculated from

$$p = p_0 \left(\frac{T_h}{T_0} \right)^{-\frac{\gamma_0}{\gamma_0 - 1}}. \quad (5.11)$$

The ideal gas equation can be used to calculate the density of the air

$$\rho = \frac{p}{RT_h}. \quad (5.12)$$

5.3 Control Variables

If a flight control system is to be implemented, the first question that has to be answered is what does a pilot or autopilot system want to control? Most fighter aircraft are still designed for the high maneuverability required in dogfights. For longitudinal control, the normal acceleration or load factor, and pitch rate are important control variables. Since the load factor is closely coupled to the angle of attack, the angle of attack is often selected as a control variable in nonlinear control approaches.

In the lateral direction the roll rate and sideslip control systems are most common. Typically, the sideslip is regulated to zero such that the aircraft is flying straight into the relative wind. However, in some occasions some degree of sideslip might be necessary, e.g. when landing the aircraft in the presence of crosswind or to restore equilibrium when flying with asymmetric aircraft. Two choices are available for roll rate control. Controlling the roll rate in F_B results in exchange of the angle of attack and sideslip. At high angles of attack this is highly undesirable, since the largest acceptable amount of sideslip during a roll is in the order of 3 – 5 degrees [44]. By rolling around the x_S -axis or x_W -axis instead this problem can be circumvented. The last type of roll is known as a *velocity-vector roll*.

There exist situations where other control variables are chosen. Examples are autopilot functions such as altitude, heading and speed hold which are functions to assist the pilot during long distance flight. Other interesting control variables are the position of the aircraft with respect to other aircraft in close formation flight to reduce drag. Additionally, control of the flight path angle γ may be of interest for automatic take-off and landing.

5.4 Control Effectors

The equations of motion of an aircraft show that the motion of an aircraft can be modified by using control effectors. These control effectors can be categorized into aerodynamic control surfaces and force generators. The control surfaces perturb the airflow around the aircraft, and this generates aerodynamic forces and moments acting on the aircraft. Engines generate thrust forces by accelerating the air. Many different aerodynamic control surface configurations for modern fighter aircraft exist, figure 5.2 shows two possibilities. On the left an F-16 aircraft with conventional control surface layout is shown. The aircraft is controlled by the horizontal stabilizers, the rudder, ailerons and has speedbrakes, leading and trailing edge flaps. On the right a Su-35 aircraft is shown which has twin tails and therefore

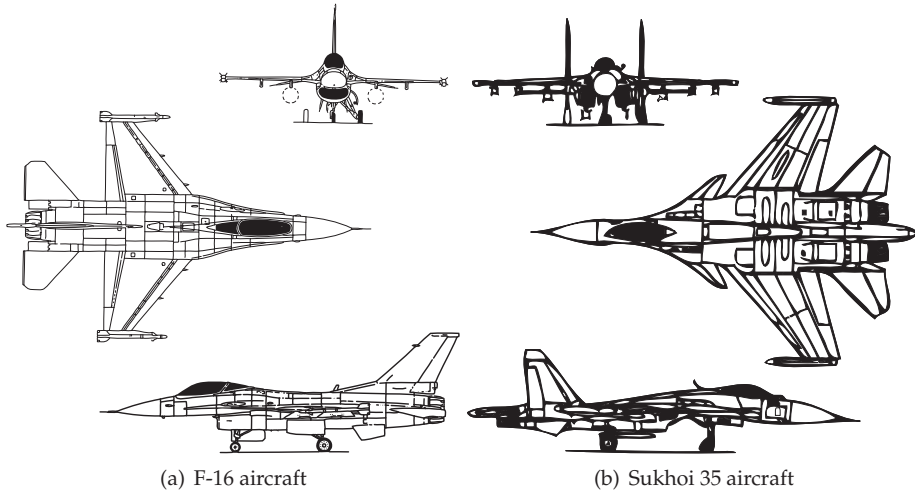


Figure 5.2: Control surface configurations of two different fighter aircraft.

double rudders, horizontal stabilizers, canards, ailerons, leading- and trailing edge flaps and speedbrakes.

5.5 High Fidelity F-16 Model

In this section the high-fidelity model of an F-16 aircraft, see figure 5.2(a), which is used in chapters 8 and 12 is introduced. First of all the available control effectors in the model are discussed. Following are the engine and aerodynamic models.

5.5.1 Aircraft Geometry

The F-16 model allows controlling the throttle, horizontal stabilizer, aileron and rudder deflections. The F-16 aircraft is equipped with leading edge flaps helping the aircraft to fly at high angles of attack. The speed brakes and trailing edge flaps are not included in the model. Additionally, in the model only symmetric horizontal stabilizers deflections are allowed, unlike the real F-16 aircraft. The geometric data for the F-16 model can be found in [126].

5.5.2 Engine Model

The F-16 aircraft is powered by a turbofan jet-engine with afterburner. The engine-thrust-lever system is modeled by means of engine thrust look-up tables, throttle gearing and engine power level lag. The power level is modeled as a first-order transfer function where the lag time constant is a function of the current engine

power and the commanded power. The commanded power level is a piece-wise linear function of the throttle setting.

$$P_c(\delta_T) = \begin{cases} 64.94\delta_T & \text{if } \delta_T \leq 0.77, \\ 217.38\delta_T - 117.38 & \text{if } \delta_T > 0.77. \end{cases} \quad (5.13)$$

The actual power level P_a is obtained through a first-order lag-filter with variable time-constant

$$\dot{P}_a = \frac{1}{\tau_{\text{eng}}^*} (P_c^* - P_a) \quad (5.14)$$

where

$$\begin{aligned} P_c^* &= P_c, \tau_{\text{eng}}^* = \frac{1}{5} && \text{if } P_c \geq 50 \text{ and } P_a \geq 50 \\ P_c^* &= 60, \tau_{\text{eng}}^* = \tau_{\text{eng}} && \text{if } P_c \geq 50 \text{ and } P_a < 50 \\ P_c^* &= 40, \tau_{\text{eng}}^* = \frac{1}{5} && \text{if } P_c < 50 \text{ and } P_a \geq 50 \\ P_c^* &= P_c, \tau_{\text{eng}}^* = \tau_{\text{eng}} && \text{if } P_c < 50 \text{ and } P_a < 50 \end{aligned}$$

$$\frac{1}{\tau_{\text{eng}}} = \begin{cases} 1.0 & \text{if } (P_c^* - P_a) \leq 25 \\ 1.9 - 0.036(P_c^* - P_a) & \text{if } 25 < (P_c^* - P_a) \leq 50 \\ 0.1 & \text{if } 50 \leq (P_c^* - P_a) \end{cases}$$

The engine thrust data is available in look-up tables as a function of the actual power setting, altitude, and Mach number. The thrust is computed as

$$T = \begin{cases} T_{\text{idle}} + (T_{\text{mil}} - T_{\text{idle}}) \frac{P_a}{50} & \text{if } P_a < 50, \\ T_{\text{mil}} + (T_{\text{max}} - T_{\text{mil}}) \frac{P_a - 50}{50} & \text{if } P_a \geq 50. \end{cases} \quad (5.15)$$

The angular momentum of the turbofan is assumed constant, with a value of $216.9 \text{ kgm}^2\text{s}^{-1}$.

5.5.3 Aerodynamic Model

The aerodynamic data of the F-16 model has been derived from low-speed static and dynamic wind-tunnel tests conducted with sub-scale models at the NASA Ames and Langley Research Centers [126]. The aerodynamic data is given in tabular form and is valid for the subsonic flight envelope for angles of attack between -20 and 90 degrees, and sideslip angles up to 30 degrees.

The total aerodynamic coefficients used in the equations of motion are composed out of several different contributing aerodynamic coefficients. One longitudinal and one lateral coefficient composition are shown here, the remaining coefficients are very similar and the complete description can be found in [126]. The force coefficient in the z_B -direction is defined as

$$\begin{aligned} C_{Z_i} &= C_Z(\alpha, \beta, \delta_h) + \delta C_{Z_{\text{lef}}}(\alpha, \beta) \left(1 - \frac{\delta_{\text{lef}}}{25}\right) \\ &\quad + \frac{q_B \bar{c}}{2V_T} \left(C_{Z_q}(\alpha) + \delta C_{Z_{q_{\text{lef}}}}(\alpha) \left(1 - \frac{\delta_{\text{lef}}}{25}\right) \right) \end{aligned}$$

where

$$\delta C_{Z_{\text{lef}}}(\alpha, \beta) = C_{Z_{\text{lef}}}(\alpha, \beta) - C_Z(\alpha, \beta, \delta_h = 0)$$

The moment coefficient around the z_B -direction, C_{n_t} , is build-up as

$$\begin{aligned} C_{n_t} = & C_n(\alpha, \beta, \delta_h) + \delta C_{n_{\text{lef}}} \left(1 - \frac{\delta_{\text{lef}}}{25} \right) + \delta C_{n_\beta}(\alpha)\beta - C_{Y_t} \frac{x_{\text{cgr}} - x_{\text{cg}}}{b} \\ & + \left(\delta C_{n_{\delta_a}} + \delta C_{n_{\delta_{a\text{lef}}}} \left(1 - \frac{\delta_{\text{lef}}}{25} \right) \right) \frac{\delta_a}{21.5} + \delta C_{n_{\delta_r}} \frac{\delta_r}{30} \\ & + \left(C_{n_p}(\alpha) + \delta C_{n_{p\text{lef}}}(\alpha) \left(1 - \frac{\delta_{\text{lef}}}{25} \right) \right) \frac{p_B b}{2V_T} \\ & + \left(C_{n_r}(\alpha) + \delta C_{n_{r\text{lef}}}(\alpha) \left(1 - \frac{\delta_{\text{lef}}}{25} \right) \right) \frac{r_B b}{2V_T} \end{aligned}$$

where

$$\begin{aligned} \delta C_{n_{\text{lef}}} &= C_{n_{\text{lef}}}(\alpha, \beta) - C_n(\alpha, \beta, \delta_h = 0) \\ \delta C_{n_{\delta_a}} &= C_{n_{\delta_a}}(\alpha, \beta) - C_n(\alpha, \beta, \delta_h = 0) \\ \delta C_{n_{\delta_{a\text{lef}}}} &= C_{n_{\delta_{a\text{lef}}}}(\alpha, \beta) - C_{n_{\text{lef}}}(\alpha, \beta) - \delta C_{n_{\delta_a}} \\ \delta C_{n_{\delta_r}} &= C_{n_{\delta_r}}(\alpha, \beta) - C_n(\alpha, \beta, \delta_h = 0). \end{aligned}$$

Note that the variables used in these look-up functions are in degrees instead of radians.

5.6 ADMIRE Model

A different, high-fidelity model of an aircraft is the Aero-Data Model In a Research Environment (ADMIRE) model developed by the Swedish Defence Agency FOI in cooperation with Saab AB. The ADMIRE is a generic model of a small single seat fighter aircraft with a delta-canard configuration. A full envelope adaptive control design with control allocation, and on-line model structure selection is made in chapter 9.

5.6.1 Aircraft Geometry

The aircraft has a delta-canard configuration, and dimensions comparable to the F-16 aircraft. The geometry of the aircraft resembles the Saab JAS 39 Gripen aircraft, increased 20% in size. The available control surfaces in the model are the left and right canards, the left and right outer elevons, the left and right inner elevons, the rudder, the leading edge flap, landing gear, air brake, and the thrust vectoring nozzle. The last three actuators are not used in this dissertation to control the aircraft. Each of the remaining control effectors, together with the throttle, can be commanded individually.

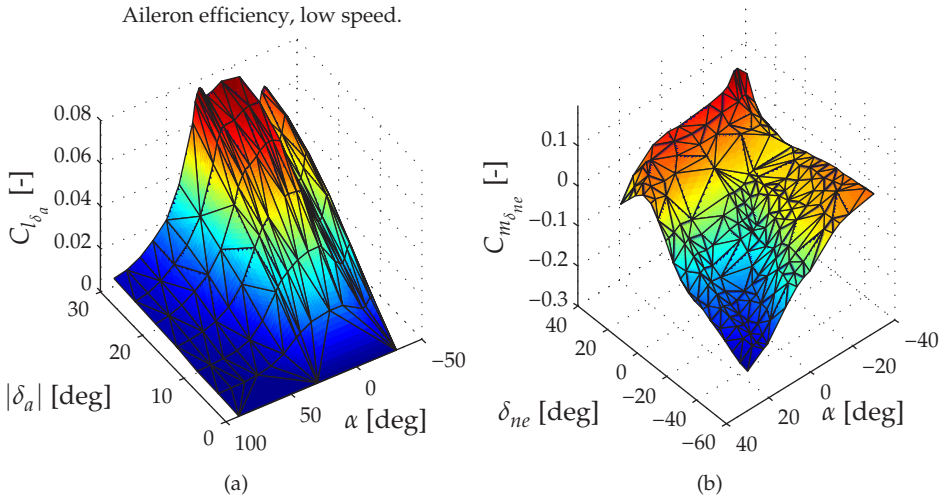


Figure 5.3: Example aerodynamic data for the ADMIRE model. In 5.3(a) the asymmetric elevon deflection effect on the rolling moment coefficient is shown, 5.3(b) shows the symmetric canard deflection effect on the pitching moment coefficient.

5.6.2 Engine Model

The engine model contains data in two 2-dimensional tables describing the produced engine thrust, with and without afterburner activated. The thrust is a function of the altitude and Mach number. The input to the engine is the throttle, taking values between 0 and 1. At throttle settings larger than 0.8 the afterburner is active. The dynamic response of the engine is modeled with a simple first order lag filter with a time constant of 2.0.

5.6.3 Aerodynamic Model

The aerodata of the model consists of aerodata tables, interpolation routines and aerodata algorithms. The aerodata is valid up to Mach numbers of 2.5, altitudes up to 20 km, angles of attack up to 30 degrees and sideslip angles up to 20 degrees. The original GAM model [6] has been extended for angles of attack up to 90 degrees at Mach numbers up to 0.5. There is considerable coupling between the longitudinal and lateral variables and coefficients, and the aerodata includes static aeroelastic effects. The full description of the aerodynamic coefficient-buildup can be found in [60]. The major difference with the F-16 model is that the aerodynamics do not have a linear-base, but rather the individual coefficients are build up from many nonlinear lookup tables. Example aerodynamic data is shown in figure 5.3.

5.7 Conclusions

In this chapter an introduction to aircraft dynamics and common control objectives for fighter aircraft was given. Two nonlinear aircraft models were introduced, the high-fidelity F-16 model, and the ADMIRE model. The aerodynamic model of both these aircraft varies nonlinearly through large flight envelopes, and hence it is expected that nonlinear control approaches can obtain better performance than linear control designs with less design effort. Furthermore, the ADMIRE model is over-actuated and thus some form of control allocation is required to control this aircraft. Finally, aircraft dynamics are typically not in lower-triangular form since the control effectors typically generate forces and moments. This has to be accounted for in the control design.

In the following chapters nonlinear adaptive control methods are applied to the flight control design to obtain excellent performance in nominal flight conditions, and improve stability and performance in post-failure flight conditions.

A COMPARISON OF ADAPTIVE CONTROL DESIGNS

In this chapter three control design approaches from chapter 4 are applied to a simplified, over-actuated fighter aircraft model. Two different design philosophies are pursued, the integrated adaptive approach where the identifier is designed simultaneously with the control law, and a modular approach which separates the control law and identifier. Since the aircraft model is over-actuated, different control allocation methods are implemented. The relation between the accuracy of the parameter estimates and the tracking performance is investigated by comparing simulation results for the combinations of backstepping and control allocation approaches.

6.1 Introduction

Each of the different adaptive backstepping options introduced in chapter 4 has its advantages and disadvantages. In this chapter the tuning-backstepping, command-filtered integrated and modular backstepping methods are applied to a simple, single flight condition, nonlinear over-actuated aircraft model. Since the aircraft model is over-actuated, meaning more control effectors than controlled variables, some form of control allocation (CA) has to be applied to distribute the desired control moment over the available control effectors.

The integrated backstepping designs that make use of Lyapunov based update laws are designed to meet a global system stability criterion, rather than minimizing the estimation error. As a result, these methods only yield a pseudo-estimate of the unknown model parameters [133]. The parameters do not necessarily converge

to their true values as this is not a requirement for stability. It is unclear what the effect of this on the control allocation since it is hard to predict the consequences of using the estimated values within the control allocation scheme. On the other hand, the least squares estimation of the modular design should be able to estimate more accurate parameter values since it uses state information directly, and not only the tracking error. The contributions of this chapter are twofold. First, a comparison of the performance of three adaptive control design methodologies on a nonlinear fighter aircraft model suffering from several types of control surface lockups is made. Second, the estimation accuracy of the designs is studied and how this accuracy affects the performance for different control allocation algorithms.

In this chapter, first of all the aircraft model is introduced and rewritten in a form suitable for the application of the backstepping methods. Then, the three different backstepping designs are introduced and their differences are clearly indicated. The backstepping designs only yield a desired control moment which has to be distributed over the available control effectors. Two methods based on the pseudo-inverse and on quadratic programming are introduced to solve this control allocation problem. Finally, using numerical simulations the different combination of control allocation and backstepping designs for four failure scenarios are evaluated on tracking performance and parameter estimation accuracy.

6.2 Aircraft Model

To effectively compare the different control designs a relatively simple, still nonlinear, aircraft model was obtained from [133]. This aircraft model has some resemblances to an F-18 aircraft. The aerodynamic data is available in the form of tables for two trimmed flight conditions: one at an altitude of 30,000 ft and Mach number of 0.7, the other at 40,000 ft and Mach number of 0.6. The model has seven surfaces which can be controlled: left and right horizontal stabilizers, left and right ailerons, collective leading edge flaps, collective trailing edge flaps, and collective rudder. A layout of the aircraft and its control surfaces is shown in figure 6.1.

The main simplifications made in the derivation of the model are the assumption of constant airspeed, and secondly that the control surface deflections do not generate lift and drag effects. This last assumption was made to transform the system into a feedback linearizable form to allow application of feedback linearization and non-filtered backstepping methods. Second order actuator dynamics have been included in the model. The magnitude, rate and bandwidth limits of the various actuators are specified in table 6.1.

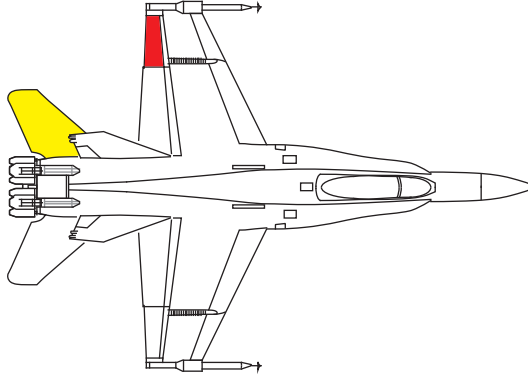


Figure 6.1: Top-view of an F-18 aircraft. The failing horizontal tail surface is marked in yellow, and the failing aileron is marked red.

Table 6.1: Actuator Specifications

Surface	Deflection Limit [deg]	Rate Limit [deg/s]	Bandwidth [rad/s]
Horizontal Stabilizer	[-24, 10.5]	± 40	50
Ailerons	[-25, 45]	± 100	50
Leading Edge Flaps	[-3, 33]	± 15	50
Trailing Edge Flaps	[-8, 45]	± 18	50
Rudder	[-30, 30]	± 82	50

The full equations of motion are given by

$$\begin{pmatrix} \dot{\alpha} \\ \dot{\beta} \\ \dot{\phi} \\ \dot{\vartheta} \\ \dot{p} \\ \dot{q} \\ \dot{r} \end{pmatrix} = \begin{pmatrix} q - p\beta + z_{\alpha}\Delta\alpha + (g_0/V)(\cos\vartheta\cos\phi - \cos\vartheta_0) \\ y_{\beta} + p(\sin\alpha_0 + \Delta\alpha) - r\cos\alpha_0 + (g_0/V)\cos\vartheta\sin\phi \\ p + q\tan\vartheta\sin\phi + r\tan\vartheta\cos\phi \\ q\cos\phi - r\sin\vartheta \\ l_{\beta}\beta + l_qq + l_r r + (l_{\beta\alpha}\beta + l_{r\alpha}r)\Delta\alpha + l_p p - i_1 q r \\ m_{\alpha}\Delta\alpha + m_q q + i_2 p r - m_{\dot{\alpha}}(g_0/V)(\cos\vartheta\cos\phi - \cos\vartheta_0) \\ n_{\beta}\beta + n_r r + n_p p + n_{p\alpha}p\Delta\alpha - i_3 p q + n_q q \end{pmatrix} \quad (6.1)$$

$$+ \begin{pmatrix} 0 & 0 & 0 & 0 & 0 & 0 & 0 \\ 0 & 0 & 0 & 0 & 0 & 0 & 0 \\ 0 & 0 & 0 & 0 & 0 & 0 & 0 \\ 0 & 0 & 0 & 0 & 0 & 0 & 0 \\ l_{\delta_{el}} & l_{\delta_{er}} & l_{\delta_{al}} & l_{\delta_{ar}} & 0 & 0 & l_{\delta_r} \\ m_{\delta_{el}} & m_{\delta_{er}} & m_{\delta_{al}} & m_{\delta_{ar}} & m_{\delta_{lef}} & m_{\delta_{tef}} & m_{\delta_r} \\ n_{\delta_{el}} & n_{\delta_{er}} & n_{\delta_{al}} & n_{\delta_{ar}} & 0 & 0 & n_{\delta_r} \end{pmatrix} \begin{pmatrix} \delta_{el} \\ \delta_{er} \\ \delta_{al} \\ \delta_{ar} \\ \delta_{lef} \\ \delta_{tef} \\ \delta_r \end{pmatrix}$$

where all the stability and control derivatives are considered to be unknown and should be estimated on-line by the parameter estimation process. The system of equations (6.1) can be rewritten in a notationally more convenient form for the control design as

$$\dot{x}_1 = f_1(x_1, x_0) + \varphi_{f_1}^T(x_1, x_0)\theta + g_1(x_1, x_0)x_2 \quad (6.2)$$

$$\dot{x}_2 = f_2(x_1, x_2, x_0) + \varphi_{f_2}^T(x_1, x_2, x_0)\theta + g_2(\theta)u \quad (6.3)$$

$$\dot{x}_0 = f_0(x_1, x_2, x_0) \quad (6.4)$$

where

$$\begin{aligned} x_1 &= [\phi \quad \alpha \quad \beta]^T, \\ x_2 &= [p \quad q \quad r]^T, \\ u &= [\delta_{el} \quad \delta_{er} \quad \delta_{al} \quad \delta_{ar} \quad \delta_{lef} \quad \delta_{tef} \quad \delta_r]^T, \end{aligned}$$

and the uncontrolled state $x_0 = \vartheta$. The known nonlinear aircraft dynamics are represented by the vector functions $f_1(x_1, x_0)$, $f_2(x_1, x_2, x_0)$ and $f_0(x_1, x_2, x_0)$ and the matrix function $g_1(x_1, x_0)$. The matrix functions $\varphi_1(x_1, x_0)$ and $\varphi_2(x_1, x_2, x_0)$ are regressor matrices for the part of the unknown dynamics that does not depend on the control input, θ is the unknown parameter vector, and $g_2(\theta)$ is a linear mapping of the control input related parameters into matrix form. The parameter vector is defined as

$$\theta = \left[z_\alpha \ y_\beta \ l_\beta \ l_p \ l_q \ l_r \ l_{\beta\alpha} \ l_{r\alpha} \ l_0 \ l_{\delta_{el}} \ l_{\delta_{er}} \ l_{\delta_{al}} \ l_{\delta_{ar}} \ l_{\delta_r} \ m_\alpha \ m_q \ m_{\dot{\alpha}} \ m_0 \ m_{\delta_{el}} \ m_{\delta_{er}} \ m_{\delta_{al}} \ m_{\delta_{ar}} \ m_{\delta_{lef}} \ m_{\delta_{tef}} \ m_{\delta_r} \ n_\beta \ n_r \ n_p \ n_{p\alpha} \ n_q \ n_0 \ n_{\delta_{el}} \ n_{\delta_{er}} \ n_{\delta_{al}} \ n_{\delta_{ar}} \ n_{\delta_r} \right]^T$$

with

$$g_2(\theta) = \begin{bmatrix} l_{\delta_{el}} & l_{\delta_{er}} & l_{\delta_{al}} & l_{\delta_{ar}} & 0 & 0 & l_{\delta_r} \\ m_{\delta_{el}} & m_{\delta_{er}} & m_{\delta_{al}} & m_{\delta_{ar}} & m_{\delta_{lef}} & m_{\delta_{tef}} & m_{\delta_r} \\ n_{\delta_{el}} & n_{\delta_{er}} & n_{\delta_{al}} & n_{\delta_{ar}} & 0 & 0 & n_{\delta_r} \end{bmatrix}.$$

6.3 Control System Design

The aircraft model has been rewritten into a form that is suitable for application of different backstepping design methods in the previous section. The static, or non-adaptive part, of both the integrated and modular backstepping designs is almost identical. The main difference is that nonlinear damping terms are not required for the integrated designs to guarantee boundedness of the state in the presence of estimation errors, but they do improve the tracking performance [88].

6.3.1 Static Backstepping Design

The control objective is to let x_1 track a smooth reference signal y_r . The reference y_r and its derivative \dot{y}_r are produced by filtering a step-like signal with a second order filter. This filter can be tuned such that desired transient response requirements are met. The first step in the design is to introduce tracking errors, which are defined as

$$z_1 = x_1 - y_r \quad (6.5)$$

$$z_2 = x_2 - x_{2,r} \quad (6.6)$$

where $x_{2,r}$ is a filtered stabilizing function for the z_1 subsystem. The dynamics of the z_1 subsystem satisfy

$$\dot{z}_1 = g_1(z_2 + \alpha_1) + f_1 + \varphi_{f_1}^T \theta - \dot{y}_r \quad (6.7)$$

using the dynamics (6.2). If the parameter vector θ is assumed known, and $z_2 = 0$, then a stabilizing function α_1 for the CLF $V_1 = \frac{1}{2}z_1^T z_1$ is defined as

$$\alpha_1 = g_1^{-1} \left(-f_1 - \varphi_{f_1}^T \hat{\theta} - C_1 z_1 + \dot{y}_r \right), \quad (6.8)$$

where $\hat{\theta}$ is the estimate of the parameter vector, and C_1 is a positive definite gain matrix. For the nominal controller, the estimate is not updated and is taken equal to some a-priori estimate of the unknown parameters. The input to the command filter to produce the reference signal for x_2 is defined as

$$x_{2,r}^0 = \alpha_1 - \Xi_2. \quad (6.9)$$

To remove the effect of command filtering from the tracking errors, the tracking error is augmented with filters that estimate the effect of filtering the control inputs. These augmented tracking errors are defined as

$$\bar{z}_1 = z_1 - \Xi_1 \quad (6.10)$$

$$\bar{z}_2 = z_2 - \Xi_2 \quad (6.11)$$

and the filter dynamics are

$$\dot{\Xi}_1 = -C_1 \Xi_1 + g_1 \left(x_{2,r} - x_{2,r}^0 \right) \quad (6.12)$$

$$\dot{\Xi}_2 = -C_2 \Xi_2 + g_2(\hat{\theta})u - M_{\text{des}} \quad (6.13)$$

where M_{des} is defined in the final backstepping step. The dynamics of the \bar{z}_2 subsystem are given by

$$\dot{\bar{z}}_2 = g_2(\hat{\theta})u + f_2 + \varphi_{f_2}^T \theta - \dot{x}_{2,r} - \dot{\Xi}_2. \quad (6.14)$$

A stabilizing function M_{des} can be defined, which serves as the desired total control effort to be produced by control surfaces

$$M_{\text{des}} = \hat{g}_2 u^0 = -C_2 z_2 - g_1^T \bar{z}_1 - f_2 - \varphi_{f_2}^T \hat{\theta} + \dot{x}_{2,r}. \quad (6.15)$$

The task to distribute M_{des} over the control surfaces is performed by the control allocation scheme, and results in desired actuator deflections u^0 . These desired control surface deflections are subsequently filtered to incorporate magnitude, rate, and bandwidth constraints to produce u .

The derivative of the CLF

$$V = \frac{1}{2} \bar{z}_1^T \bar{z}_1 + \frac{1}{2} \bar{z}_2^T \bar{z}_2 \quad (6.16)$$

along the trajectories of the closed-loop system defined by (6.7), (6.14) and the assumption that $\hat{\theta} = \theta$, is reduced to

$$\dot{V} = -\bar{z}_1^T C_1 \bar{z}_1 - \bar{z}_2^T C_2 \bar{z}_2$$

showing that the origin of (\bar{z}_1, \bar{z}_2) is UGAS. If the filter state (Ξ_1, Ξ_2) is small due to appropriate settings of the command filters, then (z_1, z_2) will be close to the origin, resulting in good tracking performance of the reference signal y_r . This concludes the common static feedback design for all methods. Nonlinear damping and integral terms can be easily added to this design. The modifications of the static design required for the three different backstepping designs are now shown, and the identification method in each approach is discussed.

6.3.2 Filtered Integrated Adaptive Backstepping Design

The CABS backstepping control law design is identical to the static design above. The parameter update law can be chosen such that global stability of the closed-loop system can be shown. Consider the CLF

$$V = \frac{1}{2} \bar{z}_1^T \bar{z}_1 + \frac{1}{2} \bar{z}_2^T \bar{z}_2 + \frac{1}{2} \tilde{\theta}^T \Gamma^{-1} \tilde{\theta}. \quad (6.17)$$

By choosing the update law

$$\dot{\hat{\theta}} = \text{Proj} \left(\Gamma \left(\varphi_{f_1} \bar{z}_1 + \varphi_{f_2} \bar{z}_2 + \varphi_u \bar{z}_2 \right) \right) \quad (6.18)$$

where $\varphi_u^T \hat{\theta} = g_2(\hat{\theta})u$, and parameter projection is applied to guarantee that $g_2(\hat{\theta})$ always has full rank, avoiding controllability issues. The CLF derivative along the trajectories of the system with the same control laws as the static backstepping design, and the update law (6.18) becomes

$$\dot{V} = -\bar{z}_1^T C_1 \bar{z}_1 - \bar{z}_2^T C_2 \bar{z}_2.$$

Using a theorem due to LaSalle-Yoshizawa 3.3, UGS of the closed-loop system and convergence of the augmented tracking error to zero can be concluded.

6.3.3 Filtered Modular Adaptive Backstepping Design

The modular backstepping design requires robustification of the static backstepping design presented above with respect to parameter estimation errors to achieve modularity of the design. Additionally, since the time derivative of the state is not always measurable swapping filters are applied to map the dynamic parametric from into static form, allowing direct use of standard identifiers. This swapping filter, see also 4.4.3, is defined by

$$\dot{\Omega}_0 = A(\Omega_0 + X) - f(x, u) \quad (6.19)$$

$$\dot{\Omega}^T = A\Omega^T + \varphi^T(x, u) \quad (6.20)$$

$$\epsilon = x + \Omega_0 - \Omega^T \hat{\theta} \quad (6.21)$$

where

$$f = \begin{bmatrix} f_1 + g_1 x_2 \\ f_2 \end{bmatrix}, \quad \varphi^T = \begin{bmatrix} \varphi_{f_1}^T \\ \varphi_{f_2}^T + \varphi_u^T \end{bmatrix}$$

$$A = A_0 - \rho \varphi^T \varphi P, \quad \rho > 0, P = P^T > 0$$

and the matrix φ_u maps the control vector u to the corresponding parameter estimates in θ such that $\varphi_u^T \hat{\theta} = gh_2(\hat{\theta})u$.

Nonlinear damping terms are added to the stabilizing functions

$$\alpha_1 = g_1^{-1} \left(-C_1 z_1 - S_1 \bar{z}_1 - f_1 - \varphi_{f_1}^T \hat{\theta} + \dot{y}_r \right) \quad (6.22)$$

$$M_{\text{des}} = -C_2 z_2 - S_2 \bar{z}_2 - f_2 - \varphi_{f_2}^T \hat{\theta} + \dot{x}_{2,r} \quad (6.23)$$

where

$$S_1 = \varphi_1^T \kappa_1 \varphi_1, \quad S_2 = (\varphi_2^T + \varphi_u^T) \kappa_2 (\varphi_2 + \varphi_u)$$

and $\kappa_1 > 0$, and $\kappa_2 > 0$ are the nonlinear damping gains. The resulting control design achieves input-to-state stability with respect to the parameter estimation error $\tilde{\theta}$. The parameter update is performed using a least squares filter with exponential forgetting

$$\dot{\hat{\theta}} = \text{Proj} \left(\frac{\Gamma \Omega \epsilon}{1 + \nu \text{tr}(\Omega^T \Gamma \Omega)} \right) \quad (6.24)$$

$$\dot{\Gamma} = \frac{-\Gamma \Omega \Omega^T \Gamma + \lambda \Gamma}{1 + \nu \text{tr}(\Omega^T \Gamma \Omega)}, \quad \lambda \geq 0, \nu \geq 0. \quad (6.25)$$

where parameter projection is applied to ensure that $g_2(\hat{\theta})$ always has full rank. By means of the CLF

$$V = \frac{1}{2} \bar{z}_1^T \bar{z}_1 + \frac{1}{2} \bar{z}_2^T \bar{z}_2 \quad (6.26)$$

ISS of the augmented tracking error with respect to the parameter estimation errors can be shown. The derivative becomes

$$\dot{V} \leq -\bar{z}_1^T C_1 \bar{z}_1 - \bar{z}_2^T C_2 \bar{z}_2 + \frac{1}{4} \bar{\theta}^T \kappa_1^{-1} \dot{\bar{\theta}} + \frac{1}{4} \bar{\theta}^T \kappa_2^{-1} \dot{\bar{\theta}}. \quad (6.27)$$

The size of the compact set to which the augmented tracking errors will converge can be controlled through the nonlinear damping gains κ . When the estimation errors are converging to zero, also the augmented errors will converge to zero.

After a period of flying, even with a small forgetting factor, the covariance matrix Γ will become very small, reducing the ability of the identification module to track rapid or sudden changes in the system parameters. Therefore, a change detector is introduced to reset the covariance matrix when a large mismatch between the estimated model and the system is detected. After a sudden failure, or during mismatch, the estimation error ϵ will be large compared to the estimation error before the failure. The current estimation error is compared with the average estimation error $\bar{\epsilon}$ taken over the last t_e seconds. An abrupt change is declared when

$$\left| \frac{\epsilon - \bar{\epsilon}}{\bar{\epsilon}} \right| > T_e \quad (6.28)$$

where T_e is a predefined threshold. On detection of a failure, i.e. a sudden change in the prediction error, the information matrix is reset. The change detector has to be tuned with caution, since a too sensitive tuning will result in the detector being triggered during normal maneuvering and a high threshold results in no triggering at all. Note that introduction of exponential forgetting and covariance resetting does not change the established properties of the closed-loop system [64, 143].

6.3.4 Tuning Function Adaptive Backstepping Design

The tuning function adaptive backstepping design removes the over-parameterization of the adaptive backstepping design by postponing the actual design of the identifier until the final stage of the design. In intermediate stages, intermediate update laws are defined for the parameter update called tuning functions. These tuning functions are extended recursively, until at the last step the complete update law for the unknown parameter is obtained. More details on this approach can be found in [87, 88, 163]. Note that in this design the command filters and the filter states Ξ are not used, therefore the CLF only contains the true tracking errors, and the analytic derivative of the virtual control law is required.

The time derivative of α_1 will be of the form

$$\dot{\alpha}_1 = \beta_1 + \beta_2^T \hat{\theta} \quad (6.29)$$

where the functions β_1 , and β_2 are obtained through tedious analytic calculations. The resulting parameter update law is summarized as

$$\dot{\hat{\theta}} = \text{Proj} \left(\Gamma \left(\varphi_{f_1} z_1 + \left(\varphi_{f_2} + \varphi_u + \beta_2 \right) z_2 \right) \right) \quad (6.30)$$

For the CLF

$$V = \frac{1}{2}z_1^T z_1 + \frac{1}{2}z_2^T z_2 + \frac{1}{2}\tilde{\theta}^T \Gamma^{-1} \tilde{\theta} \quad (6.31)$$

the tuning function design results in the CLF derivative

$$\dot{V} = -z_1^T C_1 z_1 - z_2^T C_2 z_2 \quad (6.32)$$

showing UGS of the origin of the error system, and by LaSalle-Yoshizawa it follows that $\lim_{t \rightarrow \infty} z_1 = 0$.

6.4 Control Allocation Methods

The backstepping control laws in the previous section yield a desired control moment. The task of control allocation is to distribute the desired control moment over the available control effectors in some optimal way. The control allocation problem is summarized by

$$g_2(\hat{\theta})u^0 = M_{\text{des}} \quad (6.33)$$

where u^0 are the desired control surface deflections. Without constraints on u , (6.33) describes an overdetermined system and hence has infinite solutions. In the presence of magnitude and rate constraints on u , this equation has either an infinite number of solution, a unique solution, or none at all. Two different control allocation methods are discussed in this section, one based on the (weighted) pseudo-inverse, the other based on quadratic programming. These control allocation methods are quite simple methods, and many more sophisticated methods exist. An overview of numerous control allocation techniques is presented in [14, 43, 68, 131].

6.4.1 Weighted Pseudo-inverse Control Allocation

The pseudo-inverse control allocation does not take any constraints on the control effectors into account, and should therefore be interpreted as a crude approach to control allocation. The pseudo-inverse itself can be interpreted as a least-squares fit to an over- or under-determined system of linear equations. The pseudo-inverse can be computed numerically stable through singular-value decomposition (SVD) or Cholesky decomposition. Suppose that the SVD of a matrix A is given by

$$A = U\Sigma V^H \quad (6.34)$$

then the pseudo-inverse A^\dagger is

$$A^\dagger = V\Sigma^\dagger U^H \quad (6.35)$$

where Σ^\dagger is the transpose of Σ with every nonzero entry replaced by its reciprocal, \star^H denotes the conjugate transpose.

The weighted pseudo-inverse is a slightly more sophisticated algorithm which allows to put a weight on the different parts of the least-squares fit. The solution to the optimization problem

$$\min_{Q \in \mathcal{S}} Q^T W Q, \quad \mathcal{S} = \left\{ Q \mid \|\hat{B}_2 u^0 - M_{des}\| \text{ is minimum} \right\} \quad (6.36)$$

where W is a weight matrix is given by

$$u^0 = W^{-1} \hat{B}_2^T \left(\hat{B}_2 W^{-1} \hat{B}_2^T \right)^{-1} M_{des}. \quad (6.37)$$

This gives a unique solution to the optimization problem, but does not take constraints on the control inputs into account. When $W = I$ the normal pseudo-inverse is obtained.

6.4.2 Quadratic Programming

The main disadvantage of the pseudo-inverse method is that it does not take magnitude and rate constraints on the control effectors into account. Quadratic programs (QP) can handle constraints and can be solved efficiently, therefore they are interesting for on-line applications. The QP will be feasible when the desired moment vector is within the attainable moment set, and infeasible if it is outside. Especially for on-line applications it is important that the problem is always feasible, such that a solution can always be obtained. Two approaches are available to guarantee that the QP will be feasible: direction preserving and sign preserving modification of the optimization problem. Direction preserving QP scales down the magnitude of the desired moment such that it falls within the attainable moment set, the sign-preserving method on the other hand scales down individual components of the moment vector. The difference between the scaling methods is illustrated in figure 6.2.

The sign preserving control allocation method makes more effective use of the available control authority, and therefore this method is selected. The QP is formulated by Simmons and Hodel [155] as

$$\begin{aligned} \min_{u, \sigma} \quad & \frac{1}{2} x^T H x + f^T x & (6.38) \\ \text{s.t.} \quad & g_2(\hat{\theta}) u - \Sigma^T M_{des} = 0 \\ & \begin{bmatrix} u_{lb} \\ 0 \\ 0 \\ 0 \end{bmatrix} \leq \begin{bmatrix} u \\ \sigma_{roll} \\ \sigma_{pitch} \\ \sigma_{yaw} \end{bmatrix} \leq \begin{bmatrix} u_{ub} \\ 1 \\ 1 \\ 1 \end{bmatrix} \end{aligned}$$

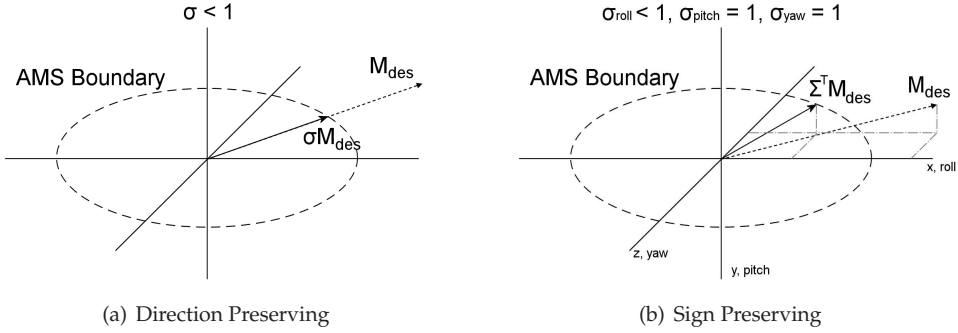


Figure 6.2: Different approaches to handle infeasible solutions [155].

where

$$x = \begin{bmatrix} u^T & \sigma_{roll} & \sigma_{pitch} & \sigma_{yaw} \end{bmatrix}^T,$$

$$\Sigma = \begin{bmatrix} \sigma_{roll} & 0 & 0 \\ 0 & \sigma_{pitch} & 0 \\ 0 & 0 & \sigma_{yaw} \end{bmatrix},$$

$$H = \begin{bmatrix} Q_u & 0 \\ 0 & Q_\sigma \end{bmatrix},$$

$$f^T = \begin{bmatrix} C_u^T & -2Q_\sigma \mathbf{1}^T \end{bmatrix}.$$

The weight matrices Q_u and Q_σ , and vector C_u are user specified. The scaling factors σ are more heavily weighted than the control inputs such that as much as possible of the available control authority is used, $Q_\sigma \gg Q_u$. Note that rate constraints can be implemented as magnitude constraints if a fixed simulation time step is taken, by selecting the most restrictive constraint of the two. Then, the modified magnitude constraints are defined as

$$\begin{aligned} \underline{\delta}(t+T) &= \max(\delta_{\min}, \delta(t) + \underline{\delta}T) \\ \bar{\delta}(t+T) &= \min(\delta_{\max}, \delta(t) + \bar{\delta}T) \end{aligned} \quad (6.39)$$

where T is the fixed time step and $\dot{\delta}$ represents the rate constraints.

6.5 Results

The combinations of the control designs and control allocation methods are evaluated on their tracking performance and parameter estimation accuracy for several failure scenarios. Two different maneuvers of 60 seconds have been flown. The control task is to track roll and angle of attack reference signals, while regulating

Table 6.2: Controller Tuning.

Controller	C_1	C_2	κ_1	κ_2	A_0	ρ	Γ_{sym}	Γ_{asym}
NOMINAL	I_3	$2I_3$	$0.01I_{36}$	$0.01I_{36}$	n/a	n/a	n/a	n/a
INTEGRATED	I_3	$2I_3$	$0.01I_{36}$	$0.01I_{36}$	n/a	n/a	10	3
TUNING	I_3	$2I_3$	$0.01I_{36}$	$0.01I_{36}$	n/a	n/a	10	3
MODULAR	I_3	$2I_3$	$0.01I_{36}$	$0.01I_{36}$	$-I_6$	0.1	1×10^3	1×10^3

the sideslip angle to zero. The tuning of the different controllers is summarized in table 6.2. The inner loop command filters implement the actuator specifications as shown in table 6.1, the outer loop filters do not implement magnitude or rate constraints. The difference in magnitude for the update gain Γ between the integrated and modular approaches is due to the fact that the integrated approaches use the tracking error signal to drive the parameter update, and the modular approach uses the filtered estimation error and regressors instead.

Numerical simulations of the controllers were performed in Mathworks Simulink environment. The simulations were performed with a fixed-time step of 0.01s and a third-order accurate solver. First the simulation scenarios are introduced, followed by an evaluation of the nominal performance. Once the reference performance of the controllers is established, the scenarios with control failures are evaluated. Finally, a specific failure scenario is highlighted and a direct comparison of the integrated and modular backstepping approach is made.

6.5.1 Simulation Scenarios

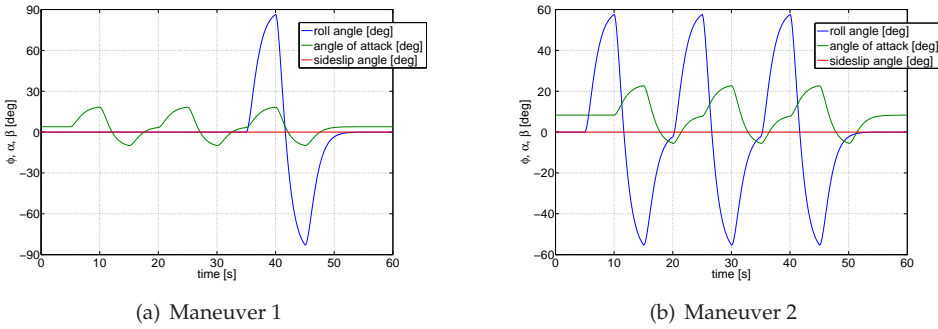
The simulated failure scenarios are limited to individual locked control surfaces at different deflections. As indicated in figure 6.1, failures of the left aileron and the left elevator surfaces are considered at both flight conditions: the left aileron locks at either $-25, -10, 0, 10, 25$ or 45 degrees, and the left elevator locks at either $-20, -10, -5, 0, 5$ or 10 degrees. A positive deflection means trailing edge down for both control surfaces. All simulations are started from the trimmed flight condition. Scenarios 1 and 2 are flown at flight condition I, scenarios 3 and 4 at flight condition II. The simulated failures are introduced 1 second into the simulation and the failed surface is deflecting to the failure position subject to the rate limit of the corresponding effector, i.e. 100 deg/s for the aileron and 40 deg/s for the elevator surface. Second order command filters are used to generate the reference signals on angle of attack and roll angle. The following two maneuvers are considered

Maneuver 1 Three angle of attack doublets of ± 15 degrees around the trim angle of attack are flown, while a roll angle double of ± 90 degrees is commanded during the third angle of attack doublet.

Maneuver 2 Three multi-axis doublets are flown, exciting the angle of attack ± 15 degrees around the trim angle of attack and the roll angle ± 60 degrees.

Table 6.3: Simulation Scenarios. Control surface positions in degrees after 1 second.

Scenario	Maneuver	Trim Condition	Failed Effector	Lock Positions
1	1	I	Left Aileron	45, 25, 10, 0, -10, -25 degrees
2	1	I	Left Hor. Stabilizer	10, 5, 0, -5, -10, -20 degrees
3	2	II	Left Aileron	45, 25, 10, 0, -10, -25 degrees
4	2	II	Left Hor. Stabilizer	10, 5, 0, -5, -10, -20 degrees

**Figure 6.3:** Maneuvers flown for the controller comparison.

The resulting, filtered, reference signals for these two maneuvers are shown in figure 6.3. The simulation scenarios are summarized in table 6.3. Each scenario and failure case is simulated for each of the control design and control allocation method combinations. Two different weight matrices are used for the weighted-pseudo inverse and QP control allocation methods, favoring horizontal tail surface deflections and favoring aileron deflections respectively

$$W_{u_1} = \text{diag} \left(\begin{bmatrix} 1 & 1 & 20 & 20 & 10 & 10 & 5 \end{bmatrix} \right), \quad (6.40)$$

$$W_{u_2} = \text{diag} \left(\begin{bmatrix} 20 & 20 & 1 & 1 & 10 & 10 & 5 \end{bmatrix} \right). \quad (6.41)$$

For each scenario, 6 failure case were performed for every control allocation method, resulting in 120 failure simulations per control design.

6.5.2 Nominal Performance

The root mean square (RMS) tracking error over the whole simulation is chosen as the evaluation criterion for the nominal performance. The RMS tracking error for the nominal simulations and all controller and control allocation method combinations is shown in table 6.4. These results show that the choice of control allocation does not have a large impact on the nominal performance. When the estimate of the control effectiveness matrix g_2 is good, and the desired control moments are

Table 6.4: Tracking performance, nominal case.

Control Allocation	NONAD	Control Design		
		TUNING	CABS	MODBS
PI	1.0013	0.8058	0.7692	1.0013
WPI W_{u_1}	1.0139	0.8891	0.8717	1.0139
WPI W_{u_2}	1.0007	0.7872	0.7402	1.0007
QP W_{u_1}	0.9964	0.8604	0.8198	0.9964
QP W_{u_2}	0.9964	0.8273	0.7953	0.9964

within the attainable moment set, the desired control moment can be realized. The performance of the two backstepping designs with Lyapunov based update law is better than the non-adaptive and modular backstepping since the integrated designs adapt the model parameters even if they are correctly initialized. In real applications this behavior could be removed by adding dead-zones. The modular backstepping design recognizes that the parameter estimates are at their correct values, and therefore does not adapt the parameters.

6.5.3 Failure Performance

The same reference tracking problem is considered with failures. To be able to present some meaningful statistics on performance, simulation cases which were terminated due to excessive tracking errors are not included in the comparison. The number of excluded cases is given in table 6.5. The adaptive control designs have considerable less terminated simulations than the non-adaptive design. The non-adaptive control law only results in satisfactory tracking for the mildest failure cases. Another striking fact is that the adaptive control laws in combination with the control allocation weight matrix W_{u_1} perform worse than with its counterpart, especially for the weighted pseudo-inverse. An exception is the modular design in combination with the quadratic programming control allocation. Weight matrix W_{u_1} gives priority to the horizontal stabilizers. If one of these surfaces fails, and its loss of effectiveness is poorly estimated, the difference between the desired moments and the actually generated moments will be big, resulting in performance degradation and large tracking errors. This effect is even larger when the weighted pseudo-inverse is used instead of a control allocation method which can incorporate constraints on the input. The failure cases that occur for the adaptive designs are the most extreme failure cases. For example, in scenario 4 with an elevator hard-over failure of 10.5 degrees, the simulation is terminated for each flight control design. Stability can still be maintained, but the commanded maneuver is too demanding for this failure at flight condition II.

The RMS of the tracking errors over the whole duration of the simulation, combined with the parameter estimation errors in the last five seconds are calculated for

Table 6.5: Number of terminated simulation cases.

Control Allocation	Controller			
	NOMINAL	TUNING	CABS	RLS-BS
PI	15	2	2	4
WPI W_{u_1}	19	18	14	15
WPI W_{u_2}	18	5	4	5
QP W_{u_1}	15	10	10	3
QP W_{u_2}	18	6	6	2
Total # of Failures	85	41	36	29

controller comparison. The results of the numerical simulations can be found in tables 6.6-6.9. Note that the results for the damaged aircraft are averaged over all *successful* failure scenarios. The average performance of the modular approach is better than that of the integrated designs. The performance of the nominal controller is included for comparison, note that the tracking performance for the mild successful failure cases already degrades when compared to the nominal performance. Not surprisingly, the average performance with the QP control allocation is better than for the (weighted) pseudo-inverse methods, and the number of successful simulations is also higher. The latter methods do not take constraints on the surface deflections into account, which can result in suboptimal use of the available control effectiveness, and thus reduced performance. Page and Steinberg [133] did similar simulations for the tuning function backstepping design in combination with the weighted pseudo-inverse and direct control allocation. Their results show that the weighted pseudo-inverse control allocation gave the best results due to the artificial lead it generates, although it is pointed out that this lead can also result in poor performance during maneuvers. However, their research did not consider actual failures, the investigation was limited to maneuvers with wrong initial estimate of the aerodynamic parameters. With control surface failures, the choice between the weighted pseudo-inverse and a more sophisticated method becomes more crucial as shown in this chapter.

A possible source for the better performance of the modular controller is a more accurate parameter estimation. To verify this hypothesis, the average errors over the last 5 seconds of the simulation between the estimate of the parameter and the true values of the post-failure parameters are calculated. The average estimation errors of parameters θ not related to the control surfaces are shown in table 6.7, table 6.8 presents the estimation errors in the unchanged part of the control effectiveness matrix, and finally, the estimation errors in the changed part of the control effectiveness matrix are shown in table 6.9. From these tables it becomes clear that the modular design estimates the parameter values closer to their true values than the other two designs. In fact, if the simulations are continued the estimates of the least squares algorithm keep converging closer to the true

Table 6.6: Tracking performance after aircraft failure (terminated cases removed).

Control Allocation	Control Design			
	NONAD	TUNING	CABS	MODBS
PI	5.7142	2.4372	2.1363	1.7437
WPI W_{u_1}	4.8384	3.7543	2.6949	2.0602
WPI W_{u_2}	4.4557	2.3611	2.3331	2.4741
QP W_{u_1}	5.7652	2.5326	2.4066	1.7660
QP W_{u_2}	4.2899	2.3884	2.3583	1.8176

Table 6.7: Average estimation error of θ unrelated to control surfaces over last 5 seconds.

Control Allocation	Control Design		
	TUNING	CABS	MODBS
PI	0.2179	0.2064	0.0589
WPI W_{u_1}	0.2693	0.2187	0.0242
WPI W_{u_2}	0.2053	0.1950	0.0413
QP W_{u_1}	0.3267	0.2805	0.0739
QP W_{u_2}	0.2400	0.2272	0.0516

Table 6.8: Average estimation error of unchanged g_2 elements over last 5 seconds.

Control Allocation	Control Design		
	TUNING	CABS	MODBS
PI	0.3070	0.3034	0.2125
WPI W_{u_1}	0.3151	0.3294	0.0691
WPI W_{u_2}	0.2785	0.2796	0.1508
QP W_{u_1}	0.2611	0.2484	0.1481
QP W_{u_2}	0.2620	0.2628	0.1310

Table 6.9: Average estimation error of changed g_2 elements due to surface failures over last 5 seconds.

Control Allocation	Control Design		
	TUNING	CABS	MODBS
PI	1.7742	1.7776	0.4046
WPI W_{u_1}	1.8362	1.0579	0.7117
WPI W_{u_2}	1.5960	1.5359	0.2266
QP W_{u_1}	2.0812	2.0979	0.2208
QP W_{u_2}	1.8665	1.8685	0.1005

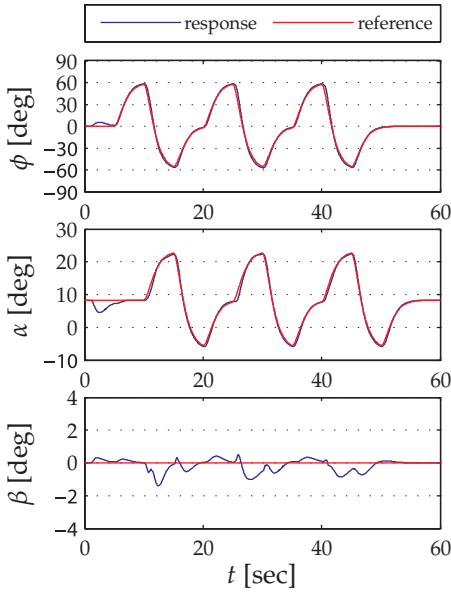
parameters for the same repeating reference signal. This is not the case for the integrated designs where usually the opposite is true [164], which is why parameter projection methods are often used to bound the values of the parameter estimation errors for an adaptive backstepping design with Lyapunov based update. Most crucial for the control allocation are the estimation errors in the effectiveness of the failed surfaces as shown in table 6.9. It is evident that the parameter estimation quality of the modular design is superior to the integrated Lyapunov based designs, which explains why this control law has the most successful reconfigurations when a weighted control allocation method is used.

6.5.4 Specific Failure Scenario Comparison

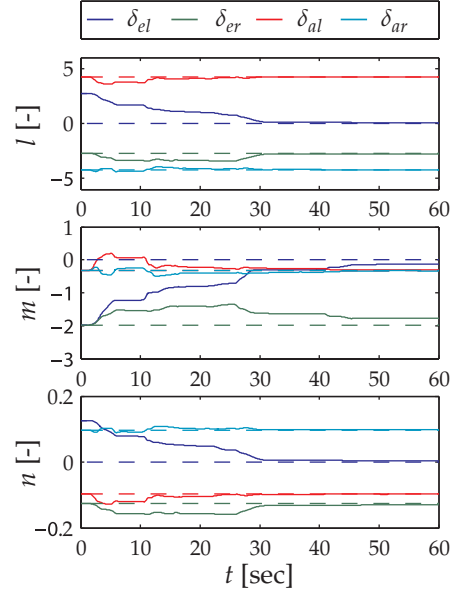
To see if the observations on the total amount of failure scenarios can be a more direct comparison of the tracking error response and parameter estimations for the modular and filtered adaptive backstepping designs is made. One of the severest failures is shown, a trailing-edge down hard-over of the left horizontal stabilizer after 1 second in the simulation. The simulation results for the modular adaptive backstepping design are shown in figure 6.4, the results for the filtered integrated adaptive backstepping design in figure 6.5, both for the QP control allocation method with weight matrix W_{u_2} , favoring aileron deflections. Both control designs manage to stabilize the aircraft quite fast after the failure occurs and both achieve excellent tracking performance after the controller is reconfigured and post-failure transients. The parameter estimates converge to constant values in both designs but only the modular control design has convergence of the parameter estimates to their true values.

6.6 Conclusions

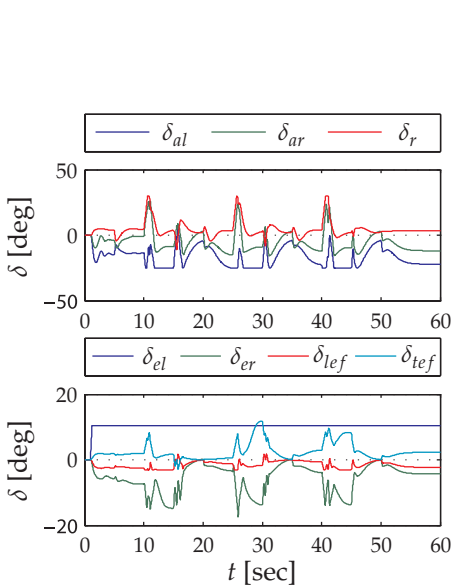
Three nonlinear adaptive control designs for a simple, over-actuated fighter aircraft model with unknown aerodynamic parameters have been studied. Two of these adaptive designs use an integrated Lyapunov based update law, while the other



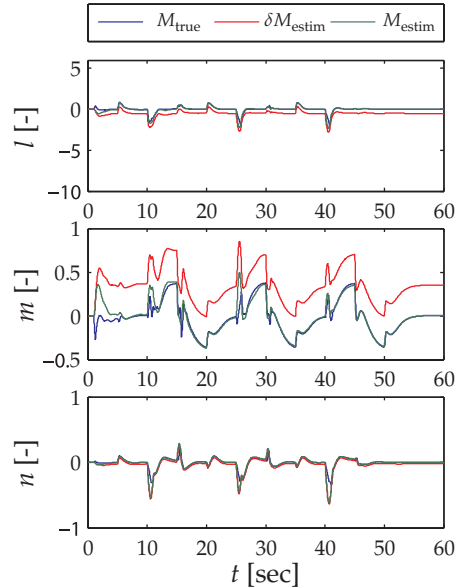
(a) Reference tracking



(b) Parameter estimation

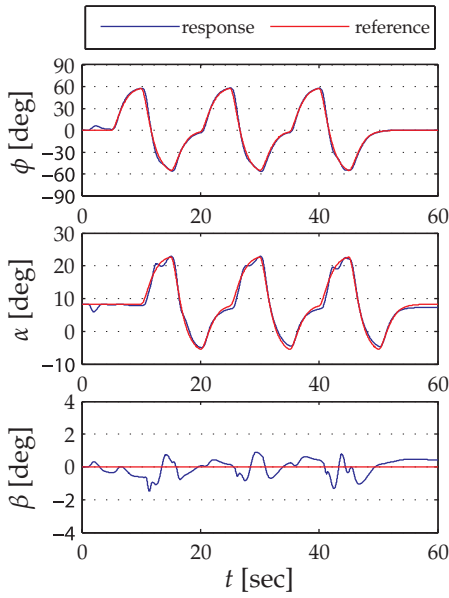


(c) Control surface deflections

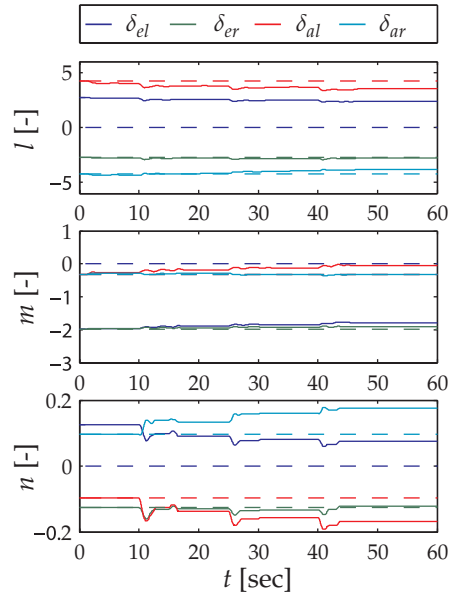


(d) Control moment

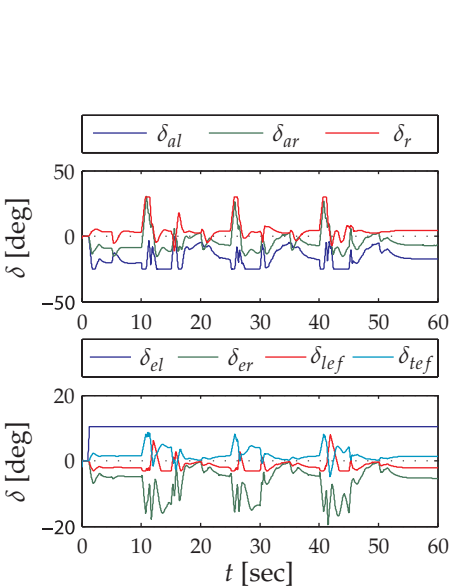
Figure 6.4: Modular adaptive backstepping simulation results for scenario 4, QP_2 control allocation, 10 degree horizontal stabilizer fault.



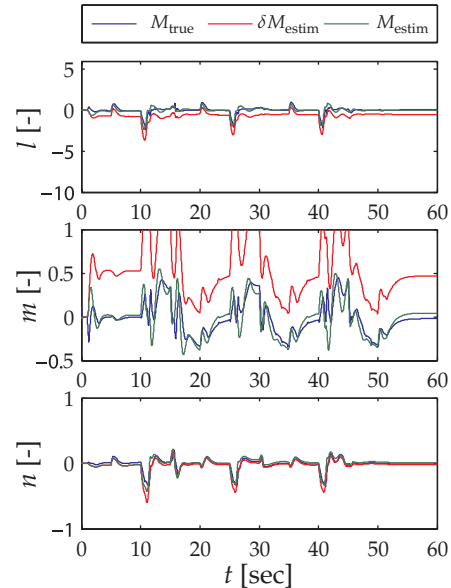
(a) Reference tracking



(b) Parameter estimation



(c) Control surface deflections



(d) Control moment

Figure 6.5: Filtered integrated adaptive backstepping simulation results for scenario 4, QP₂ control allocation, 10 degree horizontal stabilizer fault.

design is modular and uses a least-squares update law. The control designs were combined with two control allocation methods to distribute the desired control effort over the available control surfaces. A comparison based on numerical simulations of the resulting control design and control allocation combinations for different control surface failures has been made. From the comparison, conclusions can be drawn and some recommendations formulated:

- The numerical simulations show that all three adaptive control designs provide a significant improvement over a non-adaptive backstepping or NDI-like design in the presence of actuator lock-up failures. With the pseudo-inverse control allocation the reconfiguration success rate and performance of the adaptive control designs is very similar. However, in combination with more sophisticated control allocation methods the reconfiguration success rate and performance of the modular adaptive design is superior to the integrated designs. This can be mainly explained by the better parameter estimates obtained by the least squares identifier.
- In some simulation cases, the adaptive control designs managed to stabilize the aircraft and were able to track part of the desired trajectories. Following the complete desired maneuver was too challenging for the degraded aircraft. Therefore an adaptive controller alone is not sufficient to improve safety in post-failure flight conditions: both the pilot and guidance system have to be made aware of the failure characteristics and post-failure flight envelope. The problem of determining the aircraft's capabilities, or safe maneuvering envelope, is addressed in part III of this dissertation.
- The integrated adaptive designs do not require nonlinear damping terms in the design to guarantee boundedness of the closed-loop system states. These nonlinear damping terms can possibly result in high-gain feedback control and numerical instability in the modular adaptive design. Furthermore the dynamic order of the modular design with least squares identifier is considerably larger than the integrated designs.
- The choice of control allocation weights has a small influence on the tracking performance after failure when the aircraft can be reconfigured within the limits of the control surfaces and attainable moment envelope. The methods which take constraints into account perform very similar or better than the methods which do not. In the nominal case, hardly any difference was found between the different control allocation methods.
- Tuning of the integrated adaptive control designs turned out to be quite time consuming, even for this relatively simple aircraft model. Increasing the adaptation gain will result in faster parameter convergence, but on the other hand it can lead to undesirable transients in the closed-loop response. An alternative, more modular, approach called Immersion and Invariance Adaptive

Backstepping has been proposed in [163, 166] which was considerably easier to tune at the cost of an increase in the number of controller states.

ADAPTIVE OPTIMIZING NONLINEAR CONTROL DESIGN

In the previous chapter three different adaptive backstepping designs and two control allocation methods were combined, each having been designed separately. In this chapter, the control law design and control allocation are tackled simultaneously and stability of the combined design is shown through Lyapunov analysis. The resulting control designs are applied to the same aircraft model and failures as in the previous chapter, and simulation results are discussed.

7.1 Introduction

Nearly all modern aircraft, ranging from general aviation aircraft to commercial and military jets, have become over-actuated systems. While this facilitates on-line reconfiguration, it creates an additional problem for the control engineer. The main question to be answered is, what is the best way to use the available control effectors to realize the desired control effort? Hence, some kind of cost function should be formulated and optimized subject to the constraint that the total control effort is equal, or as close as possible, to the desired control effort, such that the aircraft handles as intended by the designer.

Optimizing control allocation solutions have been derived for certain classes of over-actuated systems, including aircraft, automotive vehicles and marine vessels [14, 19, 48, 68, 79, 80, 105, 106, 142, 169]. In many of these works, the control allocation problem is viewed as a static or quasi-dynamic optimization problem which is solved independently of the dynamic control problem. Johansen, Fossen, and Berge

[79] showed that it is not necessary to solve the optimization problem exactly at each time instant. The main advantage of this approach is computational efficiency and simple implementation. Furthermore, the method is able to handle non-affine cost functions and control effort mappings when convexity constraints are satisfied. Stability of the closed-loop system is shown through Lyapunov-analysis of a time-varying optimal set composed of the tracking errors, estimation error and first-order derivatives of a Lagrangian cost function.

In this chapter, first of all the problem is presented in mathematical form and some preliminaries are discussed. Afterwards, the non-adaptive high level control with dynamic control allocation scheme is introduced, and its stability and convergence results are analyzed. Then, the non-adaptive control design is extended in three different adaptive designs: integrated, modular, and composite. The composite adaptive approach is applied to the control design of the simple fighter aircraft model of chapter 6. Simulation results for two specific failure cases are demonstrated. Finally, the conclusions are presented and recommendations for future research formulated.

7.2 Problem Definition and Preliminaries

Consider a system in the form

$$\begin{aligned}
 \dot{x}_1 &= f_1(t, x, u) + \varphi_1^T(t, x, u)\theta + g_1(t, x, u)x_2 \\
 \dot{x}_2 &= f_2(t, x, u) + \varphi_2^T(t, x, u)\theta + g_2(t, x, u)x_3 \\
 &\vdots \\
 \dot{x}_{n-1} &= f_{n-1}(t, x, u) + \varphi_{n-1}^T(t, x, u)\theta + g_{n-1}(t, x, u)x_n \\
 \dot{x}_n &= f_n(t, x) + \varphi_n^T(t, x)\theta + g_n(t, x)\tau,
 \end{aligned} \tag{7.1}$$

with $\theta \in \mathbb{R}^p$, and a static mapping from the control effectors u to the virtual controls τ

$$\tau = h(t, x, u, \theta) = \varphi_u^T(t, x, u)\theta + \varphi_0^T(t, x, u). \tag{7.2}$$

Then, the system dynamics can be written in alternative form as $\dot{x} = G(t, x, u, \theta)$. Furthermore, there are actuator dynamics between the control laws and the actual system. The commanded control effector signals u_d are filtered by the actuator model to produce the actual input to the system u . This is modeled as

$$\dot{u} = m(t, x, u, u_d) \tag{7.3}$$

where the function m is assumed to be known, measurements of u are not required by the controller. Additionally, the following assumption is made on the system (7.1).

Assumption 7.1. (*Control Mapping Assumption*) The function h is twice differentiable, and there exist constants $0 < \rho_1 < \rho_2$, such that $\forall t, x, u, \theta$

$$\rho_1 I < \frac{\partial h}{\partial u}(t, x, u, \theta) \left(\frac{\partial h}{\partial u}(t, x, u, \theta) \right)^T \leq \rho_2 I. \quad (7.4)$$

This assumption can be viewed as a controllability assumption in the sense that the mapping h is surjective, and there exists a function $f_u(t, x, \theta)$ such that for all t, x, θ , $h(t, x, f_u(t, x, \theta), \theta) = \tau_d$, where τ_d is the desired control effort. The problem of finding the optimal control allocation is formulated as a static minimization problem as

$$\min_{u_d} J(t, x, u_d) \quad \text{subject to} \quad \tau_d - h(t, x, u_d, \theta) = 0. \quad (7.5)$$

where J is a cost function that incorporates objectives such as minimum power consumption, wear and tear, effects related to actuator configuration (singularity avoidance), and actuator constraints. Based on the optimization problem, the Lagrangian function

$$L(t, x, u_d, \lambda, \hat{\theta}) = J(t, x, u_d) + (h(t, x, u_d, \hat{\theta}) - \tau_d)^T \lambda \quad (7.6)$$

is introduced. The assumptions made on the cost function are

Assumption 7.2. (*Cost Function Assumptions*)

1. The cost function J is twice differentiable and $J(t, x, u_d) \rightarrow \infty$ as $|u_d| \rightarrow \infty$. Furthermore, $\frac{\partial J}{\partial u_d}$, $\frac{\partial^2 J}{\partial i \partial u_d}$ and $\frac{\partial^2 J}{\partial x \partial u_d}$ are uniformly bounded by x and u_d .
2. There exists constants $0 < k_1 < k_2$ such that $\forall t, x, \theta$ and $(u_d^T \lambda^T)^T \notin \mathcal{O}_{u\lambda}^0$, where $\mathcal{O}_{u\lambda} = \left\{ u_d^T, \lambda^T \mid \frac{\partial L}{\partial u_d} = 0, \frac{\partial L}{\partial \lambda} = 0 \right\}$,

$$k_1 I < \frac{\partial^2 L}{\partial u^2}(t, x, u_d, \lambda, \theta) \leq k_2 I, \quad (7.7)$$

where $\mathcal{O}_{u\lambda}^0$ is the interior of $\mathcal{O}_{u\lambda}$. In the interior, the lower bound is replaced by $\frac{\partial^2 L}{\partial u^2} \geq 0$.

The second order sufficient conditions posed by Nocedal and Wright [129] are satisfied for all t, x, u_d, λ and θ by these assumptions. Hence the set $\mathcal{O}_{u\lambda}$ describes global optimal solutions of the problem (7.5). The control problem is to design a controller which is able to track a reference signal $y_r(t) \in \mathbb{C}^n$ asymptotically when the parameters θ are not known, and simultaneously optimize the cost function J .

7.3 Non-adaptive Control Design

In this section the non-adaptive optimizing control design is introduced. First of all the combination of backstepping with optimizing dynamic control allocation approach is derived. The steps up until the final step are identical to the normal backstepping design, where a virtual control law for the desired control effort τ_d is derived. The task of control allocation is to generate commands for the control effectors such that the desired control effort is generated and the cost function is minimized. Closed-loop stability and convergence to the optimal solution can then be shown through Lyapunov analysis.

7.3.1 High-level Control Design

The backstepping design is performed using CLFs of the form

$$V_{i+1}(\bar{z}_1, \dots, \bar{z}_i) = V_i + \frac{1}{2} \bar{z}_i^T \bar{z}_i \quad (7.8)$$

where \bar{z}_i are the augmented tracking errors. More detail and extensive discussion can be found in chapters 3, 4 and 6. The backstepping design ends with a virtual control law for the desired total control effort τ_d . The resulting backstepping control design can be summarized as

$$z_i = x_i - x_{i_c}, \quad (7.9a)$$

$$\bar{z}_i = z_i - \Xi_i, \quad (7.9b)$$

$$\dot{\Xi}_i = -C_1 \Xi_i + g_i (x_{i+1_c} - x_{i+1_c}^0) \quad \text{for } i = 1, \dots, n-1, \quad (7.9c)$$

$$x_{i_c}^0 = \alpha_{i-1} - \Xi_i \quad \text{for } i = 2, \dots, n \quad (7.9d)$$

$$\alpha_i = g_i^{-1} \left(-f_i - \varphi_i^T \hat{\theta} - C_i z_i - g_{i-1}^T \bar{z}_{i-1} + \dot{x}_{i_c} \right) \quad (7.9e)$$

where the desired commands $x_{i_c}^0$ are filtered to produce x_{i_c} and \dot{x}_{i_c} , and the desired control effort $\tau_d = \alpha_n$. If the generated control effort τ is equal to the desired total control effort τ_d , the CLF derivative at the final step becomes

$$\dot{V}_n = - \sum_{i=1}^n \bar{z}_i^T C_i \bar{z}_i \leq 0 \quad \forall \bar{z} \neq 0 \quad (7.10)$$

showing UGAS of the equilibrium $\bar{z} = 0$, which for appropriate filter settings can be used to show stability and convergence of the tracking error z to zero.

7.3.2 Control Allocation Design

The task of the control allocation design is to transform the desired virtual control commands τ_d to actual control effector commands u_d based on the solution of the

optimization problem (7.5). This will be done by considering first-order optimality of the Lagrangian function (7.6). Update laws for the effector reference commands u_d and the Lagrangian parameter λ are then defined, such that u_d and λ converge to a set defined by the time-varying optimality condition. Stability and convergence of the closed loop system is shown for the time and state varying optimal set $\mathcal{A} = \left\{ \left(\bar{z}^T \ u^T \ \lambda^T \right)^T \mid \left(\bar{z}^T \ \frac{\partial L^T}{\partial u} \ \frac{\partial L^T}{\partial \lambda} \right)^T = 0 \right\}$. The design of the update laws is based on the following optimizing control Lyapunov function (OCLF)

$$V_{ca}(t, \bar{z}, \hat{\theta}, u_d, \lambda) = \sigma V_n(t, \bar{z}, \hat{\theta}) + \frac{1}{2} \left(\frac{\partial L^T}{\partial u_d} \frac{\partial L}{\partial u_d} + \frac{\partial L^T}{\partial \lambda} \frac{\partial L}{\partial \lambda} \right), \quad (7.11)$$

which is an extension of the CLF (7.8) with terms penalizing the first order derivatives of the Lagrangian function with respect to the desired control effector signals, and the Lagrangian parameter. The parameter $\sigma > 0$ is an arbitrary design constant used to control the relative weight of the tracking error subsystem in the OCLF. The time derivative of the OCLF along the trajectories of the system (7.1) with the control effector mapping (7.2) is given by

$$\begin{aligned} \dot{V}_{ca} &= \sigma \left(\frac{\partial V_n}{\partial t} + \frac{\partial V_n^T}{\partial \bar{z}} (G(t, x, u, \hat{\theta}) - \dot{x}_c - \dot{\Xi}) \right) \\ &\quad + \left(\frac{\partial L^T}{\partial u_d} \frac{\partial^2 L}{\partial u_d^2} + \frac{\partial L}{\partial \lambda} \frac{\partial^2 L}{\partial u_d \partial \lambda} \right) \dot{u}_d + \frac{\partial L^T}{\partial u_d} \frac{\partial^2 L}{\partial \lambda \partial u_d} \dot{\lambda} \\ &\quad + \left(\frac{\partial L^T}{\partial u_d} \frac{\partial^2 L}{\partial \bar{z} \partial u_d} + \frac{\partial L^T}{\partial \lambda} \frac{\partial^2 L}{\partial \bar{z} \partial \lambda} \right) \dot{\bar{z}} + \frac{\partial L^T}{\partial u_d} \frac{\partial^2 L}{\partial t \partial u_d} + \frac{\partial L^T}{\partial \lambda} \frac{\partial^2 L}{\partial t \partial \lambda} \\ &= -\sigma \sum_{i=1}^n \bar{z}_i^T C_i \bar{z}_i + \begin{bmatrix} \frac{\partial L}{\partial u_d} \\ \frac{\partial L}{\partial \lambda} \end{bmatrix}^T H \begin{bmatrix} \dot{u}_d \\ \dot{\lambda} \end{bmatrix} + \begin{bmatrix} \frac{\partial L}{\partial u_d} \\ \frac{\partial L}{\partial \lambda} \end{bmatrix}^T u_{ff} \end{aligned} \quad (7.12)$$

where

$$H = \begin{bmatrix} \frac{\partial^2 L}{\partial u_d^2} & \frac{\partial^2 L}{\partial \lambda \partial u_d} \\ \frac{\partial^2 L}{\partial u_d \partial \lambda} & 0 \end{bmatrix}$$

x_c is composed of y_r and the x_{i_c} , and, when $\det \left(\frac{\partial^2 L}{\partial u_d^2} \right) \geq \epsilon$

$$u_{ff} = \begin{bmatrix} \frac{\partial^2 L}{\partial t \partial u_d} \\ \frac{\partial^2 L}{\partial t \partial \lambda} \end{bmatrix} + \begin{bmatrix} \frac{\partial^2 L}{\partial \bar{z} \partial u_d} \\ \frac{\partial^2 L}{\partial \bar{z} \partial \lambda} \end{bmatrix} (G(t, x, u, \hat{\theta}) - \dot{x}_c - \dot{\Xi})$$

, else $u_{\text{ff}} = 0$. The update laws for u_d and λ now follow straightforward from the OCLF derivative, where they are used to cancel the known parts related to the cost function partial derivatives:

$$\begin{bmatrix} \dot{u}_d \\ \dot{\lambda} \end{bmatrix} = -\Gamma_{\text{ca}} H \begin{bmatrix} \frac{\partial L}{\partial u_d} \\ \frac{\partial L}{\partial \lambda} \end{bmatrix} - H^{-1} u_{\text{ff}}. \quad (7.13)$$

where Γ_{ca} is a symmetric, positive definite gain matrix. Additionally, the actuator model has been used to remove the effect of the actuator dynamics on the tracking error. Therefore, the effect of the actuator and control allocation dynamics on the tracking error is removed by the filter

$$\dot{\Xi}_n = -C_n \Xi_n + (h(t, x, u, \hat{\theta}) - \tau_d), \quad (7.14)$$

where $\hat{\theta}$ is a fixed estimate of the parameter θ in the non-adaptive design. The matrix Γ_{ca} can be time-varying to speed up convergence. For example if $\Gamma_{\text{ca}} = \gamma (H^T H)^{-1}$ for some $\gamma > 0$, then

$$\begin{bmatrix} \dot{u}_d \\ \dot{\lambda} \end{bmatrix} = -\gamma H^{-1} \begin{bmatrix} \frac{\partial L}{\partial u_d} \\ \frac{\partial L}{\partial \lambda} \end{bmatrix} - H^{-1} u_{\text{ff}} \quad (7.15)$$

where the first term is the Newton direction when L is considered the cost function to be minimized. In the case $H^T H$ is poorly conditioned, the choice $\Gamma_{\text{ca}} = \gamma (H^T H + \zeta I)^{-1}$ for a small $\zeta > 0$ can be made. Using the design (7.9), (7.13), (7.14), the OCLF derivative becomes

$$\dot{V}_{\text{ca}} = -\sigma \sum_{i=1}^n \bar{z}_i^T C_i \bar{z}_i - \begin{bmatrix} \frac{\partial L}{\partial u_d} \\ \frac{\partial L}{\partial \lambda} \end{bmatrix}^T H \Gamma_{\text{ca}} H \begin{bmatrix} \frac{\partial L}{\partial u_d} \\ \frac{\partial L}{\partial \lambda} \end{bmatrix}, \quad (7.16)$$

which shows that the set \mathcal{A} is UGAS and therefore the augmented tracking error will converge to zero when $t \rightarrow \infty$. For appropriate choices of the virtual command filters, controller gains, and within the set of constraints on x and u , Ξ is small and therefore the tracking error z_1 converges to a small neighborhood around zero. The first order partial derivatives of the cost function with respect the desired control commands and the Lagrangian parameter converge to zero, and due to the cost function being convex, the desired commands and Lagrangian parameter converge to the optimal solution.

7.4 Adaptive Control Design

So far, it has been assumed in the design that the parameter θ was known. If the parameter θ is (partially) unknown, the control design from the previous section

is not implementable. Hence, an estimate $\hat{\theta}$ and corresponding update law are introduced. Three different adaptation laws are presented, in the first the parameter update is designed simultaneously with the control laws: the integrated design. In the second design, modularity between the control laws and the identifier is achieved by means of introducing additional nonlinear damping terms, allowing non-Lyapunov based identifiers to be applied. Finally, a hybrid combination of the two former designs is proposed which has better convergence properties as it uses information from both sources to update the estimate, and does not require nonlinear damping terms.

7.4.1 Integrated Update Law

The Lyapunov-based update laws for the integrated adaptive design method are designed by extending the OCLF (7.11) with additional terms that penalize the parameter estimation error, yielding an adaptive optimizing CLF (AOCLF)

$$V_{\text{int}} = V_{\text{ca}} + \frac{1}{2} \text{tr} \left(\tilde{\theta}^T \Gamma_{\theta}^{-1} \tilde{\theta} \right) \quad (7.17)$$

where $\Gamma_{\theta}^T = \Gamma_{\theta} > 0$ is the update gain matrix, and $\tilde{\theta} = \theta - \hat{\theta}$. In this case, the task is to stabilize the set \mathcal{A}_{int} defined by

$$\mathcal{A}_{\text{int}} = \{ \eta \in \mathbb{R}^q \mid Q(\eta) = 0 \} \quad (7.18)$$

where $\eta = \left(\bar{z}^T \tilde{\theta}^T u_d^T \lambda^T \right)^T$, and $Q(\eta) = \left(\bar{z}^T \tilde{\theta}^T \frac{\partial L^T}{\partial u_d} \frac{\partial L^T}{\partial \lambda} \right)^T$. Taking the time derivative of (7.17), results in

$$\begin{aligned} \dot{V}_{\text{int}} = & -\sigma \sum_{i=1}^n \bar{z}_i^T C_i \bar{z}_i - \left[\begin{array}{c} \frac{\partial L}{\partial u_d} \\ \frac{\partial L}{\partial \lambda} \end{array} \right]^T H \Gamma_{\text{ca}} H \left[\begin{array}{c} \frac{\partial L}{\partial u_d} \\ \frac{\partial L}{\partial \lambda} \end{array} \right] - \text{tr} \left(\tilde{\theta}^T \Gamma_{\theta}^{-1} \dot{\tilde{\theta}} \right) + \sigma \sum_{i=1}^n \left(\bar{z}_i^T \varphi_i^T \tilde{\theta} \right) \\ & + \left(\frac{\partial L^T}{\partial u_d} \frac{\partial^2 L}{\partial x \partial u_d} + \frac{\partial L^T}{\partial \lambda} \frac{\partial^2 L}{\partial x \partial \lambda} \right) \varphi_u^T \tilde{\theta} + \left(\frac{\partial L^T}{\partial u_d} \frac{\partial^2 L}{\partial \hat{\theta} \partial u_d} + \frac{\partial L^T}{\partial \lambda} \frac{\partial^2 L}{\partial \hat{\theta} \partial \lambda} \right) \hat{\theta} \end{aligned} \quad (7.19)$$

where the parameter update law is used to cancel the indefinite parts, and the control allocation update law feed-forward signal now includes the parameter estimate

update:

$$\dot{\hat{\theta}} = \Gamma_{\theta} \left(\sigma \sum_{i=1}^n \varphi_i \bar{z}_i + \varphi_u \left(\frac{\partial^2 L^T}{\partial x \partial u_d} \frac{\partial L}{\partial u_d} + \frac{\partial^2 L^T}{\partial x \partial \lambda} \frac{\partial L}{\partial \lambda} \right) \right) \quad (7.20)$$

$$\begin{bmatrix} \dot{u}_d \\ \dot{\lambda} \end{bmatrix} = -\Gamma_{ca} H \begin{bmatrix} \frac{\partial L}{\partial u_d} \\ \frac{\partial L}{\partial \lambda} \end{bmatrix} - H^{-1} u_{ff}, \quad (7.21)$$

$$\begin{aligned} u_{ff} &= \begin{bmatrix} \frac{\partial^2 L}{\partial t \partial u_d} \\ \frac{\partial^2 L}{\partial t \partial \lambda} \end{bmatrix} + \begin{bmatrix} \frac{\partial^2 L}{\partial \bar{z} \partial u_d} \\ \frac{\partial^2 L}{\partial \bar{z} \partial \lambda} \end{bmatrix} (G(t, x, u, \hat{\theta}) - \dot{y}_r - \dot{\Xi}) \\ &+ \begin{bmatrix} \frac{\partial^2 L}{\partial \hat{\theta} \partial u_d} \\ \frac{\partial^2 L}{\partial \hat{\theta} \partial \lambda} \end{bmatrix} \dot{\hat{\theta}}. \end{aligned} \quad (7.22)$$

This choice of update laws results in the AOCLF time derivative

$$\dot{V}_{\text{int}} = -\sigma \sum_{i=1}^n \bar{z}_i^T C_i \bar{z}_i - \begin{bmatrix} \frac{\partial L}{\partial u_d} \\ \frac{\partial L}{\partial \lambda} \end{bmatrix}^T H \Gamma_{ca} H \begin{bmatrix} \frac{\partial L}{\partial u_d} \\ \frac{\partial L}{\partial \lambda} \end{bmatrix}, \quad (7.23)$$

which shows UGS of the set \mathcal{A}_{int} . From LaSalle-Yoshizawa's theorem 3.3 it follows that when $t \rightarrow \infty$, all solutions converge to the manifold $\begin{bmatrix} \bar{z}^T \frac{\partial L}{\partial u_d} \frac{\partial L}{\partial \lambda} \end{bmatrix}^T = 0$. It is possible to conclude UGAS of \mathcal{A}_{int} for the integrated design when certain PE conditions are satisfied, and then demonstrating that the estimation error $\varphi^T \tilde{\theta}$ converges to zero, see e.g. [186, 187].

7.4.2 Modular Update Law

The modular adaptive design aims to separate the identifier from the the Lyapunov design, to allow non-Lyapunov based parameter update laws. In order to achieve this for general nonlinear systems, nonlinear damping terms are required to make the control design robust against parameter estimation errors, see chapter 4 and 6. In this case, these nonlinear damping terms are required *both* in the high level design and the control allocation update laws. First of all swapping filters are introduced since the state derivatives are, in general, not measurable or directly available. These swapping filters are nearly identical to the swapping filters derived in chapter 4 and used in chapter 6. Two filters and a static mapping are introduced

$$\dot{\Omega}_0 = A(\Omega_0 + x) - f(t, x, u) \quad (7.24a)$$

$$\dot{\Omega}^T = A\Omega^T + F^T(t, x, u) \quad (7.24b)$$

where

$$f(t, x, u) = \begin{bmatrix} f_1(t, x, u) + g_1(t, x, u)x_2 \\ \vdots \\ f_n(t, x) + g_n(t, x)\varphi_0^T(t, x, u) \end{bmatrix},$$

$$F^T(t, x, u) = \begin{bmatrix} \varphi_1^T(t, x, u) \\ \vdots \\ \varphi_n^T(t, x) + g_n(t, x)\varphi_u^T(t, x, u) \end{bmatrix}$$

and the estimation error is defined as

$$\epsilon = (\Omega_0 + x) - \Omega^T \hat{\theta} = \Omega^T \tilde{\theta} + \tilde{\epsilon} \quad (7.25)$$

with $\tilde{\epsilon} = (\Omega_0 + x) - \Omega^T \theta$. The matrix A is negative definite, and strengthened

$$A(t, x) = A_0 - \rho F^T(t, x, u)F(t, x, u)P \quad (7.26)$$

where $\rho > 0$, and P is a constant matrix such that

$$PA_0 + A_0^T P = -I, \quad P = P^T > 0. \quad (7.27)$$

This allows the following update laws to be used, which guarantee boundedness of the estimation error

$$\dot{\hat{\theta}} = \Gamma_\theta \Omega \epsilon \quad (7.28)$$

for a gradient based update law with Γ_θ a positive definite, symmetric matrix, and

$$\dot{\hat{\theta}} = \Gamma_\theta \Omega \epsilon \quad (7.29)$$

$$\dot{\Gamma}_\theta = -\Gamma_\theta \Omega \Omega^T \Gamma_\theta \quad (7.30)$$

for a least-squares update law. Additionally, the high-level virtual control laws and control allocation update laws are augmented with nonlinear damping terms to achieve the desired separation. The virtual control laws become

$$\alpha_i = g_i^{-1} \left(-f_i - \varphi_i^T \hat{\theta} - C_i z_i - S_i \bar{z}_i - g_{i-1}^T \bar{z}_{i-1} + \dot{x}_{i_c} \right) \quad (7.31)$$

where the nonlinear damping matrices S_i are defined as

$$S_i = \varphi_i^T \kappa_i \varphi_i \quad (7.32)$$

and $\kappa_i = \kappa_i^T > 0$ are the nonlinear damping gain matrices of size $\mathbb{R}^{(p \times p)}$. Additional nonlinear damping is added in the design of the desired virtual control effort τ_d , such that S_n becomes

$$S_n = \varphi_i^T \kappa_i \varphi_i + \varphi_u^T \kappa_u \varphi_u. \quad (7.33)$$

The update laws for control allocation become

$$\begin{bmatrix} \dot{u}_d \\ \dot{\lambda} \end{bmatrix} = -\Gamma_{ca} H \begin{bmatrix} \frac{\partial L}{\partial u_d} \\ \frac{\partial L}{\partial \lambda} \end{bmatrix} - H^{-1} (u_{ff} + u_\kappa) \quad (7.34)$$

where u_{ff} is the same as for the non-adaptive control design, and u_κ is the contribution due to nonlinear damping defined as

$$u_\kappa = \begin{bmatrix} \frac{\partial^2 L}{\partial x \partial u_d} \\ \frac{\partial^2 L}{\partial x \partial \lambda} \end{bmatrix}^T \varphi_u^T \kappa_{u_d} \varphi_u \begin{bmatrix} \frac{\partial^2 L}{\partial x \partial u_d} \\ \frac{\partial^2 L}{\partial x \partial \lambda} \end{bmatrix} \begin{bmatrix} \frac{\partial L}{\partial u_d} \\ \frac{\partial L}{\partial \lambda} \end{bmatrix}. \quad (7.35)$$

Boundedness of $\Omega, \tilde{\epsilon}, \tilde{\theta}$, boundedness and square-integrability of ϵ and $\hat{\theta}$ has already been shown in chapter 4. Using the designed update laws for the parameter estimate, the high-level control laws, and the control allocation update laws, ISS of the set $\mathcal{A}_{\text{mod}} = \mathcal{A}$ with respect to the parameter estimation error and its derivative is shown by means of the following OCLF

$$V_{\text{mod}} = V_{ca}. \quad (7.36)$$

The derivative of the OCLF along the trajectories of the system (7.1), the virtual control laws (7.31), and the control allocation update laws (7.34) becomes

$$\begin{aligned} \dot{V}_{\text{mod}} &= -\sigma \sum_{i=1}^n \bar{z}_i^T C_i \bar{z}_i - \sigma \sum_{i=1}^n \bar{z}_i^T S_i \bar{z}_i + \sigma \sum_{i=1}^n \left(\bar{z}_i^T \varphi_i^T \tilde{\theta} \right) \\ &\quad + \left(\frac{\partial L^T}{\partial u_d} \frac{\partial^2 L}{\partial x \partial u_d} + \frac{\partial L^T}{\partial \lambda} \frac{\partial^2 L}{\partial x \partial \lambda} \right) \varphi_u^T \tilde{\theta} + \left(\frac{\partial L^T}{\partial u_d} \frac{\partial^2 L}{\partial \hat{\theta} \partial u_d} + \frac{\partial L^T}{\partial \lambda} \frac{\partial^2 L}{\partial \hat{\theta} \partial \lambda} \right) \hat{\theta} \\ &\quad - \begin{bmatrix} \frac{\partial L}{\partial u_d} \\ \frac{\partial L}{\partial \lambda} \end{bmatrix}^T H \Gamma_{ca} H \begin{bmatrix} \frac{\partial L}{\partial u_d} \\ \frac{\partial L}{\partial \lambda} \end{bmatrix} - \begin{bmatrix} \frac{\partial L}{\partial u_d} \\ \frac{\partial L}{\partial \lambda} \end{bmatrix}^T u_\kappa \\ &= -\sigma \sum_{i=1}^n \bar{z}_i^T C_i \bar{z}_i - \sigma \sum_{i=1}^n \left(\varphi_i \bar{z}_i - \frac{1}{2} \kappa_i^{-1} \tilde{\theta} \right)^T \kappa_i \left(\varphi_i \bar{z}_i - \frac{1}{2} \kappa_i^{-1} \tilde{\theta} \right) \end{aligned}$$

$$\begin{aligned}
& + \frac{\sigma}{4} \sum_{i=1}^n \tilde{\theta}^T \kappa_i^{-1} \tilde{\theta} - \sigma \left(\varphi_u \bar{z}_n - \frac{1}{2} \kappa_u^{-1} \tilde{\theta} \right)^T \kappa_u \left(\varphi_u \bar{z}_n - \frac{1}{2} \kappa_u^{-1} \tilde{\theta} \right) \\
& + \frac{\sigma}{4} \tilde{\theta}^T \kappa_u^{-1} \tilde{\theta} - \left[\begin{array}{c} \frac{\partial L}{\partial u_d} \\ \frac{\partial L}{\partial \lambda} \end{array} \right]^T H \Gamma_{ca} H \left[\begin{array}{c} \frac{\partial L}{\partial u_d} \\ \frac{\partial L}{\partial \lambda} \end{array} \right] \\
& - \left(\varphi_u \left[\begin{array}{c} \frac{\partial^2 L}{\partial x \partial u_d} \\ \frac{\partial^2 L}{\partial x \partial \lambda} \end{array} \right]^T \left[\begin{array}{c} \frac{\partial L}{\partial u_d} \\ \frac{\partial L}{\partial \lambda} \end{array} \right] - \frac{1}{2} \kappa_u^{-1} \tilde{\theta} \right)^T \kappa_u \left(\varphi_u \left[\begin{array}{c} \frac{\partial^2 L}{\partial x \partial u_d} \\ \frac{\partial^2 L}{\partial x \partial \lambda} \end{array} \right]^T \left[\begin{array}{c} \frac{\partial L}{\partial u_d} \\ \frac{\partial L}{\partial \lambda} \end{array} \right] - \frac{1}{2} \kappa_u^{-1} \tilde{\theta} \right) \\
& + \frac{1}{4} \tilde{\theta}^T \kappa_u^{-1} \tilde{\theta} \\
\leq & -\sigma \sum_{i=1}^n \bar{z}_i^T C_i \bar{z}_i + \frac{\sigma}{4} \sum_{i=1}^n \tilde{\theta}^T \kappa_i^{-1} \tilde{\theta} + \frac{\sigma}{4} \tilde{\theta}^T \kappa_u^{-1} \tilde{\theta} + \frac{1}{4} \tilde{\theta}^T \kappa_u^{-1} \tilde{\theta} \\
& - \left[\begin{array}{c} \frac{\partial L}{\partial u_d} \\ \frac{\partial L}{\partial \lambda} \end{array} \right]^T H \Gamma_{ca} H \left[\begin{array}{c} \frac{\partial L}{\partial u_d} \\ \frac{\partial L}{\partial \lambda} \end{array} \right]
\end{aligned} \tag{7.37}$$

From the last inequality, a positively invariant compact set can be derived to which the augmented tracking errors and control allocation states will exponentially converge. From (7.37)

$$\sigma c_0 \bar{z}^T \bar{z} + \gamma_0 \left(\frac{\partial L^T}{\partial u_d} \frac{\partial L}{\partial u_d} + \frac{\partial L^T}{\partial \lambda} \frac{\partial L}{\partial \lambda} \right) \geq \frac{1}{4} \tilde{\theta}^T \kappa_0^{-1} \tilde{\theta} \tag{7.38}$$

where $c_0 = \min_i \lambda_{\min}(C_i) \geq 0$, $\gamma_0 = \inf_t \lambda_{\min}(H \Gamma_{ca} H)$, $\kappa_0^{-1} = \sigma \sum_{i=1}^n \kappa_i^{-1} + \sigma \kappa_u^{-1} + \kappa_{u_d}^{-1}$ implies that $\dot{V} \leq 0$. Hence, the inequality therefore describes an upper bound on the invariant compact set. ISS-stability of the set \mathcal{A}_{mod} can be shown using an ISS-Lyapunov function, see appendix A.5, since existence of such a function is equivalent to the system being ISS [88, 168], if \mathcal{A}_{mod} is compact, and 0-invariant.

7.4.3 Composite Update Law

The designs above can be combined as discussed in chapter 4. This has the benefit that the nonlinear damping terms are no longer required for stability, and faster convergence of the tracking errors as well as estimation error can be achieved. The composite design makes use of the nonlinear swapping filters (7.24), and has a composite update law defined as

$$\dot{\hat{\theta}} = \Gamma_{\theta} \left(\sigma \sum_{i=1}^n \varphi_i \bar{z}_i + \varphi_u \left(\frac{\partial^2 L^T}{\partial x \partial u_d} \frac{\partial L}{\partial u_d} + \frac{\partial^2 L^T}{\partial x \partial \lambda} \frac{\partial L}{\partial \lambda} \right) + \Omega \Psi \epsilon \right) \tag{7.39}$$

with $\Psi = \Psi^T > 0$ a weight matrix to control how the adaptation law should weight information from the tracking error relative to the information coming from the

estimation error. The update gain matrix Γ_θ can be kept constant for a gradient approach or updated through the weighted least-squares update law

$$\dot{\Gamma}_\theta = -\Gamma_\theta \Omega \Psi \Omega^T \Gamma_\theta. \quad (7.40)$$

The control allocation update laws are identical to the ones in the integrated adaptive design. The AOCLF from the integrated design is augmented with a term penalizing the residual error $\tilde{\epsilon} = \Omega_0 + x - \Omega^T \theta$,

$$V_{\text{comp}} = V_{\text{int}} + \frac{1}{2} \tilde{\epsilon}^T P \Psi \tilde{\epsilon}. \quad (7.41)$$

This AOCLF will be used to show UGS of the set

$$\mathcal{A}_{\text{comp}} = \left\{ \left(\bar{z}^T \tilde{\epsilon}^T \tilde{\theta}^T u_d^T \lambda^T \right)^T \mid \left(\bar{z}^T \tilde{\theta} \tilde{\epsilon}^T \frac{\partial L^T}{\partial u_d} \frac{\partial L^T}{\partial \lambda} \right)^T = 0 \right\}. \quad (7.42)$$

The time derivative of V_{comp} along the solutions of the system, with the integrated control laws and composite update laws becomes

$$\begin{aligned} \dot{V}_{\text{comp}} &= -\sigma \sum_{i=1}^n \bar{z}_i^T C_i \bar{z}_i - \frac{1}{2} \epsilon^T \Psi \Omega^T \tilde{\theta} - \frac{1}{2} \tilde{\theta}^T \Omega \Psi \tilde{\epsilon} + \frac{1}{2} \left(\tilde{\epsilon}^T P \Psi \tilde{\epsilon} + \tilde{\epsilon}^T \Psi P \tilde{\epsilon} \right) \\ &\quad - \begin{bmatrix} \frac{\partial L}{\partial u_d} \\ \frac{\partial L}{\partial \lambda} \end{bmatrix}^T H \Gamma_{\text{ca}} H \begin{bmatrix} \frac{\partial L}{\partial u_d} \\ \frac{\partial L}{\partial \lambda} \end{bmatrix} \\ &\leq -\sigma \sum_{i=1}^n \bar{z}_i^T C_i \bar{z}_i - \frac{1}{2} \epsilon^T \Psi \epsilon + \frac{1}{2} \tilde{\epsilon}^T \Psi \tilde{\epsilon} - \frac{1}{2} \tilde{\epsilon}^T \Psi \tilde{\epsilon} - \begin{bmatrix} \frac{\partial L}{\partial u_d} \\ \frac{\partial L}{\partial \lambda} \end{bmatrix}^T H \Gamma_{\text{ca}} H \begin{bmatrix} \frac{\partial L}{\partial u_d} \\ \frac{\partial L}{\partial \lambda} \end{bmatrix} \\ &= -\sigma \sum_{i=1}^n \bar{z}_i^T C_i \bar{z}_i - \frac{1}{2} \epsilon^T \Psi \epsilon - \begin{bmatrix} \frac{\partial L}{\partial u_d} \\ \frac{\partial L}{\partial \lambda} \end{bmatrix}^T H \Gamma_{\text{ca}} H \begin{bmatrix} \frac{\partial L}{\partial u_d} \\ \frac{\partial L}{\partial \lambda} \end{bmatrix} \end{aligned} \quad (7.43)$$

showing UGS of the set $\mathcal{A}_{\text{comp}}$. The fact that the dynamics of $\tilde{\epsilon}$ are governed by (4.79) has been used to provide an upper bound on part of the AOCLF time derivative. From the LaSalle-Yoshizawa theorem it follows that when $t \rightarrow \infty$, all solutions converge to the manifold $\left[\bar{z}^T \epsilon^T \frac{\partial L^T}{\partial u_d} \frac{\partial L^T}{\partial \lambda} \right]^T = 0$. Note that the major difference between the integrated and composite designs is that in the composite design also convergence of the estimation error to zero is guaranteed. Convergence of the parameter estimation error $\tilde{\theta}$ to zero can only be guaranteed when a PE condition is satisfied.

7.5 Fighter Aircraft Model Application

The backstepping high-level control scheme with optimizing dynamic control allocation with composite update laws is applied in the control design for the aircraft

model introduced in section 6.2. The performance of the control design is evaluated at the lowest altitude flight condition, flight condition I , for the same failure scenarios as used in the previous chapter. Since the control allocation method discussed in this chapter is not able to handle actuator rate constraints, these have been removed from the design.

7.5.1 Controller Design

The control design follows the nominal backstepping design presented in chapter 6 for the high level control design. This design is extended with dynamic control allocation and parameter estimation laws according to the composite adaptive design. The following cost function has been used

$$J(u_d) = u_d^T W u_d + J_2(u_d) \quad (7.44)$$

where $W = W^T > 0$, and J_2 includes the magnitude constraints for this aircraft by means of barrier functions

$$J_2(u_d) = -w \ln(u_d - u_{d,\min}) - w \ln(-u_d + u_{d,\max}) \quad (7.45)$$

where $w > 0$ is a tuning gain, $u_{d,\min}$ and $u_{d,\max}$ represent the lower and upper bound on u_d respectively.

The numerical simulations have been performed in the MATLAB/Simulink environment, with an adaptive time-step, third-order accurate solver. The tuning parameters summarized in table 7.1 were used in the design. Additionally, covariance resetting was introduced to speed-up the estimation after a failure is detected. When a low-pass filtered version of the squared estimation error exceeds a certain threshold, and the covariance matrix is small, it is reset. Hence, the covariance matrix will only be reset if there is confidence in the estimated parameters, and there is a large estimation error.

7.5.2 Nominal Simulation Results

Before considering actuator failures, the nominal simulation results are presented. The parameter vector is initialized with the values used in the model, hence, the on-board and the actual aircraft model are identical. The tracking performance for the aircraft performing three simultaneous angle of attack and bank angle doublets is shown in figure 7.1. The desired references are tracked nearly perfect, and the sideslip angle is kept very close to zero during the whole maneuver. Due to the aircraft model and on-board model being identical, the composite adaptive controller does not update the on-board model parameters. The commanded control deflections and the realized deflections are shown in figure 7.2. Note that for this controller tuning and reference signal the leading and trailing edge flaps contribute significantly to the realized control effort.

Table 7.1: Adaptive Optimizing Controller Tuning Parameters

Parameter	Value
C_1	I_3
C_2	$2I_3$
S_0	$1 \times 10^{-1} I_{36}$
γ	500
w	$0.1 \cdot \text{diag}(1 \ 1 \ 1 \ 1 \ 1 \ 1 \ 1)$
W	$\text{diag}(1 \ 1 \ 2 \ 2 \ 2 \ 2 \ 1)$
A_0	$-100I_6$
ρ	10000
ϵ_{\min}	1×10^{-6}
Γ_{reset}	$10S_0S_0$
S_{reset}	$10I_{36}$
R	1000
λ	0.005

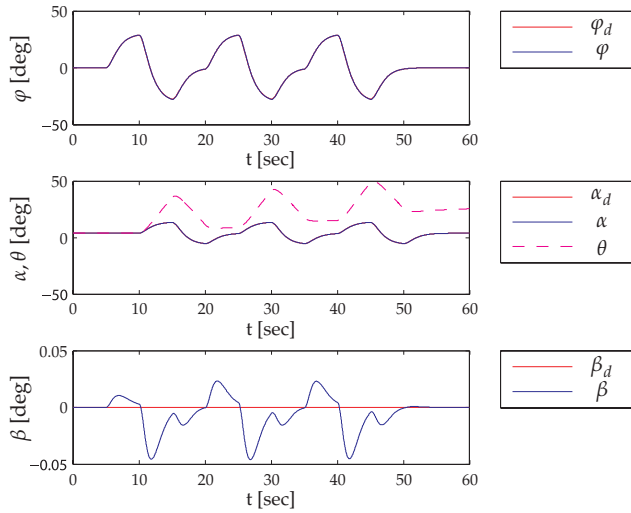


Figure 7.1: Tracking performance of the composite adaptive optimizing controller in the nominal case.

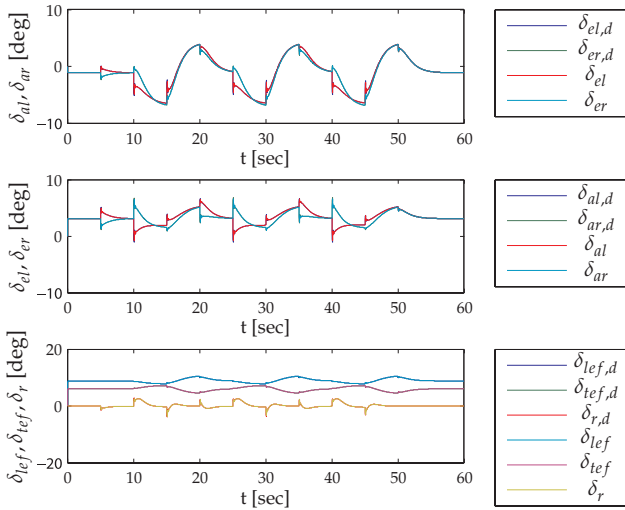


Figure 7.2: Control deflections commands and positions in the nominal case.

7.5.3 Elevator Failure

Several elevator lock-in-place failures have been investigated, only the severest considered failure is discussed here. After three seconds in the simulation, the left elevator deflects to -20 degrees and locks there. Hence, a trim moment is introduced, and the effectiveness of the left elevator seems zero. This failure is detected rapidly by the change detection mechanism, and the update gain matrix is reset. After the failure is detected, the controller reconfigures very quickly and is able to complete the maneuver with excellent tracking performance as shown in figure 7.3. After the failure is injected and detected there are fast transients in the estimated parameters, as observed in figure 7.4. After the estimates have settled near their values sufficient for convergence of the augmented tracking error, they will start converging to their true values if a PE condition is satisfied. The control deflections used by the controller are shown in figure 7.5.

7.5.4 Aileron Failure

Similar as for the elevator failures, aileron actuator failures have been investigated. Once again, only the worst case failure is discussed here. After three seconds into the maneuver, the left aileron deflects to 45 degrees trailing edge down. A transient can be observed from figure 7.6 after injection of the failure. The controller rapidly reconfigures and is able to track the reference commands very well. The failure is accommodated by asymmetric deflection of the elevators, with help from

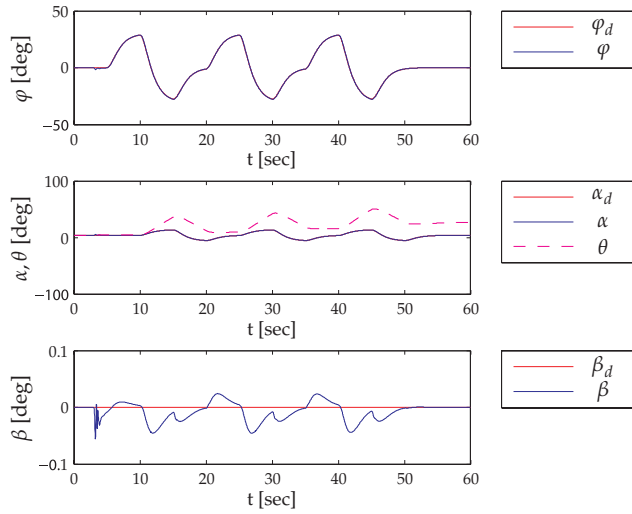


Figure 7.3: Tracking performance of the composite adaptive optimizing controller for a left elevator lock to -20 degrees after 3 seconds.

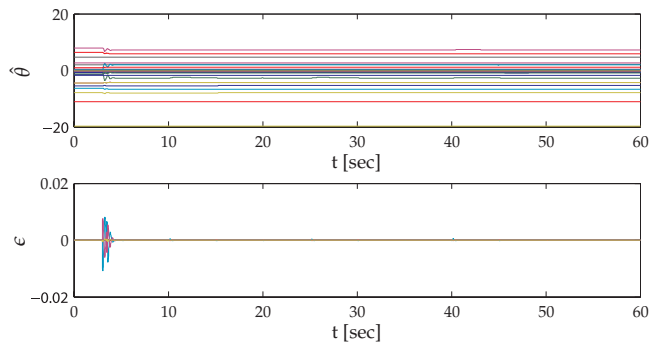


Figure 7.4: Parameter estimates and filtered estimation error for a left elevator lock to -20 degrees after 3 seconds.

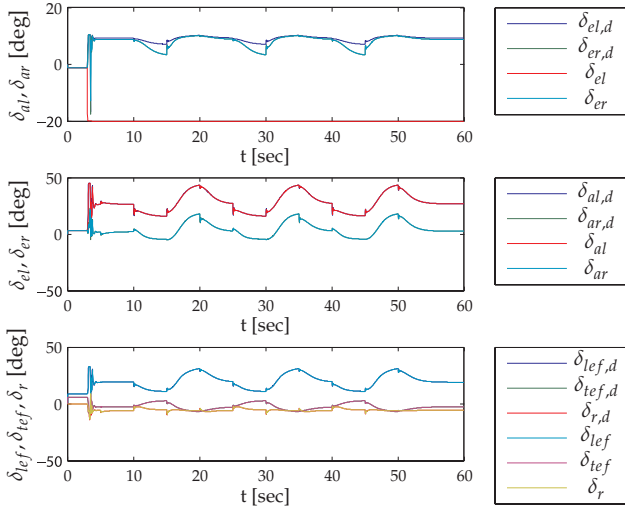


Figure 7.5: Control deflections commands and positions for a left elevator lock to -20 degrees after 3 seconds.

the remaining functional aileron as shown in figure 7.8. The parameter estimates and filtered estimation error are shown in figure 7.7, after initial transients the parameter estimates start converging to their true values and the filtered estimation error converges to zero.

7.6 Conclusions

In this chapter three adaptive control designs have been proposed for over-actuated systems with uncertain parameters, and these methods have been applied to the same aircraft model as in the previous chapter. The control design has been separated into a high-level control law, dynamic control allocation update laws, and an parameter update law. Stability of the time-varying optimal sets has been proven through Lyapunov analysis. Based on the designs and the obtained simulation results, the following observations can be made:

- Closed loop boundedness of the tracking errors can be proven by means of AOCLFs. Since the state and control effectors of a system are generally bounded, locally asymptotic tracking of the desired reference signal can be concluded. The optimizing control allocation algorithm is also defined by means of a Lyapunov function, and it does *not* solve the optimization problem exactly at each step but rather (continuously) converges to the time varying optimal solution.

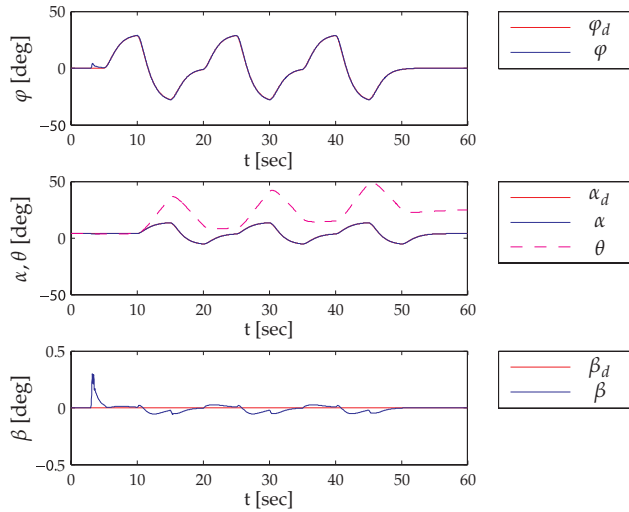


Figure 7.6: Tracking performance of the composite adaptive optimizing controller for a left aileron lock to 45 degrees after 3 seconds.

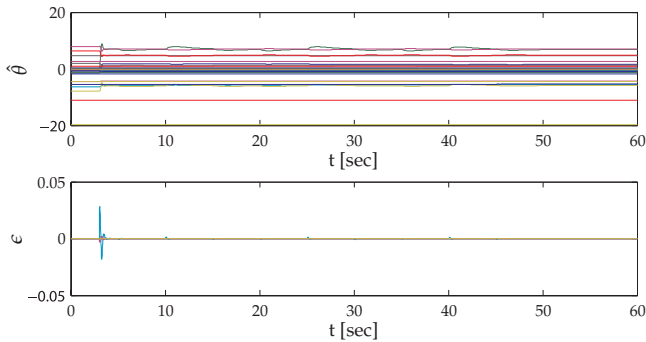


Figure 7.7: Parameter estimates and filtered estimation error for a left aileron lock to 45 degrees after 3 seconds.

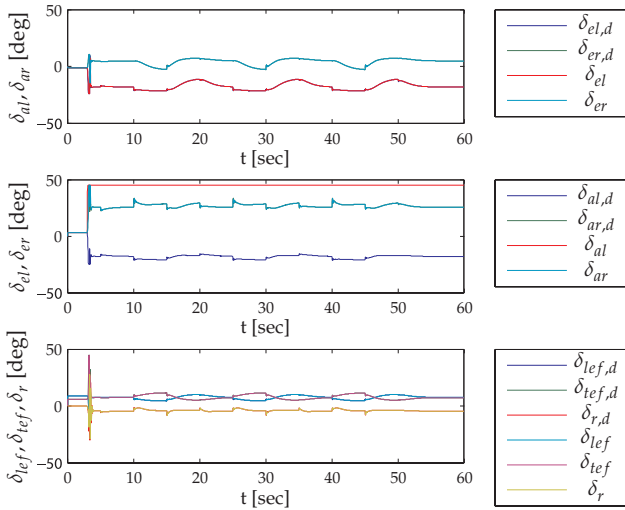


Figure 7.8: Control deflections commands and positions for a left aileron lock to 45 degrees after 3 seconds.

- The tracking performance of the adaptive control design is excellent for the nominal case and all considered failure cases. The failures are identified shortly after they are introduced to the system, and the new dynamics are rapidly identified.
- The composite adaptive design has the best convergence properties and does not require nonlinear damping to achieve this. The dynamic order of the resulting controller is equal to that of the modular adaptive design, and considerably higher than the integrated design due to inclusion of the update gain Γ_θ as states of the controller.
- The control allocation algorithm is not iterative, and does not depend on optimization software.

Some extensions of the work presented are suggested.

- The considered control scheme requires state measurements. In many applications (full) state measurements are not available, such that observers and estimators become necessary. This has to be accounted for in the control allocation design to guarantee boundedness of the tracking error.
- Extension of the method to handle non-convex optimization problems. The scheme currently will converge to a locally optimal solution, but this will not necessarily result in accurate tracking.

- Considering anti-windup strategies, and possibly slack variables to enable faster convergence and handle solution infeasibility. Furthermore, include rate constraints on the control effectors.
- Actuator models can be included in the design, and parameters of these models can be estimated on-line.

FULL ENVELOPE MODULAR ADAPTIVE CONTROL

In this chapter the modular adaptive control approach introduced in chapter 4 is applied to the control design for a high fidelity F-16 model. The flight envelope is partitioned into hyperboxes, for each hyperbox a locally valid incremental model based on the linearized equations of motion is estimated. The models from the hyperboxes are combined by means of B-spline interpolation functions to obtain a smooth model valid for the complete flight envelope. The performance of the resulting adaptive control design is evaluated for representative flight conditions, maneuvers and failure cases.

8.1 Introduction

During the last decades the flight envelope of modern fighter aircraft has become larger, and in this expanded flight envelope the performance requirements have become more demanding. Examples of modern aircraft with large flight envelopes include the F-22 Raptor and F-35 Lightning II. Most modern fighters are capable of flying at high angles of attack, and high angles of sideslip to achieve high maneuverability. At these flight conditions, unmodeled vehicle dynamics and unmodeled parametric variations can occur, due to unsteady aerodynamic effects, control surface saturation and increased longitudinal and lateral coupling [153]. In addition to this, there is an increased interest in the ability of aircraft to remain controllable and operable after faults, failures and structural damage occurring during the flight. Because of these challenges, advanced nonlinear adaptive control

techniques are typically required to address the nonlinear, uncertain and time-varying, characteristics and requirements of such vehicles.

In this chapter a modular approach based on backstepping is taken, extending the approach from chapter 6 to full flight envelope model identification, and applying it on a high fidelity nonlinear model of an F-16 aircraft. In the approach the control law is based on Input-to-State Stable (ISS) backstepping which can be combined with any identifier that guarantees bounded estimates. Command filters are used to avoid the tedious analytic computation of virtual control signal derivatives, and make it possible to apply the control design to non-lower triangular systems. The flight envelope is partitioned into hyperboxes, in each of these boxes an incremental locally valid linear-in-the-parameters model is estimated using continuous-time orthogonal least squares. The benefit of this partitioning approach over a single local model approach is that information can be stored, such that when revisiting a identified part of the flight envelope the estimated incremental model can be retrieved and estimated restarted from there instead of starting from scratch. The output of the hyperboxes is combined using tensor-product B-spline weights to obtain a smooth, nonlinear and globally valid dynamic aircraft model. Compared to multilayer neural network approaches the advantages of the B-splines are their local support and numerical stability. This local support allows updating the estimated model only at the current flight condition. Additionally, it is easier to extract model information for health monitoring and failure analysis from a model with clear physical interpretation [130].

The remaining part of this chapter is organized as follows. First the system dynamics are cast into a form convenient for the application of the control design. Then the ISS-backstepping design is discussed and its stability properties are established. Following is the design of the identifier such that the aircraft model can be estimated and stored over the full flight envelope. Simulation results are presented for application of the ISS-backstepping design with least squares identification for several failure cases on a nonlinear model of an F-16 aircraft. Finally, conclusions drawn from the simulation experiment are given.

8.2 Controller Design

Consider a nonlinear system

$$\begin{aligned}\dot{x} &= f(x, u) \\ y &= h(x)\end{aligned}\tag{8.1}$$

where $x \in \mathbb{R}^n$ is the state vector, $u \in \mathcal{U} \subset \mathbb{R}^m$ is the system control vector, and $y \in \mathbb{R}^q$ is the output vector. The function f contains both parametric and nonparametric uncertainties. The control objective is to let the system output track a known smooth reference signal y_r with bounded derivatives. In the modular backstepping approach the design of the identifier and control law is separated. This allows for more flexibility in the choice of identification method, which is therefore not

limited to Lyapunov-based identifier designs. Thus, the identification process is not only driven by the tracking error, the system state and/or its measurements can be incorporated as well by means of nonlinear swapping filters.

For linear systems the separation principle [83] holds, which allows straightforward separation of the identifier and control law. The true parameter values are simply replaced by their estimates in the control law according to the certainty equivalence principle [5, 88]. However, due to the difference in stability characteristics of linear and nonlinear systems this is not allowed for general nonlinear systems as shown in section 4.4. In systems with faster than linear growing nonlinearities (for example x^2 and $x_1 x_2$) even a small parameter estimation error can drive the state to infinity in finite time [88]. Hence, the control law has to be made robust against estimation errors and the time varying character of the parameter estimates. The estimation error is viewed as unknown disturbance and is attenuated by adding nonlinear damping terms to the control law. The complete structure of the proposed control design is shown in figure 8.1.

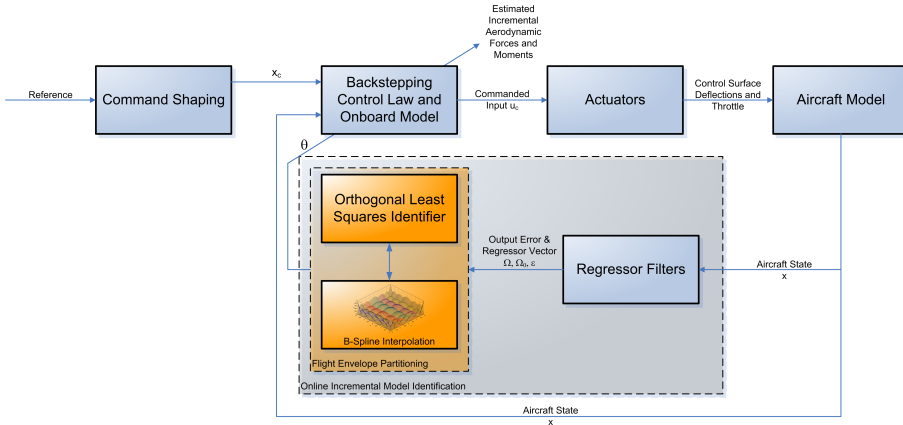


Figure 8.1: A schematic overview of the control architecture.

8.2.1 System dynamics

First of all rewrite the system dynamics (8.1) to

$$\begin{aligned} \dot{x}_i &= f_i(x, u) + g_i(x)x_{i+1} + \varphi_i^T(x, u)\theta + \delta_i(x, u, t) \\ \dot{x}_n &= f_n(x) + \left(g_{n_0}(x) + g_{n_\theta}(x, \theta)\right)u + \varphi_n^T(x, u)\theta + \delta_n(x, u, t) \end{aligned} \quad (8.2)$$

where δ represents an unknown, bounded, disturbance, f_i , g_i and g_{n_0} represent known parts of the system dynamics, g_{n_θ} uncertainty in the control effectiveness, $\varphi^T : \mathbb{R}^n \times \mathbb{R}^m \rightarrow \mathbb{R}^{n \times p}$ a known matrix function, and $\theta \in \mathbb{R}^p$ an unknown constant

vector of parameters, together these present the uncertain, or unknown part of the dynamics to be estimated. Assume that the disturbance δ is bounded as

$$|\delta(x, u, t)| \leq p^T(x, u)\psi^* \quad \forall x \in \mathbb{R}^n, \forall u \in \mathbb{R}^m, \forall t \in \mathbb{R}_+ \quad (8.3)$$

where p is a vector of known, smooth, positive functions, and $\psi^* \geq 0$ is an unknown constant parameter vector defining an upper bound on the uncertainty.

8.2.2 Backstepping Control Law Design

The ISS-backstepping scheme by Krstić, Kanellakopoulos, and Kokotović [88] is combined with command filtering and adaptive bounding [57, 59, 141]. Using this combination, the tedious analytical computation of derivatives of the intermediate control laws is avoided as shown in chapter 4, the method can be applied to systems which are not in lower triangular form, and magnitude and rate constraints on the (intermediate) control laws can be incorporated. Adaptive bounding is included in the design to robustify against a possible mismatch in model structure between the output of the interpolated linear local models and the true system.

The control law design can be summarized as

$$\bar{z}_i = x_i - x_{i_c} - \Xi_i, \quad (8.4a)$$

$$\dot{e}_i = \bar{z}_i, \quad (8.4b)$$

$$\dot{\Xi}_i = -C_i \Xi_i + g_i (x_{i+1_c} - x_{i+1_c}^0), \quad (8.4c)$$

$$x_{i_c}^0 = \alpha_{i-1} - \Xi_i, \quad (8.4d)$$

$$\omega_i = p_i(x, u) \tanh\left(\frac{x_i - x_{i_c}}{\zeta_i}\right), \quad (8.4e)$$

$$\beta_i = \psi_i \omega_i, \quad (8.4f)$$

$$\dot{\psi}_i = \Gamma_{\psi_i} (\omega_i \bar{z}_i - \sigma_i (\psi_i - \psi_0)), \quad (8.4g)$$

$$\alpha_i = g_i^{-1} \left(-f_i - \varphi_i^T \hat{\theta} - C_1 (x_i - x_{i_c}) - S_i \bar{z}_i + \dot{x}_{i_c} - K_i e_i - \beta_i - g_{i-1}^T \bar{z}_{i-1} \right), \quad (8.4h)$$

$$S_i = \varphi_i^T \kappa_i \varphi_i, \quad (8.4i)$$

$$u_c^0 = \hat{g}_n^{-1} g_n \alpha_n - \hat{g}_n^{-1} \kappa_u \bar{z}_n, \quad (8.4j)$$

where \bar{z}_i is the augmented tracking error, Ξ a filtered version of the error imposed by the command filters, e is the integrated augmented tracking error, x_c^0 the filter input, α_i the virtual control input at stage i , \hat{g}_n is the estimate of $g_n = g_{n_0} + g_{n_\theta}$, $\sigma_i \geq 0$ is a constant leakage gain to guarantee boundedness of ψ_i , $\psi_i^0 \geq 0$ is a design constant. Nonlinear damping, through S_i , is used to guarantee boundedness of the states with respect to the parameter estimation error. The parameter ζ_i is a (small) constant used to smooth the switching of the control laws at $\omega_i = 0$.

Application of the design (8.4) to the system (8.2) results in the augmented tracking error derivatives for $i = 1, \dots, n-1$, the compensated tracking error dynamics become

$$\begin{aligned}
\dot{\bar{z}}_i &= f_i + g_i x_{i+1} + \varphi_i^T \theta + \delta_i - \dot{x}_{i_c} - \dot{\Xi}_i \\
&= f_i + g_i x_{i+1_c}^0 + g_i (x_{i+1_c} - x_{i+1_c}^0) + g_i (x_{i+1} - x_{i+1_c}) + \varphi_i^T \theta \\
&\quad + \delta_i - \dot{x}_{i_c} + C_i \Xi_i - g_i (x_{i+1_c} - x_{i+1_c}^0) \\
&= f_i + g_i \alpha_i + g_i (x_{i+1} - x_{i+1_c} - \Xi_{i+1}) + \varphi_i^T \theta + \delta_i - \dot{x}_{i_c} + C_i \Xi_i \\
&= -(C_i + S_i) \bar{z}_i + g_i \bar{z}_i + \varphi_i^T \tilde{\theta} + \delta_i - \beta_i - K_i e_i - g_{i-1}^T \bar{z}_{i-1},
\end{aligned} \tag{8.5}$$

with $g_0 = 0$, $\bar{z}_0 = 0$. For \bar{z}_n they become

$$\begin{aligned}
\dot{\bar{z}}_n &= f_n + g_n u + \varphi_n^T \theta + \delta_n - \dot{x}_{n_c} - \dot{\Xi}_n \\
&= f_n + \hat{g}_n u_c^0 - \dot{x}_{n_c} + \hat{g}_n (u - u_c^0) + (g_n - \hat{g}_n) u + \varphi_n^T \theta \\
&\quad + \delta_n + C_n \Xi_n - \hat{g}_n (u - u_c^0) \\
&= f_n + \hat{g}_n \alpha_n - \dot{x}_{n_c} + \varphi_n^T \theta + C_n \Xi_n \\
&\quad - \kappa_u \bar{z}_n + \delta_n + (g_n - \hat{g}_n) u \\
&= -(C_n + S_n) \bar{z}_n + \varphi_n^T \tilde{\theta} + \delta_n - \beta_n - g_{n-1}^T \bar{z}_{n-1} \\
&\quad - \kappa_u \bar{z}_n - K_n e_n + \hat{g}_n u,
\end{aligned} \tag{8.6}$$

where $\tilde{\theta} = \theta - \hat{\theta}$, and $\hat{\theta}$ is the estimate of the unknown parameter vector. Now consider the Control Lyapunov Function (CLF) candidate

$$\mathcal{V}(\bar{z}, \chi, e) = \frac{1}{2} \sum_{i=1}^n \left(\bar{z}_i^T \bar{z}_i + \chi_i^T \Gamma_{\psi_i}^{-1} \chi_i + e_i^T K_i e_i \right) \tag{8.7}$$

where $\chi_i = \psi_i - \psi_i^M$, $\psi_i^M = \max(\psi_i^*, \psi_i^0)$. The time derivative of the CLF (8.7) along the solutions of Eqs. (8.5)–(8.6) satisfies

$$\begin{aligned}
\dot{\mathcal{V}} &= \bar{z}_1^T \left(-C_1 \bar{z}_1 - K_1 e_1 - \varphi_1^T \kappa_1 \varphi_1 \bar{z}_1 + g_1 \bar{z}_2 + \varphi_1^T \tilde{\theta} + \delta_1 - \beta_1 \right) \\
&\quad + \sum_{i=2}^{n-1} \bar{z}_i^T \left(-C_i \bar{z}_i - K_i e_i - \varphi_i^T \kappa_i \varphi_i \bar{z}_i - g_{i-1} \bar{z}_{i-1} + g_i \bar{z}_{i+1} \right. \\
&\quad \left. + \varphi_i^T \tilde{\theta} + \delta_i - \beta_i \right) + \bar{z}_n^T \left(-C_n \bar{z}_n - K_n e_n - \varphi_n^T \kappa_n \varphi_n \bar{z}_n \right. \\
&\quad \left. - g_{n-1} \bar{z}_{n-1} + \varphi_n^T \theta + \delta_n - \beta_n - \kappa_u \bar{z}_n + (g_n - \hat{g}_n) u \right) \\
&\quad + \sum_{i=1}^n \chi_i^T \left(\omega_i z_i - \sigma_i (\psi_i - \psi_i^0) \right) + \sum_{i=1}^n \bar{z}_i^T K_i e_i
\end{aligned}$$

$$\begin{aligned}
&= - \sum_{i=1}^n \bar{z}_i^T C_i \bar{z}_i - \sum_{i=1}^n \bar{z}_i^T \varphi_i^T \kappa_i \varphi_i \bar{z}_i + \sum_{i=1}^n \varphi_i^T \tilde{\theta} \bar{z}_i + \sum_{i=1}^n (\delta_i - \beta_i) \bar{z}_i \\
&\quad - \bar{z}_n^T \kappa_u \bar{z}_n + \bar{z}_n^T (g_n - \hat{g}_n) u + \sum_{i=1}^n \chi_i^T \left(\omega_i \bar{z}_i - \sigma_i (\psi_i - \psi_i^0) \right) \\
&= - \sum_{i=1}^n \bar{z}_i^T C_i \bar{z}_i - \sum_{i=1}^n \left(\varphi_i \bar{z}_i - \frac{1}{2} \kappa_i^{-1} \tilde{\theta} \right)^T \kappa_i \left(\varphi_i \bar{z}_i - \frac{1}{2} \kappa_i^{-1} \tilde{\theta} \right) \\
&\quad + \sum_{i=1}^n \frac{1}{4} \tilde{\theta}^T \kappa_i^{-1} \tilde{\theta} - \left(\bar{z}_n - \frac{1}{2} \kappa_u^{-1} \tilde{g}_n u \right)^T \kappa_u \left(\bar{z}_n - \frac{1}{2} \kappa_u^{-1} \tilde{g}_n u \right) \\
&\quad + \frac{1}{4} u^T \tilde{g}_n^T \kappa_u^{-1} \tilde{g}_n u + \sum_{i=1}^n \left(\delta_i \bar{z}_i - (\psi_i^M)^T \omega_i \bar{z}_i - \frac{1}{2} \chi_i^T \sigma_i \chi_i \right. \\
&\quad \left. - \frac{1}{2} (\psi_i - \psi_i^0)^T \sigma_i (\psi_i - \psi_i^0) + \frac{1}{2} (\psi_i^M - \psi_i^0)^T \sigma_i (\psi_i^M - \psi_i^0) \right) \\
&\leq - \sum_{i=1}^n \bar{z}_i^T C_i \bar{z}_i + \frac{1}{4} \sum_{i=1}^n \tilde{\theta}^T \kappa_i^{-1} \tilde{\theta} + \frac{1}{4} u^T \tilde{g}_n^T \kappa_u^{-1} \tilde{g}_n u \tag{8.8} \\
&\quad + \frac{1}{2} \sum_{i=1}^n (\psi_i^M)^T \zeta_i + (\psi_i^M - \psi_i^0)^T \sigma_i (\psi_i^M - \psi_i^0)
\end{aligned}$$

which uses a claim by Polycarpou and Ioannou [141] for the adaptive bounding of disturbances. The second and third terms at the first line of the inequality in (8.8) are due to the nonlinear damping, the last two terms are due to the adaptive bounding. The result in (8.8) shows that the tracking error states and desired control input are bounded when the parameter estimation errors are bounded, and that the tracking error states converge exponentially to a positively invariant compact set. Using results by Freeman, Krstić, and Kokotović [61] the robustness bounds of the controller can be derived. Tracking performance can be improved by either increasing the nonlinear damping gains and adaptive bounding update gains, or reducing the parameter estimation error using online identification. Suppose that (8.8) could be rewritten as

$$\dot{V} \leq -\bar{z}^T C_0 \bar{z} + \frac{1}{4} \tilde{\theta}^T \kappa_0^{-1} \tilde{\theta} + \frac{1}{4} u^T \tilde{g}_n^T \kappa_u^{-1} \tilde{g}_n u + \Lambda$$

where

$$\begin{aligned}
C_0 &= \min_{1 \leq i \leq n} \lambda_{\min} C_i, \\
\kappa_0 &= \left(\sum_{i=1}^n \kappa_i^{-1} \right)^{-1}, \\
\Lambda &= \frac{1}{2} \left[(\psi^M)^T \zeta + (\psi^M - \psi^0)^T \sigma (\psi^M - \psi^0) \right]
\end{aligned}$$

and $\Lambda > 0$ since $\zeta_i > 0, \psi_i^M > 0, \sigma > 0$ by their definitions. Therefore

$$\bar{z}^T C_0 \bar{z} \geq \left[\frac{1}{4} \tilde{\theta}^T \kappa_0^{-1} \tilde{\theta} + \frac{1}{4} u^T \tilde{g}_n^T \kappa_u^{-1} \tilde{g}_n u + \Lambda \right]$$

implies that $\dot{V} < 0$ and therefore gives an upper bound on the invariant compact set to which \bar{z} will converge.

8.2.3 Nonlinear Swapping Filters

Similar to their use in linear modular designs the swapping filters are used as an analytical device which uses regressor filtering to account for the time-varying nature of the parameter estimates [88]. The filters transform a time-varying system into a static mapping, such that only state measurements are required and not their derivatives. Two types of nonlinear swapping can be applied, either to the tracking error system, or to the system dynamics. In this work x-swapping filters are selected to achieve the greatest similarity to NDI with RLS estimation technique used by Lombaerts, Huisman, Chu, Mulder, and Joosten [97]. Note that the function of this filter is not state estimation, but rather to extract the unknown dynamics from the state and control feedback. First rewrite the system (8.2) in the form

$$\dot{x} = f(x, u) + F^T(x, u)\theta + \Delta(t, x, u) \quad (8.9)$$

where

$$f(x, u) = \begin{bmatrix} g_1 x_2 + f_1(x_1) \\ \vdots \\ g_{n-1} x_n + f_{n-1}(x) \\ g_{n_0} u + f_n(x) \end{bmatrix}, \quad F^T(x, u) = \begin{bmatrix} \varphi_1^T(x, u) \\ \vdots \\ \varphi_{n-1}^T(x, u) \\ \varphi_n^T(x, u) \end{bmatrix}.$$

The x-swapping filters are applied

$$\dot{\Omega}_0 = A(t)(\Omega_0 + x) - f(x, u), \quad \Omega_0 \in \mathbb{R}^n \quad (8.10a)$$

$$\dot{\Omega}^T = A(t)\Omega^T + F^T(x, u), \quad \Omega \in \mathbb{R}^{p \times n}. \quad (8.10b)$$

The matrix $A(t)$ is an exponentially stable matrix, that is a matrix with all eigenvalues in the left half plane, defined as

$$A(t) = A_0 - \rho F^T F P, \quad (8.11)$$

where $\rho > 0$ and A_0 is an arbitrary negative definite matrix such that

$$P A_0 + A_0^T P = -I, \quad P = P^T > 0,$$

to stabilize the scheme against fast parameter and regressor variations. Since $A_0 < 0, \rho > 0, P > 0$ and $F^T F > 0$, the matrix $A(t) < 0 \forall t$. For the identification

algorithm discussed in the following section the output Ω is used as the regressor, and the output vector $\mathcal{Y} = \Omega_0 + x$ as the dependent variable. The estimation error is defined as

$$\epsilon = \Omega_0 + x - \Omega^T \tilde{\theta} \quad (8.12)$$

which satisfies

$$\epsilon = \Omega^T \tilde{\theta} + \tilde{\epsilon} \quad (8.13)$$

where $\tilde{\epsilon}$ is the filtered disturbance

$$\dot{\tilde{\epsilon}} = A(t)\tilde{\epsilon} + \Delta. \quad (8.14)$$

Since $A(t)$ is exponentially stable, and Δ is bounded, $\tilde{\epsilon}$ is bounded and even converges to zero exponentially for $\Delta = 0$. Therefore, ϵ is bounded, and converges to zero when $\Delta = 0$. Since ϵ is \mathcal{L}_2 , F is smooth, and all states are bounded, $\tilde{\epsilon}$ is also bounded. Therefore, $\dot{\tilde{\epsilon}}$ is uniformly continuous. Since $\epsilon(t) \rightarrow 0$ for $\Delta = 0$, then

$$\lim_{t \rightarrow \infty} \int_0^t \dot{\epsilon}(\tau) d\tau = \lim_{t \rightarrow \infty} \epsilon(t) - \epsilon(0) = -\epsilon(0) < -\infty. \quad (8.15)$$

By Barbalat's lemma, $\dot{\epsilon}(t) \rightarrow 0$. Since $\dot{\hat{\theta}} \in \mathcal{L}_\infty \cap \mathcal{L}_2$ and $\tilde{\theta} \in \mathcal{L}_\infty$, it hence follows that $\dot{\hat{\theta}} \rightarrow 0$.

8.3 Identifier Design

In the case that the on-board model is correct, the control law design from the previous section stabilizes the system, and achieves good tracking performance on the aircraft. Generally, the model used to predict the aerodynamic forces and moments is uncertain, or, in some flight conditions or failure conditions even unknown or unavailable. Therefore the on-board model is updated during the flight, to match the true aircraft behavior as close as possible. Since fighter aircraft dynamics vary nonlinearly through a large operating regime, the flight envelope is partitioned into small regions, which will be called hyperboxes. Each of these hyperboxes will contain a local linear-in-the-parameters-model. By combining the output of all of the local models together by means of smooth interpolation, a global nonlinear aerodynamic model is obtained. The main advantage of this approach is that the complexity of the local models can be relatively low, while still being able to obtain an accurate global approximation.

First of all the least squares method used to update the local models is discussed, after which the interpolation technique based on tensor B-splines is presented.

8.3.1 Local Model Update

The introduced backstepping scheme can be combined with all identifiers which guarantee boundedness of the estimation error and its derivative. A recursive least

squares (RLS) filter is selected here, since by design it can guarantee convergence of the parameter estimates to constant values. Instead of selecting an RLS filter in combination within the modular backstepping framework applied in previous work[194, 198], an Orthogonal Least Squares (OLS) technique is applied to update the local models. The motivation for this is the planned extension towards online structure selection of the local linear models in future research. The current application of the OLS is equivalent to the continuous least squares formulation and therefore yields the same results. The continuous OLS description is started from the continuous time recursive least squares definition

$$\min_{\theta(t)} \int_0^t e^{\lambda(\tau-t)} \left(y(\tau) - \varphi(\tau)^T \theta(t) \right)^2 d\tau \quad (8.16)$$

where the entries of $\varphi(\tau) \in \mathbb{R}^p$ and $y(\tau)$ are given signals, and the entries of $\theta(t) \in \mathbb{R}^p$ are unknown scalar constants. The scalar $\lambda \geq 0$ is a forgetting rate, determining the relative importance of the past input. Instead of directly solving this optimization problem, we perform a Cholesky factorization of the correlation matrix $N = \langle \varphi, \varphi^T \rangle = R^T \langle q, q^T \rangle R = R^T R$, where R is the Cholesky factor of N and q is a vector of orthogonal vectors. Thus, (8.16) can now be rewritten as $\min_{\theta} \langle y, y \rangle - 2 \langle y, \varphi^T \rangle \theta + \theta^T N \theta$, and the solution follows from $N \theta = \langle \varphi, y^T \rangle$, or $R^T R \theta = R^T \langle q, y^T \rangle$. Therefore R and $\langle q, y^T \rangle$ need to be tracked. This can be achieved by adding an additional component to the input, $\hat{\varphi} = \begin{bmatrix} \varphi^T & y^T \end{bmatrix}^T$. However, instead of tracking the Cholesky factor \hat{R} of the augmented correlation matrix \hat{N} , tracking the inverse Cholesky factor $\hat{S} = \hat{R}^{-1}$ allows extraction of the parameter estimate without matrix inversion or backsubstitution. From $\dot{\hat{N}} = \hat{\varphi} \hat{\varphi}^T - \lambda \hat{N}$ and the lemma which relates the evolution of a matrix and its Cholesky factor by Dehaene, Moonen, and Vandewalle [38] the following is obtained

$$\dot{\hat{S}} = -\hat{S} \text{upph} \left(\hat{S}^T \hat{\varphi} \hat{\varphi}^T \hat{S} \right) + \frac{\lambda}{2} \hat{S} \quad (8.17)$$

where upph , the upper triangular half-part, is defined by

$$Y = \text{upph}(X) \iff \begin{cases} y_{i,j} = x_{i,j} & i < j \\ y_{i,j} = \frac{1}{2} x_{i,j} & i = j \\ y_{i,j} = 0 & i > j \end{cases} . \quad (8.18)$$

For the application with the backstepping control law designed earlier the input matrix becomes

$$\hat{\varphi}^T = \begin{bmatrix} \Omega^T & (\Omega_0 + x) \end{bmatrix} \quad (8.19)$$

The parameter estimate $\hat{\theta}$ can be extracted easily by

$$\hat{\theta}_i = -\hat{S}_{i,p+1} / \hat{S}_{p+1,p+1} . \quad (8.20)$$

The relation between the forgetting rate used in continuous time and the more commonly known forgetting factor for discrete time is given by

$$T_s \lambda = -\ln \lambda_d, \quad (8.21)$$

where T_s is the sampling time of the discrete system, and λ_d is the discrete forgetting factor. For example, at a sampling rate of 50 Hz and a discrete forgetting factor of 0.98 the equivalent continuous time forgetting rate is about 1.

Naturally, the parameters of the model cannot be accurately determined unless some conditions are imposed on the input signal. For adaptive control with online identification, convergence of the residual modeling error to zero is more important than convergence of the model parameters. When the input signal is persistently exciting (PE) the estimates will converge to constant values. By definition, φ satisfies a persistency of excitation condition if positive constants ρ_1, ρ_2 and T exist such that the following condition is satisfied $\forall t \geq 0$

$$\rho_1 I \leq \int_t^{t+T} \varphi(\tau) \varphi(\tau)^T d\tau \leq \rho_2 I. \quad (8.22)$$

The reference trajectory can be made PE by superimposing a sinusoidal signal on the reference signal, as discussed by Stepanyan and Hovakimyan [175]. Another method is by using an intelligently exciting signal [22, 23], which decays with trajectory tracking and parameter estimation errors.

8.3.2 Full Envelope Interpolation

Naturally, the estimation method described previously could be used to fit a model to the complete dynamics of the aircraft. However, to be able to achieve a reasonably accurate fit throughout the whole flight envelope such a model would be extremely complex and large. For such a large model, the covariance matrix would become very large since its number of elements scales quadratically, increasing the computational load of the identification scheme dramatically. Therefore an approach is selected which splits the complete flight envelope into partitions, the output of the smaller partitions is combined using smooth interpolation functions. It is desired to only update the model in the *active* part of the flight envelope, and therefore interpolating functions with local support are selected: B-splines.

A B-spline is a spline function that has minimal support with respect to a given degree, smoothness and domain partition [34].

Definition 8.1 (B-spline basis function). : Let U be a set of $m + 1$ nondecreasing numbers, $u_0 \leq u_1 \leq \dots \leq u_m$. The u_i are called knots, the set U the knot vector, and the half-open interval $[u_i, u_{i+1})$ the i^{th} knot span. If a knot u_i appears k times, where $k > 1$, u_i is a multiple knot of multiplicity k , written as $u_i(k)$. Otherwise it is called a simple knot. The knots can be considered as division points that subdivide the interval $[u_0, u_m]$ into knot spans. All B-spline basis functions are supposed to have their domain on $[u_0, u_m]$. To define

B-spline basis functions one more parameter is required, the degree of these basis functions, p . The i th B-spline basis function of degree p , written as $N_{i,p}(u)$, is defined recursively as follows:

$$F_{i,0}(u) = \begin{cases} 1 & \text{if } u_i \leq u < u_{i+1} \\ 0 & \text{otherwise} \end{cases}$$

$$F_{i,p}(u) = \frac{u - u_i}{u_{i+p} - u_i} F_{i,p-1}(u) + \frac{u_{i+p+1} - u}{u_{i+p+1} - u_{i+1}} F_{i+1,p-1}(u)$$

This formula is usually referred to as the Cox-de Boor recursion formula.

The B-splines have two characteristics that make them very suitable for online identification:

1. Only a small number of B-spline basis functions is nonzero at any given point in the flight envelope. Therefore only a small number of local models has to be updated, resulting in lower computational load. Additionally, since the update is local, the model has memory capabilities. Moving through the complete flight envelope model information is stored.
2. The spline output is always positive and normalized, resulting in a numerical stable process.

In figure 8.2(a) the output of a cubic B-spline network is shown, along with the individual B-splines and the control points. The B-spline is generalized for higher input dimensions by taking the tensor product of the B-spline basis functions in each of dimension, for example in three dimensions this yields

$$\gamma_{ijk} = \gamma_i \otimes \gamma_j \otimes \gamma_k. \quad (8.23)$$

Figure 8.2(b) shows the degree of membership for a cubic B-spline basis function for two input dimensions with knot vectors

$x_{knot} = y_{knot} = [-2 \ -2 \ -2 \ -2 \ -1 \ 0 \ 1 \ 2 \ 2 \ 2 \ 2]$. Note that the shape of the basis functions changes near the edges of the domain to keep the sum of all individual degrees of membership equal to 1. The degree of membership γ_i , the B-spline output, is used to distribute the current measurement over the active local models as a weight on their derivative.

$$\hat{S}_i = -\hat{S}_i \text{upph} \left(\hat{S}_i^T \hat{\phi} \gamma_i \hat{\phi}^T \hat{S}_i \right) + \frac{\lambda \gamma_i}{2} \hat{S}_i \quad (8.24)$$

For the inactive local models, with $\gamma_j = 0$

$$\hat{S}_j = 0. \quad (8.25)$$

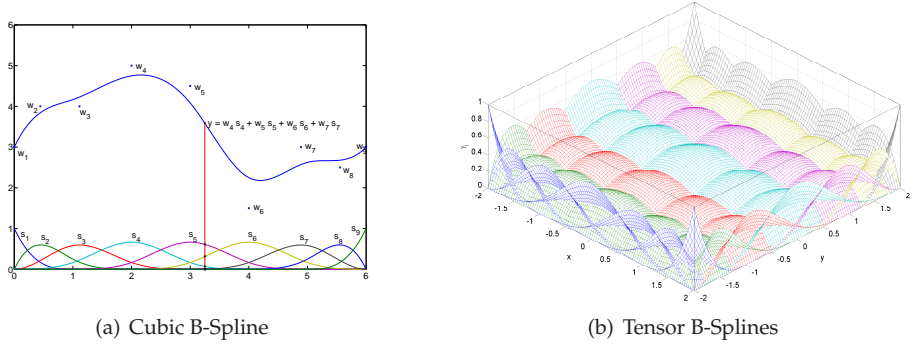


Figure 8.2: A cubic B-Spline function output is shown in (a). The output at a given input point is the weighted sum of the active B-Splines. The Degree of local membership determined by cubic B-spline basis functions in two dimensions with knot vectors $x_{knot} = y_{knot} = [-2 \ -2 \ -2 \ -2 \ -1 \ 0 \ 1 \ 2 \ 2 \ 2 \ 2]$ is shown in (b).

The output at any given point in the flight envelope can be obtained by summing the weighted output of the local models as

$$\hat{\theta} = \sum_i \gamma_i \hat{\theta}_i \tag{8.26}$$

where θ_i is the output of the i -th local model.

8.3.3 Covariance Resetting

The covariance matrix generally becomes very small after a period of tracking without any noticeable mismatch between the on-board model and the true aircraft behavior, despite using a forgetting factor in (8.24). This reduces the ability of the identifier to adjust to abrupt changes in the system dynamics. For aircraft, and especially fighter aircraft, slow adaptation to the new dynamics could cause the aircraft to reach dangerous or unrecoverable regions of the state space. Therefore, a mechanism is applied to reset the covariance matrix to enable fast adaptation when an abrupt change is detected. After a sudden change, the residual vector ϵ will in general be large. By monitoring the residual, and comparing it with a degree of membership weighted predefined threshold, abrupt changes can be detected and consequently reset the covariance matrix of that particular hyperbox, i.e.

$$\gamma_i |\epsilon| \geq W_\epsilon. \tag{8.27}$$

The trace of the inverse covariance matrix has to be below a certain threshold, to avoid repeated and continuous resetting after a failure. Note that the estimated parameters are not reset to zero, only their “update gain”.

8.4 Application to the F-16 Model

The control design presented in the preceding sections is applied to a nonlinear model of the F-16 [126]. The aerodynamic data tables are valid in the subsonic regime, with an angle of attack between -20 and 90 degrees, and sideslip angle of $|\beta| \leq 30$ degrees. The tabular data in the model is obtained from wind-tunnel tests and captures the nonlinear behavior of the total aerodynamic force and moment coefficients. A quaternion representation of the attitude is used to avoid the 90 degree pitch singularity.

8.4.1 F-16 Aircraft Model and Assumptions

The F-16 model allows for control over thrust-lever, horizontal stabilizer, ailerons, and rudder. Additionally the assumption is made that either thrust measurement or an accurate thrust model is available. The control inputs are defined positive in the conventional way: a positive control deflection results in a negative force or moment in the body-axes. The F-16 is equipped with automatic leading edge flaps, which are deflected according to a transfer function dependent on angle of attack α and a bias depending on the ratio of dynamic pressure and static pressure (Mach number)[126]

$$\delta_{LEF_c} = 1.38 \frac{2s + 7.25}{s + 7.25} \alpha - 9.05 \frac{\bar{q}}{p_{static}} + 1.45$$

The control surfaces of the F-16 are driven by servo-controlled actuators to produce the deflections commanded by the flight control system, u , which are the true control variables. The actuators of the control surfaces are modeled as a first-order low-pass filters with fixed gain and saturation limits in range and deflection rate, see table 8.1. The time constants of the actuators are 0.136 for the leading edge flaps and 0.0495 for the other control surfaces. The throttle response used in the F-16 is modeled as low-pass filter with time constant 1.0 .

Table 8.1: The control input units and maximum values

Control	Unit	Min.	Max.	Rate limit
Thrust-lever	-	0	1	$\pm 5 \text{ s}^{-1}$
Horizontal Tail	deg	-25.0	25.0	$\pm 60 \text{ deg/s}$
Ailerons	deg	-21.5	21.5	$\pm 80 \text{ deg/s}$
Rudder	deg	-30.0	30.0	$\pm 120 \text{ deg/s}$
Leading edge flap	deg	0.0	25.0	$\pm 25 \text{ deg/s}$

The original nonlinear model is not affine in the control surface inputs, the horizontal stabilizer appears as an input to several lookup tables. Therefore an

affine approximation of these tables is made, introducing an model-mismatch. For example, the moment coefficient C_m is approximated as

$$C_m(\alpha, \beta, \delta_e) \approx C_{m_0}(\alpha, \beta, \delta_e) + C_{m_{\delta_e}}(\alpha, \beta, \delta_e)\delta_e \quad (8.28)$$

since the current deflection δ_e is known through the command filters. This approximation is valid over a small range of elevator deflections around the current operating point. By partitioning on the stabilizer deflection, an accurate approximation is obtained for the full range of elevator deflections. Other similar coefficients which have a non-affine dependence on the stabilizer deflection are approximated similarly. This approximation does however create a mismatch between the true aircraft dynamics and the modeled aircraft dynamics, thereby introducing an unknown disturbance which is modeled as δ in (8.2). Using the adaptive bounding technique, the controller is robustified against this unknown model mismatch.

8.4.2 Partition Model Structure

The incremental model estimated on-board the aircraft is based on the linearized system equations [41]. The local models of the different hyperboxes is not necessarily the same: for example partitions at extreme angles of attack and sideslip angles can have a more complex model structure to capture all the nonlinear phenomena occurring. In this work the following local model structure has been selected for all hyperboxes

$$\begin{aligned} \delta C_X &= \begin{bmatrix} 1 & \frac{q\bar{c}}{2V_T} & \delta_e \end{bmatrix} \begin{bmatrix} \delta C_{X_0} & \delta C_{X_q} & \delta C_{X_{\delta_e}} \end{bmatrix}^T, \\ \delta C_Y &= \begin{bmatrix} 1 & \frac{pb}{2V_T} & \frac{rb}{2V_T} & \delta_a & \delta_r \end{bmatrix} \begin{bmatrix} \delta C_{Y_0} & \delta C_{Y_p} & \delta C_{Y_r} & \delta C_{Y_{\delta_a}} & \delta C_{Y_{\delta_r}} \end{bmatrix}^T, \\ \delta C_Z &= \begin{bmatrix} 1 & \frac{q\bar{c}}{2V_T} & \delta_e \end{bmatrix} \begin{bmatrix} \delta C_{Z_0} & \delta C_{Z_q} & \delta C_{Z_{\delta_e}} \end{bmatrix}^T, \\ \delta C_l &= \begin{bmatrix} 1 & \frac{pb}{2V_T} & \frac{rb}{2V_T} & \delta_a & \delta_e & \delta_r \end{bmatrix} \begin{bmatrix} \delta C_{l_0} & \delta C_{l_p} & \delta C_{l_r} & \delta C_{l_{\delta_a}} & \delta C_{l_{\delta_e}} & \delta C_{l_{\delta_r}} \end{bmatrix}^T, \\ \delta C_m &= \begin{bmatrix} 1 & \alpha & \frac{q\bar{c}}{2V_T} & \delta_e \end{bmatrix} \begin{bmatrix} \delta C_{m_0} & \delta C_{m_\alpha} & \delta C_{m_q} & \delta C_{m_{\delta_e}} \end{bmatrix}^T, \\ \delta C_n &= \begin{bmatrix} 1 & \frac{pb}{2V_T} & \frac{rb}{2V_T} & \delta_a & \delta_e & \delta_r \end{bmatrix} \begin{bmatrix} \delta C_{n_0} & \delta C_{n_p} & \delta C_{n_r} & \delta C_{n_{\delta_a}} & \delta C_{n_{\delta_e}} & \delta C_{n_{\delta_r}} \end{bmatrix}^T. \end{aligned}$$

The regressor functions are block-diagonally stacked together to form the full regressor matrix, all the incremental unknown parameters are stacked to form a large column-vector with 27 parameters.

8.4.3 F-16 Control Law Design

The controller design discussed in the previous sections is applied to the F-16 aircraft model. The application of the proposed control scheme is not presented in great detail since it is very similar to the examples from chapter 4 and the F-18 application of chapter 6. A tracking controller for the total airspeed, angle of attack, sideslip angle, and velocity vector roll rate is designed.

First define the outer loop subsystem as

$$x_1 = \begin{bmatrix} V_T & \alpha & \beta \end{bmatrix}^T \quad (8.29)$$

with dynamics

$$\dot{x}_1 = f_1 + F_1 + g_1 [p_S \quad q_S \quad r_S]^T + g_{1_T} [T \quad 0 \quad 0]^T \quad (8.30)$$

where

$$f_1 = \begin{bmatrix} -p_S \tan \beta + \frac{1}{mV_T} \frac{g_1}{\cos \beta} (-T \sin \alpha + mg_3) \\ \frac{1}{mV_T} (-T \cos \alpha \sin \beta + mg_2) \end{bmatrix},$$

$$F_1 = \frac{1}{m} \begin{bmatrix} -\cos \alpha \cos \beta & \sin \beta & \sin \alpha \cos \beta \\ \frac{\sin \alpha}{V_T \cos \beta} & 0 & \frac{\cos \alpha}{V_T \cos \alpha} \\ -\frac{\cos \alpha \sin \beta}{V_T} & \frac{\cos \beta}{V_T} & -\frac{\sin \alpha \sin \beta}{V_T} \end{bmatrix} \begin{bmatrix} \bar{X} \\ \bar{Y} \\ \bar{Z} \end{bmatrix},$$

$$g_1 = \begin{bmatrix} 0 & 0 & 0 \\ 0 & 1 & 0 \\ 0 & 0 & -1 \end{bmatrix}, \quad g_{1_T} = \begin{bmatrix} \frac{\cos \alpha \cos \beta}{m} & 0 & 0 \\ 0 & 0 & 0 \\ 0 & 0 & 0 \end{bmatrix}.$$

Note that this differs slightly from the system description given by (8.2) due to the presence of the control input T . The thrust input can be obtained from this outer loop for airspeed control. For the inner loop subsystem state is

$$x_2 = [p_S \quad q_S \quad r_S]^T \quad (8.31)$$

with dynamics

$$\dot{x}_2 = f_2 + F_2 + g_2 [\delta_a \quad \delta_e \quad \delta_r]^T$$

where

$$f_2 = -T_{B \rightarrow S} J^{-1} (\omega_B \times J \omega_B) + \dot{T}_{B \rightarrow S} \omega_B,$$

$$F_2 = T_{B \rightarrow S} J^{-1} \begin{bmatrix} L_0 \\ M_0 \\ N_0 \end{bmatrix},$$

$$g_2 = T_{B \rightarrow S} J^{-1} \begin{bmatrix} L_{\delta_a} & L_{\delta_e} & L_{\delta_r} \\ 0 & M_{\delta_e} & 0 \\ N_{\delta_a} & N_{\delta_e} & N_{\delta_r} \end{bmatrix}.$$

The aerodynamic forces and moments appearing in the above equations in the design are split into a part that is assumed known, or the nominal model, and a

contribution from the estimated incremental on-board model. For example, the total aerodynamic force in x -body direction can be written as

$$\bar{X} = \bar{q}S \left(\underbrace{C_X + C_{X_q} \frac{q\bar{c}}{2V_T}}_{\text{nominal}} + \underbrace{\delta C_{X_0} + \delta C_{X_q} \frac{q\bar{c}}{2V_T} + \delta C_{X_{\delta_e}} \delta_e}_{\text{incremental}} \right). \quad (8.32)$$

Thus known nonlinearities from aerodynamics and inertia coupling, are included in the function f_1, f_2 . The functions F_1 and F_2 define an incremental (nonlinear) aerodynamic model. The matrix B_2 defines the aerodynamic control effectiveness and is composed out of a known part, and an incremental part.

8.5 Simulation Scenarios and Results

This section presents the numerical simulation results from the application of the complete control design to the F-16 model of the previous section for a number of failure scenarios and flight conditions. The controller is evaluated on tracking performance and estimation accuracy. The control design has been implemented in the MATLAB/Simulink[©] environment by means of S-functions written in C++. First the tuning of the design will be discussed, followed by an introduction of the failure scenarios and flight conditions. After this, the simulations results will be presented and discussed. The simulations performed run in real time on a 2.4 Ghz desktop machine.

8.5.1 Controller Tuning

First of all the command shaping filters, see figure 8.1, are discussed. The purpose of the filters is to transform step-like input signals from the pilot or outer-loop flight path controller to smooth reference signals as input to the controller. These filters can be tuned and scheduled such that level 1 handling qualities can be achieved through the whole flight envelope, by scheduling their tuning on the flight conditions [163]. In this work a single tuning is selected for the whole flight envelope to simplify the design, since the main focus is on the feasibility of the control law design with online incremental model identification. The command filters are second-order low pass filters with magnitude constraints, the dynamics of these filters are

$$\begin{bmatrix} \dot{x}_c(t) \\ \ddot{x}_c(t) \end{bmatrix} = \begin{bmatrix} q_1 \\ q_2 \end{bmatrix} = \begin{bmatrix} 2\zeta\omega_n \left[S_R \left(\frac{\omega_n^2}{2\zeta\omega_n} \left[S_M(x^0) - q_1 \right] \right) - q_2 \right] \end{bmatrix} \quad (8.33)$$

where $S_M(\cdot)$ and $S_R(\cdot)$ represent the magnitude and rate limit functions respectively. The tuning parameters for the filters are shown in table 8.2. A different

Table 8.2: Command filter parameters.

Variable	Bandwidth	Damping	Magnitude Constraints
V_T	0.2	1.0	-
α	1.5	$\sqrt{2}/2$	-
β	2.0	$\sqrt{2}/2$	-
p_S	2.0	$\sqrt{2}/2$	-
q_S	100	$\sqrt{2}/2$	± 50 deg/s
r_S	100	$\sqrt{2}/2$	± 15 deg/s

damping ratio for the speed control has been selected to prevent overshooting the desired setting. Furthermore the bandwidth of the V_T command filter is small since the speed dynamics are relatively slow, especially compared to the other controlled variables. Additionally, accurate speed tracking is not the prime focus of the control design, the flown maneuvers are relatively short and highly dynamic.

The Lyapunov design only requires the controller gains to be negative definite, although it is natural to select the inner loop gains higher than the outer loop gains to achieve good tracking performance. The controller tracking error gains are selected as,

$$C_1 = \begin{bmatrix} 0.5 & 0 & 0 \\ 0 & 0.5 & 0 \\ 0 & 0 & 0.5 \end{bmatrix}, C_2 = \begin{bmatrix} 1.5 & 0 & 0 \\ 0 & 1.0 & 0 \\ 0 & 0 & 1.0 \end{bmatrix}$$

and the integrated tracking error gain only on the integrated stability axis roll rate

$$K_1 = \begin{bmatrix} 0 & 0 & 0 \\ 0 & 0 & 0 \\ 0 & 0 & 0 \end{bmatrix}, K_2 = \begin{bmatrix} 0.25 & 0 & 0 \\ 0 & 0 & 0 \\ 0 & 0 & 0 \end{bmatrix}.$$

The nonlinear damping gains κ are tuned to small values, if the parameter estimation is fast and accurate their contribution to the tracking performance is small. Therefore they are selected as $0.01I$ with I the identity matrix of appropriate size. The adaptive bounding gains are chosen small too since the assumption is made that the local model structure and the flight envelope partitioning will result in an accurate incremental model. The update gain Γ and leakage term σ are selected as

$$\begin{aligned} \Gamma &= \text{diag}([1 \times 10^{-6} \quad 1 \times 10^{-1} \quad 1 \times 10^{-1} \quad 1 \times 10^{-1} \quad 1 \times 10^{-1} \quad 1 \times 10^{-1}]) \\ \sigma &= 1 \times 10^{-1} I_6 \end{aligned}$$

The nonlinear swapping tuning parameters are selected such that the relevant dynamics of the aircraft can be captured. The swapping filter matrix is chosen as $A_0 = -100I_6$ and the damping gain $\rho = 0.01$. The flight envelope is partitioned

Table 8.3: Flight envelope partitioning.

Variable	min. (deg)	max. (deg)	step (deg)	hyperbox partitions
Angle of attack	-20	90	5	24
Sideslip angle	-30	30	5	14
Horizontal stabilizer deflection	-25	25	5	12
Total				4032

in three dimensions for the incremental model: the angle of attack, the sideslip angle, and horizontal stabilizer deflection, equivalent to most lookup tables in the existing model. Each input dimension of the B-spline basis functions is partitioned uniformly since this resulted in good tracking performance in earlier work [164]. The flight envelope partitioning is defined in table 8.3. The number of hyperbox partitions is a trade-off between local model complexity, required onboard storage capacity, and model accuracy. The order of the B-spline interpolation functions is a trade-off between the smoothness of the estimated model, and the number of active local models. Second order B-splines are used for all the input dimensions, since this produces a smooth nonlinear model, while limiting the number of active local models at any given point in the flight envelope to $3 \times 3 \times 3 = 27$.

A very mild forgetting rate of $\lambda = 0.005$ has been selected for all the partitions, this would correspond to a discrete forgetting factor of 0.9999 at 50 Hz sampling. The partitions are initialized with small values of the Cholesky factor of the covariance matrix, and a reset is triggered when an element of the partition weighted absolute estimation error vector exceeds

$$W_{\epsilon} = 1 \times 10^{-6} [1 \ 1 \ 1 \ 1 \ 1 \ 1]^T$$

the Cholesky factor for that particular partition is reset to

$$\hat{S}_{\text{reset}} = \text{diag} \left(\begin{array}{cccccccccccccccc} 10^2 & 10^4 & 10^3 & 10^2 & 10^2 & 10^2 & 10^3 & 10^3 & 10^2 & 10^3 & 10^3 & 10^2 & 10^2 & 10^2 \\ 10^4 & 10^4 & 10^4 & 10^2 & 10^3 & 10^5 & 10^3 & 10^2 & 10^2 & 10^4 & 10^4 & 10^4 & 1 & \end{array} \right)$$

to encourage fast adaptation to the changed system dynamics.

8.5.2 Simulation Scenarios

Three types of simulation scenarios are defined, the nominal case for which no faults occur, secondly a scenario where the center of gravity suddenly shifts in longitudinal direction, and finally scenarios in which the right aileron surface moves to a specified position and locks up. All simulations last 60 seconds. The simulations have been performed at two flight conditions, one at low altitude, 1000m at Mach 0.3, the other at cruise altitude of 10000m and Mach 0.8. Since the aircraft's maneuverability is different at these flight conditions, also different maneuvers have been performed at these flight conditions. In figure 8.3 the input commands for the two flight conditions is shown.

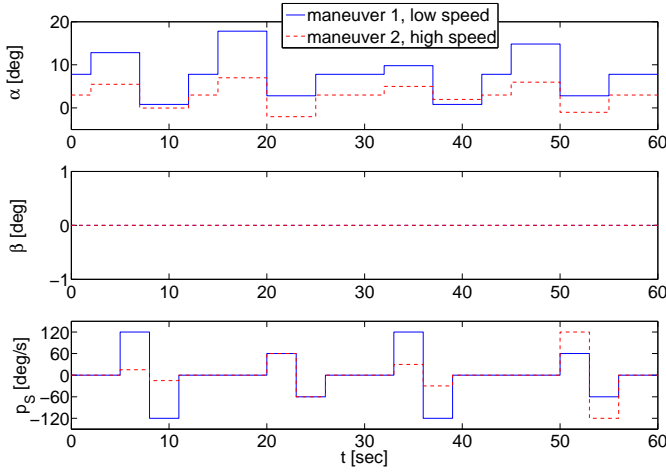


Figure 8.3: Input commands for the different maneuvers at different flight conditions.

The aileron faults are introduced after 7 seconds in the simulation, and they occur when the aircraft is rolling and pitching simultaneously. Three different lock positions are considered: locking at zero-deflection, lock at half deflection of 10.75 degrees, and a lock at full deflection or full hard-over of 21.5 degrees. Note that this aircraft model does not contain differential stabilizer inputs, hence only the rudder and the left aileron can be used to compensate the roll moment disturbance in this fault scenario.

In the last type of scenarios the center of gravity is suddenly shifted by 5% of the mean aerodynamic chord in longitudinal direction after 6 seconds into the simulation, which results in a change of longitudinal stability of the aircraft.

8.5.3 Simulation Results

First the nominal simulation results are presented to show that when the on-board model is accurate, excellent tracking performance of the angle of attack, sideslip angle, and velocity vector roll rate is achieved and the estimated incremental model parameters are practically zero. Figure 8.4 shows the tracking response and tracking errors, and figure 8.5 shows the estimated local model parameters during the maneuvers. Tracking of the velocity command is difficult due to the relatively slow response of the engine compared to the dynamics of the aircraft. Additionally, it is not possible to give negative thrust and speedbrakes are not included in the model. When there is no change of the onboard dynamics, the identifier does not estimate

a noticeable change in the incremental model parameters, tracking performance is excellent for both flight conditions and maneuvers.

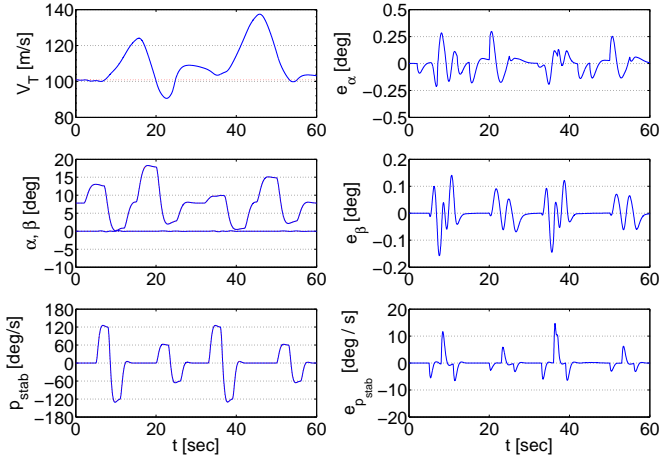
A more demanding and interesting scenario for the proposed adaptive controller is a sudden shift of the center of gravity in longitudinal direction. The pitching and yawing coefficients will change as a result of this shift according to

$$\begin{aligned}\Delta C_m &= C_Z \Delta x_{cg} \bar{c} \\ \Delta C_n &= C_Y \Delta x_{cg} \bar{b}\end{aligned}$$

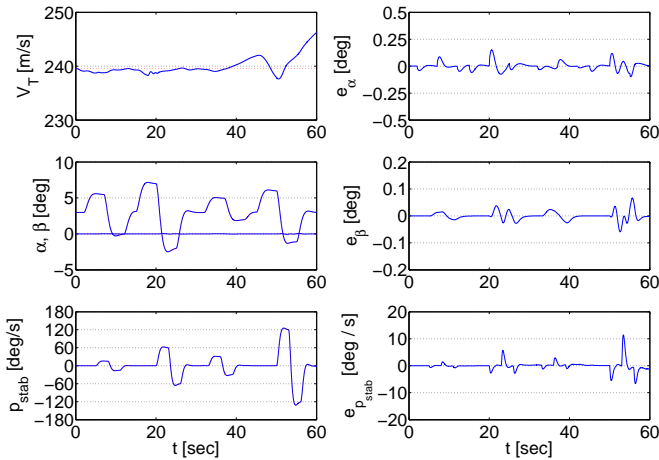
where Δx_{cg} is the shift in longitudinal direction in percentage of the chord length, ΔC_m is the increment in pitch moment coefficient, and ΔC_n the increment in yaw moment coefficient. No inertia model was available, therefore the mass and moments of the aircraft do not change. Normally, aircraft and their control laws are designed for a range of possible center of gravity positions. Especially for model based controllers a *known* change of position is therefore not a problem, a sudden unknown change on the other hand can cause degraded tracking performance and even stability problems. Figure 8.6(a) shows the tracking performance for a destabilizing shift of 5% of the mean aerodynamic chord, or 0.1725 m. In figure 8.6(b) the control deflections are compared with the nominal center of gravity position deflections. Figure 8.7(a) shows the response and tracking error of the proposed control scheme without any adaptation, i.e. $\hat{\theta} = 0, \psi = 0$. Clearly the tracking performance has decreased a lot caused by the mismatch between the onboard model and the true aircraft dynamics. A direct comparison of the tracking errors between the adaptive control design (left) and non-adaptive control design (right) is possible in figure 8.8.

The filtered residual error signals (8.14) are shown in figure 8.9, which shows that when a new part of the flight envelope is visited after the failure, first the filtered residuals increase after which they converge back to zero when the estimates for the active partitions are updated. The estimated incremental model parameters during the simulation are shown in figure 8.10(a). The failure is detected very rapidly, as seen in figure 8.10(b), and several of the active partitions are reset almost immediately. When a different part of the flight envelope is visited during the maneuvering, also the partitions that become active and have not been updated yet, are reset. To show that the update is only local, figure 8.11 shows the estimated δC_m at the end of the simulation compared to a cross-section of the interpolated lookup table value $C_Z(\alpha, \beta, \delta_e)$ at $\beta = 0$, which is a main contributor to the effect of the center of gravity shift. The figure shows that the identifier only estimated in the part of the envelope where the aircraft has flown, and that the estimation is accurate.

The proposed control design with a single partition, i.e. one local model, for the whole flight envelope has been simulated. The tracking performance of the controller is of the same level as the partitioned controller as shown in figure 8.12, however the scheme has less capability to store its estimated data for different parts of the flight envelope. Although the single incremental model control design

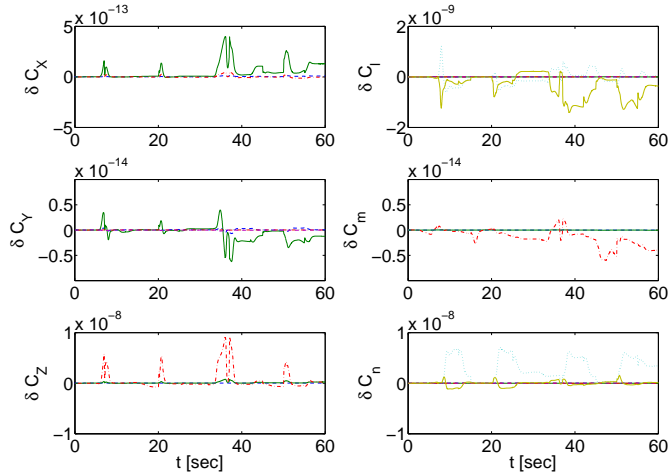


(a) Response FC1 nominal

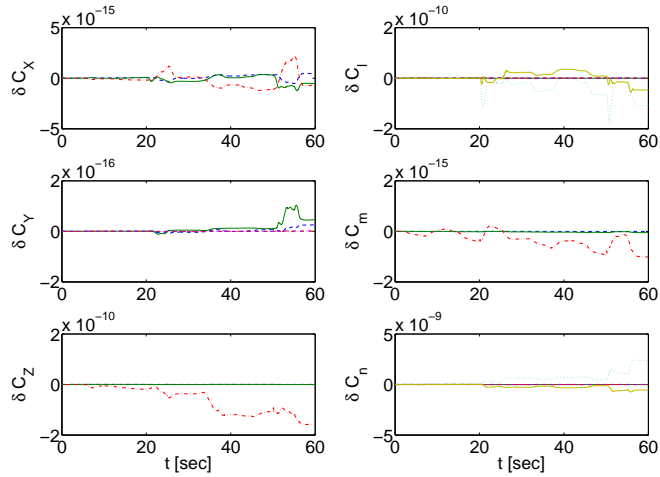


(b) Response FC2 nominal

Figure 8.4: Tracking response for two different maneuvers executed at two different flight conditions. The tracking response for the low altitude, slow flight is shown in 8.4(a) . The tracking response for the cruise altitude and velocity is shown in 8.4(b).

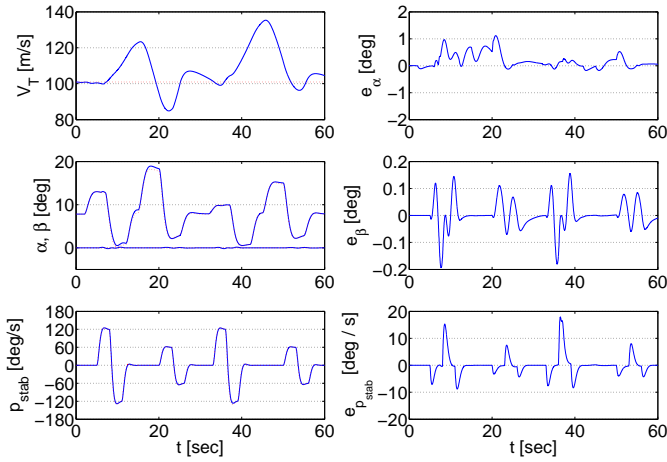


(a) Estimation FC1 nominal

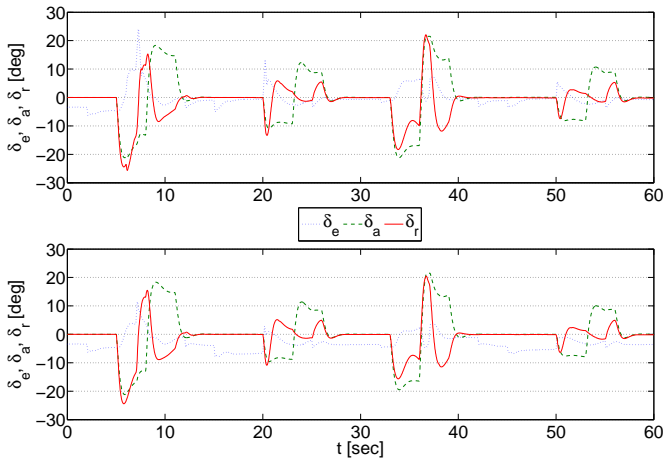


(b) Estimation FC2 nominal

Figure 8.5: Incremental model parameters estimated during the nominal tracking maneuvers at two different flight conditions. The model parameters for low altitude, slow flight, are shown in 8.5(a). The model parameters for cruise altitude and velocity flight are shown in 8.5(b).

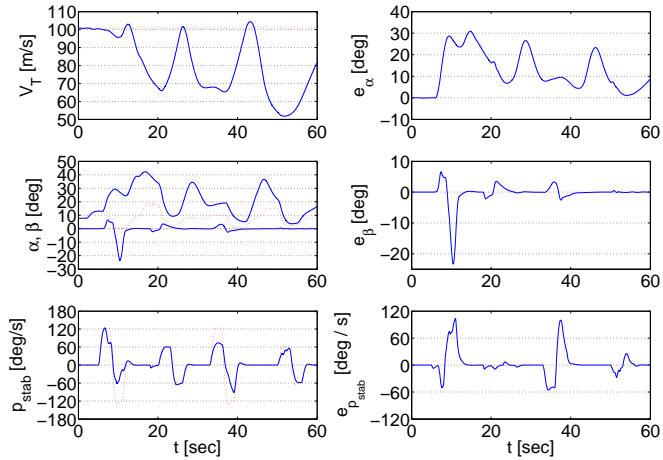


(a) Response for c.g. shift - adaptive

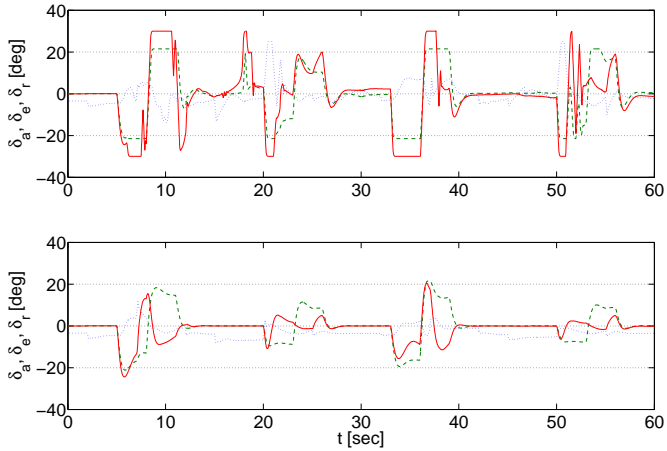


(b) Actuator input for c.g. shift - adaptive

Figure 8.6: The response of the aircraft for a sudden center of gravity shift after 6 seconds at low altitude, low speed flight is shown in 8.6(a). The control surface deflections for the shifted center of gravity location at the top of 8.6(b), and the nominal deflections the bottom.



(a) Reponse for c.g. shift - non-adaptive



(b) Actuator input for c.g. shift - non-adaptive

Figure 8.7: The response and tracking errors of the aircraft with non-adaptive controller for a sudden center of gravity shift after 6 seconds at low altitude, low speed flight are shown in 8.7(a). The control deflections for the aircraft with changed c.g. location are shown at the top of 8.7(b), and the nominal deflections at the bottom.

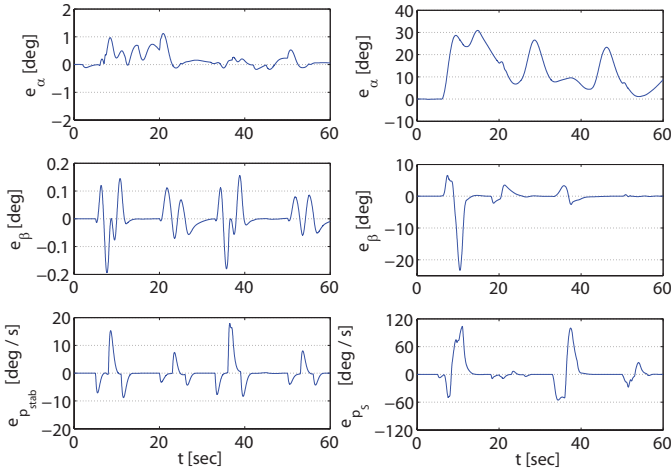


Figure 8.8: Tracking errors for the adaptive control design (left) and non-adaptive control design (right) for a sudden center of gravity shift.

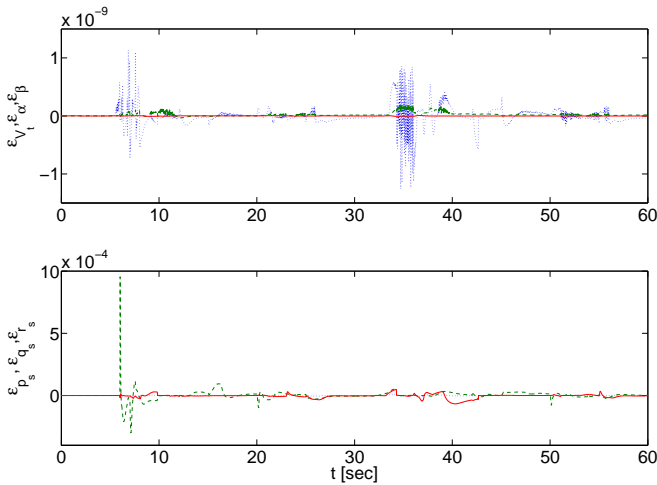


Figure 8.9: The filtered residuals for the adaptive controller for a sudden center of gravity shift after 6 seconds.

is capable of approximating the incremental dynamics accurately over a limited portion of the flight envelope, it will never yield a globally valid approximation using the same model structure as is used in each of the partitions of the fully partitioned flight envelope. This limitation is illustrated in figure 8.11, the single partition controller achieves a good approximation of δC_m for a small portion of the complete envelope: it fits a tangent plane to the true function. The fully partitioned envelope only approximates accurately in the visited part of the flight envelope, and its estimate in the unvisited parts is equal to zero. Increasing the order and complexity of the regressor would increase the approximation capabilities of the identifier in the single partitioned case. Unfortunately, it is not always clear which basis functions to include in the model such that the basis functions have physical interpretation, and increase the approximation capabilities. This problem is approached in the next chapter through on-line structure selection.

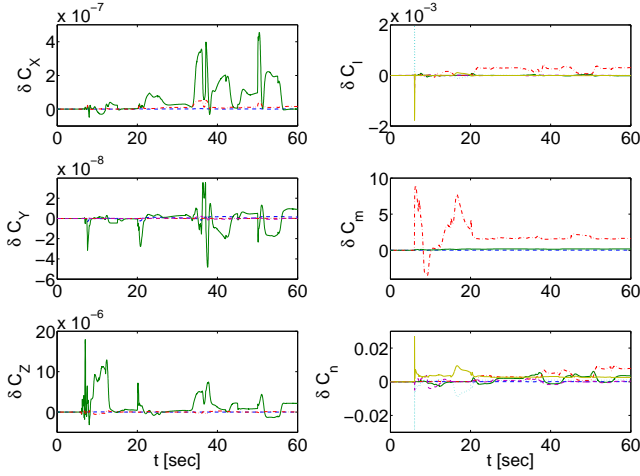
Finally the results of one of the aileron experiments are shown: the case with a full hard-over of the right aileron at the cruise altitude and velocity. The response is shown in figure 8.13(a). Due to the reduced control authority around the lateral axis, the aircraft is not able to track the roll command, tracking of the angle of attack command is excellent however. Additionally, despite the locked aileron, the sideslip angle is very small: in the order of a half degree. The estimated incremental model parameters are shown in figure 8.14(a). Clearly the change in dynamics is detected, and the identifier estimates mainly in the lateral directions. However, the incremental model estimates do not yet converge to their true values, not enough information to estimate the correct parameters can be obtained from the flown maneuver. The control surface deflections are compared to the nominal case in figure 8.13(b).

8.6 Conclusions

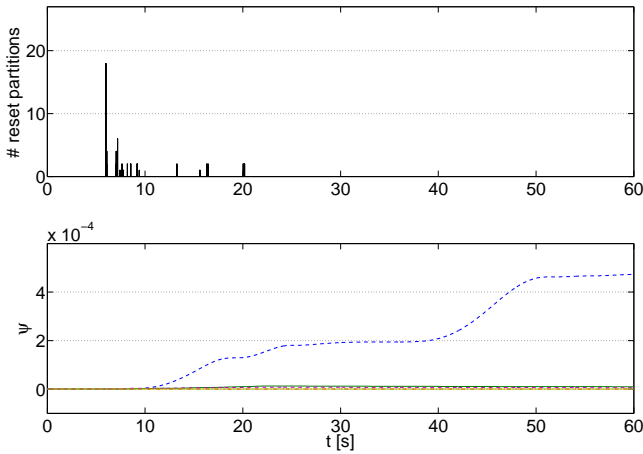
In this chapter a modular control design is presented for a high-fidelity nonlinear of an F-16 aircraft. The controller is based on the backstepping approach, combined with a orthogonal least squares identifier. The flight envelope is partitioned into hyperboxes, in each of these hyperboxes a local linear-in-the-parameters model is estimated, and using second-order B-spline interpolation a smooth model is obtained for the complete flight envelope. The developed control design was tested in three different simulation scenarios: a nominal scenario without failures, a sudden shift of the center of gravity, and a full hard-over of right aileron.

Based on the simulations the following conclusions can be drawn.

- The performance of the adaptive control design is identical in the nominal case as for a non-adaptive controller with the same tuning. An incremental model to the on-board model is estimated to account for mismatch between the true and modeled dynamics. If the input signals are sufficiently rich, this



(a) Estimation for c.g. shift



(b) Resetting and adaptive bounding for c.g. shift

Figure 8.10: The estimated incremental model parameters are shown in 8.10(a). 8.10(b) shows the number of partitions reset at a certain time instant at the top, and at the bottom shows the adaptive bounding estimate ψ .

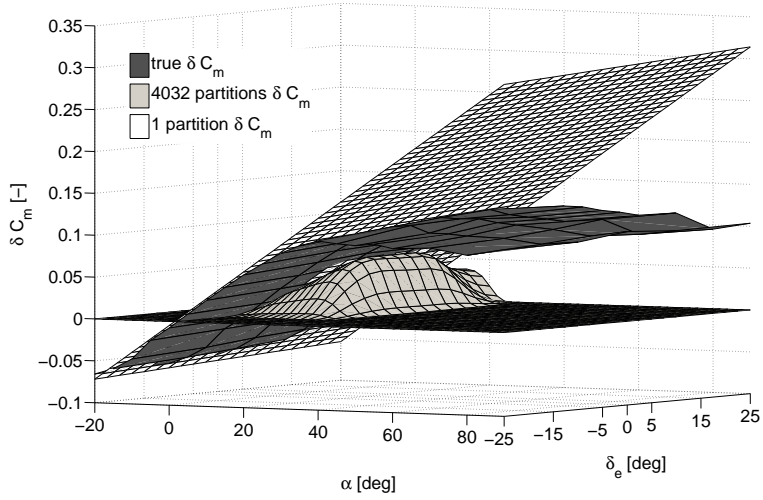


Figure 8.11: A 3d-view of an intersection at $\beta = 0$ of the estimated δC_m due to a change in the center of gravity position for a fully partitioned flight envelope, a single partition flight envelope, and the true change of the C_m coefficient caused by this shift.

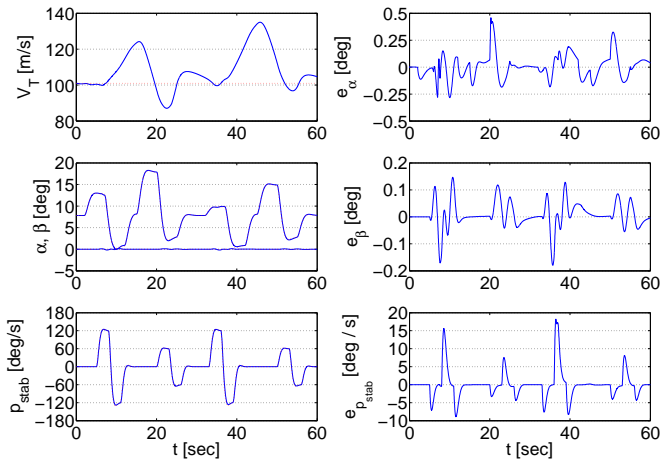
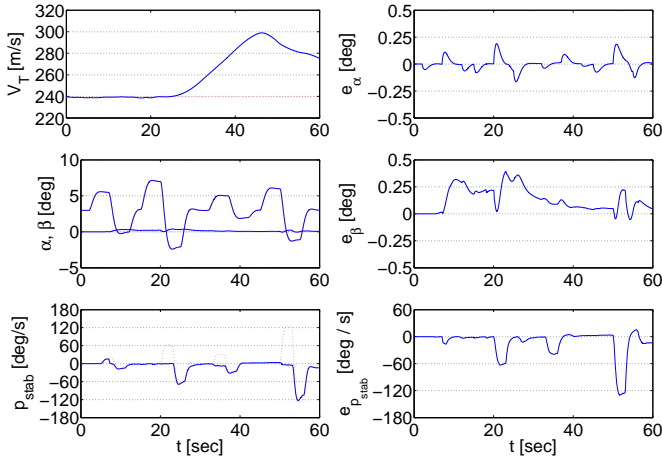
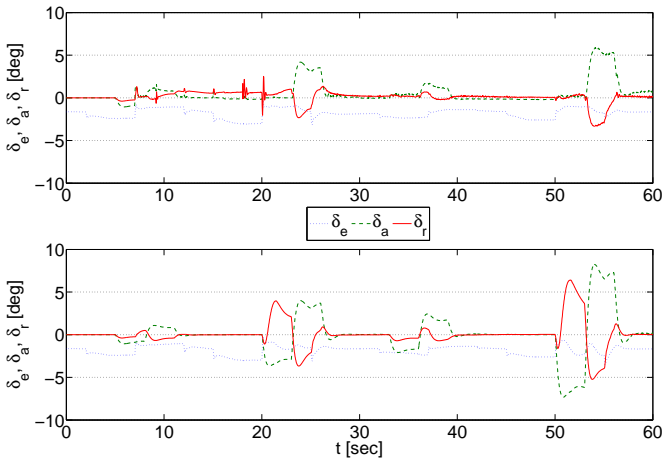


Figure 8.12: Response and tracking error of the adaptive controller with single partition incremental model for a sudden center of gravity shift after 6 seconds at low altitude, low speed flight.

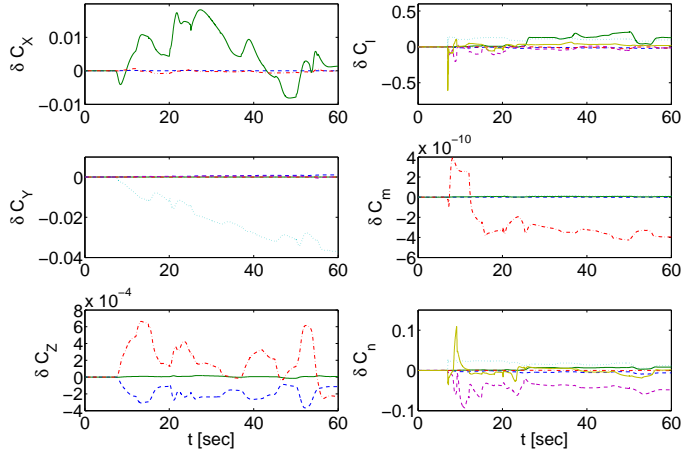


(a) Response for aileron hardover

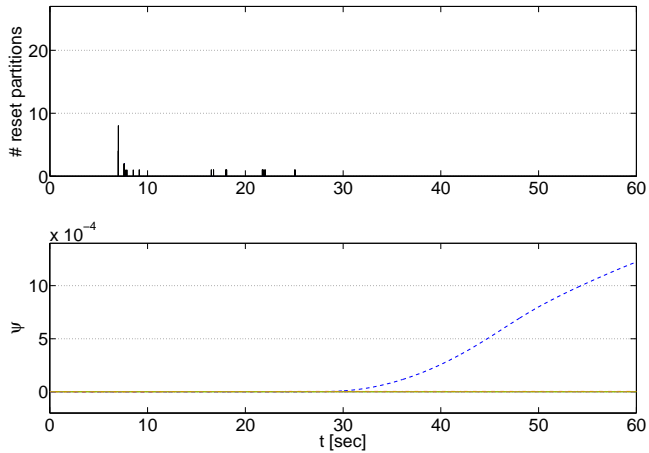


(b) Actuator input for aileron hardover

Figure 8.13: The response of the aircraft after a full right aileron hardover occurring after 7 seconds at high altitude, cruise speed flight is shown in 8.13(a). The control surface deflections for the aircraft with full right aileron hard-over at the top of 8.13(b), and the nominal deflections the bottom.



(a) Estimation for aileron hardover



(b) Resetting and adaptive bounding for aileron hardover

Figure 8.14: The estimated incremental model parameters are shown in 8.14(a). The number of partitions resetting at a certain time instant is shown at the top of 8.14(b), and the bottom shows the adaptive bounding estimate ψ .

incremental model approximates the difference between the a-priori model and the true dynamics.

- In the simulation scenario with a sudden shift of the center of gravity in longitudinal direction, tracking performance was excellent and the correct change in the dynamics was estimated. The performance of the non-adaptive control design degraded considerably.
- Longitudinal tracking performance was excellent while lateral tracking performance was partially restored for the aileron failure scenario.
- Partitioning the flight envelope into smaller partitions allows the use of relatively simple incremental models, and keeps the number of *active* identifier states within acceptable bounds. Additionally, it helps to reduce the required local model complexity to obtain an accurate fit to the true dynamics.

Improvements can be made on the control design as well.

- The lateral tracking performance was only partially restored in the case of an aileron failure. If the estimated model can be used to predict the maneuvering capabilities of the aircraft before and after failures, this information would be incredibly valuable for the (auto)pilot.
- The structure of lookup-tables of the nominal F-16 model is highly similar to that of the chosen local models. Hence, the design approach should also be evaluated when this is not the case, possibly with automatic structure selection of the local models.

FULL ENVELOPE ADAPTIVE CONTROL WITH STRUCTURE SELECTION AND CONTROL ALLOCATION

In this chapter several techniques used in the preceding chapters are combined to design an adaptive control design for the ADMIRE aircraft model. The flight envelope partitioning approach from chapter 8 is extended with structure selection in each partition, and then combined with the adaptive optimizing control allocation approach from chapter 7. Simulation results are presented for different failures and center of gravity shifts.

9.1 Introduction

For many indirect-adaptive flight control applications the model structure is considered fixed, and only aerodynamic parameters are estimated, for example by means of a least-squares procedure. However, the model structure that has been selected for the nominal design may be invalid during highly dynamic maneuvers and in post-failure situations. In these conditions, it is very probable that the nominal model structure has to be extended with additional nonlinear and/or coupling terms. Unfortunately, it is not known during the design which independent variables will have a significant influence on the dependent variable in post failure flight conditions. Inclusion of all possible regressor candidates (or independent variables) in the regressor set will lead to many small coefficients with large standard deviations. Additionally, these coefficients perturb the estimation of the coefficients for the significant regressors and destroy the extrapolation properties

[99]. Therefore, proper model identification including structure selection is nearly unavoidable for aircraft with large changes or variations in their aerodynamics due to for example component failures and airframe damage, especially for fault diagnosis and isolation purposes.

The combined problem of structure selection and parameter estimation (SSPE) can be stated as selecting a subset of regressor candidates and finding the corresponding parameter estimate which adequately fits the data [26]. A possible approach to the SSPE problem is applying some optimal multiple selection method based on the theory of hypothesis testing like stepwise regression[40, 85]. For on-line applications however these methods are not suitable since the measurement data becomes available sequentially. A suboptimal method based on orthogonal decompositions and forward selection is more promising for on-line applications. The idea of using OLS in nonlinear aerodynamic modeling problems is not new. The similar idea of generating multivariate orthogonal modeling functions from measured data, ranking those functions by fit error reduction capability, and using the predicted square error (PSE) was developed by Klein and Morelli [85], Morelli [121]. Moreover, orthogonal functions were used by Mulder [122] in optimization of multi-dimensional input signals for dynamic flight test maneuvers. The use of recursive OLS combined with model selection was introduced by Luo and Billings [104]. This approach was used in combination with an NDI-design for a Boeing 747 aircraft by Lombaerts, Oort, Chu, Mulder, and Joosten [99].

In this chapter, first the equations of motion for a rigid body aircraft are revisited in vector form. Then, a Lyapunov based control design is presented to control these dynamics, including optimizing control allocation and parameter estimation based on a composite update law. Then, a structure selection algorithm is introduced based on orthogonal least squares decompositions. This approach is then extended to full envelope modeling by partitioning the flight envelope into small partitions, with a local incremental model in each model to be identified. Simulation results are presented for the application of the resulting control design on the ADMIRE model under different failure and flight conditions. Finally, conclusions are drawn and some directions for future research are indicated.

9.2 Aircraft Dynamics and Problem Statement

The aircraft is assumed to be a rigid body with mass m and inertia tensor J . Its motion will be described in a body-fixed coordinate system, with the origin at the center of mass. Then, the aircraft dynamics can be described by

$$m\dot{V} = F - \omega \times mV \quad (9.1)$$

$$J\dot{\omega} = \tau - \omega \times J\omega \quad (9.2)$$

where V is the velocity, and ω is the angular velocity. F is the external force resulting from gravity, aerodynamics and engine thrust. τ is the external torque

due to aerodynamics and engine thrust. The velocity vector can be decomposed into

$$V = V_T \hat{V} = V_T \begin{bmatrix} \cos \alpha \cos \beta \\ \sin \beta \\ \sin \alpha \cos \beta \end{bmatrix} \quad (9.3)$$

Then, the velocity dynamics (9.1) can be split into a part related to the magnitude of the vector, or total airspeed, as

$$\dot{V}_T = \frac{\hat{V}^T F}{m} \quad (9.4)$$

and a part considering the direction of the vector

$$\dot{\hat{V}} = \hat{V} \times \frac{F}{mV_T} \times \hat{V} - \omega \times \hat{V}. \quad (9.5)$$

This description of the aircraft dynamics assumes that the external forces and moments acting on the aircraft are completely known. However, even in the nominal case this is not entirely true since there will nearly always exist a mismatch between the true and the modeled aircraft dynamics. Therefore, the velocity vector direction and angular velocity dynamics are rewritten as

$$\dot{\hat{V}} = \hat{V} \times \frac{F_0(t, x, u) + \varphi_F^T(t, x, u)\theta + \delta_F(t, x, u)}{mV_T} \times \hat{V} - \omega \times \hat{V} \quad (9.6)$$

$$J\dot{\omega} = \tau(t, x, u, \theta) - \omega \times J\omega \quad (9.7)$$

where F_0 represents the known or a-priori estimate of the external force, x is the state of the system composed out of \hat{V} and ω , u are the control effector states or inputs, φ_F is a known function, θ is an unknown constant parameter, and δ_F an unknown smooth function representing function uncertainty. Additionally, there exists a mapping from the control effectors u to the torque on the aircraft

$$\tau(t, x, u, \theta) = \tau_0(t, x, u) + \varphi_\tau^T(t, x, u)\theta + \delta_\tau(t, x, u) \quad (9.8)$$

where τ_0 is the a-priori estimate of the external moment, φ_τ a known function, and δ_τ represents function uncertainty. The system dynamics can be described in compact form by

$$\dot{x} = K(t, x, u, \theta) \quad (9.9)$$

If an actuator model is available, the effect of the actuators can be removed from the tracking error in the command filtering approach by introducing an estimated control effector state u with dynamics

$$\dot{u} = m(t, x, u, u_d). \quad (9.10)$$

where u_d represents the commanded deflections.

The control task is to track a reference signals for the direction of the velocity vector and the velocity vector roll rate, or wind-axis roll rate. The available control effectors are the control surfaces that generate aerodynamic forces and moments on the aircraft, and the engine thrust. To handle the over-actuation of aircraft with many control effectors, and the uncertainty in the model structure and model parameters an adaptive backstepping approach with optimizing control allocation, command filtering, and online structure selection is chosen.

9.3 Control Law Design

In this section the control law design is discussed. Many of the introduced backstepping design techniques in the preceding part of the dissertation come together in the design. First a vectorized backstepping approach to velocity vector direction and roll-rate control is introduced when the aircraft dynamics are completely known. Then, this control design is extended with command filters to remove the need of analytical derivatives of the intermediate control laws. The filtered backstepping design is extended with parameter update law to estimate the unknown parameter, and the optimizing control allocation approach from chapter 7. Finally, the controller is made robust against the function uncertainty δ to reduce transient response effects.

9.3.1 Vector Backstepping

The control goal is to track a reference signal for the direction of the velocity vector, and the rotation rate around this velocity vector, or wind-axis roll-rate. First the high level control design is made for the case that there is no uncertainty: $\theta = 0$, $\delta = 0$. The tracking errors are defined as

$$z_1 = \hat{V} - \hat{V}_r \quad (9.11)$$

$$z_2 = \omega - \omega_c \quad (9.12)$$

where \hat{V}_r is the reference velocity vector direction, and ω_r the reference angular rate. A speed controller can be added by designing a desired throttle setting based on equation (9.4). The first step is to design a control law which renders the origin asymptotically stable when $z_2 = 0$. Consider the CLF candidate $W_1 = \frac{1}{2}z_1^T z_1$ with

time derivative

$$\begin{aligned}
 \dot{W}_1 &= \dot{z}_1^T z_1 \\
 &= (\dot{\hat{V}} - \dot{\hat{V}}_r)^T (\hat{V} - \hat{V}_r) \\
 &= \left(\hat{V} \times \frac{F_0}{mV_T} \times \hat{V} - \omega \times \hat{V} - \dot{\hat{V}}_r \right)^T (\hat{V} - \hat{V}_r) \\
 &= \left(\hat{V} \times \frac{F_0}{mV_T} \times \hat{V} - z_2 \times \hat{V} - \alpha_1 \times \hat{V} + \omega_{\hat{V}_r} \times \hat{V}_r \right)^T (\hat{V} - \hat{V}_r) \quad (9.13)
 \end{aligned}$$

such that with

$$\alpha_1 = \omega_c = -C_1 (\hat{V} \times \hat{V}_r) - \frac{F_0}{mV_T} \times \hat{V} + \omega_{\hat{V}_r} + p_{W_{\text{ref}}} \hat{V}, \quad C_1 = C_1^T > 0 \quad (9.14)$$

the time derivative of W_1 becomes

$$\begin{aligned}
 \dot{W}_1 &= \left(-z_2 \times \hat{V} + C_1 (\hat{V} \times \hat{V}_r) \times \hat{V} - \omega_{\hat{V}_r} \times \hat{V} + \omega_{\hat{V}_r} \times \hat{V}_r \right)^T (\hat{V} - \hat{V}_r) \\
 &= -(\hat{V} \times \hat{V}_r)^T C_1 (\hat{V} \times \hat{V}_r) < 0, \quad \hat{V} \neq \pm \hat{V}_r.
 \end{aligned}$$

In this derivation the relation $a^T (b \times c) = b^T (c \times a) = c^T (a \times b)$ has been used. In the second step of the backstepping design a desired torque is designed. The CLF is augmented with a term penalizing the angular rate tracking error

$$W_2 = W_1 + \frac{1}{2} z_2^T z_2. \quad (9.15)$$

The time derivative of this CLF along the solutions of (9.6), (9.7), and intermediate control law (9.14) becomes

$$\begin{aligned}
 \dot{W}_2 &= -(\hat{V} \times \hat{V}_r)^T C_1 (\hat{V} \times \hat{V}_r) - z_2^T (\hat{V} \times z_1) \\
 &\quad + z_2^T \left(J^{-1} (\tau - \omega \times J\omega) - \dot{\omega}_c \right) \quad (9.16)
 \end{aligned}$$

which can be rendered negative definite by the choice

$$\tau_{\text{des}} = \omega \times J\omega + J (\hat{V} \times z_1) + J\dot{\alpha}_1 - JC_2 z_2. \quad (9.17)$$

With this choice of intermediate control laws, the CLF derivative becomes

$$\dot{W}_2 = -(\hat{V} \times \hat{V}_r)^T C_1 (\hat{V} \times \hat{V}_r) - z_2^T C_2 z_2 < 0, \quad \hat{V} \neq \pm \hat{V}_r, \quad z_2 \neq 0.$$

showing UGAS of the origin of the tracking error system.

9.3.2 Command Filtering

The backstepping design can be modified to include command filters, removing the need for the analytic derivative of the virtual control law (9.14) and (9.17). The effect of filtering the virtual control laws to produce their time derivatives, and the effect of actuator dynamics is estimated by special filters. Define augmented tracking errors as

$$\bar{z}_1 = z_1 - \Xi_1 \quad (9.18)$$

$$\bar{z}_2 = z_2 - \Xi_2, \quad (9.19)$$

and the filter dynamics become

$$\dot{\Xi}_1 = -C_1 \hat{V} \times \Xi_1 \times \hat{V} - \omega_{\hat{V}_r} \times z_1 - (\omega_c - \omega_c^0) \times \hat{V} \quad (9.20)$$

$$\dot{\Xi}_2 = -C_2 \Xi_2 + J^{-1} \left(\tau(t, x, u, \hat{\theta}) - \tau_{\text{des}}^0 \right). \quad (9.21)$$

where τ_{des}^0 is the desired torque, and τ is the estimated torque generated on the aircraft at the current operating point. The derivative of α_1 in (9.17) is replaced with the derivative output of the filter

$$\tau_{\text{des}}^0 = \omega \times J\omega + J(\hat{V} \times z_1) + J\dot{\omega}_c - JC_2 z_2. \quad (9.22)$$

Then, the time-derivative of the CLF $V_2 = \frac{1}{2} \bar{z}_1^T \bar{z}_1 + \frac{1}{2} \bar{z}_2^T \bar{z}_2$ becomes

$$\dot{V}_2 = -(\hat{V} \times (\hat{V}_r + \Xi_1))^T C_1 (\hat{V} \times (\hat{V}_r + \Xi_1)) - \bar{z}_2^T C_2 \bar{z}_2 \leq 0.$$

showing UGAS of the origin of the augmented tracking error system. If the filter settings are chosen appropriately, the signals Ξ will be small, and therefore the tracking error z will be small.

9.3.3 Optimizing Control Allocation

The desired torque τ cannot be directly commanded to the aircraft, it is influenced by the control effectors. Since on modern aircraft there exist many different control effectors some form of control allocation is required to distribute the desired torque over the control effectors. This can be formulated as a static optimization problem as done in (7.5) and transformed into a Lagrangian function (7.6) with assumptions 7.2. Suppose there exists a cost function $J(t, x, u_d)$, which together with the desired torque can be transformed into the Lagrangian function

$$L(t, x, u_d, \lambda, \theta) = J(t, x, u_d) + (\tau(t, x, u_d, \theta) - \tau_{\text{des}})^T \lambda. \quad (9.23)$$

In the nominal situation, where θ and δ are assumed to be zero, introduce the OCLF

$$V_{\text{ca}}(t, \bar{z}, u_d, \lambda) = \sigma W_2 + \frac{1}{2} \left(\frac{\partial L^T}{\partial u_d} \frac{\partial L}{\partial u_d} + \frac{\partial L^T}{\partial \lambda} \frac{\partial L}{\partial \lambda} \right), \quad (9.24)$$

which is an extension of the V_2 with terms penalizing the first order derivatives of a Lagrangian function with respect to the desired control effector signals, and the Lagrangian parameter. The update laws for the control allocation part become

$$\begin{bmatrix} \dot{u}_d \\ \dot{\lambda} \end{bmatrix} = -\gamma H^{-1} \begin{bmatrix} \frac{\partial L}{\partial u_d} \\ \frac{\partial L}{\partial \lambda} \end{bmatrix} - H^{-1} u_{\text{ff}} \quad (9.25)$$

where

$$H = \begin{bmatrix} \frac{\partial^2 L}{\partial u_d^2} & \frac{\partial^2 L}{\partial \lambda \partial u_d} \\ \frac{\partial^2 L}{\partial u_d \partial \lambda} & 0 \end{bmatrix}$$

and

$$u_{\text{ff}} = H^{-1} \begin{bmatrix} \frac{\partial^2 L}{\partial t \partial u_d} \\ \frac{\partial^2 L}{\partial t \partial \lambda} \end{bmatrix} + H^{-1} \begin{bmatrix} \frac{\partial^2 L}{\partial \bar{z} \partial u_d} \\ \frac{\partial^2 L}{\partial \bar{z} \partial \lambda} \end{bmatrix} (K(t, x, u, \theta) - \dot{x}_c - \dot{\bar{z}}).$$

With these update laws, the OCLF derivative becomes

$$\dot{V}_{\text{ca}} = -\sigma \sum_{i=1}^2 \bar{z}_i^T C_i \bar{z}_i - \begin{bmatrix} \frac{\partial L}{\partial u_d} \\ \frac{\partial L}{\partial \lambda} \end{bmatrix}^T H \Gamma_{\text{ca}} H \begin{bmatrix} \frac{\partial L}{\partial u_d} \\ \frac{\partial L}{\partial \lambda} \end{bmatrix}.$$

9.3.4 Adaptive Optimizing Control Allocation

The design is now extended in two directions, the parametric uncertainty is taken into account and the desired virtual control commands M_{des} are transformed to control effector commands u_d based on the solution of an optimization problem. The approach taken is identical to the adaptive control allocation schemes introduced in chapter 7.

First, introduce the swapping filters required for the modular and composite adaptive approaches when state derivative measurements are not available. The swapping filter states are defined by

$$\dot{\Omega}_0 = A(\Omega_0 + Gx) - f(t, x, u) \quad (9.26)$$

$$\dot{\Omega}^T = A\Omega^T + F^T(t, x, u) \quad (9.27)$$

where

$$G = \begin{bmatrix} I_3 & 0 \\ 0 & J \end{bmatrix},$$

$$f(t, x, u) = \begin{bmatrix} \hat{V} \times \frac{F_0}{mV_T} \times \hat{V} - \omega \times \hat{V} \\ \tau_0 - \omega \times J\omega \end{bmatrix},$$

$$F^T(t, x, u) = \begin{bmatrix} \hat{V} \times \frac{\varphi_F^T}{mV_T} \times \hat{V} \\ \varphi_\tau \end{bmatrix}.$$

The estimation error is defined as

$$\epsilon = (\Omega_0 + Gx) - \Omega^T \hat{\theta} = \Omega^T \tilde{\theta} + \tilde{\epsilon}. \quad (9.28)$$

The matrix A is negative definite, and defined as in (7.26). With the parameter estimate available, the intermediate control law is modified to cancel the estimated incremental force in (9.6) and a nonlinear damping term

$$\alpha_1 = -(C_1 + S_1) (\hat{V} \times \hat{V}_r) - \frac{F_0 + \varphi_F^T \hat{\theta}}{mV_T} \times \hat{V} + \omega_{\hat{V}_r} + p_{W_{ref}}, \quad (9.29)$$

where

$$S_1 = \left(\hat{V}_\times \frac{\varphi_F^T}{mV_T} \right)^T \kappa_1 \left(\hat{V}_\times \frac{\varphi_F^T}{mV_T} \right), \quad \kappa_1 = \kappa_1^T > 0.$$

Additionally, nonlinear damping is added to the desired torque

$$\tau_{des}^0 = \omega \times J\omega + J(\hat{V} \times z_1) + J\dot{\omega}_c - J(C_2 + S_2)z_2 \quad (9.30)$$

where

$$S_2 = J^{-1} \varphi_\tau^T \kappa_2 \varphi_\tau J^{-T}, \quad \kappa_2 = \kappa_2^T > 0.$$

Then, the OCLF is extended with a term penalizing the estimation error $\tilde{\theta}$, and the residual $\tilde{\epsilon} = \Omega_0 + Gx - \Omega^T \theta$, resulting in an AOCLF. With the time derivative of this AOCLF the composite update law for the parameter estimate $\hat{\theta}$ can be designed

$$V_{comp} = V_{ca} + \frac{1}{2} \tilde{\theta}^T \Gamma_\theta^{-1} \tilde{\theta} + \frac{1}{2} \tilde{\epsilon}^T P \Psi \tilde{\epsilon} \quad (9.31)$$

where $\Psi = \Psi^T > 0$ is a weight matrix to control how the adaptation law should weight information from the tracking error relative to the information coming from the estimation error. The resulting composite update law is

$$\dot{\hat{\theta}} = \Gamma_\theta \left(\sigma \frac{\varphi_F}{mV_T} \hat{V}_\times^T \bar{z}_1 + \varphi_\tau \left(J^{-T} \bar{z}_2 + \frac{\partial^2 L^T}{\partial x \partial u_d} \frac{\partial L}{\partial u_d} + \frac{\partial^2 L^T}{\partial x \partial \lambda} \frac{\partial L}{\partial \lambda} \right) + \Omega \Psi \epsilon \right), \quad (9.32)$$

with the update of Γ_θ defined as

$$\dot{\Gamma}_\theta = -\Gamma_\theta \Omega \Psi \Omega^T \Gamma_\theta + \lambda \Gamma_\theta, \quad \lambda \geq 0. \quad (9.33)$$

Since the parameter estimate is now time-varying, it is included in the feed-forward path of the optimizing control allocation update laws, additionally nonlinear damping terms are added to the design to improve the transient response. The adaptive optimizing control allocation update laws become

$$\begin{bmatrix} \dot{u}_d \\ \dot{\lambda} \end{bmatrix} = -\Gamma_{ca} H \begin{bmatrix} \frac{\partial L}{\partial u_d} \\ \frac{\partial L}{\partial \lambda} \end{bmatrix} - H^{-1} (u_{ff} + u_\kappa) \quad (9.34)$$

with

$$u_{\text{ff}} = \begin{bmatrix} \frac{\partial^2 L}{\partial t \partial u_d} \\ \frac{\partial^2 L}{\partial t \partial \lambda} \end{bmatrix} + \begin{bmatrix} \frac{\partial^2 L}{\partial \bar{z} \partial u_d} \\ \frac{\partial^2 L}{\partial \bar{z} \partial \lambda} \end{bmatrix} (K(t, x, u, \hat{\theta}) - \dot{x}_c - \dot{\Xi}) + \begin{bmatrix} \frac{\partial^2 L}{\partial \hat{\theta} \partial u_d} \\ \frac{\partial^2 L}{\partial \hat{\theta} \partial \lambda} \end{bmatrix} \dot{\hat{\theta}}$$

$$u_\kappa = \begin{bmatrix} \frac{\partial^2 L}{\partial x \partial u_d} \\ \frac{\partial^2 L}{\partial x \partial \lambda} \end{bmatrix}^T J^{-1} \varphi_\tau^T \kappa_u \varphi_\tau J^{-T} \begin{bmatrix} \frac{\partial^2 L}{\partial x \partial u_d} \\ \frac{\partial^2 L}{\partial x \partial \lambda} \end{bmatrix} \begin{bmatrix} \frac{\partial L}{\partial u_d} \\ \frac{\partial L}{\partial \lambda} \end{bmatrix}.$$

The Ξ filters are additionally modified to guarantee global boundedness of the augmented tracking error:

$$\dot{\Xi}_1 = -(C_1 + S_1) \hat{V} \times \Xi_1 \times \hat{V} - \omega_{\hat{V}_r} \times z_1 - (\omega_c - \omega_c^0) \times \hat{V} \quad (9.35)$$

$$\dot{\Xi}_2 = -(C_2 + S_2) \Xi_2 + J^{-1} (\tau(t, x, u, \hat{\theta}) - \tau_{\text{des}}^0). \quad (9.36)$$

The resulting AOCLF derivative becomes

$$\dot{V}_{\text{comp}} \leq -\sigma \sum_{i=1}^n \bar{z}_i^T C_i \bar{z}_i - \frac{1}{2} \epsilon^T \Psi \epsilon + \frac{1}{4} \hat{\theta}^T (\sigma \kappa_1^{-1} + \sigma \kappa_2^{-1} + \kappa_u^{-1}) \tilde{\theta}$$

$$- \begin{bmatrix} \frac{\partial L}{\partial u_d} \\ \frac{\partial L}{\partial \lambda} \end{bmatrix}^T H \Gamma_{\text{ca}} H \begin{bmatrix} \frac{\partial L}{\partial u_d} \\ \frac{\partial L}{\partial \lambda} \end{bmatrix} \quad (9.37)$$

which shows boundedness of the augmented tracking error, the residual error, and the first order partial derivatives of the Lagrangian function with respect to the parameter estimation error.

9.3.5 Nonparametric Robustness Modification

There is no guarantee that the model structure selected in the structure selection process correctly captures the structure of the aircraft's dynamics at each time instant. This modeling error results in function uncertainty which can potentially destroy the claims about stability of the resulting closed-loop system. Therefore, the control design is augmented with robustifying terms similar to the robust backstepping approach of section 3.4.

Add robustness improving terms in the intermediate control law α_1^0 and the control allocation update law to guarantee boundedness of the tracking error, and the partial derivatives with respect to the function uncertainty δ

$$\alpha_1^0 = - (C_1 + S_1 + S_{\delta_F}) (\hat{V} \times \hat{V}_r) - \frac{F_0 + \varphi_F^T \hat{\theta}}{m V_T} \times \hat{V} + \omega_{\hat{V}_r} + p_{W_{\text{ref}}} \quad (9.38)$$

$$\tau_{\text{des}}^0 = \omega \times J \omega + J \hat{V} \times z_1 + J \dot{\omega}_c - J (C_2 + S_2) z_2 \quad (9.39)$$

$$u_\kappa = \begin{bmatrix} \frac{\partial^2 L}{\partial x \partial u_d} \\ \frac{\partial^2 L}{\partial x \partial \lambda} \end{bmatrix}^T J^{-1} (\kappa_{\delta_u} + \varphi_\tau^T \kappa_u \varphi_\tau) J^{-T} \begin{bmatrix} \frac{\partial^2 L}{\partial x \partial u_d} \\ \frac{\partial^2 L}{\partial x \partial \lambda} \end{bmatrix} \begin{bmatrix} \frac{\partial L}{\partial u_d} \\ \frac{\partial L}{\partial \lambda} \end{bmatrix} \quad (9.40)$$

with

$$S_{\delta_F} = \frac{\hat{V}_\times}{mV_T} \kappa_{\delta_F} \frac{\hat{V}_\times}{mV_T}$$

$$S_2 = J^{-1} \kappa_2 J^{-T}.$$

The Ξ -filters are also modified to achieve the desired closed-loop stability

$$\dot{\Xi}_1 = -(C_1 + S_1 + S_{\delta_F})\Xi_1 - \omega_{\hat{V}_r} \times z_1 - (\omega_c - \omega_c^0) \times \hat{V} \quad (9.41)$$

$$\dot{\Xi}_2 = -(C_2 + S_2)\Xi_2 + (\tau(t, x, u, \hat{\theta}) - \tau_{\text{des}}^0) \quad (9.42)$$

The AOCLF derivative becomes

$$\begin{aligned} \dot{V}_{\text{comp}} \leq & -\sigma \sum_{i=1}^n \bar{z}_i^T C_i \bar{z}_i - \frac{1}{2} \epsilon^T \Psi \epsilon + \frac{1}{4} \tilde{\theta}^T (\sigma \kappa_1^{-1} + \kappa_u^{-1}) \tilde{\theta} \\ & - \begin{bmatrix} \frac{\partial L}{\partial u_d} \\ \frac{\partial L}{\partial \lambda} \end{bmatrix}^T H \Gamma_{\text{ca}} H \begin{bmatrix} \frac{\partial L}{\partial u_d} \\ \frac{\partial L}{\partial \lambda} \end{bmatrix} + \frac{1}{4} \delta_F^T \kappa_{\delta_F}^{-1} \delta_F + \frac{1}{4} \delta_\tau^T (\sigma \kappa_2^{-1} + \kappa_{\delta_u}^{-1}) \delta_\tau. \end{aligned} \quad (9.43)$$

showing boundedness of the augmented tracking error, the residual, and the first order partial derivatives of the Lagrangian function with respect to the parameter estimation error, and the function uncertainty.

9.4 Model Structure Selection and Identification

A control law has been designed which is able to stabilize the aircraft when a nominal and incremental aerodynamic model are available. The remaining task is to select the structure of the incremental model such that the combination of the nominal model and the incremental model matches the actual aircraft dynamics. Most structure selection approaches are based on an orthogonal decomposition of the regressor matrix Φ , and essentially seek to include the regressor candidates that have a correlation to the dependent variable. The procedure is equivalent to pivoting, a very common technique in linear algebra.

9.4.1 Least Squares and Orthogonal Decompositions

The numerical solution of a linear least squares problem through orthogonal decomposition of the matrix Φ is well established and will be shown here for discrete signals. For discrete signals, denote by $\hat{\Phi}^T = [\Phi^T \ y]$ the $n \times (m+1)$ matrix formed by adjoining Φ^T and y . Suppose that this matrix can be decomposed as $\hat{\Phi}^T = \hat{Q} \hat{R}$,

where \hat{R} is an upper triangular $(m+1) \times (m+1)$ matrix, and \hat{Q} is an $n \times (m+1)$ matrix with orthogonal matrix. Write $\hat{Q} = [Q \ q]$ and

$$\hat{R} = \begin{bmatrix} R & r \\ 0 & \hat{r} \end{bmatrix}$$

then the decomposition $\hat{\Phi}^T = \hat{Q}\hat{R}$ can be written as $[\Phi \ y] = [Q \ q] \hat{R}$ with $\Phi^T = QR$ and $y = Qr + \hat{r}q$. Since the columns of \hat{Q} are orthogonal, $q^T Q = 0$, and the norm of the residual can be written as

$$\begin{aligned} \|\Phi^T \theta - y\|^2 &= (\Phi^T \theta - y)^T (\Phi^T \theta - y) \\ &= (QR\theta - Qr - \hat{r}q)^T (QR\theta - Qr - \hat{r}q) \\ &= (QR\theta - Qr)^T (QR\theta - Qr) + \hat{r}^2 q^T q - 2\hat{r}q^T Q (R\theta - r) \\ &= \|Q(R\theta - r)\|^2 + \hat{r}^2 \|q\|^2. \end{aligned} \quad (9.44)$$

Therefore, if θ^* satisfies $R\theta^* = r$, then θ^* minimizes the norm of $\Phi^T \theta - y$. Since R is upper triangular, the equation $R\theta^* = r$ can be easily solved for the parameter estimate θ^* by backsubstitution.

9.4.2 Error Analysis

Before introducing the model structure selection procedure, the effects of ignoring columns of Φ^T on the error of the least squares solution are analyzed. First, from (9.44), it follows that the residual squared error is $\hat{r}^2 \|q\|^2$ when $R\theta^* = r$. Suppose that only the first m_s columns of Φ^T have been selected, and the remaining $m - m_s$ are ignored. If necessary, the selected columns of Φ^T can be moved to the first m_s columns by permutation of the matrix Φ^T . These columns are denoted Φ_s^T , and the remaining columns are Φ_e^T , such that $\Phi^T = [\Phi_s^T \ \Phi_e^T]$. Similarly, partition $Q = [Q_s \ Q_e]$. Let θ_s and r_s be the first m_s elements of θ and r , respectively, and θ_e and r_e the remaining elements. The orthogonal decomposition of $\hat{\Phi}^T$ then becomes

$$\begin{bmatrix} \Phi_s^T & \Phi_e^T & y \end{bmatrix} = \begin{bmatrix} Q_s & Q_e & q \end{bmatrix} \begin{bmatrix} R_s & R_{se} & r_s \\ 0 & R_e & r_e \\ 0 & 0 & \hat{r} \end{bmatrix}.$$

Therefore $y = Q_s r_s + Q_e r_e + \hat{r}q$. Setting $\theta_e = 0$, (9.44) can be written as

$$\|\Phi^T \theta - y\|^2 = \|Q_s (R_s \theta_s - r_s)\|^2 + \|Q_e r_e\|^2 + \hat{r}^2 \|q\|^2. \quad (9.45)$$

A minimum is achieved when $\theta_s = R_s^{-1} r_s$. Note that this is *not* the same as simply setting the last $m - m_s$ terms of θ^* to zero, since $\theta^* = R_s^{-1} (r_s - R_{se} R_e^{-1} r_e)$. The

columns of Q_e are just $\hat{q}_{m_s+1}, \dots, \hat{q}_m$ and therefore

$$\|Q_e r_e\|^2 + \hat{r}^2 \|q\|^2 = \sum_{i=m_s+1}^m r_i + \hat{r}^2,$$

where r_i is the i th component of $r = [r_s \ r_e]^T$. Thus, r_i is the length of the projection of y onto the i th column of Q . It can be interpreted as the change in error by switching from keeping the first $i - 1$ columns, to keeping the first i .

9.4.3 Model Structure Selection

The error analysis forms the basis of the selection techniques used by Billings, Korenberg, and Chen [12], Chen, Billings, and Luo [26], Korenberg, Billings, Liu, and McLloy [86], Stark [170]. Suppose that at the i^{th} selection step several columns have been chosen already $\hat{q}_1, \dots, \hat{q}_{i-1}$, and recall that \hat{q}_i is a scalar multiple of the projection of $\hat{\Phi}_i^T$ onto the orthogonal complement of the space spanned by $\hat{q}_1, \dots, \hat{q}_{i-1}$. The order of the columns of Φ^T is essentially arbitrary, hence there is nothing special about $\hat{\Phi}_i$. Therefore, it might be better to use one of the remaining columns $\hat{\Phi}_i^T, \dots, \hat{\Phi}_m^T$ to construct \hat{q}_i . Billings, Korenberg, and Chen [12] point out that (9.44) suggests that $\hat{\Phi}_{j_i}^T T$ from $\hat{\Phi}_i^T, \dots, \hat{\Phi}_m^T$ to maximize the resulting r_i . Incorporation of $\hat{\Phi}_{j_i}^T$ then leads to largest decrease in the residual error. Introduce an orthonormal permutation matrix Π such that $\Phi^T = QR\Pi^T$. The matrix Π is the composition of m_s transpositions, one each for each selection step of the algorithm. The m_s^{th} transposition swaps the m_s^{th} and i^{th} columns of $\hat{\Phi}^T$. Note that the last column of $\hat{\Phi}^T$ always contains the data to be fitted, and hence plays a special role.

Several criteria can be used to decide how many columns have to be incorporated in the model, i.e. when to terminate the model selection procedure. Several stopping criteria haven been suggested in literature. Chen, Billings, and Luo [26], Stark [170] suggest selecting m_s so that

$$1 - \sum_{i=1}^{m_s} [\text{ERR}]_i \leq \mu, \mu \in [0, 1] \quad (9.46)$$

such that the model given by the first m_s columns explains all but a proportion μ of the variation in y . More sophisticated tests are based on variations of Akaike's Information Criterion (AIC). A good overview of different candidate stopping criteria and their comparison is given by Barron [9], de Gooijer, Abraham, Gould, and Robinson [35], Mendes and Billings [113]. The resulting structure selection scheme operating on $\hat{\Phi}^T$ is summarized in algorithm 1.

Algorithm 1: Forward Structure Selection on Φ^T .

```

begin
   $m_s = 0$ 
  repeat
     $m_s = m_s + 1$ 
    for  $j = m_s \rightarrow m$  do
       $q_j^{(m_s)} = \varphi_j - \sum_{i=1}^{m_s-1} \frac{\varphi_j^T q_i}{q_i^T q_i} q_i$ 
       $[\text{ERR}]_j^{(m_s)} = \frac{\left(y^T q_j^{(m_s)}\right)^2}{y^T y \left(q_j^{(m_s)}\right)^T q_j^{(m_s)}}$ 
    end
     $i_{m_s} = \arg \max_{m_s \leq j \leq m} [\text{ERR}]_j^{(m_s)}$ 
     $[\text{ERR}]_{m_s} = [\text{ERR}]_{i_{m_s}}^{(m_s)}$ 
     $q_{m_s} = q_{i_{m_s}}^{(m_s)}$ 
    Swap  $m_s^{\text{th}}$  and  $i_{m_s}^{\text{th}}$  columns of  $\Phi^T$ 
    Swap  $m_s^{\text{th}}$  and  $i_{m_s}^{\text{th}}$  columns of  $\Pi$ 
  until stopping criterion is satisfied or  $m_s = m$ 
end

```

9.4.4 Selection on the Cholesky and QR Factorizations

The model structure selection scheme is very closely related to orthogonal decomposition. Suppose that the regressor matrix Φ^T is premultiplied by an orthogonal matrix P . Clearly, the orthogonal decomposition of $\hat{P}\hat{\Phi}^T = \tilde{Q}\tilde{R}$ with $\tilde{Q} = \hat{P}\hat{Q}$ and $\tilde{R} = \hat{R}$. Thus, the upper triangular part of the decomposition is invariant under orthogonal coordinate changes. If the special selection $\hat{P} = \hat{Q}^{-1}$ is made, then $\hat{P}\hat{\Phi}^T = \hat{R}$ and structure selection can be applied on \hat{R} directly, yielding the same column selection as performing structure selection on Φ^T [170]. Note that only the matrix R has to be updated recursively in an on-line scheme, tracking the matrix \hat{Q} is not necessary, reducing the required amount of storage.

The Cholesky factorization of the matrix $\hat{\Phi}^T$ is closely related to the Gram-Schmidt factorization. The inverse of this matrix is also upper triangular and is denoted by S , the Cholesky Inverse Root (CIR) of $\hat{\Phi}^T$. The CIR has several important statistical properties for model structure selection [69]

Property 9.1. In the i^{th} column of S , $r_i^2 = s_{ii}^{-2}$ is the residual sum of squares when x_i is regressed on the set x_1, \dots, x_{i-1} . The coefficient related to x_j in this regression is $-s_{ji}/s_{ii}$.

Property 9.2. If $k > i$, the residual sum of squares of the regression of x_i on $(x_1, \dots, x_{i-1}, x_{i+1}, \dots, x_k)$ is

$$r_i^2 = \left(\sum_{j=i}^k s_{ij}^2 \right)^{-1} \quad (9.47)$$

Property 9.3. If M is any diagonal matrix and $y = Mx$, then the CIR of y is SM^{-1} and scale changes have an innocuous effect on the CIR.

These properties can be used for structure selection using only the matrix \hat{S} . At the k^{th} stage of the selection process, pivot the data row to the row below the selected regressor column and retriangularize the matrix. Then, the residual sum of squares for the model including the regressor located at the row below the data row can be calculated using property 9.2. By means of row permutations and retriangularization the regressor can be added to the set of selected regressors which yields the largest reduction in the residual sum of squares. The resulting structure selection procedure is summarized in algorithm 2. Note that in the structure selection algorithm on the CIR the data row is swapped to directly after the the selected regressors.

Algorithm 2: Structure Selection on CIR.

```

begin
   $m_s = 0$ 
  repeat
     $m_s = m_s + 1$ 
    Swap data row to row  $m_s$  and retriangularize  $\hat{S}$ 
    Swap  $(m_s - 1)^{\text{th}}$  and  $m_s^{\text{th}}$  columns of  $\Pi$ 
    for  $k = m_s + 1 \rightarrow m$  do
      Swap row  $k$  to row  $m_s + 1$  and retriangularize  $\hat{S}$ 
       $r_k^{(m_s)} = \left( s_{m_s, m_s}^2 + s_{m_s, m_s + 1}^2 \right)^{-1}$ 
    end
     $i_{m_s} = \arg \min_{m_s + 1 \leq k \leq m} r_k^{(m_s)}$ 
    Swap row  $i_{m_s}$  to row  $m_s$ 
    Swap  $m_s^{\text{th}}$  and  $i_{m_s}^{\text{th}}$  columns of  $\Pi$ 
  until stopping criterion is satisfied or  $m_s = m$ 
end
```

9.4.5 Updating the Decomposition

Since data becomes available in a continuous stream during on-line operations and the model structure selection operates only on the triangular parts of the decomposition, the triangular part has to be updated continuously with the new information. The derivative of the correlation matrix $\hat{N} = \hat{\Phi}^T \hat{\Phi} = \Pi R^T R \Pi^T$ is given by

$$\dot{\hat{N}} = \dot{\hat{\Phi}}^T \hat{\Phi} + \hat{\Phi}^T \dot{\hat{\Phi}} - \lambda \hat{N} \quad (9.48)$$

where $\dot{\hat{\Phi}}^T = \left[\Omega^T (\Omega_0 + Gx) \right]$. Then, the derivative of the Cholesky factor R is given by

$$\dot{\hat{R}} = \text{upph} \left(\hat{R}^{-T} \Pi^T \dot{\hat{\Phi}} \hat{\Phi}^T \Pi \hat{R}^{-1} \right) \hat{R} - \frac{\lambda}{2} \hat{R}. \quad (9.49)$$

where upph, the upper triangular half-part, is defined by

$$Y = \text{upph}(X) \iff \begin{cases} y_{i,j} = x_{i,j} & i < j \\ y_{i,j} = \frac{1}{2}x_{i,j} & i = j \\ y_{i,j} = 0 & i > j \end{cases}. \quad (9.50)$$

This update requires on-line matrix inversion which can be avoided by considering the inverse of the matrix \hat{R} , or the CIR. The update for the CIR is defined as

$$\dot{\hat{S}} = -\hat{S} \text{upph} \left(\hat{S}^T \Pi^T \dot{\hat{\Phi}} \hat{\Phi}^T \Pi \hat{S} \right) + \frac{\lambda}{2} \hat{S}, \quad (9.51)$$

with the additional advantage that $\hat{\theta}$ can be extracted very easily through property 9.1.

Since the designed law design in the previous section also contains a direct update component, this has to be added to the update of the matrix \hat{S} . The parameter estimate is effectively contained in the $(m_s + 1)^{\text{th}}$ column of the matrix \hat{S} and hence only that column of the matrix is affected. The direct part of the update law is defined by

$$\dot{\hat{\theta}}_{\text{direct}} = \Gamma_{\theta} \left(\Pi_{1:m_s, \star} \right)^T \left(\sigma \frac{\varphi_F}{m V_T} \hat{V}_{\times}^T \bar{z}_1 + \varphi_{\tau} \left(\frac{\partial^2 L^T}{\partial x \partial u_d} \frac{\partial L}{\partial u_d} + \frac{\partial^2 L^T}{\partial x \partial \lambda} \frac{\partial L}{\partial \lambda} \right) \right) \quad (9.52)$$

where Γ_{θ} is defined by $\hat{S}_{m_s, m_s} \hat{S}_{m_s, m_s}^T$, the product of the upper-left block of size $m_s \times m_s$ of the matrix \hat{S} with its transpose. This direct update is added in the least square update to the first m_s elements of the $(m_s + 1)^{\text{th}}$ column of the matrix \hat{S} as

$$-\dot{\hat{\theta}}_{\text{direct}} \hat{S}_{m_s+1, m_s+1}. \quad (9.53)$$

9.5 Full Envelope Aerodynamic Modeling

The estimation and structure selection method introduced above could be used to fit a model to the complete dynamics of an aircraft over the whole flight envelope. For complex aircraft dynamics with many control effectors, the required set of regressors to accurately model the dynamics would become incredibly large. For such large size models, the covariance matrix would become very large since its number of elements scales quadratically with increasing model size, increasing the computational load of the identification scheme dramatically. Therefore an approach is taken which splits the complete flight envelope into partitions with a locally valid model in each partition. The output of these models is combined using smooth interpolation functions. It is desired to only update the model in the *active* part of the flight envelope to limit the computational requirements. Therefore interpolating functions with local support are selected, resulting in a local receptive field approach.

9.5.1 Local Model Structure

For an accurate fit of the total aerodynamic model for the aircraft, there is a trade-off between the local model complexity or number of regressor candidates, and the total number of partitions required. On the other hand, the structure of the local models can be used to extract information about the system behavior. As an example, the sign of the aerodynamic derivative C_{m_α} can be used to make claims about the static stability of an aircraft. Besides the linear independent variables commonly found in aerodynamic models, there are also nonlinear and cross-coupling regressor candidates. Especially for aircraft with damage, the coupling between the longitudinal and lateral modes becomes stronger, requiring inclusion of additional coupled regressor candidates in the model. As a compromise between the local model complexity and the total number of partitions required Taylor expansion terms up to second order can be included. Then, the following set of regressor candidates for each total force and moment coefficient is obtained

- longitudinal linear: $1, \alpha, \frac{q_B \bar{c}}{2V_T}$ and longitudinal control surface deflections such as δ_e ,
- longitudinal nonlinear: $\alpha^2, \alpha \frac{q_B \bar{c}}{2V_T}, \alpha \delta_e$,
- lateral linear: $\beta, \frac{p_B b}{2V_T}, \frac{r_B b}{2V_T}$ and lateral control surface deflections such as δ_a and δ_r ,
- lateral nonlinear: $\beta^2, \beta \frac{p_B b}{2V_T}, \beta \frac{r_B b}{2V_T}, \beta \delta_a, \beta \delta_r$,
- coupled nonlinear: $\alpha \beta, \alpha \frac{p_B b}{2V_T}, \beta \frac{q_B \bar{c}}{2V_T}, \alpha \frac{r_B b}{2V_T}, \alpha \delta_a, \beta \delta_e, \alpha \delta_r$.

When an aircraft has more control effectors, their aerodynamic contribution can be included in similar fashion as done for the common control surfaces. It is possible to enforce a specific order in which the model structure candidates are allowed to enter the selection process. For example, it seems logical to first include linear terms in the regression before considering the nonlinear terms [96].

9.5.2 Local Model Updating and Resetting

The norm of the residual error ϵ is filtered by a low-pass filter to remove faulty measurements and noise. Based on this filtered residual the required action for the partition is selected. If the filtered residual is above the threshold η_1 , structure selection is performed for the partition. When the filtered residual exceeds a second threshold η_2 and the standard deviation of all coefficients included in the model is below the third threshold η_3 , all measurement data is thrown away by resetting the partition. If the standard deviation is small, and there is a large residual, a change in the system dynamics is indicated. Furthermore, structure selection is performed when a partition has been active for a certain amount of time T_{ss} , and the time the partition has been active is reset to zero. This results in regular structure selection, even if the residual error is small for the current model. If the residual falls below the threshold ϵ_{\min} , no (additional) regressors are selected, regardless of whether the stopping criterion is satisfied or not.

9.6 ADMIRE Application and Simulation Results

The ADMIRE is a generic model of a small single-seat fighter aircraft with a delta-canard configuration. Available control effectors are the right and left canard, leading edge flaps, four elevons, rudder and throttle setting. The aerodynamic model is based on the Generic Aerodata Model (GAM) developed by Saab AB available as aerodata tables with associated interpolation routines and algorithms. The aerodata varies with Mach number, and contains static aeroelastic effects as well as coupling between lateral and longitudinal dynamics. The model has been discussed in more detail in chapter 5, and the full details can be found in [60].

9.6.1 Controller Tuning

A simple quadratic cost function with barrier functions to implement magnitude constraints on the desired control effector signals is used. This cost function is defined as

$$J(u_d) = u_d^T W u_d - w \ln(u_d - u_{d,\min}) - w \ln(u_{d,\max} - u_d) \quad (9.54)$$

where $W = W^T > 0$ and $w = w^T > 0$ are tuning gains, $u_{d,\min}$ and $u_{d,\max}$ represent the lower and upper bounds on u_d respectively. The tuning parameters of the controller are specified in table 9.1. Covariance resetting when a change is detected

Table 9.1: ADMIRE Controller Tuning Parameters.

Parameter	Setting
C_1	$2I_3$
C_2	$5I_3$
Ψ	$10I_3$
γ	50
w	$0.1 \cdot \text{diag}(2 \ 2 \ 1 \ 1 \ 1 \ 1 \ 1 \ 0.5 \ 1)$
W	$1000 \cdot \text{diag}(2 \ 2 \ 1 \ 1 \ 1 \ 1 \ 1 \ 0.5 \ 1)$
A_0	$-100I_3$
κ	$1 \times 10^{-3} I_{42}$
η_1	0.1
η_2	0.5
η_3	10
T_{ss}	10
S_0	$1 \times 10^{-7} I_{42}$
S_{reset}	$10I_{42}$
λ	0.1
ω_ϵ	50.0
ϵ_{\min}	1×10^{-12}

Table 9.2: Reference Filter Parameters.

Variable	Bandwidth	Damping
V_T	0.5	1.0
α	2.0	1.0
β	2.0	1.0
p_W	4.0	1.0
ω_c	10.0	1.0

has been applied. The reference filters for the aerodynamic angles, and angular rates have been chosen according to table 9.2.

9.6.2 Incremental Aerodynamic Model

The flight envelope has been partitioned in three dimensions: the angle of attack, sideslip angle, and the Mach number using B-spline basis functions as discussed in chapter 8. The partitioning structure is shown in table 9.3. This partitioning has been chosen since the step size for the angle of attack and sideslip angle resulted in adequate performance for the F-16 aircraft model. Second order interpolation is used for angle of attack and sideslip to achieve smooth and continuous transition

Table 9.3: Flight Envelope Partitioning.

Variable	Knots	Order	Hyperbox Partitions
Angle of attack	[-20 -20 -20 -15 -10 ... 80 85 90 90 90]	2	24
Sideslip angle	[-30 -30 -30 -25 -20 ... 20 25 30 30 30]	2	14
Mach number	[0 0 0.4 0.5 1.0 1.5 3 3]	1	6
Total			2016

between partitions. The knot locations for the Mach partitioning have been chosen to roughly match the structure in the aerodynamic model of the aircraft, first order interpolation is used to have continuity in the model parameters between partitions. A finer partitioning for the Mach number can be chosen in the high subsonic and transonic region if a change in control strategy is implemented, for example a switch to load-factor control.

The local model structure is relatively simple and consists of 42 candidate regressors, 14 for each component of the torque vector. The candidate regressor variables are the 8 individual actuator deflections, the 3 dimensionless angular rotation rates in the body axes, the 2 aerodynamic angles, and a bias term for each of the components of the torque vector.

9.6.3 Nominal Simulation Results

First of all nominal simulation results are presented to show the capabilities of the control design on the nominal aircraft. A maneuver is flown at low airspeed, $M = 0.3$, at 1000m altitude, with simultaneous pitching and rolling of the aircraft. The resulting aircraft response is shown in figure 9.1 and the associated commanded and realized actuator signals are shown in figure 9.2. The reference signals are tracked accurately, and during the maneuver the sideslip angle is kept within ± 1 degree. The actuator commands are well within their magnitude bounds and hence there is room to accommodate actuator failures. In figure 9.3 the Euler angles are shown, and an impression of the flown maneuver is shown in figure 9.4. The maneuver is a velocity vector roll, followed by a pitch and simultaneous velocity vector roll in the opposite direction returning to return to level flight.

9.6.4 Changes in Aerodynamic Coefficients

The structure selection and estimation capabilities of the adaptive controller are first tested by introducing a failure which can be completely accommodated by the set of available regressor candidates. After two seconds in the simulation, a failure is introduced which decreases the static stability coefficient $C_{m_{\alpha}}$ by 0.2, and the pitch stability coefficient $C_{m_{\dot{q}}}$ by 0.3. This change causes a bias in the angle of attack tracking response of the nominal controller which is not shown here. The response of the adaptive controller is shown in figure 9.5. Comparing with the nominal re-

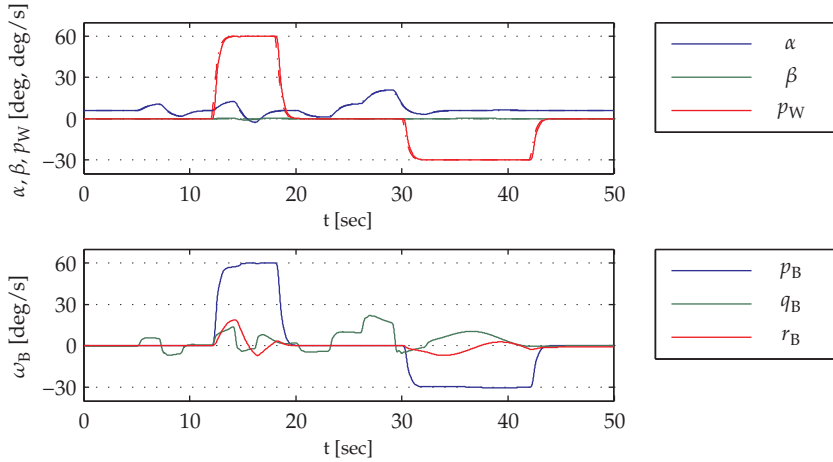


Figure 9.1: Aircraft response in the nominal case with non-adaptive controller.

sponse of figure 9.1, the change in the aerodynamic coefficients is hardly noticeable because the controller rapidly detects the change, and resets the active partitions to quickly estimate the incremental aerodynamic model. Figure 9.6 shows the control deflections, which are considerably smaller compared with the control deflections required in the nominal case as seen in figure 9.2. Finally, the estimation results are shown in figure 9.7. A clear peak is visible in the residual error directly after introducing the change in the coefficients. During the maneuver the parameters are estimated, and by the end of the simulation the correct structure and parameter values have been identified. The variation in the estimated parameter after 27 seconds is explained by the fact that the aircraft enters a different part of the flight envelope, where no incremental model has been identified yet.

9.6.5 Actuator Failures

Two different actuator failures are considered. First, a lock of the right canard and right outer elevon at their center position of 0 degrees after two seconds in the simulation. This causes a small positive rolling moment and a small negative pitching moment due to the imbalance between the left and right sides of the aircraft. The maneuver is flown at a velocity ranging from 100 m/s at the start of the simulation to 180 m/s at the end. The response of the aircraft is shown in figure 9.8, the actuator commands and realized deflections in figure 9.9. Finally, the estimated incremental model parameters and residual error are shown in figure 9.10. The tracking performance is very good despite the lock of the surfaces at their center position. The desired control torque is realized by the remaining functional control

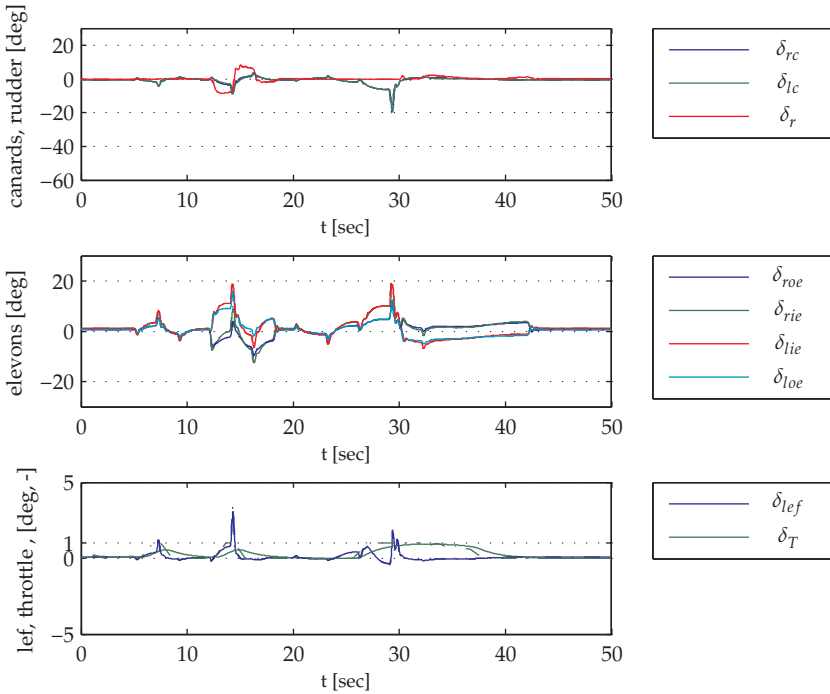


Figure 9.2: Actuator commands and deflections in the nominal case with non-adaptive controller.

surfaces as can be seen by comparing figures 9.2 and 9.9. During the maneuver the residual errors converge to a small neighborhood around zero.

Secondly, an actuator failure is considered which suddenly lets the right outer elevon deflect to 15 degrees trailing edge up. This causes a rolling moment to the right. This failure is identified rapidly by the identifier as seen in figure 9.13, although there still exists a residual error after identification. This indicates that this failure cannot be fully accommodated within the chosen set of regressor candidates. Hence, either a larger set of regressor candidates has to be chosen, or a finer partitioning of the flight envelope has to be made. The tracking response is excellent despite the residual error as shown in figure 9.11. The resulting control effector commands and realized signals are shown in figure 9.12.

9.6.6 Center of Gravity Shift

As the last “failure” condition, a sudden center of gravity shift is introduced into the system. A mismatch between the real aircraft’s center of gravity and the esti-

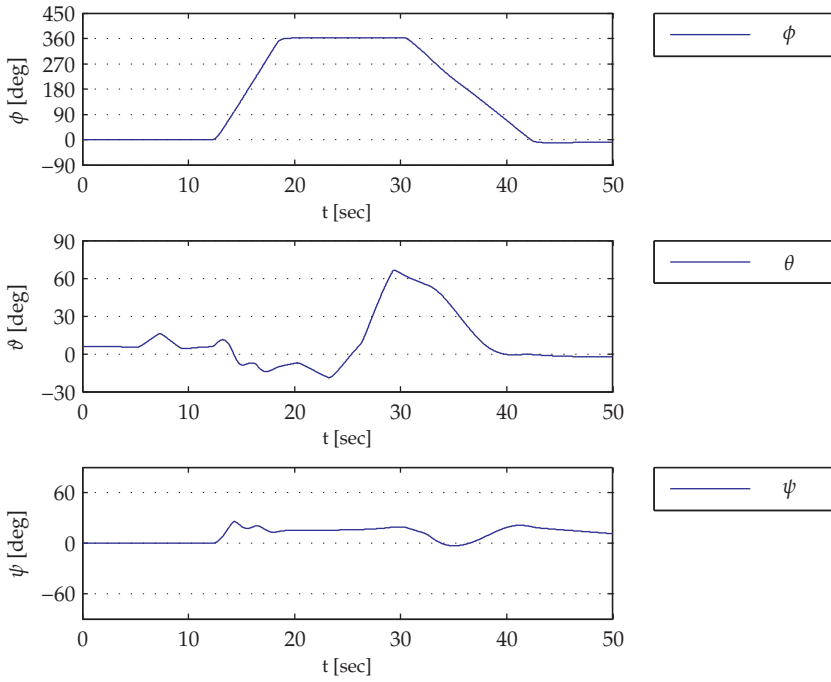


Figure 9.3: Euler angles for the nominal case with non-adaptive controller.

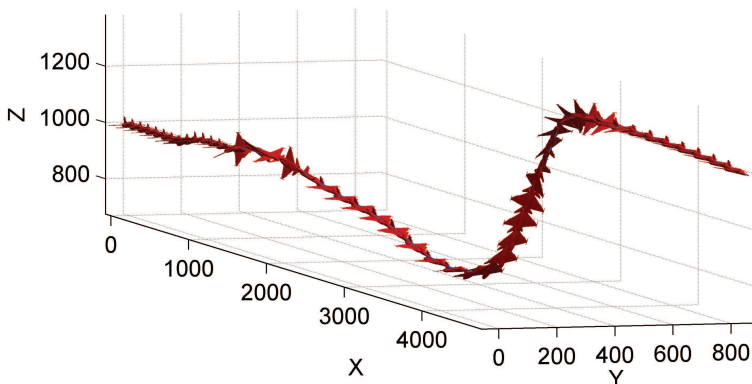


Figure 9.4: Impression of the trajectory flown by the aircraft.

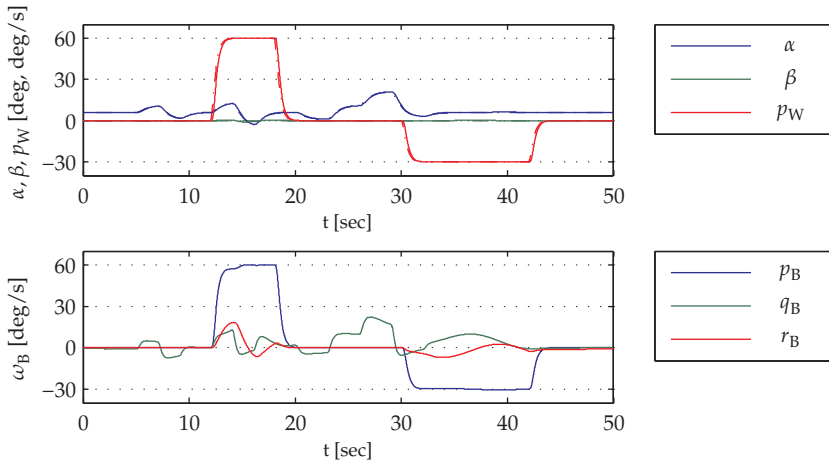


Figure 9.5: Aircraft response with adaptive controller for a sudden change in the pitch stability coefficients.

mated location of the center of gravity used by the control law can be caused by a faulty fuel or weapon-store sensor, or damage to the airframe. Especially for model inversion controllers without adaptation, these kind of failures result in bad tracking performance or even instability [164, 197, 199]. The center of gravity is shifted 20 cm forwards and 10 cm to the left with respect to its original location, additionally the aerodynamic model of the pitching moment is changed by modifying the pitch stability coefficients with opposite signs. The center of gravity shift causes increased coupling between the longitudinal and lateral axes of the aircraft, leading to a deterioration of tracking performance of the non-adaptive controller. The response of the aircraft with adaptive controller is shown in figure 9.14. Clearly, the tracking performance is still excellent. A considerable change in control effector activation compared to the nominal case can be observed by comparing figures 9.15 and 9.2. The estimated parameters and the residual error are shown in figure 9.16. Quite a large number of regressors is selected to accurately model the influence of the aerodynamic force on the aerodynamic moments due to the mismatch between the aerodynamic center and the center of gravity.

9.7 Conclusions

In this chapter many design techniques introduced during the preceding part of the dissertation are brought together to create a controller which is able to achieve excellent tracking performance for nonlinear, over-actuated, aircraft. The controller is designed within the backstepping framework and combines a high level control

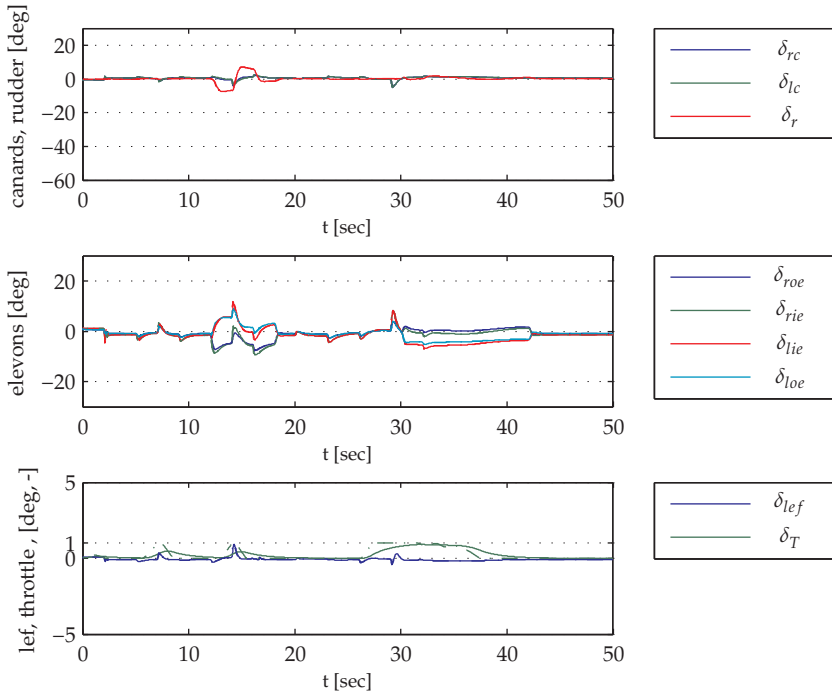


Figure 9.6: Actuator commands and deflections of the aircraft with adaptive controller for a sudden change in the pitch stability coefficients.

design with dynamic optimizing control allocation using a composite update law for estimation of the unknown parameter. The flight envelope has been divided into a smaller partitions, for each partition a locally valid model is created. Both the structure and model parameter values are identified on-line based on a orthogonal least squares identification scheme. Global stability of the closed-loop system, and convergence of the estimated parameter can be proven using a single Lyapunov function. The control design is evaluated with numerical simulations. Based on these simulation results, several observations can be made.

- The proposed control design shows excellent performance for a variety of simulated fault and failure cases ranging from a simple change in the aerodynamic coefficients, to actuator failures and center of gravity shifts. The tracking performance of non-adaptive model based control designs deteriorates significantly for these kinds of failures.
- When the failure is in the space spanned by the set of available regressor candidates, the correct model structure can be identified, and the correct param-

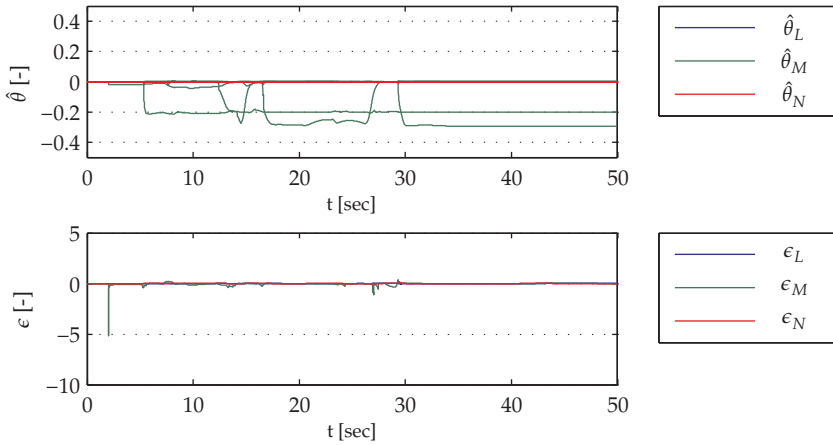


Figure 9.7: Estimated parameters and residual error for a sudden change in the pitch stability coefficients.

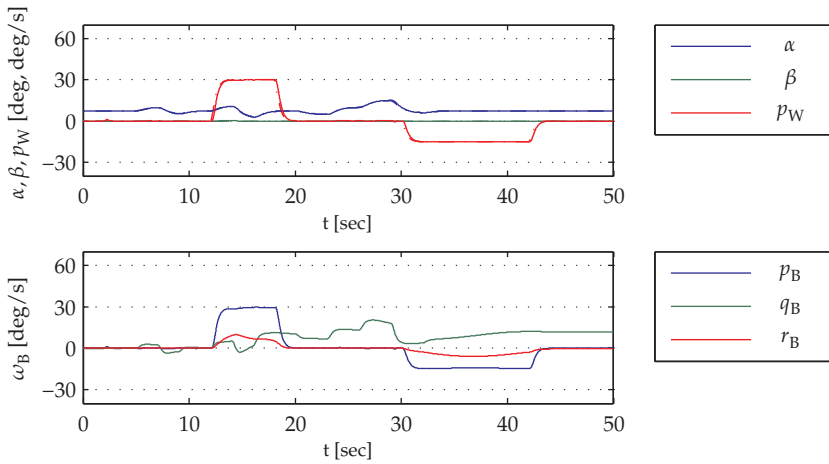


Figure 9.8: Aircraft response with adaptive controller for a sudden lock of the right canard and outer elevon.

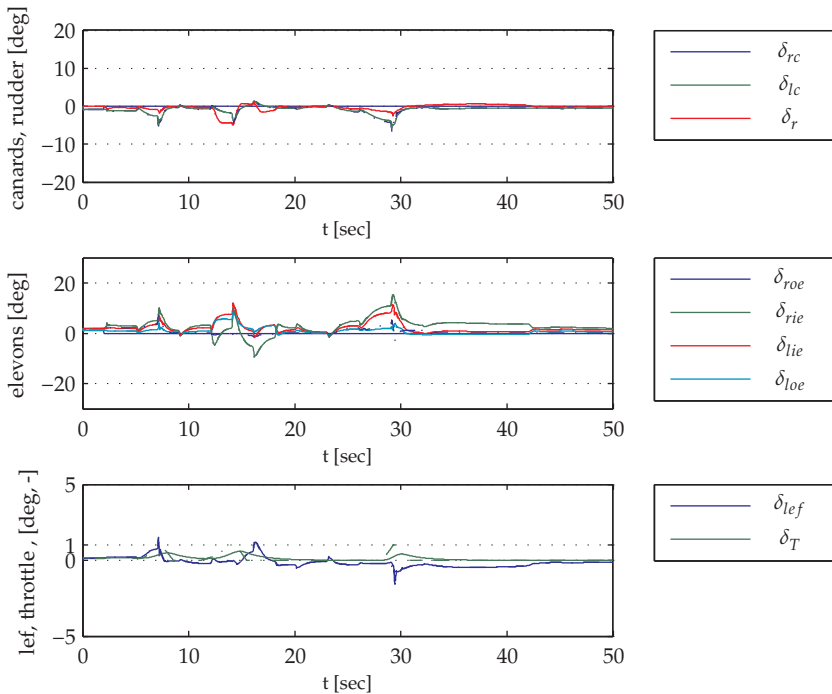


Figure 9.9: Actuator commands and deflections of the aircraft with adaptive controller for a sudden lock of the right canard and outer elevon.

eter values are estimated if a persistency of excitation condition is satisfied. Even if the failure cannot be completely characterized by the available set of regressor candidates, tracking performance can be very good as long as the residual error between the estimated model and the true behavior is small.

- Splitting the complete flight envelope into smaller partitions allows real-time implementation of the control design, and the identified information can be stored efficiently for later use, when the same part of the envelope is visited again.
- Tuning of the controller is straightforward since the update gain of the parameter adaptation is tuned automatically by the least squares filter, and the remaining tuning parameters can be chosen independently. However, care has to be taken in the selection of the structure selection and covariance resetting parameters.

The control design presented can be extended in different directions for future research.

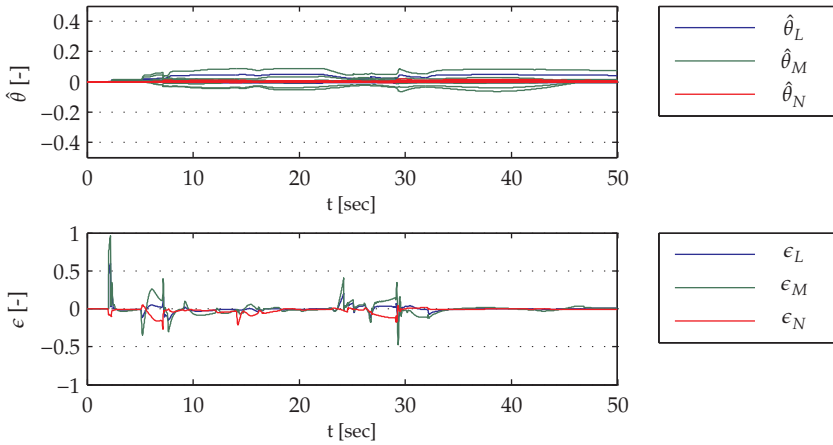


Figure 9.10: Estimated parameters and residual error for a sudden lock of the right canard and outer elevon.

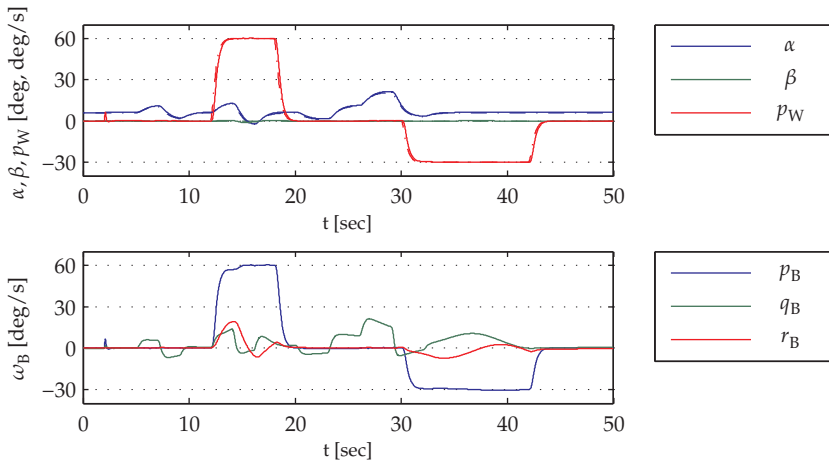


Figure 9.11: Aircraft response with adaptive controller for a sudden lock of the right outer elevon at 15 degrees.

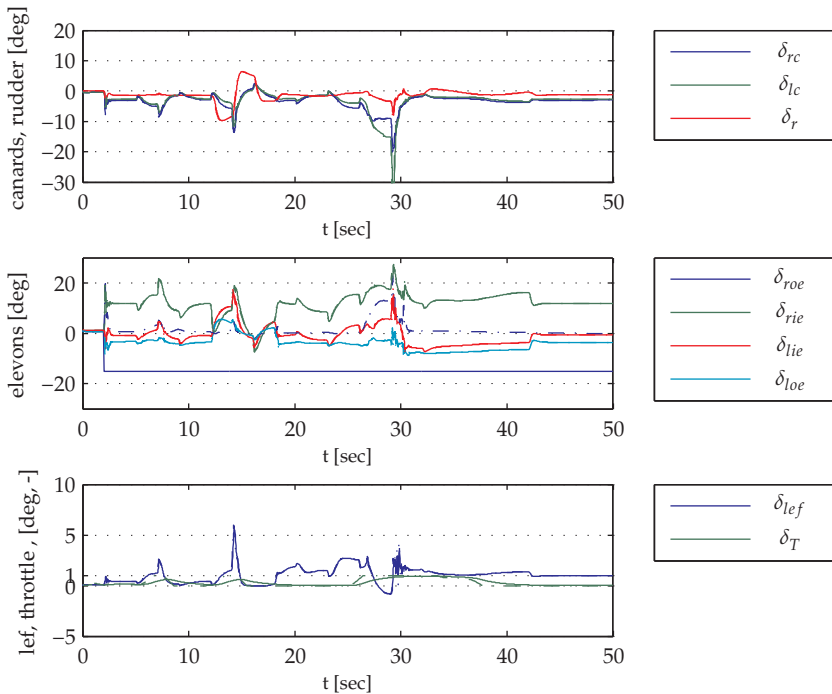


Figure 9.12: Actuator commands and deflections of the aircraft with adaptive controller for a sudden lock of the right outer elevon at 15 degrees.

- Implement a more advanced control allocation scheme by including control effector rates and constraints in the cost function such that for demanding maneuvers the full capabilities of the control effectors are used. An example of such demanding maneuvers would be high angle of attack maneuvering at low-airspeed using thrust vectoring.
- Extend the cost function and the control design with airspeed control such that for example at cruise the control deflections can be chosen which minimize the aircraft drag and hence minimizing fuel consumption.
- Investigate the trade-off between local model structure and level of partitioning required to accurately model the aircraft dynamics over the full envelope. Increasing the number of regressor candidates causes the number of identifier states to increase in quadratic order, increasing the computational load. Therefore, this investigation is very important before attempting online applications.

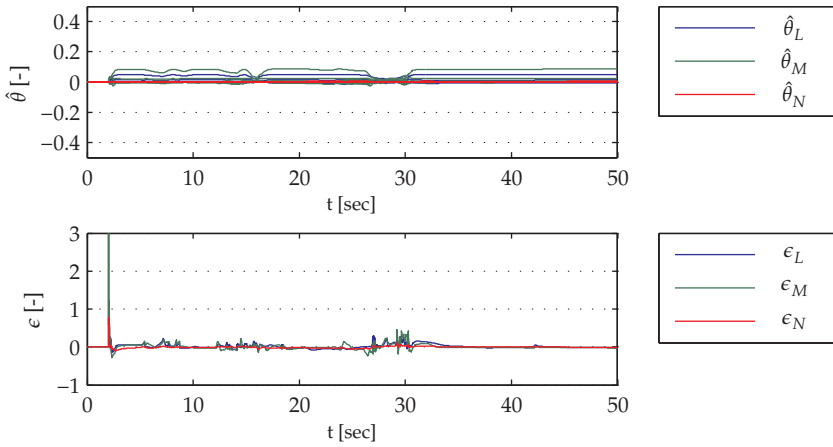


Figure 9.13: Estimated parameters and residual error for a sudden lock of the right outer elevon at 15 degrees.

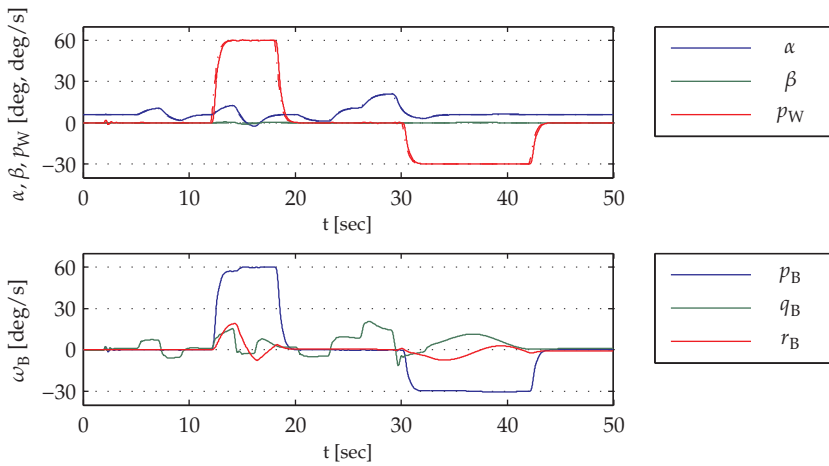


Figure 9.14: Aircraft response with adaptive controller for a sudden center of gravity shift.

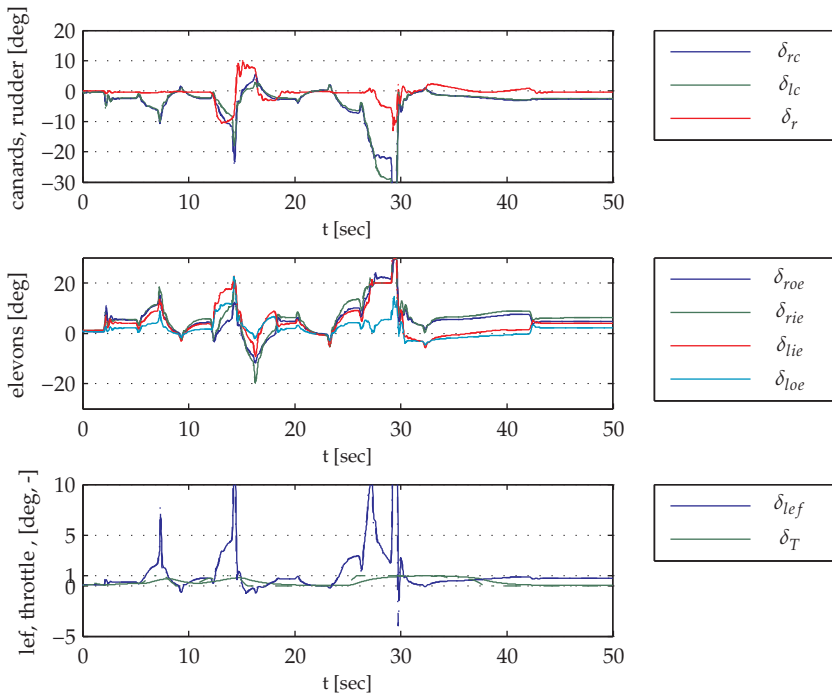


Figure 9.15: Actuator commands and deflections of the aircraft with adaptive controller for a sudden center of gravity shift.

- Modify the control design such that for higher Mach numbers instead of angle of attack the normal load factor is controlled. Simultaneously, the desired response of the aircraft can be scheduled over the flight envelope for the best possible handling qualities.
- Extend the set of regressor candidates with longitudinal/lateral coupling and nonlinear terms, and additionally estimate an incremental aerodynamic force model.
- Another interesting option is to replace the tensor B-spline partitioning with local models to model the aerodynamic coefficients by simplex B-splines as proposed by de Visser, Chu, and Mulder [37].

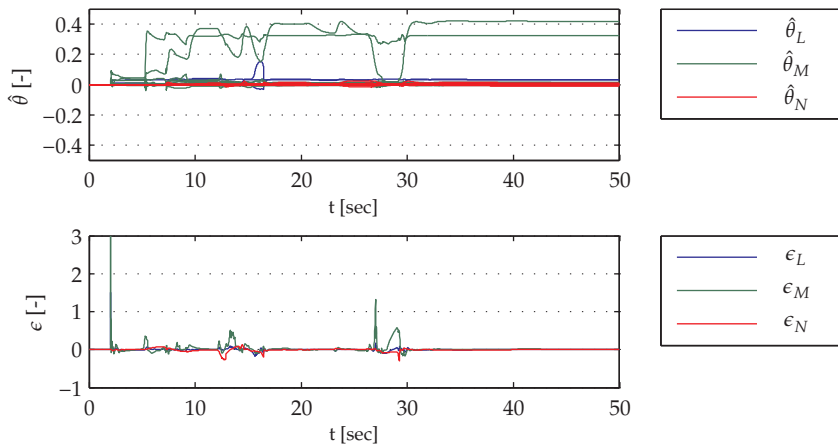


Figure 9.16: Estimated parameters and residual error for a sudden center of gravity shift.

BIBLIOGRAPHY

- [5] K. J. Åström and B. Wittenmark. *Adaptive Control*. Addison Wesley Longman, 1995.
- [6] H. Backström. *Report on the usage of the Generic Aerodata Model*. Tech. rep. Saab Aircraft AB, 1997.
- [7] B. J. Bacon and I. M. Gregory. "General Equations of Motion for a Damaged Asymmetric Aircraft". In: *Proceedings of the AIAA Atmospheric Flight Mechanics Conference and Exhibit*. 2007-6306. AIAA. Hilton Head, South Carolina, USA, Aug. 2007.
- [9] A. R. Barron. "Self-organizing Methods in Modeling". In: ed. by S. J. Farlow. New York, NY, USA: Marcel Dekker, Inc, 1984. Chap. Predicted Squared Error: A Criterion for Automatic Model Selection, pp. 87–104.
- [12] S. A. Billings, M. J. Korenberg, and S. Chen. "Identification of nonlinear output-affine systems using an orthogonal least squares algorithm". In: *International Journal of Systems Science* 19 (1988), pp. 1559–1568.
- [14] M. Bodson. "Evaluation of Optimization Methods for Control Allocation". In: *Journal of Guidance, Control, and Dynamics* 25.4 (2002), pp. 703–711.
- [19] J. M. Buffington, D. F. Enns, and A. R. Teel. "Control Allocation and Zero Dynamics". In: *Journal of Guidance, Control, and Dynamics* 21.3 (1998), pp. 458–464.
- [22] C. Cao and N. Hovakimyan. "Vision-Based Aerial Tracking using Intelligent Excitation". In: *American Control Conference, 2005. Proceedings of the*. Vol. 7. June 2005, pp. 5091–5096.
- [23] C. Cao, N. Hovakimyan, and J. Wang. "Intelligent Excitation for Adaptive Control With Unknown Parameters in Reference Input". In: *Automatic Control, IEEE Transactions on* 52.8 (Aug. 2007), pp. 1525–1532.
- [26] S. Chen, S. A. Billings, and W. Luo. "Orthogonal Least Squares Methods and their Applications to Non-linear System Identification". In: *International Journal of Control* 50.5 (1989), pp. 1873–1896.
- [34] C. de Boor. "A Practical Guide to Splines". In: Springer-Verlag, 1978, pp. 87, 109.

- [35] J. G. de Gooijer, B. Abraham, A. Gould, and L. Robinson. "Methods for Determining the Order of an Autoregressive-Moving Average Process: A Survey". In: *International Statistical Review* 53.3 (1985), pp. 301–329.
- [37] C. C. de Visser, Q. P. Chu, and J. A. Mulder. "A new approach to linear regression with multivariate splines". In: *Automatica* 45.12 (Dec. 2009), pp. 2903–2909.
- [38] J. Dehaene, M. Moonen, and J. Vandewalle. "Continuous-Time Recursive Least-Squares Estimation, Adaptive Neural Networks and Systolic Arrays". In: *IEEE Transactions on Circuits and Systems I: Fundamental Theory and Applications* 42.2 (1995), pp. 116–119.
- [40] N. Draper and H. Smith. *Applied Regression Analysis*. John Wiley & Sons, Inc., 1981.
- [41] E. L. Duke, R. F. Antoniewicz, and K. D. Krambeer. *Derivation and Definition of a Linear Aircraft Model*. Tech. rep. RP-1207. NASA Ames Research Center Dryden Flight Research Facility, 1988.
- [43] W. C. Durham. "Constrained Control Allocation". In: *Journal of Guidance, Control, and Dynamics* 16.4 (1993), pp. 717–725.
- [44] W. C. Durham, F. H. Lutze, and W. Mason. "Kinematics and aerodynamics of the velocity vector roll". In: *Journal of Guidance, Control, and Dynamics* 17.6 (1994), pp. 1228–1233.
- [48] D. F. Enns. "Control Allocation Approaches". In: *Proceedings of the AIAA Guidance, Navigation, and Control Conference and Exhibit*. Boston MA, USA, 1998, pp. 98–108.
- [57] J. A. Farrell, M. Sharma, and M. Polycarpou. "Backstepping Based Flight Control with Adaptive Function Approximation". In: *Journal of Guidance, Control and Dynamics* 28.6 (Jan. 2005), pp. 1089–1102.
- [59] J. A. Farrell and M. M. Polycarpou. *Adaptive Approximation Based Control, Unifying Neural, Fuzzy and Traditional Adaptive Approximation Approaches*. John Wiley & Sons, Inc., 2006.
- [60] L. Forssell and U. Nillsson. *ADMIRE The Aero-Data Model in a Research Environment Version 4.0, Model Description*. Tech. rep. FOI-R-1624-SE. FOI - Swedish Defence Research Agency, 2005.
- [61] R. A. Freeman, M. Krstić, and P. V. Kokotović. "Robustness of Adaptive Nonlinear Control to Bounded Uncertainties". In: *Automatica* 34 (1998), pp. 1227–1230.
- [64] G. Goodwin and D. Mayne. "A Parameter Estimation Perspective of Continuous Time Model Reference Adaptive Control". In: *Automatica* 23 (1987), pp. 55–70.

- [68] O. Härkegård. "Backstepping and Control Allocation with Applications to Flight Control". PhD thesis. Linköping, Sweden: Linköping University, 2003.
- [69] D. M. Hawkins and W. J. R. Eplett. "The Cholesky Factorization of the Inverse Correlation or Covariance Matrix in Multiple Regression". In: *Technometrics* 24.3 (1982), pp. 191–198.
- [79] T. A. Johansen, T. I. Fossen, and S. P. Berge. "Constrained Nonlinear Control Allocation with Singularity Avoidance using Sequential Quadratic Programming". In: *Control Systems Technology, IEEE Transactions on* 12.1 (2004), pp. 211–216.
- [80] T. A. Johansen, T. I. Fossen, and P. Tøndel. "Efficient Optimal Constrained Control Allocation via Multi-parametric Programming". In: *Journal of Guidance, Control, and Dynamics* 28.3 (2005), pp. 506–515.
- [83] H. K. Khalil. *Nonlinear Systems*. 3rd ed. Prentice Hall, 2002.
- [85] V. Klein and E. A. Morelli. *Aircraft System Identification: Theory and Practice*. Education Series. AIAA, 2006.
- [86] M. J. Korenberg, S. A. Billings, Y. P. Liu, and P. J. McIlroy. "Orthogonal parameter estimation algorithm for non-linear stochastic systems". In: *International Journal of Control* 48 (1988), pp. 193–210.
- [87] M. Krstić, I. Kanellakopoulos, and P. V. Kokotović. "Adaptive Nonlinear Control without Overparameterization". In: *Systems and Control Letters* 19 (1992), pp. 177–185.
- [88] M. Krstić, I. Kanellakopoulos, and P. V. Kokotović. *Nonlinear and Adaptive Control Design*. John Wiley and Sons, 1995.
- [96] T. J. J. Lombaerts. "Fault Tolerant Flight Control, A Physical Model Approach". PhD thesis. Delft University of Technology, Faculty of Aerospace Engineering, 2010.
- [97] T. J. J. Lombaerts, H. O. Huisman, Q. P. Chu, J. A. Mulder, and D. A. Joosten. "Nonlinear Reconfiguring Flight Control Based on Online Physical Model Identificatin". In: *Journal of Guidance, Control, and Dynamics* 32.3 (2009), pp. 727–748.
- [99] T. J. J. Lombaerts, E. R. van Oort, Q. P. Chu, J. A. Mulder, and D. A. Joosten. "Online Aerodynamic Model Structure Selection and Parameter Estimation for Fault Tolerant Control". In: *Journal of Guidance, Control, and Dynamics* 33.3 (2010), pp. 707–723.
- [104] W. Luo and S. A. Billings. "Adaptive model selection and estimation for nonlinear systems using a sliding data window". In: *Signal Processing* 46.2 (1995), pp. 179–202.

- [105] Y. Luo, A. Serrani, S. Yurkovich, D. Doman, and M. Oppenheimer. "Dynamic Control Allocation with Asymptotic Tracking of Time-varying Control Input Commands". In: *Proceedings of the American Control Conference*. Portland, OR, USA, 2005, pp. 2098–2103.
- [106] Y. Luo, A. Serrani, S. Yurkovich, D. Doman, and M. Oppenheimer. "Model Predictive Dynamic Control Allocation with Actuator Dynamics". In: *Proceedings of the American Control Conference*. Vol. 2. Boston, MA, USA, 2004, pp. 1695–1700.
- [113] E. M. A. M. Mendes and S. A. Billings. "An Alternative Solution to the Model Structure Selection Problem". In: *IEEE Transactions on Systems, Man, and Cybernetics* 31.6 (2001), pp. 597–608.
- [121] E. A. Morelli. "Global nonlinear aerodynamic modeling using multivariate orthogonal functions". In: *Journal of Aircraft* 32 (1995), pp. 270–277.
- [122] J. A. Mulder. "Design and evaluation of dynamic flight test manoeuvres". PhD thesis. Delft University of Technology, Faculty of Aerospace Engineering, 1986.
- [126] L. T. Nguyen, M. E. Ogburn, W. P. Gilbert, et al. *Simulator Study of Stall/Post-stall Characteristics of a Fighter Airplane with Relaxed Longitudinal Static Stability*. Tech. rep. 1538. NASA Langley Research Center, 1979.
- [129] J. Nocedal and S. J. Wright. "Numerical Optimization". In: 2nd ed. Springer, 2006. Chap. 12, pp. 304–351.
- [130] J. Oliveira, Q. P. Chu, J. A. Mulder, H. M. N. K. Balini, and W. M. Vos. "Output Error Method and Two Step Method for Aerodynamic Model Identification". In: *Proceedings of the AIAA Guidance, Navigation and Control Conference and Exhibit*. San Francisco, California, USA, Aug. 2005.
- [131] M. Oppenheimer and D. Doman. "A Method for Including Control Effector Interactions in the Control Allocation Problem". In: *Proceedings of the AIAA Guidance, Navigation and Control Conference and Exhibit*. AIAA-2007-6418. Hilton Head, SC, USA, 2007.
- [133] A. B. Page and M. L. Steinberg. "Effects of Control Allocation Algorithms on a Nonlinear Adaptive Design". In: *Proceedings of the AIAA Guidance, Navigation, and Control Conference and Exhibit, Portland, OR*. Aug. 1999.
- [141] M. M. Polycarpou and P. A. Ioannou. "A Robust Adaptive Nonlinear Control Design". In: *Automatica* 32.3 (1996), pp. 423–427.
- [142] V. Poonamallee, S. Yurkovich, A. Serrani, and D. Doman. "A Nonlinear Programming Approach for Control Allocation". In: *Proceedings of the American Control Conference*. Vol. 2. Boston, MA, USA, 2004, pp. 1689–1694.
- [143] L. Praly, G. Bastin, J. B. Promet, and Z. Jiang. *Foundations of Adaptive Control*. Berlin: Springer-Verlag, 1991. Chap. Adaptive Stabilization of Nonlinear Systems, pp. 347–434.

- [153] Y. Shin, A. J. Calise, and M. D. Johnson. "Adaptive Control of Advanced Fighter Aircraft in Nonlinear Flight Regimes". In: *Journal of Guidance, Control, and Dynamics* 31.5 (2008), pp. 1464–1477.
- [155] A. T. Simmons and A. S. Hodel. "Control Allocation for the X-33 using Existing and Novel Quadratic Programming Techniques". In: *Proceedings of the 2004 American Control Conference*. Boston, Massachusetts, USA, 2004.
- [163] L. Sonneveldt. "Adaptive Backstepping Control for Modern Fighter Aircraft". PhD thesis. Delft University of Technology, Faculty of Aerospace Engineering, July 2010.
- [164] L. Sonneveldt, Q. P. Chu, and J. A. Mulder. "Nonlinear Flight Control Design using Constrained Adaptive Backstepping". In: *Journal of Guidance, Navigation, and Dynamics* 30.2 (2007), pp. 322–336.
- [166] L. Sonneveldt, E. R. van Oort, Q. P. Chu, and J. A. Mulder. "Immersion and Invariance Based Nonlinear Adaptive Flight Control". In: *Proceedings of the AIAA Guidance, Navigation, and Control Conference*. 2010-7690. AIAA. Toronto, Ontario, Canada, 2010.
- [168] E. D. Sontag and Y. Wang. "On Characterizations of Input-to-State Stability with Respect to Compact Sets". In: *Proceedings of the IFAC Non-linear Control Systems Design Symposium*. Tahoe City, CA, USA, 1995, pp. 226–231.
- [169] O. J. Sørtdalen. "Optimal Thrust Allocation for Marine Vessels". In: *Control Engineering Practice* 5.9 (1997), pp. 1223–1231.
- [170] J. Stark. "Adaptive Model Selection Using Orthogonal Least Squares Methods". In: *Proceedings: Mathematical, Physical and Engineering Sciences* 453.1956 (1997), pp. 21–42.
- [175] V. Stepanyan and N. Hovakimyan. "Adaptive Disturbance Rejection Controller for Visual Tracking of a Maneuvering Target". In: *Journal of Guidance, Control, and Dynamics* 30.4 (2007), pp. 1090–1106.
- [186] J. Tjønnås. "Nonlinear and Adaptive Dynamic Control Allocation". PhD thesis. Trondheim, Norway: Norwegian University of Science, Technology, Faculty of Information Technology, Mathematics, and Electrical Engineering, 2008.
- [187] J. Tjønnås and T. A. Johansen. "Optimizing Nonlinear Adaptive Control Allocation". In: *Proceedings of the 16th IFAC World Congress*. Prague, Czech Republic, 2005.
- [194] E. R. van Oort, L. Sonneveldt, Q. P. Chu, and J. A. Mulder. "A Comparison of Adaptive Nonlinear Control Designs for an Over-actuated Fighter Aircraft Model". In: *AIAA Guidance, Navigation, and Control Conference and Exhibit*. Honolulu, Hawaii, USA, Aug. 2008.

- [197] E. R. van Oort, L. Sonneveldt, Q. P. Chu, and J. A. Mulder. "Full Envelope Modular Adaptive Control of a Fighter Aircraft using Orthogonal Least Squares". In: *Journal of Guidance, Navigation and Dynamics* 33.5 (2010), pp. 1461–1472.
- [198] E. R. van Oort, L. Sonneveldt, Q. P. Chu, and J. A. Mulder. "Modular Adaptive Input-to-state Stable Backstepping of a Nonlinear Missile Model". In: *AIAA Guidance, Navigation, and Control Conference and Exhibit*. Hilton Head, South Carolina, USA, Aug. 2007.
- [199] J. A. M. M. Wedershoven. "Analysis of Nonlinear Dynamic Inversion based Control Law Designs". MA thesis. Delft University of Technology, Faculty of Aerospace Engineering, June 2010.

PART



SAFE FLIGHT ENVELOPE

In the preceding part of the dissertation adaptive control designs have been applied to different fighter aircraft models. Although these control designs are able to stabilize the aircraft in post-failure flight conditions, it is still unclear what the remaining maneuvering capability and flight envelope of the aircraft is. Knowledge of the flight envelope is extremely important to prevent loss-of-control accidents from occurring. In this part, a method is proposed which can be used to determine the safe flight envelope using a model of the aircraft dynamics, and it is applied to a nonlinear fighter aircraft model to show its capabilities.

FLIGHT ENVELOPE PROTECTION

In this chapter an introduction to the flight envelope and flight envelope protection concepts is given. The importance of knowledge about the safe flight envelope is discussed and the question how this knowledge can enhance the safety of flight and aid the aircraft designer during the design and development phases is answered. Then, different interpretations of flight envelope are discussed. A literature review of existing approaches to aircraft flight envelope determination and protection is given. Finally, some conclusions and research objectives based on this literature review are given.

10.1 Introduction

During the last decades adaptive control, in its many forms, has received a lot of attention within the flight control community. These control algorithms are able to deal with changes in the system's dynamics due to possible system component faults and failures. A question that still remains unanswered is which parts of the state space are safe to operate in, often even when the dynamics of the system are fully known they are not completely understood. This question is of fundamental importance in the safety verification of control systems and system validation.

The relevance of knowledge of the flight envelope is emphasized by means of two accidents which are both the result of a violation of the safe flight envelope. On October 4, 1992 El-Al flight 1862, a Boeing 747 cargo plane crashed into two apartment buildings in the Bijlmermeer neighborhood of Amsterdam, near Schiphol Airport. Engine number three separated from the right wing of the aircraft shortly after take-off, damaging the wing flaps, and striking engine number four which then also separated. The damage to the airframe sustained by the aircraft after the

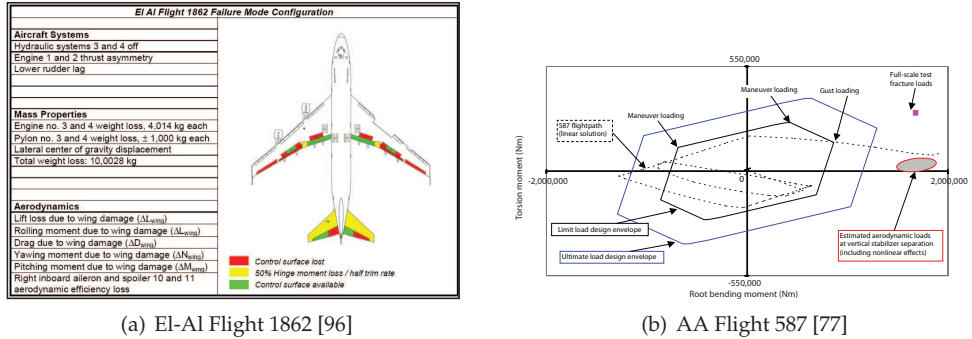


Figure 10.1: Structural damage for El-Al Flight 1862 10.1(a) and the reconstructed loads on the vertical stabilizer of AA 587 in 10.1(b).

separation of the right inboard engine is illustrated in figure 10.1(a). Post crash analysis showed that the aircraft still had marginal controllability left in a severely restricted flight envelope [161]. Simulator experiments using various fault tolerant flight control approaches have shown that landing the aircraft safely at Schiphol airport was still possible [2, 98, 178]. Additional simulations showed that a very experienced pilot was able to land the aircraft using the standard control system when he was informed about the severely restricted flight envelope. However, the Boeing 747 aircraft does not have such a fault tolerant control system and, more importantly, the pilots did not have any knowledge about the restricted flight envelope of the aircraft. When the crew tried to reduce the speed for landing the aircraft banked sharply to the right without any chance of recovery: control of the aircraft was completely lost with disastrous results.

One could argue that the cause of the preceding accident was the damage the aircraft sustained, and that a crash might have been inevitable with the information available at that time. Therefore, another example is presented in which the structural damage and fatal crash was actually caused by excessive pilot input. American Airlines Flight 587, an Airbus A300, departing from John F. Kennedy International Airport and encountered heavy turbulence due to the wake of a preceding aircraft shortly after take-off. The pilots tried to keep the plane upright with aggressive rudder inputs which eventually caused the aircraft's vertical stabilizer to snap off entirely. This caused complete loss-of-control of the aircraft and eventually a crash. The reconstructed loads on the vertical stabilizer and its design limits are shown in figure 10.1(b).

Spin is an aggravated stall that results in auto-rotation. The flight path is a downward spiral, in which the aircraft descends while rotating about a vertical axis, rolling, yawing, pitching and sideslipping as a consequence of being at some angle of attack between stall and 90 degrees. The combination of separated flows, high rotational rates, and high coupling in lateral and directional axes make spin

a very complicated motion. Simultaneously, the pilot can be very disoriented and might not be able to give the required control input to get the aircraft back to a stable state. Combined, this results in major difficulties in spin recovery and therefore prediction and analysis of spin characteristics together with recovery strategies have received great interest.

Recent statistics show that the majority of accidents in aviation nowadays are due to Loss-of-Control (LOC) [15, 145]. It is very hard to obtain a definition of LOC in analytical terms [91, 202], but it is generally associated with flight outside of the normal flight envelope, nonlinear behavior, and inability of the pilot to control the aircraft [90]. This also shows that LOC is not a phenomenon solely attributed to military aircraft, but that it is a real problem for commercial aircraft and general aviation as well. One definition of LOC is that the (auto)pilot is not able to return to a *normal* flight condition from the current flight condition: the aircraft has exceeded its *safe flight envelope*. A very striking fact is that this category of accident causes is one of the few, if not the only one, which has not decreased in frequency over the last decades. Therefore, safety of aviation can be potentially be improved by paying effort in flight envelope protection and upset prevention to avoid LOC situations.

10.2 The Flight Envelope

The conventional definition of the flight envelope is “[the flight envelope] describes the area of altitude and airspeed where an airplane is constrained to operate.” [147]. The flight envelope boundaries are defined by various limitations on the performance of the airplane, for example available engine power, stalling and buffet characteristics, structural considerations and requirements on noise production. A very common way to present the flight envelope is the *doghouse*-plot. In figure 10.2 a doghouse plot for the F-16 aircraft is shown which relates the altitude, velocity and some other variables at which the aircraft can safely fly.

The boundaries defined on the flight envelope in the doghouse plot are quite adequate during normal operation of aircraft. The main problem with this conventional definition of flight envelope is that only constraints on quasi-stationary aircraft states are taken into account, for example for coordinated turns and cruise flight. Additionally, constraints posed on the aircraft state by the environment are not part of the conventional definition of flight envelope. The aircraft’s dynamic behavior can pose additional constraints on the flight envelope, for example due to inertia coupling effects. Such constraints would be especially important for military and acrobatic aircraft, aircraft having experienced upset, and aircraft with airframe and/or actuator damage or malfunctions. Thus, a different, extended definition of the flight envelope is required. The definition of the safe flight envelope used in this dissertation is presented below, which is more restrictive than the definition based on performance and structural limitations alone.

Definition 10.1 (Safe Flight Envelope). *The safe flight envelope is the part of the state space for which safe operation of the aircraft and safety of its cargo can be guaranteed and*

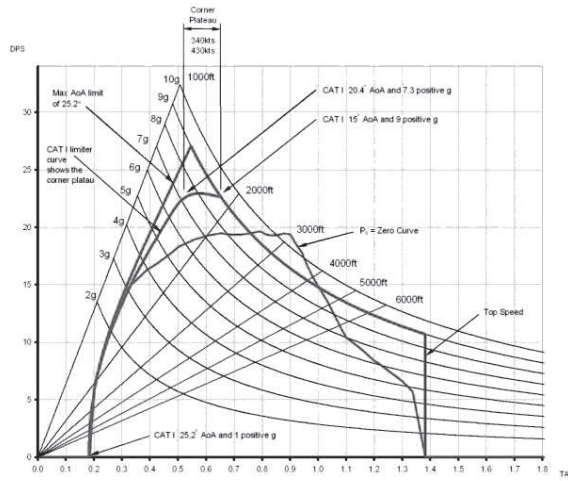


Figure 10.2: Doghouse-plot for an F-16 aircraft model [162].

externally posed constraints will not be violated.

The safe flight envelope can be defined by the intersection of three envelopes:

Dynamic Envelope Constraints posed on the envelope by the dynamic behavior of the aircraft, due to its aerodynamics and kinematics.

Structural and Comfort Envelope Constraints posed by the airframe, pilot, passengers and cargo. These constraints are usually defined through maximum accelerations and loads.

Environmental Envelope Constraints due to the environment in which the aircraft operates.

The last two envelopes pose *external* constraints on the flight envelope, constraints which are generally well-known and can be quantified easily. Examples of such external constraints are the terrain around the aircraft (see figure 10.3(a)), weather, and the maximum load-factor the airframe can sustain before breaking (see figure 10.3(b)). The first example given in the introduction is considered to be a violation of the dynamic flight envelope, while the structural envelope was violated by the aircraft in the second example. The focus of the research in this dissertation is on the first type, i.e. the flight envelope that is *internal* to the system itself and depends on its dynamic behavior. A more formal definition of the *dynamic flight envelope* is given below.

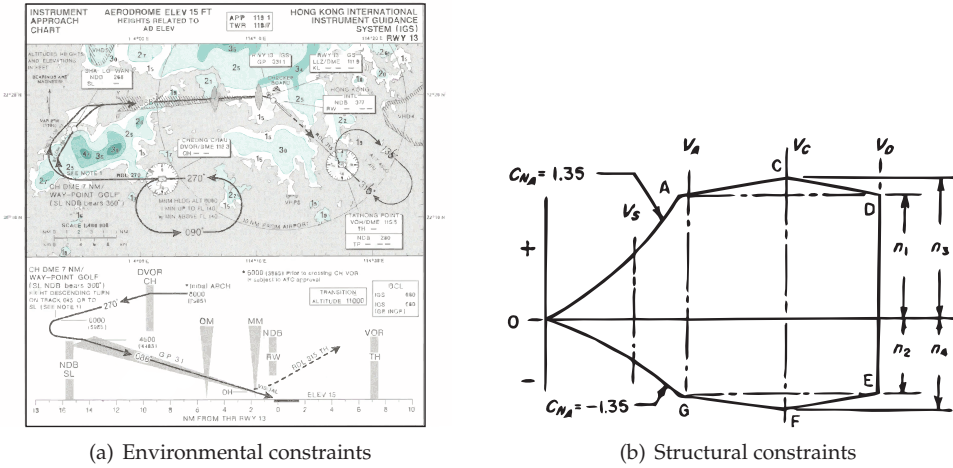


Figure 10.3: External constraints posed on the flight envelope

Definition 10.2 (Dynamic Flight Envelope). *The region of the aircraft’s state space in which the aircraft can be safely controlled and no loss-of-control events can occur.*

Constraints posed on the aircraft by the dynamic flight envelope are for example a maximum roll-rate at a certain angle of attack in order to prevent the aircraft from entering a potentially hazardous inertia coupling or spin phenomenon. Similar constraints can be obtained to prevent aircraft from entering stall and deep-stall, or even unstable limit cycles. Simultaneously, the dynamic flight envelope provides excellent insight in the aircraft maneuvering capabilities, and the envelope results can for example be used to develop evasive and attack maneuvers. Furthermore, when an CFD model with uncertainty bounds on the parameters is available a preliminary flight envelope model can be created to support flight testing outside the conventional regime, or identify and address potentially hazardous parts of the flight envelope already during the design phase.

10.3 Flight Envelope Protection Methods

As noted by Lambregts, Nesemeier, Wilborn, and Newman [91] one of the most promising techniques to prevent LOC-related accidents is envelope protection. Envelope protection methods use the safe flight envelope (and add a margin of safety) to prevent pilots from commanding control inputs that would push the aircraft outside that flight envelope. For example, if the pilot uses the rearward side-stick to pitch the aircraft nose up, the control computers creating the flight envelope protection will prevent the pilot pitching the aircraft beyond the stalling angle of

attack. As a result, even if the pilot tried to apply more and more rearward control, the flight envelope protection would cause the aircraft to ignore this command. Flight envelope protection can in this way increase aircraft safety by allowing the pilot to apply maximum allowable control effort in an emergency, while at the same time not pushing the aircraft outside the margins of its operational safety. Whether the pilot is allowed to override the constraints posed by the flight computer is a still the subject of an ongoing debate. A prerequisite for flight-envelope protection systems is a fly-by-wire (FBW) system. In the FBW, the pilot's inputs are sent to a computer which then calculates the desired commands, i.e. there is no direct link between the pilot and the controls. Such systems have existed for over 30 years but are currently only available in military aircraft, several commercial aircraft and some general aviation aircraft. The task of envelope protection can be split into two parts:

1. determination/calculation of the safe flight envelope, and
2. guaranteeing that the aircraft state stays within that safe flight envelope.

Quite a lot of research has been done on the second aspect of envelope protection and the constraints posed on the aircraft states by the safe flight envelope can be incorporated in the control design such that the (auto)pilot is either unable to steer the aircraft outside its safe operating regime (hard-constrained, for example the Airbus A320 aircraft), or is informed that the aircraft is *pushing the envelope* (soft-constrained, for example the Boeing 777 aircraft). It is important to note that envelope protection does not only enable aircraft to safely operate within their envelope, but should do so without restricting the aircraft to a smaller region of its operational envelope.

Switching logic with PID-control is used by Well [200] and Falkena, Borst, and Mulder [54] to develop controllers which keep a fighter and a general aviation aircraft respectively within a restricted part of the flight envelope. Limit detection and avoidance schemes based on neuro-adaptive techniques have also been proposed and flight tested on rotorcraft UAVs [72, 73, 81, 205]. Tang, Roemer, Ge, et al. [181] emphasize the integration of online flight envelope estimation and protection functions as a total solution, and feasibility of the concept and proposed architecture is shown through simulation studies on the NASA GTM model. This architecture combined with adaptive flight control is illustrated in figure 1.3.

10.4 Survey of (Safe) Flight Envelope Estimation

Although the nonlinear problems in aircraft flight dynamics and control have been well recognized and widely documented since the dawn of aviation [1], their prediction and solution was limited by both the lack of analytical tools and poor simulation capabilities [136]. One of the first problems to draw attention was the inertia-coupling problem as predicted by Phillips [139]. Reviews of early work on these

problems have been provided by Hacker and Oprisiu [67] and Murphy [123]. Approximate analytical methods were used to predict conditions for onset of instability, which were not always reliable. Due to increasing computing power, greater reliance was placed on numerical simulations to predict instability onset and post-instability nonlinear dynamical behavior. Increasing demands on aircraft agility and performance have since then pushed the operating range of modern fighter aircraft (far) beyond the linear range of aerodynamics [70]. This introduced new nonlinear problems due to flight at high angles of attack and critical flight regimes, typically under post-stall conditions.

Initial flight envelope and clearance results can be obtained by means of wind-tunnel tests, CFD-calculations and experience with comparable airframe and actuator configurations. Usually, this information is verified and corrected through an expensive flight testing program.

An important development in the field was the introduction of bifurcation and continuation methods by Carroll and Mehra [24] and Zagaynov and Goman [209]. These techniques made it possible to smartly compute an entire family of steady state solutions for varying values of a control parameter, for example the elevator deflection. By means of numerical differentiation it is possible to obtain the linearized dynamics at each trim state, and compute the stability of each trim state. Continuation algorithms have been very helpful in computing and characterizing limit cycle oscillations in terms of their onset, stability, amplitude, and frequency [136]. Bifurcation and continuation methods have been mainly used as analysis tools during the design of aircraft and for clearance of flight control laws and envelope. For excellent overviews and state of the art of bifurcation theory applied to flight the dynamics, the interested reader is referred to Cummings [31], Lowenberg [103], Goman, Zagaynov, and Khramtsovsky [63], and Sinha [157]. Examples of the application of bifurcation and continuation methods to aircraft dynamics are given by Paranjape, Sinha, and Ananthkrishnan [136], flight clearance metrics for autonomous UAVs through continuation analysis were derived by Panella [135].

Concepts directly related to safety are reachability, viability and invariance. These concepts were explicitly linked for aviation safety in flight control analysis [108] and analysis of a traffic alert and collision avoidance system [95] for example. An indirect approach to address the reachability questions is using optimal control methods, where the reachable sets are characterized as levels sets of the value function of an appropriate optimal control problem [116]. A basic flight envelope was derived through reachable set analysis combined with neuro-dynamic programming by Djeridane and Lygeros [39]. The safe envelope for an aircraft in different landing configurations was investigated by Bayen, Mitchell, Oishi, and Tomlin [10] in the reachable set framework. Five dimensional reachable set computations have been implemented on a glider submarine at the French Department of Defense [146]. The safety of closely-spaced parallel approaches was investigated and demonstrated by Teo, Jang, and Tomlin [182], Teo and Tomlin [183].

The theory of reachable set analysis has been applied to linear parameter varying (LPV) systems by Shin [152]. Many nonlinear methods based on Lyapunov's

stability theory, see 3, have been proposed and applied successfully as a region of attraction (ROA) prediction tool [66, 180, 185, 188]. ROA methods are able to predict a stable set in the state space around a given equilibrium point for which the system will return to the equilibrium. Hence, an application scenario would be a trimmed aircraft experiencing an upset condition due to atmospheric phenomena. Knowledge whether such conditions could potentially destabilize the aircraft without chance of recovery is vital to verify safety. A combination of LPV reachability and region of attraction analysis is applied to the NASA GTM model investigating the safe envelope by Pandita, Chakraborty, Seiler, and Balas [134].

The methods discussed so far are off-line methods, requiring a fixed, a-priori aircraft model. Real time estimation of stability margins has also been investigated. Frequency response analysis based stability margin determination was first demonstrated on the X-36 aircraft by Balough [8], Lichter, Bateman, and Balas [94] demonstrated run-time margin estimation on NASA Langley's AirSTAR testbed. In [125] on-line stability metrics were derived on-line for a small-scale Cessna 182 aircraft.

10.5 Conclusions

In this chapter the concept of flight envelope was discussed. The safe flight envelope is defined as the region in the state space for which safe operation of the aircraft and safety of its cargo can be guaranteed and externally posed constraints will not be violated. This region in the state space can be defined as the intersection between the dynamical, structural and environmental envelopes. Statistical data shows that the majority of aircraft accidents in the past decade has been related to excursions of the aircraft beyond its safe flight envelope. Therefore, both knowledge of the safe flight envelope and some form of protection is required to keep the aircraft within the safe flight envelope. Since determination of the actual limits is important not to constrain the operational envelope too much, this will be the focus of the research in the remainder of this part of the dissertation.

LEVEL SET METHODS

This chapter introduces the theory used by the proposed method to determine the safe dynamic flight envelope of aircraft. First the reachable set concept is introduced, and its use in safe flight envelope determination is discussed. After this, the explicit and implicit descriptions of sets are introduced. Dynamics are added to the implicit description by means of the level set equation, such that the set can be evolved in time to obtain the reachable set. Different solution methods for the level set equation, a Hamilton Jacobi partial differential equation for systems with inputs, exist. Three different solution approaches are introduced, as well as their advantages and disadvantages. The potential of the level set approach for reachability analysis is illustrated by means of several examples. These examples are additionally used to perform a comparison of computation time required for the different solution methods. Finally, conclusions are drawn from the analysis of the examples.

11.1 Forwards and Backwards Reachable Sets

Reachable set analysis is a useful tool in the safety verification of systems. The reachable set for a given initial set describes the set of states that can be reached within a certain time. In this section, the concept will be defined formally, and the difference between forwards and backwards reachable sets is illustrated.

Consider a system

$$\begin{aligned} \dot{x} &= f(x(t), u(t), d(t)) \\ x(0) &\in \mathcal{S}_0 \text{ or } x(t_f) \in \mathcal{T}_f \\ t &\in [0, t_f] \end{aligned} \tag{11.1}$$

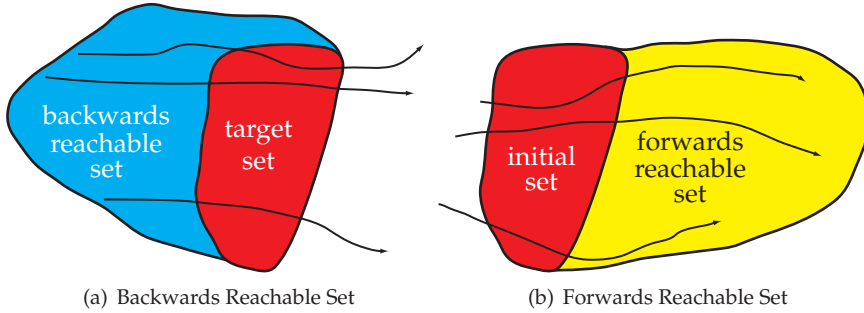


Figure 11.1: Backwards (left) and forwards (right) reachable set definitions

where $0 \leq t_f < \infty$, $x \in \mathbb{R}^n$ is the state, $u \in U \subset \mathbb{R}^m$ is the control input, $d \in D \subset \mathbb{R}^q$ is the disturbance input, $\mathcal{S}_0 = \{x \in \mathbb{R}^n \mid S(x) \leq 0\}$ is a set of initial states, and $\mathcal{T}_f = \{x \in \mathbb{R}^n \mid T(x) \leq 0\}$ is a set of target states. The function f is assumed to be Lipschitz continuous. The spaces of admissible control and disturbance input trajectories are denoted as the spaces of the piecewise continuous functions $\mathcal{U} = \{u(\cdot) \in PC^0 \mid u(t) \in U, 0 \leq t \leq t_f\}$, and $\mathcal{D} = \{d(\cdot) \in PC^0 \mid d(t) \in D, 0 \leq t \leq t_f\}$ respectively.

The dynamics defined by (11.1) can be evolved backwards and forwards in time resulting in the backwards and forwards reachable sets respectively. The difference between these two sets is illustrated in figure 11.1. Formally, these sets are defined below [75].

Definition 11.1 (Backwards Reachable Set). *The backwards reachable set $\mathcal{T}(\tau)$ at time τ ($0 \leq \tau < t_f$), of the system (11.1) for the target set \mathcal{T}_f , is the set of all states $x(\tau)$, such that there exists a control input $u(t) \in \mathcal{U}(\tau \leq t \leq t_f)$, for all disturbance inputs $d(t) \in \mathcal{D}(\tau \leq t \leq t_f)$, for which some $x(t_f) \in \mathcal{T}_f$ are reachable from $x(\tau)$ along a trajectory satisfying (11.1).*

Definition 11.2 (Forwards Reachable Set). *The forwards reachable set $\mathcal{S}(\tau)$ at time τ ($0 < \tau \leq t_f$) of the system (11.1) for the initial set \mathcal{S}_0 , is the set of all states $x(\tau)$, such that there exists a control input $u(t) \in \mathcal{U}(\tau \leq t \leq t_f)$, for all disturbance inputs $d(t) \in \mathcal{D}(\tau \leq t \leq t_f)$, for which $x(\tau)$ is reachable from some $x(0) \in \mathcal{S}_0$ along a trajectory satisfying (11.1).*

11.2 The Flight Envelope and Reachable Set Analysis

With the concepts of forwards and backwards reachability, the safe envelope can be defined. First, pose the initial and target set as a set of known safe states, for

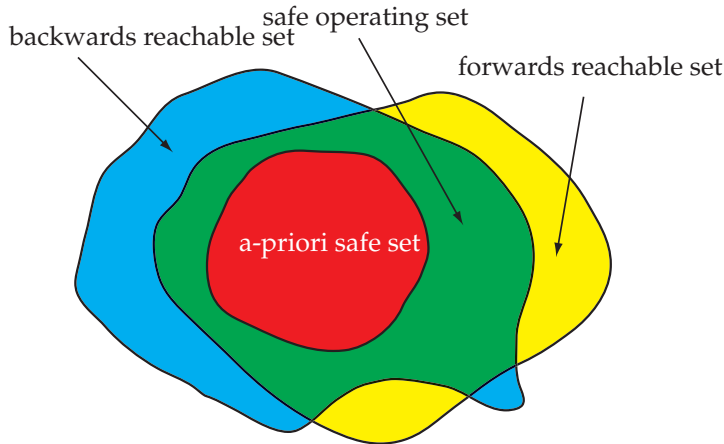


Figure 11.2: The safe envelope for a known safe set is defined by the intersection of the forwards and backwards reachable sets.

example a set of trimmable states at normal flight conditions. The backwards reachable set then contains the set of states that can be controlled back to a state within the trim set using a control signal within the control effector constraints and for any disturbance realization included in the model, for example wind or uncertain aerodynamic parameters. Similarly, the forwards reachable set describes the set of states that can be reached from the trim states, allowing investigation of the full maneuvering capabilities of an aircraft, and what influence different control constraints and disturbance levels have on maneuverability, stability and performance.

The safe maneuvering envelope can be obtained by the intersection of the forwards and backwards reachable sets, as illustrated in figure 11.2. The end time for the calculations and disturbance constraints do not have to be the same equivalent. For example, one can allow a longer time period for the backwards reachable set for highly maneuverable aircraft, or, increase the magnitude constraints on the disturbance in the backwards reachable set to obtain safer bounds on the safe envelope. Regions in the flight envelope that are part of the forwards reachable set, but are not part of the backwards reachable set, are potentially hazardous.

11.3 Connection to Lyapunov Theory

A very interesting connection to Lyapunov theory can be drawn, one of the main subjects of part I in this dissertation. Suppose that it is possible to find a positive definite function V where the trim set corresponds to some level set of V . Then, if additionally the safe maneuvering envelope can be encoded in the function V as a different, higher value, level set, this Lyapunov function can be used to prevent

the aircraft state from exceeding the safe maneuvering envelope. It is possible to interpret the Lyapunov function value as a distance measure to the trim set. This could then for example be used in a receding horizon controller. In [144] a connection between the Hamilton-Jacobi-Bellman equation and a modified version of Sontag's formula is drawn to create a control law based on a CLF, which solves the HJB equation.

11.4 Implicit Functions and Surfaces

Sets or regions in some space, can be defined in different ways. This section introduces the explicit and implicit representations and discusses their advantages and disadvantages.

In one spatial dimension, the real line can be divided into three distinct pieces, by using the points $x = -1$ and $x = 1$. Three intervals are defined as $(\infty, -1)$, $(-1, 1)$ and $(1, \infty)$ as three sub-domains. The part $\Omega^- = (-1, 1)$ will be referred to as the *inside* part of the domain, and $\Omega^+ = (\infty, -1) \cup (1, \infty)$ as the *outside* part. The border between the inside and outside consists of two points $\partial\Omega = \{-1, 1\}$, and is defined as the *interface*. Therefore, in one spatial dimension the inside and outside regions are one-dimensional (a line), while the interface is zero-dimensional (a point). More generally, in \mathbb{R}^n , the sub-domains are n -dimensional, while the interface has dimension $n - 1$.

In an *explicit* representation of the interface, all segments that are part of the interface are explicitly defined, as in the example in one dimension above. An alternative description is the *implicit* definition of the interface as an isocontour of some function. For example, the zero isocontour of the function $\phi(x) = |x| - 1$ is the set of all points where $\phi(x) = 0$. Figure 11.3 shows this implicit description of the interface $\partial\Omega$. Note that the function $\phi(x)$ is defined over the whole domain, while the interface, or isocontour, is defined on a domain that is one dimension lower.

The explicit interface definition requires specification of all points that belong to the interface. While this task is achievable for simple geometric and low dimensional shapes, it becomes increasingly difficult for more complex interface shapes and/or higher dimensions. A convenient way of approximating an explicit representation is to discretize the interface into a finite number of points. The approximated interface can then be obtained by triangulation of these points. The interface can then be evolved in time by evolving each discretization point through time.

An implicit representation of the interface might seem wasteful on the other hand, since the function is defined on the whole (computational) domain, while only the interface is of interest. One possible solution for this is by clustering the computational nodes near the interface, and allowing a coarser grid further away from the interface. The implicit interface description allows the use of a very powerful tool to evolve the interface: the level set method.

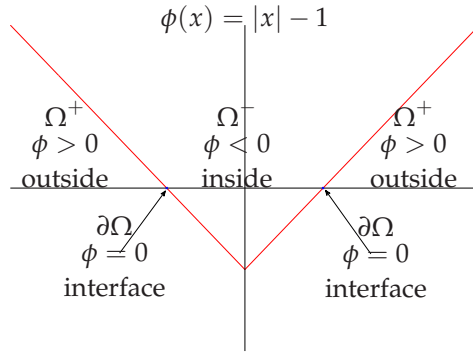


Figure 11.3: Implicit function $\phi(x) = |x| - 1$ defining the region Ω^- and Ω^+ as well as the boundary $\partial\Omega$.

11.5 Level Set Method

The level set method adds dynamics to implicitly defined set descriptions. The book by Osher and Fedkiw [132] provides an excellent introductory reference about the level set method and dynamic implicit surfaces. The interface, or boundary of a set, needs to be evolved in time to obtain the reachable set for the defined initial or target set. Suppose that the velocity of each point on the interface is given by some externally generated velocity field $f(x)$. Then, every point on the interface can be evolved in time using this velocity field. The simplest way to achieve this is by solving the ordinary differential equation (ODE)

$$\frac{dx}{dt} = f(x) \tag{11.2}$$

for every point that is part of the interface. This is a *Lagrangian* formulation of the interface evolution equation. If the connectivity of the discretized interface points does not change, and the surface elements are not distorted too much, the interface can be evolved relatively easy in this fashion. Unfortunately, even rather trivial velocity fields can cause large distortions of the boundary elements, and hence the accuracy of this method deteriorates quickly if the interface description is not regularized and smoothed often.

Instead of directly evolving the interface, the implicit function ϕ is used to both represent the interface, and to evolve it in time. The simple convection equation.

$$\phi_t + \nabla\phi \cdot f(x) = 0, \tag{11.3}$$

where subscript t denotes a temporal partial derivative in the time variable t , defines the evolution of the implicit function ϕ . Note that the function $f(x)$ should

now be defined on the whole domain of interest to correctly evolve the interface. This partial differential equation (PDE) often needs to be solved numerically for non-trivial velocity fields, for which various methods exist. In section 11.7 some of these methods will be discussed in more detail. In the next section the level set equation, or Hamilton Jacobi PDE, for systems with inputs is derived.

11.6 Reachable Sets and Differential Games

A connection between reachable sets and optimal control can be made. This connection allows transformation of the reachable set problem described in section 11.1 using the level set approach of the previous section into a terminal value Hamilton Jacobi partial differential equation (HJ PDE).

11.6.1 The Hamilton-Jacobi PDE

Consider the dynamical system

$$\dot{x} = f(x, a, b) \quad (11.4)$$

where a and b are inputs to the system. A trajectory of this system is defined by $\xi_f(\cdot; x, t, a(\cdot), b(\cdot))$, where

$$\begin{aligned} \xi_f(\cdot; x, t, a(\cdot), b(\cdot)) &= x, \\ \frac{d}{dt} \xi_f(s; x, t, a(\cdot), b(\cdot)) &= f(x, a(s), b(s)). \end{aligned}$$

A finite horizon differential game is played over the time horizon $[-T, 0]$, with dynamics governed by (11.4). The terminal cost of a trajectory is given by

$$C(x, t, a(\cdot), b(\cdot)) = G(\xi_f(\cdot; x, t, a(\cdot), b(\cdot))).$$

One player will try to maximize this cost, while the other player tries to minimize it. If player a tries to minimize the cost and player b tries to maximize it, the value function of the differential game is defined by

$$\begin{aligned} V(x, t) &= \inf_{a(\cdot) \in \mathcal{A}} \sup_{b(\cdot) \in \mathcal{B}} C(x, t, a(\cdot), b(\cdot)), \\ &= \inf_{a(\cdot) \in \mathcal{A}} \sup_{b(\cdot) \in \mathcal{B}} G(\xi_f(0; x, t, a(\cdot), b(\cdot))). \end{aligned} \quad (11.5)$$

If the value function would be differentiable, it is straightforward to show using Bellman's optimality principle [11] and a Taylor expansion of the value function

that the differential game can be reformulated as a Hamilton-Jacobi Isaacs PDE. If the dynamic programming principle holds, the value function can be rewritten as

$$V(x, t) = \min_{a \in \mathcal{A}} \max_{b \in \mathcal{B}} V\left(\xi_f(t + \Delta t; x, t, a(\cdot), b(\cdot)), t + \Delta t\right)$$

for $-T \leq t \leq t + \Delta t \leq 0$ and $V(x, 0) = G(x)$. A first order Taylor expansion of the value function under the assumption that the function is differentiable is now given by

$$V(\xi_f(t + \Delta t; x, t, a(\cdot), b(\cdot)), t + \Delta t) \approx V(x, t) + V_t(x, t)\Delta t + V_x(x, t) \cdot \Delta x.$$

Re-arranging terms in the expression defined by the principle of optimality and dividing by Δt yields

$$\min_{a \in \mathcal{A}} \max_{b \in \mathcal{B}} \frac{V(\xi_f(t + \Delta t; x, t, a(\cdot), b(\cdot)), t + \Delta t) - V(x, t)}{\Delta t} = 0$$

Now insert the Taylor expansion of the value function and letting $\Delta t \rightarrow 0$ gives

$$\begin{aligned} \min_{a \in \mathcal{A}} \max_{b \in \mathcal{B}} \left[\frac{d}{dt} V(x, t) \right] &= 0 \\ \frac{\partial}{\partial t} V(x, t) + \min_{a \in \mathcal{A}} \max_{b \in \mathcal{B}} \frac{\partial}{\partial x} V(x, t) \cdot f(x, a, b) &= 0 \quad (11.6) \\ \frac{\partial}{\partial t} V(x, t) + H(x, \frac{\partial}{\partial x} V(x, t)) &= 0, \end{aligned}$$

where the Hamiltonian $H(x, p) = \inf_{a(\cdot) \in \mathcal{A}} \sup_{b(\cdot) \in \mathcal{B}} p \cdot f(x, a, b)$. Unfortunately, the assumption that $V(x, t)$ is differentiable is often violated. Therefore, this derivation is not technically correct. If shocks and rarefactions are present, a classical solution to an HJ PDE may not exist. A non-classical or weak solution to the PDE is defined through a viscosity solution, which first appeared in [30] and was rewritten in a more useful form in [29]. A bounded, uniformly continuous function $\phi(x, t)$ is a *viscosity solution* to the HJ PDE

$$\frac{\partial}{\partial t} \phi(x, t) + H(x, \frac{\partial}{\partial x} \phi(x, t)) = 0,$$

provided that for each infinitely differentiable test function $\psi(x, t)$

- if $\phi(x_0, t_0) - \psi(x_0, t_0)$ is a local maximum of the function $\phi - \psi$, then

$$\frac{\partial}{\partial t} \psi(x_0, t_0) + H(x_0, \frac{\partial}{\partial x} \psi(x_0, t_0)) \leq 0$$

- if $\phi(x_0, t_0) - \psi(x_0, t_0)$ is a local minimum of the function $\phi - \psi$, then

$$\frac{\partial}{\partial t} \psi(x_0, t_0) + H(x, \frac{\partial}{\partial x} \psi(x_0, t_0)) \geq 0$$

Note that viscosity solutions are *not* the same as vanishing viscosity solutions which are the solutions $\phi^{(\epsilon)}(x, t)$ in the limit $\epsilon \rightarrow 0$ of the linear second order PDE

$$\frac{\partial \phi^{(\epsilon)}}{\partial t} + H(x, \frac{\partial \phi^{(\epsilon)}}{\partial x}) = \epsilon \frac{\partial^2 \phi^{(\epsilon)}}{\partial x^2} \quad (11.7)$$

Lemma 11.3. *The value function $\phi(x, t)$ of the game (11.5) is the viscosity solution of a Hamilton-Jacobi terminal value PDE.*

$$\begin{aligned} \frac{\partial}{\partial x} \phi(x, t) + H\left(x, \frac{\partial}{\partial x} \phi(x, t)\right) &= 0, \text{ for } t \in [-T, 0], x \in \mathbb{R}^n \\ \phi(x, 0) &= G(x) \text{ for } x \in \mathbb{R}^n \end{aligned} \quad (11.8)$$

where

$$H(x, p) = \min_{a \in \mathcal{A}} \max_{b \in \mathcal{B}} p^T f(x, a, b) \quad (11.9)$$

Proof. This lemma is a special case of Theorem 4.1 in [53] □

11.6.2 HJ PDE for the Backwards and Forwards Reachable Sets

The connection between the HJ PDE and reachable sets has been shown. Now, the HJ PDE can be derived for the backwards and forwards reachable set formulations. It will be assumed that the task of the player a will be to use the control input to get away from the initial or target set as far as possible, while the task of player b will be to remain as close to the initial or target set as possible.

Therefore, the Hamiltonians for these respective problems are defined as

$$\begin{aligned} H_b(x, p, t) &= \min_{u \in \mathcal{U}} \max_{d \in \mathcal{D}} p \cdot f(x, u, d) \\ H_f(x, p, t) &= \max_{u \in \mathcal{U}} \min_{d \in \mathcal{D}} p \cdot f(x, u, d) \end{aligned} \quad (11.10)$$

The following relation

$$H_l(x, p, t) = -H_r(x, -p, t) \quad (11.11)$$

allows the transformation of an initial value problem, denoted by subscript l , related to forwards reachable sets into an equivalent terminal value HJ PDE [112],

denoted by subscript r . The HJ PDE for the backwards and forwards reachable set determination are [89]

$$\begin{aligned}\frac{\partial}{\partial t}\phi_b + H_b(x, p, t) &= 0 \\ H_b(x, p, t) &= \min_{u \in \mathcal{U}} \max_{d \in \mathcal{D}} p^T f(x, u, d) \\ \phi_b(x, 0) &= T(x),\end{aligned}\tag{11.12}$$

and

$$\begin{aligned}\frac{\partial}{\partial t}\phi_f + H_f(x, p, t) &= 0 \\ H_f(x, p, t) &= \max_{u \in \mathcal{U}} \min_{d \in \mathcal{D}} p^T f(x, u, d) \\ \phi_f(x, 0) &= S(x)\end{aligned}\tag{11.13}$$

respectively. Note that the backwards reachable set is solved from time $t = 0$ backwards to $t = -t_f \leq 0$. A modification can be made such that the reachable set only is allowed to grow, meaning that states that have been part of the reachable set are marked as reachable for the whole timespan considered. For more detail on this modification, the reader is referred to [116], the implementation basically make sure that only flow inwards over the interface is allowed by scaling the dynamics. The modified Hamilton is defined as

$$\tilde{H}(x, t, p) = \min [0, H(x, t, p)].\tag{11.14}$$

11.7 HJ-PDE Solution Methods

Various methods exists to obtain a solution to a Hamilton-Jacobi partial differential equation, or the level set equation. In this section, three different approaches to solving the equation are discussed. The methods can be distinguished by the way the interface is defined and how it is propagated in time. The methods will not be discussed in full detail, references will be given to the interested reader instead.

11.7.1 Lagrangian-methods

The Lagrangian methods can be considered as tracking methods, which track the evolution of the interface in a Lagrangian fashion, for example by evolving marker particles using the velocity field. This concept is illustrated in figure 11.4. The fundamental problem in the Lagrangian methods is the distortion of the locations of the computational elements, particles, resulting in an inaccurate description of the interface. Therefore, a regularization procedure is necessary to compensate for this problem and hence maintain the accuracy of the method. Several rather ad-hoc procedures have been proposed such as particle insertion and deletion. In

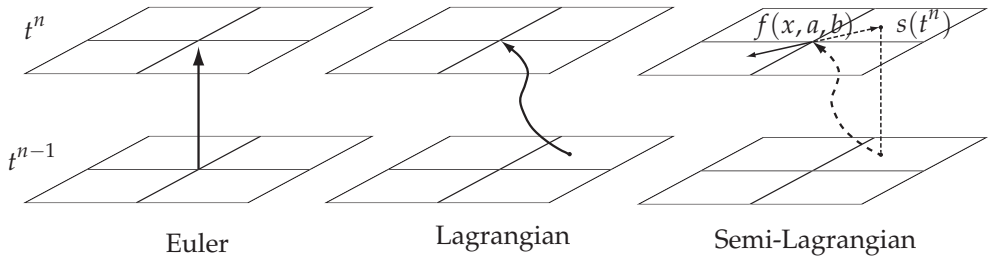


Figure 11.4: Euler, Lagrangian, and semi-Lagrangian schemes for the Level Set equation.

[71] a Lagrangian particle level set method was proposed which regularizes the particles by a remeshing procedure after each time-step to avoid this distortion of the calculation grid. Another problem with this method is that for the evolution of systems with inputs, the optimal inputs have to be solved. The optimal inputs depend on the state as well as the co-state. When the particles or computational elements located only near or on the interface, the co-state or directional derivative of the value function, is nearly impossible to obtain. Thus, determination of the optimal inputs as they appear in (11.10) is hard and rather inaccurate, resulting in a bad approximation of the true reachable set solution.

11.7.2 Euler-methods

The Euler-methods discretize the state space by means of a grid. On this grid, sets can be defined easily by an isocontour of an implicit surface as described in section 11.4. The Hamilton-Jacobi PDE is then solved by numerical integration of the implicit function values on the grid nodes in time. Usually, a Lax-Friedrichs approximation of the Hamiltonian is used to ensure stability of the numerical scheme by adding artificial viscosity. The spatial derivatives in (11.12) and (11.13) can be computed using (weighted) essentially non-oscillatory (ENO) schemes. Time-integration is performed by second- or third-order total variation diminishing (TVD) explicit Runge-Kutta schemes.

The biggest disadvantage of this approach is that the time-step is restricted by the Courant-Friedrichs-Lewy-condition (CFL condition) [27]. This is a necessary condition to ensure converge of the solution when using explicit time-marching schemes. In essence, it states that the domain of dependence must include the analytical domain of dependence in order to assure that the scheme can access the information required to form the solution: the solution is not allowed to travel more than one grid cell. Therefore, when the desired accuracy of the solution is high, the allowed time step can become extremely small.

The CFL time step restriction in one dimension becomes

$$\Delta t \leq \frac{\Delta x}{\max |u|} \quad (11.15)$$

where $\max |u|$ is chosen to be the largest value of $|u|$ over the entire Cartesian grid. A multi-dimensional CFL-condition can be written as

$$\Delta t \max \left\{ \sum_i \frac{|v_i|}{\Delta x_i} \right\} = \alpha \quad (11.16)$$

where $\alpha \leq 1$ is a safety factor and the maximization is over the computational domain. This condition clearly poses a stringent constraint on the allowed time-step for high resolution grids: for a small Δx_i and fast dynamics, or large $|v_i|$, the allowed Δt to comply with the CFL-condition will be very small.

11.7.3 Semi-Lagrangian methods

The time restriction posed by the CFL-condition can be eliminated by allowing unbounded stencils [177]. The time-step can be decoupled from the CFL-condition by using an explicit unconditionally stable time-stepping scheme. These schemes can be interpreted as semi-Lagrangian time-stepping schemes. For first-order hyperbolic problems, these schemes satisfy the CFL-condition with large time steps by shifting the stencil. The difference between the Euler and semi-Lagrangian approach is illustrated in figure 11.4. A semi-Lagrangian approach based on particle level sets was taken in [49] for systems without inputs. Consider the simplest linear hyperbolic PDE

$$\phi_t + \nabla \phi \cdot f(x, t) = 0. \quad (11.17)$$

This partial differential equation propagates the ϕ values along the characteristic curves $s(t)$ defined by

$$\dot{s}(t) = f(s(t), t). \quad (11.18)$$

Therefore, the value of ϕ at any time t can be determined by finding the characteristic curve passing through (x, t) and following it backwards to some previous point (x_0, t_0) where the value of ϕ is known: then $\phi(x, t) = \phi(x_0, t_0)$. This observation forms the basis of the “backwards characteristic”, or the CIR-scheme due to Courant, Isaacson and Rees [28] the simplest semi-Lagrangian scheme. Given ϕ at time t_n the CIR-scheme approximates $\phi(x, t_{n+1})$ at any point x at time $t_{n+1} = t_n + \Delta t$ by evaluating the velocity $F(x, t_n)$, approximating the backwards characteristic through x by a straight line

$$x - (t_{n+1} - t)f(x, t_{n+1}) \approx s(t), \quad (11.19)$$

and interpolating ϕ linearly at time t_n to the point

$$x - \Delta t F(x, t_n) \approx s(t_n). \quad (11.20)$$

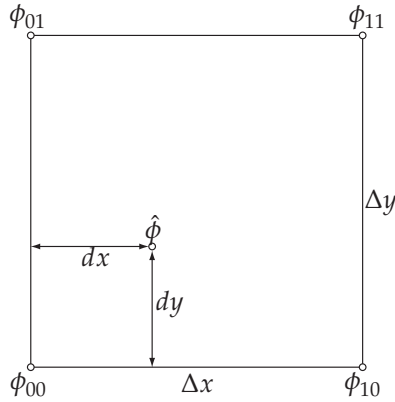


Figure 11.5: Bilinear interpolation of off-grid value for the semi-Lagrangian level set.

Then $\phi(x, t_{n+1})$ is set equal to the interpolated value. For linear PDEs the Lax-Richtmyer equivalence theorem guarantees that the CIR scheme converges to the exact solution when $\delta t, \delta x \rightarrow 0$, if the PDE is stable and consistent [177]. The linear interpolation scheme in the two-dimensional case results in

$$\begin{aligned} \hat{\phi}(s(t^k)) &= \left(1 - \frac{dx}{\Delta x}\right)\left(1 - \frac{dy}{\Delta y}\right)\phi_{00} + \frac{dx}{\Delta x}\left(1 - \frac{dy}{\Delta y}\right)\phi_{10} \\ &\quad + \left(1 - \frac{dx}{\Delta x}\right)\frac{dy}{\Delta y}\phi_{01} + \frac{dx}{\Delta x}\frac{dy}{\Delta y}\phi_{11} \end{aligned} \quad (11.21)$$

and is illustrated in figure 11.5.

11.7.4 Hybrid methods

The methods discussed can be combined with each other. For example, the Euler-approach can be combined with marker particles evolved in Lagrangian fashion fairly easily. Impressive results have been obtained with a combination of a grid-based solver and marker particles in [101]. The marker particles are used to obtain a high resolution definition of the interface, while the grid is used to define the flow in regions further away from the interface. Additionally, the marker particles can be used to correct the implicit interface definition on the grid. Unfortunately, the marker particles do not help resolving the time-restriction problem posed by the CFL-condition directly. Furthermore, marker particles can not be used when shocks are developed in the solution as this phenomenon is incorrectly resolved by the Lagrangian method.

11.8 Reachable Set Examples

To illustrate the capabilities of reachable set calculations using level set methods, and to investigate which method is the most suitable for aircraft flight envelope determination, several examples are presented. These examples have been selected since they have some connection to the aircraft envelope reachability problem, and since the results for some of the examples are freely available in literature. This allows comparison between the different solution methods as well as verification of their implementation.

11.8.1 Double Integrator

Most mechanical systems can be interpreted as a chain of integrators from the input to the “output” of the system. The double integrator system

$$\dot{x} = f(x, u) = \frac{d}{dt} \begin{bmatrix} x_1 \\ x_2 \end{bmatrix} = \begin{bmatrix} x_2 \\ u \end{bmatrix} \quad (11.22)$$

can be interpreted as a very simple mechanical system: a cart on rails, where x_1 represents the cart’s position, x_2 the velocity of the cart, and the input u is the specific acceleration. In this case the target set is created artificially as a region where a measure of total energy in the system is below a certain threshold. This measure is defined as

$$E(x_1, x_2) = \frac{1}{2} (x_1^2 + x_2^2). \quad (11.23)$$

The target set is then defined as the set $\mathcal{T} = \{(x_1, x_2) \in \mathbb{R}^2 \mid E(x_1, x_2) \leq 0.5\}$. The Hamilton-Jacobi PDE for this problem back- and forwards in time is described by

$$\frac{\partial}{\partial t} \phi(x, t) + \min_u \frac{\partial}{\partial x} \phi(x, t) \cdot f(x, u) \quad \text{for } t \in [-t_f, 0] \quad (11.24)$$

and

$$\frac{\partial}{\partial t} \phi(x, t) + \max_u \frac{\partial}{\partial x} \phi(x, t) \cdot f(x, u) \quad \text{for } t \in [-t_f, 0] \quad (11.25)$$

respectively. For this example, symmetric constraints were posed on the control input $u \in [-1.0, +1.0]$. The optimal control input u^* in the HJ PDEs (11.24) and (11.25) depends both on the direction of time, and the sign of the second co-state. For the forwards reachable set the optimal control input is

$$u^* = \begin{cases} u_{\max} & \text{if } p_2 \geq 0 \\ u_{\min} & \text{otherwise.} \end{cases} \quad (11.26)$$

and vice-versa for the backwards reachable set. The resulting forwards and backwards reachable sets for the semi-Lagrangian and Euler approach are shown in

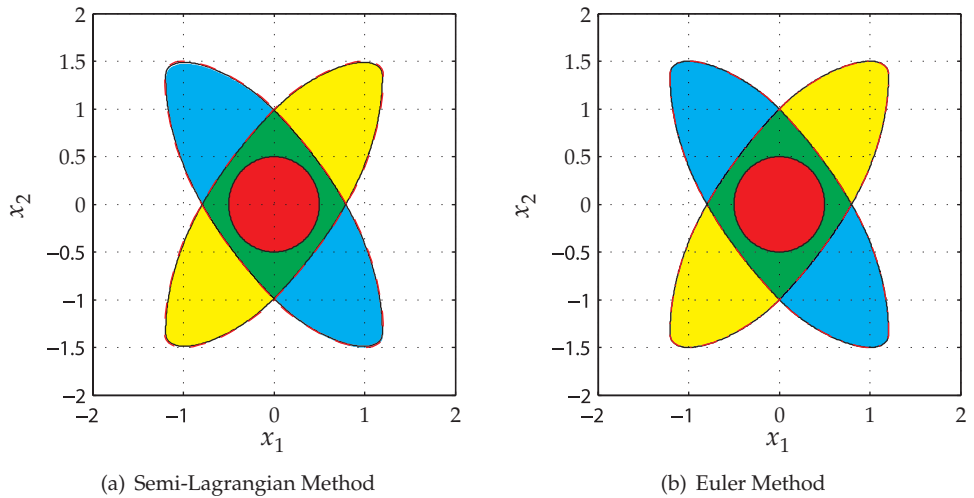


Figure 11.6: Forwards (yellow) and backwards (cyan) reachable sets for the double integrator example system. On the left the results for the Semi-Lagrangian approach are shown, on the right the results for the Euler approach.

figure 11.6. Unfortunately, it is not straightforward to obtain an analytical solution for this problem for the given target set. Therefore, a relatively large number of simulations was performed with the initial state on the boundary of the target set, the convex hull of all intermediate and end-points was taken as the true reachable set. This set is defined by the dash-dotted red contour in figure 11.6.

The adaptive nature of the semi-Lagrangian approach on kd-tree grids is demonstrated in figure 11.7 which shows the nodes at the start and end of the computation. Clearly, the highest level of grid refinement is achieved near the interface, or at values of the value function close to the value describing the set of interest.

11.8.2 Acoustic Capture

The acoustic capture example is included to show the power of the level set method to automatically merge the interface. The reachable set develops a hole in the solution which potentially could also happen in the case of the aircraft flight envelope, for example by limit cycle oscillations. It is very difficult to correctly obtain this reachable set through simulations alone, and the Lagrangian method even requires ad-hoc procedures or may even fail to find the solution altogether.

In the acoustic capture example, the evader is free to travel in any direction, while the pursuer has a limited turn radius. The evader's limited speed is reduced even further if the pursuer gets too close, trying to avoid making too much noise and getting caught. This differential game can be analyzed in two dimensional relative

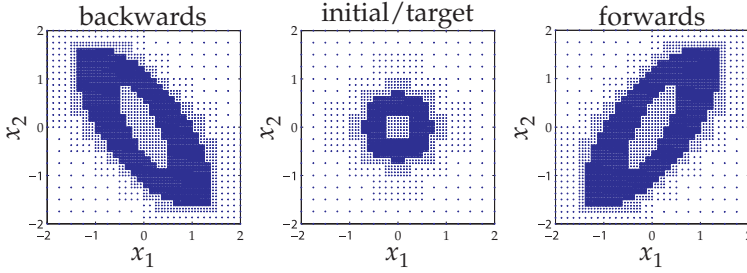


Figure 11.7: Grid nodes of the adaptive kd-tree grid semi-Lagrangian method for a 128^2 effective resolution grid.

Table 11.1: Parameters for the Acoustic Capture Example.

Variable	Explanation	Value
a	velocity vector and input of the evader	$\mathbb{B}^2[0, 1]$
b	angular velocity and input of pursuer	$[-1, 1]$
W_e	speed of evader	1.3
W_p	speed of pursuer	1.0
R	turn radius of pursuer	0.8
S	radius beyond which evader can safely use maximum speed	0.5

coordinates with the pursuer fixed at the origin. The relative dynamics are

$$\begin{aligned} \dot{x} &= \frac{d}{dt} \begin{bmatrix} x_r \\ y_r \end{bmatrix} = f(x, a, b) \\ &= W_p \begin{bmatrix} 0 \\ -1 \end{bmatrix} + \frac{W_p}{R} \begin{bmatrix} y_r \\ -x_r \end{bmatrix} b + 2W_e \min \left(\sqrt{x_r^2 + y_r^2}, S \right) a \end{aligned} \tag{11.27}$$

where the problem specific parameters are defined in table 11.1. The optimal control inputs in this case are defined as

$$\begin{aligned} a &= \frac{p}{\|p\|} \in \mathbb{B}^2(0, 1) \\ b &= -\text{sgn}(p_1 y_r - p_2 x_r) \in [-1, 1]. \end{aligned} \tag{11.28}$$

where $\mathbb{B}^2(0, 1)$ is the Banach-space in \mathbb{R}^2 with the Euclidean norm bounded to 1.

The capture region of the pursuer is defined by the box $\mathcal{T} = [-3.5, 3.5] \times [-0.2, 0] \subset \mathbb{R}^2$. The reachable set is defined only backwards in time, and represents the set of states for which the pursuer is able to capture the evader. The evolution

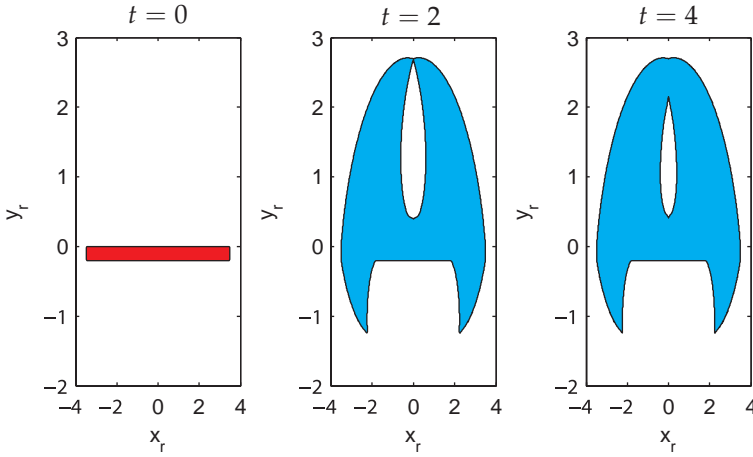


Figure 11.8: Evolution of the capture region for the acoustic capture example using a semi-Lagrangian level-set method.

of the reachable set backwards in time is shown in figure 11.8 and figure 11.9 for the semi-Lagrangian and Euler approach respectively. Unfortunately, determination of the analytic solution for this problem is hard, probably the best non-analytical approach would be creating many simulated trajectories for a large number of input combinations. Comparing the results of the Euler and the semi-Lagrangian method shows that the methods produce results that are very similar. The results produced by the Euler approach are more accurate since second-order time integration was used, in combination with a second-order ENO scheme for the spatial derivative. The semi-Lagrangian approach is only first order accurate in time, and first order accurate spatial derivatives were used.

11.8.3 Aircraft Collision Avoidance

The example section is concluded with an application of reachability analysis for aircraft collision avoidance. This example can also be interpreted as application of the reachability analysis in determining part of the *environmental envelope*. In this case the pursuer airplane wants to create a collision by getting within the minimum separation distance of the evader airplane: the reachable is therefore the set for which the pursuer is able to enter the minimum-separation zone of the evader. In literature, this problem is also referred to as the game of two identical vehicles [114].

The dynamics of this system with the evader fixed at the origin are described by

$$\dot{x} = \frac{d}{dt} \begin{bmatrix} x_r \\ y_r \\ \psi_r \end{bmatrix} = \begin{bmatrix} -v_e + v_p \cos \psi_r + u_e y_r \\ v_p \sin \psi_r - u_e x_r \\ u_p - u_e \end{bmatrix} = f(x, u_e, u_p) \quad (11.29)$$

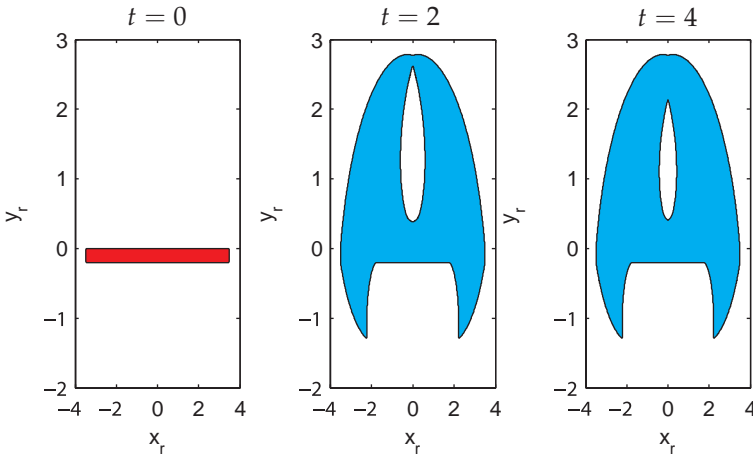


Figure 11.9: Evolution of the capture region for the acoustic capture example using an Euler level-set method.

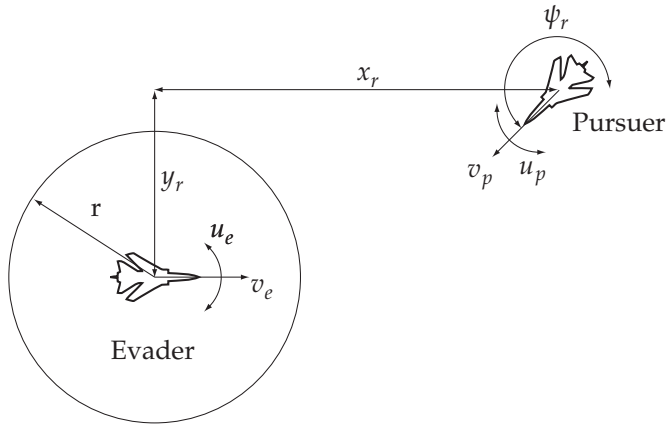


Figure 11.10: Coordinate system for the game of two identical aircraft.

where $x \in \mathbb{R}^2 \times [0, 2\pi[$, v_e the velocity of the evading aircraft, $u_e \in U_e$ is the control input of the evading aircraft, v_p the velocity of the pursuer aircraft, and $u_p \in U_p$ is the input of the pursuing aircraft. The coordinate system is shown in figure 11.10.

Since a collision is allowed to occur at any relative heading, the target set \mathcal{T}_f only depends on the relative coordinates x_r and y_r , and includes any state within a

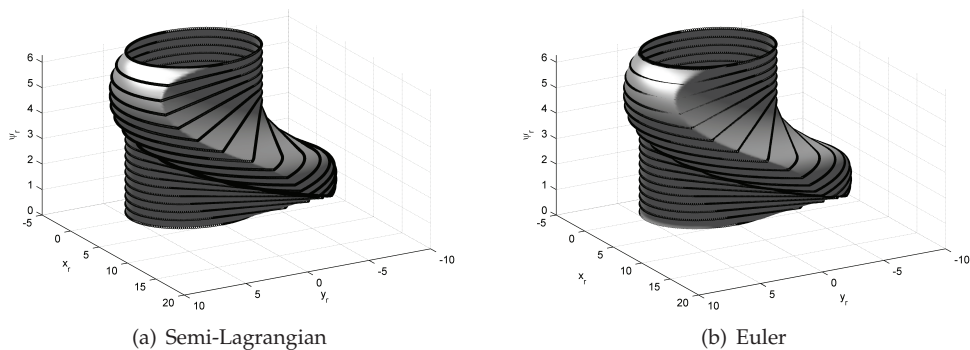


Figure 11.11: Semi-Lagrangian (a) and Euler (b) unsafe-set results for the aircraft collision avoidance example, 128^3 grid resolution.

distance r of the planar origin:

$$\begin{aligned} \mathcal{T}_f &= \left\{ x \in \mathbb{R}^2 \times [0, 2\pi[\mid x_r^2 + y_r^2 \leq r^2 \right\} \\ T(x) &= \sqrt{x_r^2 + y_r^2} - r \end{aligned} \quad (11.30)$$

for the target condition of the backwards reachable set. Analytical results used to verify the resulting reachable set were obtained from [117]. The following parameters were used for this example

$$\begin{aligned} r &= 5 \\ v_p &= v_e = 5 \\ U_e &= U_p = [-1, 1] \end{aligned}$$

The resulting reachable set for the Euler approach on a 128^3 grid is shown in figure 11.11(b) and compared with the analytical solution represented by barrier points on the interface. Only barrier points on the top half of the surface are shown since the solution is symmetric. The resulting reachable set for the semi-Lagrangian approach for an effective resolution of 128^3 is shown in figure 11.11(a). Once again, the Euler approach has better accuracy, due to the higher order integration method and more accurate derivative approximation. The semi-Lagrangian method actually gives an under-approximation of the true reachable set solution in this case.

11.8.4 Computational Load

For the generation of the reachable set of these examples two different level set methods were used. The first is the Level Set Toolbox by Ian Mitchell [115], which implements the Euler approach for uniform grids in MATLAB. The second method

Table 11.2: Computation time for the Euler and semi-Lagrangian level set methods for various examples.

Example	Resolution	Euler	Semi-Lagrangian
Double integrator	128^2	2.3	6.8
	256^2	22.5	18.4
Acoustic capture	128^2	48.7	135
	256^2	373	600
Collision avoidance	64^3	524	552
	128^3	9812	5537

implements a semi-Lagrangian method on adaptive kd-tree grids. The effective resolution for both methods has been selected the same. The first method allows the user to select an accuracy level which determines which kind of derivative approximation method and time integration method is used. Implementing the Euler level set method in a more low-level programming language would probably increase the speed of the method, although the code is vectorized and makes use of the LAPACK libraries.

From table 11.2 it becomes clear that for low dimensional grids the non-adaptive Euler approach gives the best results. Additionally, the Euler method achieves better accuracy for lower, or computation time of the same order. Unfortunately, the computational load increases dramatically when the dimension of problem is increased due to both the CFL condition and the number of grid elements growing exponentially. The adaptive semi-Lagrangian method is slower for low dimensional and low resolution grids due to grid adaptation and has lower accuracy due to the selected time integration and spatial derivative approximation methods. Adaptation of the grid on the other hand has clear benefits when the dimension is increased: the most computational effort is spent on the most interesting regions of the domain. Therefore, the semi-Lagrangian approach is selected as the most promising solution method for application to aircraft flight envelope determination by means of reachable set analysis.

11.9 Conclusions

In this chapter, the level set method for reachability analysis has been introduced, and its relation to the flight envelope problem has been discussed. Different solution methods to solve the level set equation were presented: the Euler, Lagrangian, and semi-Lagrangian approaches. Only the first and last are considered to be applicable to the flight envelope problem, while the Lagrangian method can be used as auxiliary method to improve the resolution of the solution locally.

Three different examples were presented to demonstrate the capabilities of reachable set analysis through the level set approach: a double integrator, acoustic cap-

ture, and an aircraft collision avoidance example. These examples were also used to perform a comparison between the Euler and semi-Lagrangian solution methods. The semi-Lagrangian appears to scale best with increasing grid resolution and dimension, and acceptable accuracy. Therefore, the semi-Lagrangian approach is selected to be used for safe flight envelope determination through reachability analysis. In the next chapter, the semi-Lagrangian method is applied to a nonlinear, longitudinal, high-fidelity F-16 aircraft model.

Several recommendations can be made to improve the speed and accuracy of the semi-Lagrangian method. First of all the efficiency of the code can be improved, and an extension to use multiple cores or even distribution of tasks can be implemented to increase solution speed. The accuracy of the method can be improved by more accurate derivative approximation, and higher-order time integration and interpolation methods. It would be interesting to combine the method with particles, tracking the flow in Lagrangian fashion, to further improve the accuracy as proposed by Losasso, Gibou, and Fedkiw [102].

F-16 LONGITUDINAL ENVELOPE

In this chapter the semi-Lagrangian level set method on adaptive kd-tree grids is applied to a nonlinear model of the longitudinal F-16 dynamics. First of all the model will be introduced and the simplifications made are discussed. After this, the trim-set for the model is derived which serves as the starting point for the level set algorithm. Results obtained for different aircraft configurations at different flight conditions are presented and discussed. Finally, the conclusions drawn from the application and the results are presented and some recommendations for future research are made.

12.1 Aircraft Model and Assumptions

To research whether the reachable set approach can yield promising results for determining the safe flight envelope of modern aircraft, the method is applied to a simplified nonlinear model of the longitudinal F-16 dynamics. The main simplifications made to the model are

Assumption I The dynamics have been made affine in the control and disturbance inputs,

Assumption II Only magnitude constraints on the control and disturbance inputs are taken into account,

Assumption III The altitude and therefore the air density as well as gravitational acceleration are kept constant during the maneuver.

Assumption IV The aircraft has a plane of symmetry, the engine thrust lies in this plane of symmetry.

When the full maneuvering capabilities of an aircraft are considered the reachable set calculations have to be run in at least 9 dimensional space if the altitude is considered to be fixed: three states related to the airspeed and its direction, three rotational rates, and three defining the attitude of the aircraft with respect to Earth. Rate constraints on the control input and actuators can in principal be taken into account by augmenting the system with actuator dynamics. Such an application would be too computationally demanding to run with acceptable resolution on a single desktop computer at the moment of writing however. In this application example only the longitudinal dynamics are considered to reduce the computational load, and additionally simplify the presentation of the maneuver set in figures. Therefore, only four states need to be considered: the total airspeed V_T , the angle of attack α , the pitch rate q_B , and the pitch attitude defined through a quaternion component q_2 . The engine thrust T and horizontal stabilizer deflection δ_h are considered as control inputs. In the results presented in this chapter no disturbance inputs were taken into account, however the extension of the HJ PDE including uncertainty on the aerodynamic parameters, aircraft parameters, and wind as disturbance inputs is straightforward. The HJ PDE with control inputs and aerodynamic uncertainty is presented. By solving this HJ PDE, the worst-case safe maneuvering envelope can be obtained.

The model of the longitudinal dynamics is given by

$$\dot{V}_T = \frac{1}{m} [-D + T \cos \alpha + mg_1] \quad (12.1)$$

$$\dot{\alpha} = q_B + \frac{1}{mV_T} [-L - T \sin \alpha + mg_3] \quad (12.2)$$

$$\dot{q}_2 = \frac{1}{2} q_B q_0 \quad (12.3)$$

$$\dot{q}_B = \frac{M}{I_{yy}} \quad (12.4)$$

where the lift, drag forces and pitch moment are described by

$$D = \frac{1}{2} \rho V_T^2 S [-C_{X_T} \cos(\alpha) - C_{Z_T} \sin(\alpha)]$$

$$L = \frac{1}{2} \rho V_T^2 S [C_{X_T} \sin(\alpha) - C_{Z_T} \cos(\alpha)]$$

$$M = \frac{1}{2} \rho V_T^2 S [C_{m_T} + C_{Z_T} (x_{cg} - x_{cgr})].$$

The force and moment coefficients in the body-axes are specified in [126]. The gravity components g_1 and g_3 are defined by

$$g_1 = [-2q_0 q_2 \cos \alpha + (q_0^2 - q_2^2) \sin \alpha] g_0$$

$$g_3 = [2q_0 q_2 \sin \alpha + (q_0^2 - q_2^2) \cos \alpha] g_0,$$

and the quaternion component q_0 is derived from the constraint $q_0^2 + q_2^2 = 1$ as $q_0 = \sqrt{1 - q_2^2}$. A more detailed overview of the aerodynamic model and all the individual lookup tables can be found in [126]. The horizontal stabilizer deflection is constrained to ± 25 degrees in the nominal case, and the engine thrust is constrained between 0 and 75000 Newton. The leading edge flap also available in the model has not been used during any of the simulations.

12.2 Trim Set

The trim set is used as the initial *safe* set for the level set algorithm. Therefore, definition of this trim set is extremely important in order to obtain the correct safe flight envelope: an unsafe state that is part of the initial set will destroy all claims made about the safety of the resulting flight envelope. The trim-set can be found through various methods: analytically, by means of numerical optimization, interval-analysis [189], and bifurcation and continuation methods [3, 62].

As discussed in the previous chapter, both the Euler- and semi-Lagrangian approaches require that at least one cell of the grid is part of the initial or target set in order to be able to propagate the interface in time. If this is not the case, the methods can evolve the implicit surface yet the reachable set will be empty as there is no meaningful iso-contour to define the set. The aircraft trim set is a very thin hypersurface if a requirement on the trim condition is that the aircraft is non-rotating and the flight path angles are constant. This is illustrated in figure 12.1(a) which shows the trim-curve for symmetric, non-climbing flight at different altitudes and c.g. positions. Alternatively one can perform the trim for non-zero rotational rates and a wide range of flight path angles. This would yield a much larger set of trimmable states for which an implicit surface description has to be made, and most of the considered flight conditions would not generally be considered as *normal* flight conditions. Another alternative is assuming that all states within a certain weighted distance of the trim-curve belong to the trimmable-set. This approach immediately yields an implicit surface description of the trimmable set, and the distance can be chosen such that all states within the resulting trimmable-set are actually (quasi-)trimmed states. This can be verified by comparing the results from the last approach with the full trim approach. Figure 12.1(b) shows the results of including states within a certain distance of the trim-curve as part of the trimmable-set.

12.3 Level Set Problem and Solver Settings

The reachability problem has four dimensions. In this section the HJ PDE will be derived which has to be solved to obtain the forwards and backwards reachable sets, and hence the safe flight envelope. Due to the first assumption, the total

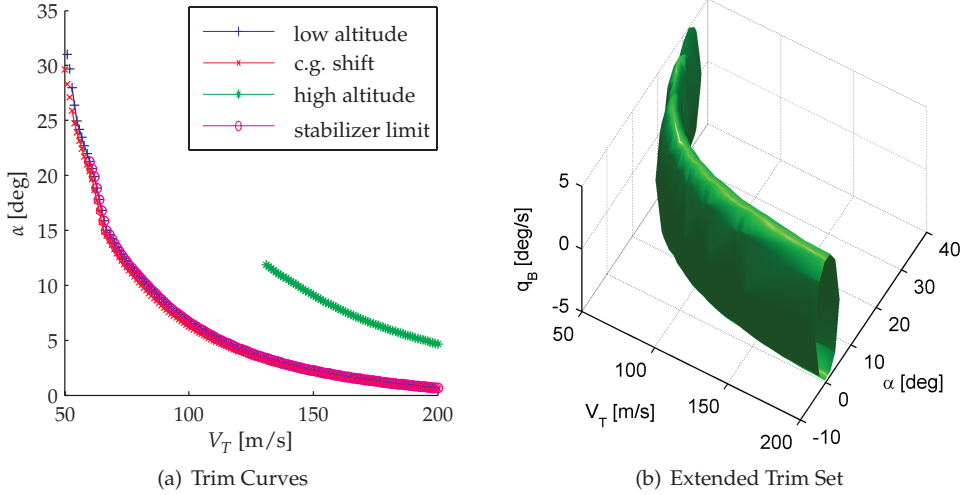


Figure 12.1: Longitudinal, symmetric, level, trim curve at different altitudes and c.g. positions (a). Slices of the extended trim set for the F-16 aircraft at low altitude flight in (b).

aerodynamic forces and moment coefficients can be written as

$$\begin{aligned} C_{X_T} &= C_{X_0} + C_{X_{\delta_h}} \delta_h + C_{X_\Delta} \Delta, \\ C_{Z_T} &= C_{Z_0} + C_{Z_{\delta_h}} \delta_h + C_{Z_\Delta} \Delta, \\ C_{m_T} &= C_{m_0} + C_{m_{\delta_h}} \delta_h + C_{m_\Delta} \Delta. \end{aligned}$$

where Δ is the disturbance signal. Inserting these coefficients into the equations of motion then results, and then considering the forwards reachable set results in the following HJ PDE

$$\begin{aligned} 0 &= \frac{\partial V}{\partial t} + \max_u \min_{\Delta} \frac{\partial V^T}{\partial x} f(x, u, \Delta) \\ &= \frac{\partial V}{\partial t} + \frac{\partial V}{\partial V_T} \left(g_1 + \frac{\bar{q}S}{m} (C_{X_0} \cos \alpha + C_{Z_0} \sin \alpha) \right) + \frac{\partial V}{\partial q_2} \frac{1}{2} q_B q_0 \\ &\quad + \frac{\partial V}{\partial \alpha} \left(q_B + \frac{1}{m V_T} (m g_3 - \bar{q}S (C_{X_0} \sin \alpha - C_{Z_0} \cos \alpha)) \right) \\ &\quad + \frac{\partial V}{\partial q_B} \bar{q}S \bar{c} C_{m_0} + \max_{\delta_h} \left(\frac{\partial V}{\partial V_T} \frac{\bar{q}S}{m} (C_{X_{\delta_h}} \cos \alpha + C_{Z_{\delta_h}} \sin \alpha) \right. \\ &\quad \left. - \frac{\partial V}{\partial \alpha} \frac{\bar{q}S}{m V_T} (C_{X_{\delta_h}} \sin \alpha - C_{Z_{\delta_h}} \cos \alpha) + \frac{\partial V}{\partial q_B} \bar{q}S \bar{c} C_{m_{\delta_h}} \right) \delta_h \end{aligned} \quad (12.5)$$

Table 12.1: Solver settings for the reachable set calculations.

Parameter	Setting
min. level	0
max. level	6
domain	$[50, 200] \times [-20, 50] \times [-60, 60] \times [-1, 1]$
final time	1.0 second
dt	0.01 second
scale factor	45

$$\begin{aligned}
& + \max_T \left(\frac{\partial V}{\partial V_T} \frac{1}{m} \cos \alpha - \frac{\partial V}{\partial \alpha} \frac{1}{m V_T} \sin \alpha \right) T \\
& + \min_{\Delta} \left(\frac{\partial V}{\partial V_T} \frac{\bar{q} S}{m} \left(C_{X_{\Delta}} \cos \alpha + C_{Z_{\Delta}} \sin \alpha \right) \right. \\
& \left. - \frac{\partial V}{\partial \alpha} \frac{\bar{q} S}{m V_T} \left(C_{X_{\Delta}} \sin \alpha - C_{Z_{\Delta}} \cos \alpha \right) + \frac{\partial V}{\partial q_B} \bar{q} S \bar{c} C_{m_{\Delta}} \right) \Delta.
\end{aligned}$$

The optimal input values for δ_h , T and Δ for each grid node can be derived by simply evaluating the parts of the HJ PDE where they appear. Using these optimal input values at each grid node, the flow field over the whole domain can be calculated, and the value function can be propagated using the semi-Lagrangian level set method.

12.4 Nominal Aircraft Results

In this section the results of applying the semi-Lagrangian level set method to the aircraft model described above are presented. The calculations were performed by an implementation of the semi-Lagrangian level set method in C++ on a desktop computer. More details about the implementation can be found in appendix C. The settings for the solver are given in table 12.1 below.

The safe flight envelope computations are performed with four different model settings. An overview of the considered scenarios is given in table 12.2. First the nominal aircraft is investigated at an altitude of 0m. To compare the maneuverability of the aircraft at different altitudes, the envelope is also determined at a flight level used for cruise, 10000m. The influence of the center of gravity position on the aircraft's flight envelope is investigated by shifting it backwards compared with the nominal low altitude simulations. This causes the aircraft to have a smaller stability margin. Finally, the effect of damage to the horizontal stabilizer actuators is investigated by reducing the deflection limits of the stabilizer.

The following legend is used in the figures: the trim set is shown in red, the forwards reachable set in yellow, the backwards reachable set in blue, and the intersection or the safe flight envelope in green.

Table 12.2: Simulation Scenarios.

scenario	description	altitude	stabilizer limits	c.g. position
I	nominal, low	0	$[-25, 25]$	$0.30\bar{c}$
II	nominal, high	10000	$[-25, 25]$	$0.30\bar{c}$
III	cg	0	$[-25, 25]$	$0.36\bar{c}$
IV	stabilizer	0	$[-5, 5]$	$0.3\bar{c}$

12.4.1 Low Altitude Maneuverability

First of all the maneuverability of the F-16 aircraft at low altitude is investigated by comparison of the safe envelope at three flight conditions with different airspeed. Figures 12.2(a), 12.2(b), and 12.3(a) show the reachable sets and safe envelope at airspeed of 60, 100 and 150 m/s respectively, at a c.g. location of $0.30\bar{c}$ and nominally constrained horizontal stabilizer. Clearly, with increasing dynamic pressure due to increasing velocity, the aircraft becomes more maneuverable as can be observed from the increased size of the safe maneuver set. Furthermore, the expected relations between the angle of attack and the pitch attitude, the angle of attack and pitch rate, and the pitch attitude and pitch rate can all be observed from the plots. Especially for the airspeed of 100 m/s a clear difference between the forwards and backwards reachable sets exists; states can be reached within one second that cannot be returned to the set of assumed safe sets within one second. It is expected that at least part of these states are within the safe maneuver envelope evaluated for a longer time period.

12.4.2 High Altitude Results Altitude Comparison

There exists a large difference between the trim curves of the aircraft at low and high altitude as can be observed from figure 12.1(a). The lookup tables of the used F-16 model do not depend on Mach number. Therefore, the difference between the maneuver set of the aircraft at different altitudes for the same airspeed is explained by the difference in air density, and hence dynamic pressure. This difference can be observed by comparing Fig. 12.3(a) and Fig. 12.3(b). The dynamic pressure resulting from flying at 10000m and 150 m/s is about 75% of the dynamic pressure for flying at 0m and 100 m/s. The same ratio can be observed in the size of the maneuver sets shown in figure 12.2(b) and figure 12.3(b).

12.5 Center of Gravity Shift Comparison

The center of gravity location has considerable influence on the maneuverability of an aircraft. Normally when the center of gravity is moved backwards, the static stability margin of the aircraft is reduced, and maneuverability is increased. The safe maneuvering envelope of the aircraft with the center of gravity shifted aft

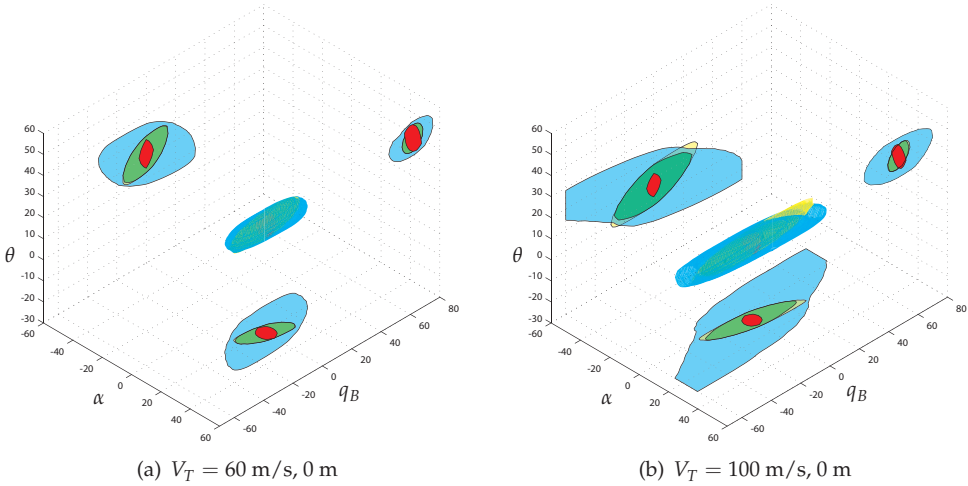


Figure 12.2: Initial, forwards, backwards, and safe maneuver set for the F-16 aircraft at $V_T = 60 \text{ m/s}$ (a) and $V_T = 100 \text{ m/s}$ (b) at 0m altitude.

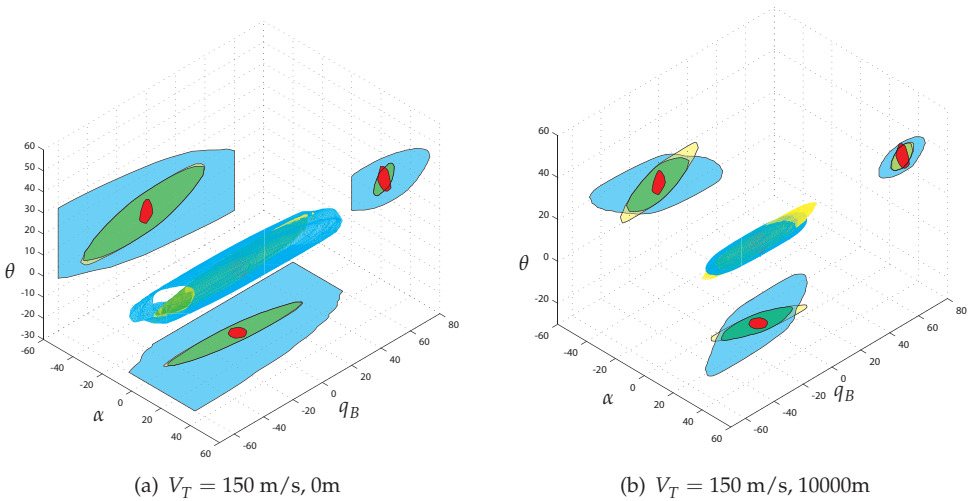


Figure 12.3: Initial, forwards, backwards, and safe maneuver set for the F-16 aircraft at $V_T = 150 \text{ m/s}$ at 0m and 10000m altitude.

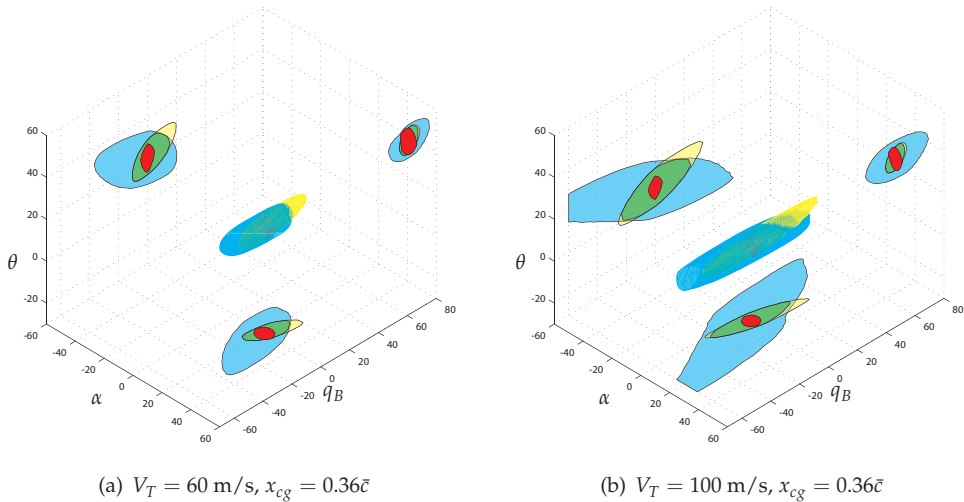


Figure 12.4: Initial, forwards, backwards, and safe maneuver set for the F-16 aircraft at $V_T = 60 \text{ m/s}$, and $V_T = 100 \text{ m/s}$ for $x_{cg} = 0.36\bar{c}$.

by 6% of the chord at an altitude of 0m is shown in figures 12.4(a), 12.4(b), and 12.5(a) for airspeeds of 60, 100, and 150 m/s respectively. At all airspeeds the safe maneuvering set is quite comparable in size with the results obtained at the nominal center of gravity location. However, it seems that the forwards reachable set has become larger while the backwards reachable set has become smaller; it has become easier to maneuver away from the safe set but harder to return to it.

12.6 Constrained Actuator Comparison

Unfortunately there is no aerodynamic failure model for the F-16 aircraft available and therefore no simulations could be performed to investigate the influence of realistic aerodynamic changes in the dynamics on the safe maneuvering envelope. Instead, an actuator failure is considered to simulate an aircraft with reduced safe maneuvering envelope. The trim curve does not change much due to this failure, only part of the curve is cut off as seen in Fig. 12.1(a). The safe maneuvering envelope of the aircraft with reduced horizontal stabilizer deflection capability for three different airspeeds of 60, 100, and 150 m/s at an altitude of 0m is shown in figures 12.5(b), 12.6(a), and 12.6(b) respectively. At low airspeed there is little left of the maneuvering capability of the aircraft. When the airspeed is increased, the safe maneuvering envelope grows slightly. This illustrates that aircraft with failures can have severely reduced maneuvering capability. Hence, in order to guarantee safety, knowledge of the post-failure maneuvering envelope is extremely important

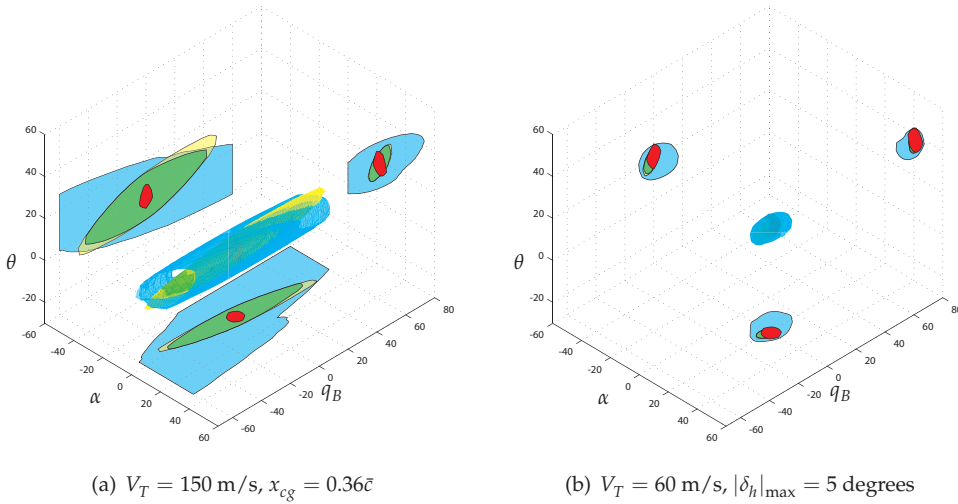


Figure 12.5: Initial, forwards, backwards, and safe maneuver set for the F-16 aircraft at $V_T = 150 \text{ m/s}$, $x_{cg} = 0.36\bar{c}$, at $V_T = 60 \text{ m/s}$ with constrained horizontal stabilizer to $|\delta_h|_{\max} = 5 \text{ degrees}$.

to prevent loss-of-control incidents and accidents.

12.7 Conclusions

In this chapter the safe longitudinal envelope for a high-fidelity, nonlinear, F-16 aircraft model has been derived using the semi-Lagrangian level set method introduced in the previous chapter, demonstrating the capabilities of the reachable set approach for safe envelope determination. From the results, several conclusions can be drawn.

- The semi-Lagrangian approach is able to solve the level set equations to obtain the safe flight envelope for a high-fidelity aircraft model. Hence, the approach can potentially be an aid in the design and (flight) testing phases of aircraft development.
- The shape of the forwards and backwards reachable sets matches with what is expected from flight dynamics. At higher altitude the aircraft becomes less maneuverable for the same airspeed. When the center of gravity is shifted in longitudinal direction, the aircraft becomes more unstable, resulting in larger maneuverability, but at the cost of greater difficulty to get the aircraft back to a trim condition.

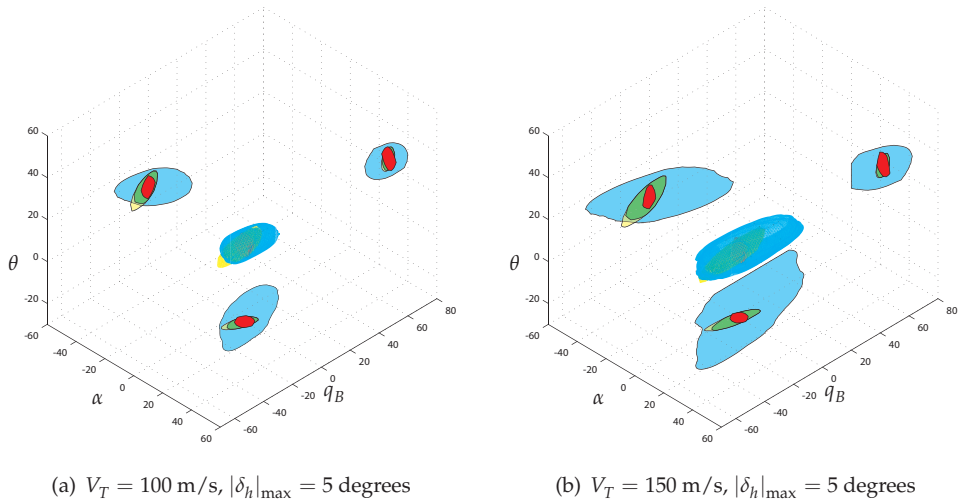


Figure 12.6: Initial, forwards, backwards, and safe maneuver set for the F-16 aircraft at $V_T = 100 \text{ m/s}$ and $V_T = 150 \text{ m/s}$, $|\delta_h|_{\max} = 5 \text{ deg}$.

- In the case of a loss in hydraulic pressure, resulting in more stringent constrained horizontal stabilizer deflections, the maneuvering capabilities of the aircraft severely degrade at low airspeeds. At higher airspeeds there is more maneuvering capability left, and this information could be extremely beneficial for a safe approach and landing. If the post-failure flight envelope would have been available in the El-Al Flight 1862 discussed in chapter 10, a crash might have been prevented.
- The method is not yet feasible for on-line applications due to the computational power required. Instead of calculating the envelope on-line using an estimated model, a database of flight envelopes for different failure cases and aircraft configurations can be carried on-board as proposed by [181]. Then, using fault detection and isolation schemes, an appropriate safe flight envelope can be selected from the database.

The research yielded several ideas for future investigation. Especially for general aviation and commercial aircraft, it would be interesting to investigate whether the full envelope determination problem can be split into fast, and slow dynamics by means of time-scale separation arguments. This would simplify the dynamic envelope problem into five and four dimensional subproblems which are far more computationally tractable than the original problem, and might even be solved on current hardware within reasonable amounts of time. Another problem requiring attention is the determination of the initial safe set. An alternative solution is

to start with very small grid resolution, and evolve the level set backwards and forwards over a small amount of time. Then, the resulting safe flight envelope can be used to initiate the calculations on a larger and coarser resolution domain.

BIBLIOGRAPHY

- [1] M. J. Abzug and E. E. Larrabee. *Airplane Stability and Control - A History of the Technologies That Made Aviation Possible*. Ed. by M. J. Rycroft. Cambridge University Press, 1997.
- [2] H. Alwi, C. Edwards, O. Stroosma, and J. A. Mulder. "Fault Tolerant Sliding Mode Control Design with Piloted Simulator Evaluation". In: *Journal of Guidance, Control, and Dynamics* 31.5 (2008), pp. 1186–1201.
- [3] N. Ananthkrishnan and N. K. Sinha. "Level Flight Trim and Stability Analysis Using Extended Bifurcation and Continuation Procedure". In: *Journal of Guidance, Control, and Dynamics* 24.6 (2001), pp. 1225–1228.
- [8] D. L. Balough. "Determination of X-36 Stability Margins Using Real-Time Frequency Response Techniques". In: *Proceedings of the AIAA Atmospheric Flight Mechanics Conference and Exhibit*. AIAA 1998-4154. Boston, MA, USA, 1998.
- [10] A. M. Bayen, I. M. Mitchell, M. M. K. Oishi, and C. J. Tomlin. "Aircraft Autolander Safety Analysis Through Optimal Control-Based Reach Set Computation". In: *Journal of Guidance, Control, and Dynamics* 30.1 (2007), pp. 68–77.
- [11] R. E. Bellman. *Dynamic Programming*. Princeton, NJ: Princeton University Press, 1957.
- [15] Boeing Company. *Statistical Summary of Commercial Jet Airplane Accidents: Worldwide Operations since 1959*. Tech. rep. Boeing Commercial Airplanes, 2009.
- [24] J. V. Carroll and R. K. Mehra. "Bifurcation analysis of nonlinear aircraft dynamics". In: *Journal of Guidance, Control, and Dynamics* 5.5 (1982), pp. 529–536.
- [27] R. Courant, K. Friedrichs, and H. Lewy. "Über die partiellen Differenzgleichungen der mathematischen Physik". In: *Mathematische Annalen* 100.1 (1928), pp. 32–74.
- [28] R. Courant, E. Isaacson, and M. Rees. "On the solution of nonlinear hyperbolic differential equations by finite differences". In: *Communications on Pure and Applied Mathematics* 5 (1952), pp. 243–255.

- [29] M. G. Crandall, L. C. Evans, and P. L. Lions. "Some properties of viscosity solutions of Hamilton-Jacobi equations". In: *Transactions of the American Mathematical Society* 282.2 (1984), pp. 487–502.
- [30] M. G. Crandall and P.-L. Lions. "Viscosity solutions of Hamilton-Jacobi equations". In: *Transactions of the American Mathematical Society* 277.1 (1983), pp. 1–42.
- [31] P. A. Cummings. *Continuation Method for Qualitative Analysis of Aircraft Dynamics*. Tech. rep. CR-2004-213035. NASA Langley Research Center, July 2004.
- [39] B. Djeridane and J. Lygeros. "Neural approximation of PDE solutions: An application to reachability computations". In: *Decision and Control, 2006 45th IEEE Conference on*. Dec. 2006, pp. 3034–3039.
- [49] D. Enright, F. Losasso, and R. Fedkiw. "A Fast and Accurate Semi-Lagrangian Particle Level Set Method". In: *Computers & Structures* 83.6-7 (Feb. 2005), pp. 479–490.
- [53] L. C. Evans and P. E. Souganidis. "Differential games and representation formulas for solutions of Hamilton-Jacobi-Isaacs equations". In: *Indiana University Mathematics Journal* 33.5 (1984), pp. 773–797.
- [54] W. Falkena, C. Borst, and J. A. Mulder. "Investigation of Practical Flight Envelope Protection Systems for Small Aircraft". In: *Proceedings of the AIAA Guidance, Navigation, and Control Conference*. 2010-7701. AIAA. Toronto, Ontario, Canada, Aug. 2010.
- [62] M. G. Goman and A. V. Khrantsovsky. "Computational framework for investigation of aircraft nonlinear dynamics". In: *Advances in Engineering Software* 39 (2008), pp. 167–177.
- [63] M. G. Goman, G. I. Zagaynov, and A. V. Khrantsovsky. "Application of Bifurcation Theory to Nonlinear Flight Dynamcis Problems". In: *Progress in Aerospace Sciences* 33.9 (1997), pp. 539–586.
- [66] O. Hachicho and B. Tibken. "Estimating Domains of Attraction of a Class of Nonlinear Dynamical Systems with LMI Methods Based on Theory of Moments". In: *Proceedings of the IEEE Conference on Decision and Control*. 2002, pp. 3150–3155.
- [67] T. Hacker and C. Oprisiu. "A Discussion of the Roll-Coupling Problem". In: *Progress in Aerospace Sciences* 15 (1974), pp. 151–180.
- [70] W. H. Herbst. "Dynamics of Air Combat". In: *Journal of Aircraft* 20.7 (1983), pp. 594–598.
- [71] S. E. Hieber and P. Koumoutsakos. "A Lagrangian Particle Level Set Method". In: *Journal of Computational Physics* 210 (2005), pp. 342–367.

- [72] J. F. Horn, A. J. Calise, and J. V. R. Prasad. "Flight Envelope Cueing on a Tilt-Rotor Aircraft Using Neural Network Limit Prediction". In: *Journal of the American Helicopter Society* 46.1 (Jan. 2001), pp. 23–31.
- [73] J. F. Horn, A. J. Calise, and J. V. R. Prasad. "Flight Envelope Limit Detection and Avoidance for Rotorcraft". In: *Journal of the American Helicopter Society* 47.4 (Oct. 2002), pp. 253–262.
- [75] I. Hwang, D. M. Stipanović, and C. J. Tomlin. "Applications of Polytopic Approximations of Reachable Sets to Linear Dynamic Games and a Class of Nonlinear Systems". In: *American Control Conference. Proceedings of the 2003*. Vol. 6. 2003, pp. 4613–4619.
- [77] *In-Flight Separation of Vertical Stabilizer American Airlines Flight 587*. Tech. rep. NTSB/AAR-04/04. National Transportation Safety Board, 2001.
- [81] E. Johnson and S. Kannan. "Adaptive Trajectory Control for Autonomous Helicopters". In: *Journal of Guidance, Control, and Dynamics* 28.3 (2005), pp. 524–538.
- [89] A. B. Kurzhanski and P. Varaiya. "Dynamic Optimization for Reachability Problems". In: *Journal of Optimization Theory and Applications* 108.2 (Feb. 2001), pp. 227–251.
- [90] H. G. Kwatny, J.-E. T. Dongmo, R. C. Allen, B. Chang, and G. Bajpai. "Loss-of-Control: Perspectives on Flight Dynamics and Control of Impaired Aircraft". In: *Proceedings of the AIAA Guidance, Navigation, and Control Conference*. 2010-8005. AIAA. Toronto, Ontario, Canada, Aug. 2010.
- [91] A. A. Lambregts, G. Nesemeier, J. E. Wilborn, and R. L. Newman. "Airplane Upsets: Old Problems, New Issues". In: *AIAA Modeling and Simulation Technologies Conference and Exhibit*. AIAA-2008-6867. Honolulu, Hawaii, Aug. 2008.
- [94] M. D. Lichter, A. J. Bateman, and G. J. Balas. "Flight Test Evaluation of a Run-time Stability Margin Estimation Tool". In: *Proceedings of the AIAA Guidance, Navigation, and Control Conference*. AIAA 2009-6257. Chicago, IL, USA, 2009.
- [95] C. Livadas, J. Lygeros, and N. Lynch. "High-level modeling and analysis of the traffic alert and collision avoidance system (TCAS)". In: *Proceedings of the IEEE* 88.7 (July 2000), pp. 926–948.
- [96] T. J. J. Lombaerts. "Fault Tolerant Flight Control, A Physical Model Approach". PhD thesis. Delft University of Technology, Faculty of Aerospace Engineering, 2010.
- [98] T. J. J. Lombaerts, E. R. van Oort, Q. P. Chu, and J. A. Mulder. "On-line Aerodynamic Model Structure Selection and Parameter Estimation for Fault Tolerant Control". In: *AIAA Guidance, Navigation, and Control Conference*. AIAA-2009-5725. Chicago, Illinois, Aug. 2009.

- [101] F. Losasso, J. O. Talton, N. Kwatra, and R. Fedkiw. "Two-way coupled SPH and Particle Level Set Fluid Simulation". In: *IEEE Transactions on Visualization & Computer Graphics* 14.4 (2008), pp. 797–804.
- [102] F. Losasso, F. Gibou, and R. Fedkiw. "Simulating water and smoke with an octree data structure". In: *SIGGRAPH '04: ACM SIGGRAPH 2004 Papers*. Los Angeles, California: ACM, 2004, pp. 457–462.
- [103] M. Lowenberg. "Bifurcation and Continuation Method". In: ed. by C. Fielding, A. Varga, S. Bennani, and M. Selier. Vol. 283. *Advanced Techniques for Clearance of Flight Control Laws*, Lecture Notes in Control and Information Sciences. Springer-Verlag, 2002. Chap. 6, pp. 89–106.
- [108] J. Lygeros. "On reachability and minimum cost optimal control". In: *Automatica* 40.6 (2004), pp. 917–927.
- [112] A. Melikyan, A. Akhmetzhanov, and N. Hovakimyan. "On Initial Value and Terminal Value Problems for Hamilton-Jacobi Equations". In: *System & Control Letters* 56 (2007), pp. 714–721.
- [114] A. W. Merz. "The game of two identical cars". In: *Journal of Optimization Theory and Applications* 9.5 (1972), pp. 324–343.
- [115] I. M. Mitchell. *A Toolbox of Level Set Methods*. Tech. rep. TR-2007-11. UBC Department of Computer Science, June 2007.
- [116] I. M. Mitchell. "Application of Level Set Methods to Control and Reachability Problems in Continuous and Hybrid Systems". PhD thesis. Stanford University, 2002.
- [117] I. M. Mitchell. *Games of two Identical Vehicles*. Tech. rep. 740. Stanford University Department of Aeronautics and Astronautics, 2001.
- [123] C. H. Murphy. "Symmetric Missile Dynamic Instabilities". In: *Journal of Guidance, Control, and Dynamics* 4.5 (1981), pp. 464–471.
- [125] J. C. Neidhoefer, J. Ryan, K. Al-Ali, A. Ishihara, and N. Kulkarni. "Experimental Validation of Metrics-Driven Enhanced-Safety (ME) Adaptive Control". In: *Proceedings of the AIAA Guidance, Navigation, and Control Conference and Exhibit*. AIAA 2008-6984. 2008.
- [126] L. T. Nguyen, M. E. Ogburn, W. P. Gilbert, et al. *Simulator Study of Stall/Post-stall Characteristics of a Fighter Airplane with Relaxed Longitudinal Static Stability*. Tech. rep. 1538. NASA Langley Research Center, 1979.
- [132] S. Osher and R. Fedkiw. *Level Set Methods and Dynamic Implicit Surfaces*. Springer-Verlag, 2003.
- [134] R. Pandita, A. Chakraborty, P. Seiler, and G. Balas. "Reachability and Region of Attraction Analysis Applied to GTM Dynamic Flight Envelope Assessment". In: *AIAA Guidance, Navigation, and Control Conference*. 2009.

- [135] I. Panella. "Flight Clearance Metrics for Autonomous UAVs". In: *Proceedings of the AIAA Guidance, Navigation, and Control Conference and Exhibit*. AIAA 2005-6412. San Francisco, CA, USA, 2005.
- [136] A. Paranjape, N. K. Sinha, and N. Ananthkrishnan. "Use of Bifurcation and Continuation Methods for Aircraft Trim and Stability Analysis - A state-of-the-art". In: *45th AIAA Aerospace Sciences Meeting and Exhibit, 8-11 January 2007, Reno, Nevada*. AIAA 2007-1051. AIAA, 2007.
- [139] W. H. Phillips. *Effect of steady rolling on longitudinal and directional stability*. Tech. rep. TN 1627. NACA, 1948.
- [144] J. A. Primbs, V. Nevistić, and J. C. Doyle. "Nonlinear Optimal Control: A Control Lyapunov Function and Receding Horizon Perspective". In: *Asian Journal of Control* 1.1 (Mar. 1999), pp. 14–24.
- [145] H. Ranter. *Airliner Accident Statistics 2006*. Tech. rep. Aviation Safety Network, 2007.
- [146] S. Rigal. *Guidage d'un Véhicule Sous Marin de Type Glider par des M'ethodes de Viabilité*. Tech. rep. Nantes, France: Ecole Centrale de Nantes, 2001.
- [147] G. J. J. Ruijgrok. *Elements of Airplane Performance*. Delft University Press, 1996.
- [152] J. Shin. *Analysis of Linear Parameter Varying System Model Based on Reachable Sets*. Tech. rep. CR-2001-211231. NASA Langley Research Center, Oct. 2001.
- [157] N. K. Sinha. "Application of Bifurcation Methods to Nonlinear Aircraft Dynamics". In: *Journal of the Aeronautical Society of India* 53.4 (2001), pp. 253–270.
- [161] M. H. Smaili and J. A. Mulder. "Flight data reconstruction and simulation of El Al Flight 1862". In: *AIAA Modeling and Simulation Technologies Conference and Exhibit*. AIAA-2000-4586. Washington, DC, 2000.
- [162] L. Smith. *Falcon Flight Model Evolution*. Tech. rep. SimHQ, 2004.
- [177] J. Strain. "Semi-Lagrangian Methods for Level Set Equations". In: *Journal of Computational Physics* 151 (1999), pp. 498–533.
- [178] O. Stroosma, M. H. Smaili, T. J. J. Lombaerts, and J. A. Mulder. "Piloted Simulator Evaluation of New Fault-Tolerant Flight Control Algorithms for Reconstructed Accident Scenarios". In: *AIAA Modeling and Simulation Technologies Conference and Exhibit, Honolulu, Hawaii, Aug 18 - 21*. AIAA 2008-6534. 2008.
- [180] W. Tan. "Nonlinear Control Analysis and Synthesis using Sum-of-Squares Programming". PhD thesis. Berkeley, California, USA: University of California, 2006.
- [181] L. Tang, M. Roemer, J. Ge, et al. "Methodologies for Adaptive Flight Envelope Estimation and Protection". In: *AIAA Guidance, Navigation, and Control Conference*. AIAA 2009-6260. Chicago, IL, 2009.

- [182] R. Teo, J. S. Jang, and C. J. Tomlin. "Flight Demonstration of Provably Safe Closely Spaced Parallel Approaches". In: *Proceedings of the AIAA Guidance, Navigation, and Control Conference and Exhibit*. 2005-6197. AIAA. San Francisco, California, USA, Aug. 2005.
- [183] R. Teo and C. J. Tomlin. "Computing Danger Zones for Provably Safe Closely Spaced Parallel Approaches". In: *Journal of Guidance, Control, and Dynamics* 26.3 (2003), pp. 434–442.
- [185] B. Tibken and Y. Fan. "Computing the Domain of Attraction for Polynomial Systems via BMI Optimization Methods". In: *Proceedings of the American Control Conference*. 2006, pp. 117–122.
- [188] U. Topcu, A. Packard, and P. Seiler. "Local Stability Analysis using Simulations and Sum-of-Squares Programming". In: *Automatica* 44.10 (2008), pp. 2669–2675.
- [189] E. van Kampen, Q. P. Chu, J. A. Mulder, and M. H. van Emden. "Nonlinear Aircraft Trim using Interval Analysis". In: *Proceedings of the AIAA Guidance, Navigation and Control Conference and Exhibit*. Hilton Head, South Carolina, USA, 2007.
- [200] K. H. Well. "Aircraft Control Laws for Envelope Protection". In: *Proceedings of the AIAA Guidance, Navigation, and Control Conference and Exhibit*. 2006-6055. AIAA. Keystone, Colorado, USA, Aug. 2006.
- [202] J. E. Wilborn and J. V. Foster. "Defining Commercial Aircraft Loss-of-Control: A Quantative Approach". In: *Proceedings of the AIAA Atmospheric Flight Mechanics Conference and Exhibit*. 2004-4811. AIAA. Providence, Rhode Island, USA, Aug. 2004.
- [205] I. Yavrucuk, J. V. R. Prasad, and S. Unnikrishnan. "Envelope Protection for Autonomous Unmanned Aerial Vehicles". In: *Jorunal of Guidance, Control, and Dynamics* 32 (2009), pp. 248–261.
- [209] G. I. Zagaynov and M. G. Goman. "Bifurcation analysis of critical aircraft flight regimes". In: *Proceedings of the 14th congress of ICAS*. 84-4.2.1. Toulouse, France, 1984.

PART

IV

**CONCLUSIONS AND
RECOMMENDATIONS**

CONCLUSIONS AND RECOMMENDATIONS

This dissertation describes the development of an adaptive flight control approach for modern fighter aircraft, and the determination of the safe flight envelope for such high performance aircraft. In this chapter the main conclusions of this research are summarized. Based on these conclusions and other observations made during the research, new research objectives and questions can be formulated in the form of recommendations for future research.

13.1 Conclusions

The conclusions are directly linked to the research goals postulated in the introduction. These research goals are summarized here:

- *Damaged Aircraft Control* A control scheme has to be developed which achieves the desired performance characteristics over the whole flight envelope of the aircraft. Additionally, in the presence of faults and failures in the system, the control law has provable stability and state boundedness characteristics. Combined with on-line model identification the control design clearly enhances performance and survivability in post-failure flight conditions.
- *Control Allocation* Modern aircraft have many different control effectors. While this property allows on-line reconfiguration as it provides redundancy, it poses an additional problem in the control design since the desired control effect has to be distributed over the available control effectors. This distribution is performed optimally with respect to a cost criterion and takes the individual

control effector characteristics into account. Stability of the control law with control allocation can be shown.

- *Damaged Aircraft Identification* Aircraft failures or damage influence the dynamics of the system, which need to be identified on-line to allow active reconfiguration of the control design and restore control performance. Severe failures cause changes in the required model structure, and additionally, asymmetric damage contributes to the complexity of the required model structure. When the model structure and estimated parameters match the underlying physics of the system, the estimated model can be used for fault diagnosis and derivation of the safe flight envelope post-failure. Therefore, development of on-line model structure selection methods is required and the estimated model has to be stored efficiently onboard.
- *Flight Envelope Determination* Especially for highly maneuverable aircraft and aircraft with faults and failures the aircraft dynamics pose important constraints on the safe maneuvering space. In post-failure flight conditions knowledge of the safe envelope can be the difference between an inevitable accident or safe (crash) landing. Thus, a method has to be developed which calculates the safe envelope, based on a available model of the aircraft, and takes input constraints and disturbances into account.

13.1.1 Damaged Aircraft Control

The research on adaptive control described in this dissertation is focused on a physical modeling approach where knowledge of flight dynamics is used in the design of indirect adaptive backstepping flight control designs for different aircraft models. Starting from the adaptive backstepping framework, the approach was extended with control allocation, and full envelope model estimation and model structure selection.

Adaptive backstepping is a recursive, Lyapunov-based, nonlinear design method which makes use of parameter update laws to deal with parametric uncertainties in the system. The main idea of backstepping is to design the control law recursively by considering some of the state variables as “virtual control inputs”, and designing stabilizing functions for these. With the inclusion of command filters, the backstepping design is applicable to non-triangular systems and the whole design is simplified considerably as the need for analytic derivatives of the “virtual control inputs” is removed.

Different parameter update laws can be designed, resulting in the integrated, modular, and composite update law designs. The integrated design employs a Lyapunov based update law, while the modular update law allows the use of a recursive least squares identifier. However, nonlinear damping terms are required in the control law to achieve the modularity between the controller and identifier. The composite update law combines the integrated and modular designs, and has the best parameter convergence properties of all three designs.

In chapter 6 three nonlinear adaptive control designs for a simple, over-actuated fighter aircraft model with unknown aerodynamic parameters have been studied. Two of these adaptive designs use an integrated Lyapunov based update law, while the other design is modular and uses a least-squares update law. The control designs were combined with two control allocation methods to distribute the desired control effort over the available control surfaces. A comparison based on numerical simulations of the resulting control design and control allocation combinations for different control surface failures has been made.

The main observation that can be made from the simulation results is that all three adaptive flight control designs provide a significant improvement over a non-adaptive model based design in the presence of actuator failures. With the pseudo-inverse control allocation the reconfiguration success rate and performance of the adaptive control designs is very similar. However, in combination with more sophisticated control allocation methods the reconfiguration success rate and performance of the modular adaptive design is superior to the integrated designs. This can be mainly explained by the better parameter estimates obtained by the least squares identifier.

In some simulation cases, the adaptive control designs managed to stabilize the aircraft and were able to track part of the desired trajectories. Following the complete desired maneuver was too challenging for the degraded aircraft. Therefore an adaptive controller alone is not sufficient to improve safety in post-failure flight conditions: both the pilot and guidance system have to be made aware of the failure characteristics and post-failure flight envelope. The problem of determining the aircraft's capabilities, or safe maneuvering envelope, is addressed in part III of this dissertation.

Tuning of the integrated adaptive control designs turned out to be quite time consuming, even for this relatively simple aircraft model. Increasing the adaptation gain will result in faster parameter convergence, but on the other hand it can lead to undesirable transients in the closed-loop response. The modular design requires inclusion of nonlinear damping terms to guarantee boundedness of the closed-loop response. These nonlinear damping terms can result in high-gain control, and possibly undesirable numerical effects.

13.1.2 Control Allocation

In chapter 7 three adaptive control designs have been proposed for over-actuated systems with uncertain parameters: an integrated, modular and composite design. The control design is split into a high-level control law and a dynamic control allocation update law. The last update law does not solve the control allocation problem directly as was done in chapter 6, but rather converges to the optimal solution continuously. Closed loop boundedness of the system states and desired control effector signals can be proven by means of adaptive optimizing control Lyapunov functions, and locally, asymptotic tracking of the desired reference signal is concluded.

The composite adaptive design has the best convergence properties and does not require nonlinear damping unlike the fully modular design. The tracking performance of the composite control design is excellent in the nominal case as well as for all considered failure cases. After introduction of a failure to the model, the correct model parameters are rapidly estimated. The dynamic order of the resulting controller is equal to that of the modular adaptive design, but considerably higher than for the integrated design due to the presence of the dynamic update gain.

13.1.3 Damaged Aircraft Identification

In chapter 9 many design techniques introduced earlier are brought together to create a controller which is able to achieve excellent tracking performance for nonlinear, over-actuated, aircraft. The controller is designed within the backstepping framework and combines a high level control design with dynamic optimizing control allocation using a composite update law for the unknown parameter. The flight envelope has been divided into small partitions, for each partition a locally valid model is created. Both the structure and model parameter values are identified online based on a orthogonal least squares identification scheme. Global stability of the closed-loop system, and convergence of the estimated parameter can be proven using a single Lyapunov function. The control design is evaluated with numerical simulations.

The proposed control design shows excellent performance for a variety of simulated fault and failure cases ranging from a simple change in the aerodynamic coefficients, to actuator failures and center of gravity shifts. The tracking performance of non-adaptive model based control designs deteriorates significantly for these kinds of failures. When the failure is in the space spanned by the set of available regressor candidates, the correct model structure can be identified, and the correct parameter values are estimated if a persistency of excitation condition is satisfied. Even if the failure cannot be completely characterized by the available set of regressor candidates, tracking performance can be very good as long as the residual error between the estimated model and the true behavior is small.

Splitting the complete flight envelope into smaller partitions allows real-time implementation of the control design, and the identified information can be stored efficiently for later use, when the same part of the envelope is visited again. Tuning of the controller is very straightforward since the update gain of the parameter adaptation is tuned automatically by the least squares filter, and the remaining tuning parameters can be chosen independently.

13.1.4 Flight Envelope Determination

The second part is considered with determination of the safe flight envelope. Statistical data shows that the majority of aircraft accidents in the past decade has been related to excursions of the aircraft beyond its safe flight envelope. Therefore, both knowledge of the safe flight envelope and some form of protection is required to

keep the aircraft within its safe flight envelope. The safe flight envelope is defined as the region in the state space for which safe operation of the aircraft can be guaranteed and externally posed constraints will not be violated. This region in the state space can be defined as the intersection of the dynamical, structural and environmental envelopes.

In chapter 11 the level set method for reachability analysis has been introduced, and its relation to the flight envelope problem has been discussed. The dynamic flight envelope can be obtained by evaluating the forwards and backwards reachable set of a set of known, safe states. Different solution methods to solve the level set equation are presented: the Euler, Lagrangian, and semi-Lagrangian approaches. Only the first and last are considered to be applicable to the flight envelope problem, while the Lagrangian method can be used as auxiliary method to improve the resolution of the solution locally.

Three different examples were presented to demonstrate the capabilities of reachable set analysis through the level set approach: a double integrator, acoustic capture, and an aircraft collision avoidance example. These examples were also used to perform a comparison between the Euler and semi-Lagrangian solution methods. The semi-Lagrangian appears to scale best with increasing grid resolution and dimension, and acceptable accuracy. Therefore, the semi-Lagrangian approach is selected to be used for safe flight envelope determination through reachability analysis.

In chapter 12 the safe longitudinal envelope for a high-fidelity, nonlinear, F-16 aircraft model is derived using the semi-Lagrangian level set method introduced in chapter 11, demonstrating the capabilities of the reachable set approach for safe envelope determination. The semi-Lagrangian approach is able to solve the level set equations to obtain the safe flight envelope for a high-fidelity aircraft model. Hence, the approach can potentially be an aid in the design and (flight) testing phases of aircraft development.

The shape of the forwards and backwards reachable sets matches with what is expected from a flight dynamics analysis. At higher altitude the aircraft becomes less maneuverable for the same true airspeed due to reduction of dynamic pressure. When the center of gravity is shifted in longitudinal direction, the aircraft becomes more unstable, resulting in larger maneuverability, but at the cost of greater difficulty to get the aircraft back to a trim condition. In the case of a loss in hydraulic pressure, resulting in smaller deflection limits of the horizontal stabilizers, the maneuvering capabilities of the aircraft severely degrade at low airspeed. At higher airspeed there is more maneuvering capability left, and this information could be extremely beneficial for a safe approach and landing. If the post-failure flight envelope would have been available in the El-Al Flight 1862 accident introduced in chapter 10, a crash might have been prevented.

13.1.5 Final Conclusions

The conclusions can be summarized for each of the research objectives as

- Adaptive control improves the tracking performance in post-failure flight conditions considerably over non-adaptive designs, while the nominal performance is identical or slightly better. However, the improved performance comes at the cost of a larger computing power requirement due to the increased order of the control design.
- The over-actuation of modern aircraft facilitates on-line reconfiguration. With control allocation methods, the available control effectors can be used optimally with respect to a cost criterion taking individual effector characteristics into account. By incorporation of control allocation into the backstepping framework, closed loop boundedness and stability can be shown through Lyapunov analysis.
- Full envelope model identification is made possible by partitioning the flight envelope into small regions or hyperboxes. Each hyperbox has its own locally valid model for which the model structure and parameters can be identified. The full model is obtained by B-spline interpolation between the local models. Due to the local support of these B-splines, only a limited amount of hyperboxes has to be evaluated and updated for each flight condition.
- The safe flight envelope for a given aircraft can be derived by means of reachability analysis, provided that an accurate model of the vehicle dynamics is available and the magnitude of the control inputs and disturbances is known.

13.2 Recommendations and Future Prospects

New research questions and objectives are formulated based on the research presented in this dissertation.

Adaptive Flight Control

The contributions in adaptive flight control are obtained from numerical flight simulations with pre-programmed maneuvers, no piloted simulations have been performed. The interaction between pilots and adaptive control designs is still an area open for research. Investigating the handling qualities of adaptive flight control designs just after injection of a failure, and after the estimated model has converged would make a very interesting study.

No accurate failure models of realistic structural damage were available for modern fighter aircraft. Therefore, the evaluation of the adaptive flight control designs was limited to simulation scenarios with actuator failures, shifts of the center of gravity, and uncertainties on individual aerodynamic coefficients. It would be very interesting to analyze whether the proposed control designs achieve adequate performance for asymmetric failure modes such as partial wing surface loss. In that case, the set of regressor candidates would have to be extended with additional

coupled longitudinal-lateral and nonlinear terms to be able to correctly identify the new dynamics.

The developed control designs can be enhanced with Fault Detection and Isolation (FDI) modules for actuator failures, performing actuator health monitoring, simplifying the task of on-line model identification and control reconfiguration. This was not done in the present research to make the limited failure scenarios more challenging for the controller, including such a module would be a very logical step when actuator models and more challenging aerodynamic failure cases are available. Similarly, in this research full, perfect, state measurement was assumed while this is not always possible in real applications. Therefore, the extension of the design with state observers has still to be investigated.

Currently, a fixed partitioning of the flight envelope has been used in combination with structure selection for each partition. An interesting extension would be automatic partitioning of the flight envelope, similar to what is proposed by [124]. The automatic partitioning recruiting and shape optimization can then be used together with structure selection to achieve an accurate fit of the aerodynamic model, even in the presence of asymmetric failures. Another possibility would be to replace the tensor B-splines partitioned envelope with local models in each hyperbox by simplex splines to model the aerodynamic coefficients [37].

No adaptive control designs are currently reported to be in operational use. The main reason is that there are no certification guidelines or requirements for adaptive control designs, and therefore these novel designs cannot be applied to commercial aircraft in production yet. Currently, many of the analysis tools used for certification and verification are based on linear system theory. With the emergence of nonlinear control designs, such as for example in the Lockheed-Martin F-35 aircraft, there exists a need for new validation and verification methods which are applicable to nonlinear control designs and nonlinear aircraft models.

Safe Flight Envelope

Several recommendations can be made to improve the speed and accuracy of the semi-Lagrangian method. First of all the efficiency of the code can be improved, and an extension to use multiple cores or even distribution of tasks can be implemented to decrease the required time to calculate the solution. The accuracy of the method can be improved by more accurate derivative approximation, and higher-order time integration and interpolation methods. It would be interesting to combine the method with particles, tracking the flow in Lagrangian fashion by “floating” along streamlines, to further improve the accuracy as proposed by Losasso, Gibou, and Fedkiw [102].

Especially for general aviation and commercial aircraft, it should be investigated whether the full envelope determination problem can be split into fast, and slow dynamics by means of time-scale separation arguments. This would simplify the dynamic envelope problem into five and four dimensional subproblems which are far more computationally tractable than the original problem, and might even

be solved on current hardware within reasonable amounts of time. The information obtained using these calculations might be valuable during the design process to identify problem areas in the flight envelope.

Another problem requiring attention is the determination of the initial safe set. An alternative solution is to start with very small grid resolution, and evolve the level set backwards and forwards over a small amount of time. Next, the resulting safe flight envelope can be used to initiate the calculations on a larger and coarser resolution domain.

It would be extremely interesting to apply the approach to the El-Al Boeing 747 accident and determine whether indeed the aircraft would become uncontrollable below a certain airspeed, and, secondly, determine the optimal flight path to the runway that could still have been flown by the aircraft.

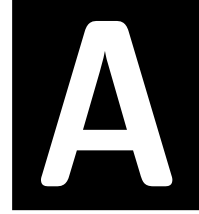
Future Prospects

Most probable first applications of adaptive control techniques are in small and relatively cheap UAV utilized in reconnaissance missions by the military, police and similar organizations. These UAVs are then able to complete their mission while flying over hazardous areas, for example enemy territory, by coping with airframe damage and actuator and sensor failures. When the technology has matured more, it will eventually find its way to manned military aircraft and commercial aircraft, to increase the safety of aviation.

Additionally, adaptive control and on-line system identification techniques have clear benefits in flight testing, reducing both the required time and budget to execute the test program. The adaptive control techniques do not have to be implemented on the final products, but can be used to obtain flight test data in unconventional regimes of the flight envelope, for example flight at high angle of attack.

Further developments should be aimed at increasing the technology readiness level of the designed algorithms. In The Netherlands at least two aircraft exist which can be employed to test the development algorithms during real flights: the Orange Jumper F-16 aircraft from the RNLAF and the Cessna Citation II laboratory aircraft of the NLR and Delft University of Technology. At the current stage, demonstrating of the developed fault tolerant control and identification techniques in a realistic environment is the next logical step in the development process.

APPENDICES



SYSTEM AND STABILITY CONCEPTS

The following comparison functions are useful tools for stability analysis.

Definition A.1. A continuous function $\alpha : [0, a) \rightarrow \mathbb{R}_+$ is said to be of class \mathcal{K} if it is strictly increasing and $\alpha(0) = 0$. It is said to be of class \mathcal{K}_∞ if $a = \infty$ and $\lim_{r \rightarrow \infty} \alpha(r) = \infty$.

Definition A.2. A continuous function $\beta : [0, a) \times \mathbb{R}_+ \rightarrow \mathbb{R}_+$ is said to be of class \mathcal{KL} if for each fixed s the mapping $\beta(s, r)$ is of class \mathcal{K} with respect to r and, for each fixed r , the mapping $\beta(r, s)$ is decreasing with respect to s and $\beta(r, s) \rightarrow 0$ as $s \rightarrow \infty$. It is said to be of class \mathcal{KL}_∞ if, in addition, for each fixed s the mapping $\beta(r, s)$ belongs to class \mathcal{K}_∞ with respect to r .

Lyapunov analysis can be used to show stability of sets through the following claims [158].

Definition A.3. If the system $\dot{x} = f(x)$ is forward complete, then for this system a closed, forward invariant set \mathcal{A} is:

- Uniformly Stable (US) if there exists $\delta(\cdot) \in \mathcal{K}_\infty$ such that for any $\epsilon > 0$,

$$|x_0|_{\mathcal{A}} \leq \delta(\epsilon), t \geq 0 \rightarrow |x(t, x_0)|_{\mathcal{A}} \leq \epsilon. \quad (\text{A.1})$$

- Uniformly Globally Asymptotically Stable (UGAS) if it is US and Uniformly Attractive (UA), that is, for each $\epsilon > 0$ and $r > 0$ there exists $T > 0$ such that

$$|x_0|_{\mathcal{A}} \leq r, t \geq T \rightarrow |x(t, x_0)|_{\mathcal{A}} \leq \epsilon. \quad (\text{A.2})$$

Definition A.4. The system $\dot{x} = f(x, u, t)$ is input-to-state stable (ISS) with respect to a closed, 0-invariant set \mathcal{A} if there exists $\beta \in \mathcal{KL}$ and $\gamma \in \mathcal{K}$ such that for each $u \in \mathcal{L}_\infty^m$ and all initial states x_0 , the solution $x(t, x_0, u)$ is defined for all $t \geq 0$ and satisfies

$$|x(t, x_0, u)|_{\mathcal{A}} \leq \beta(|x_0|_{\mathcal{A}}, t) + \gamma(\|u\|_{[0,t]}) \quad (\text{A.3})$$

for each $t \geq 0$.

Definition A.5. An ISS Lyapunov function with respect to the compact subset $\mathcal{A} \subseteq \mathbb{R}^n$ for system Σ is a smooth function $V : \mathbb{R}^n \rightarrow \mathbb{R}_+$ which satisfies the following conditions:

1. V is proper and positive definite with respect to the set \mathcal{A} , that is, there exist $\alpha_1, \alpha_2 \in \mathcal{K}_\infty$ such that for all $\xi \in \mathbb{R}^n$,

$$\alpha_1(|\xi|_{\mathcal{A}}) \leq V(\xi) \leq \alpha_2(|\xi|_{\mathcal{A}}), \quad (\text{A.4})$$

2. there exist functions $\alpha_3 \in \mathcal{K}_\infty$ and $\sigma \in \mathcal{K}$ such that

$$\nabla V(\xi)f(\xi, v) \leq -\alpha_3(|\xi|_{\mathcal{A}}) + \sigma(|v|) \quad (\text{A.5})$$

for all $\xi \in \mathbb{R}^n$ and for all $v \in \mathbb{R}^m$.

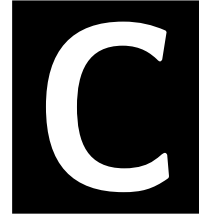
F-18 AERODYNAMIC MODEL DATA

Table B.1: Aircraft model parameters for trim condition I, $h = 30000$ ft and $M = 0.7$

$l_\beta = -11.04$	$l_q = 0$	$l_r = 0.4164$	$l_{\beta\alpha} = -19.72$	$l_{r\alpha} = 4.709$	$l_p = -1.4096$
$z_\alpha = -0.6257$	$y_\beta = -0.1244$	$m_\alpha = -5.432$	$m_{\dot{\alpha}} = -0.1258$	$m_q = -0.3373$	$n_\beta = 2.558$
$n_r = -0.1122$	$n_p = -0.0328$	$n_{p\alpha} = -0.0026$	$n_q = 0$	$l_{\delta_{el}} = 6.3176$	$l_{\delta_{er}} = -6.3176$
$l_{\delta_{al}} = 7.9354$	$l_{\delta_{ar}} = -7.9354$	$l_{\delta_r} = 1.8930$	$i_1 = 0.7966$	$i_2 = 0.9595$	$i_3 = 0.6914$
$m_{\delta_{el}} = -4.5176$	$m_{\delta_{er}} = -4.5176$	$m_{\delta_{al}} = -0.8368$	$m_{\delta_{ar}} = 0.8368$	$m_{\delta_{ief}} = -1.2320$	$m_{\delta_{ief}} = 0.9893$
$m_{\delta_r} = 0$	$g_0 = 9.80665$	$n_{\delta_{el}} = 0.2814$	$n_{\delta_{er}} = -0.2814$	$n_{\delta_{al}} = -0.0698$	$n_{\delta_{ar}} = -0.0698$
$n_{\delta_r} = -1.7422$	$V = 212.14$	$\alpha_0 = 0.0681$	$\theta_0 = 0.0681$		

Table B.2: Aircraft model parameters for trim condition II, $h = 40000$ ft and $M = 0.6$

$l_\beta = -7.0104$	$l_q = 0$	$l_r = 0.3529$	$l_{\beta\alpha} = -16.4015$	$l_{r\alpha} = 1.0461$	$l_p = -0.7331$
$z_\alpha = -0.2876$	$y_\beta = -0.0700$	$m_\alpha = -1.4592$	$m_{\dot{\alpha}} = -0.0177$	$m_q = -0.1286$	$n_\beta = 1.3612$
$n_r = -0.0619$	$n_p = -0.0177$	$n_{p\alpha} = 0.0696$	$n_q = 0$	$l_{\delta_{el}} = 2.7203$	$l_{\delta_{er}} = -2.7203$
$l_{\delta_{al}} = 4.2438$	$l_{\delta_{ar}} = -4.2438$	$l_{\delta_r} = 0.8920$	$i_1 = 0.7966$	$i_2 = 0.9595$	$i_3 = 0.6914$
$m_{\delta_{el}} = -1.9782$	$m_{\delta_{er}} = -1.9782$	$m_{\delta_{al}} = -0.3183$	$m_{\delta_{ar}} = -0.3183$	$m_{\delta_{ief}} = -0.4048$	$m_{\delta_{ief}} = 0.3034$
$m_{\delta_r} = 0$	$g_0 = 9.80665$	$n_{\delta_{el}} = 0.1262$	$n_{\delta_{er}} = -0.1262$	$n_{\delta_{al}} = -0.0963$	$n_{\delta_{ar}} = -0.0963$
$n_{\delta_r} = -0.8018$	$V = 177.09$	$\alpha_0 = 0.1447$	$\theta_0 = 0.1447$		



SEMI-LAGRANGIAN LEVEL SET IMPLEMENTATION

C.1 kd-tree Grids

The interface is the most interesting region of the state space, as it defines the level set of interest. Hence, the computational effort should be concentrated in a band around the interface. This can be achieved by refining the grid closer to the interface by splitting grid cells, and coarsening the grid by merging grid cells further away from the interface. Interpolation methods can be used within the grid cells to advance the level set in semi-Lagrangian fashion.

Every cell vertex has a value, which can be interpreted as the level set value. Hence, when any of a cell's vertices has a value closer to the value of the interface, the cell is split into smaller cells. When all vertices of the parent cell and its children have values larger than twice the maximum allowed value, the children are merged together to the parent cell. In two dimensions, the resulting grid is a quadtree grid [33], see figure C.1(a). In three dimensions the result is an octree grid where each parent has 8 children, see figure C.1(b). This concept generalizes to n -dimensional space, where each parent has 2^n -children.

C.2 Spatial Derivative Approximation

Since the grid is not regular any more, the distances to the left and right neighbors of a node are not necessarily equal. Furthermore, some nodes will have virtual

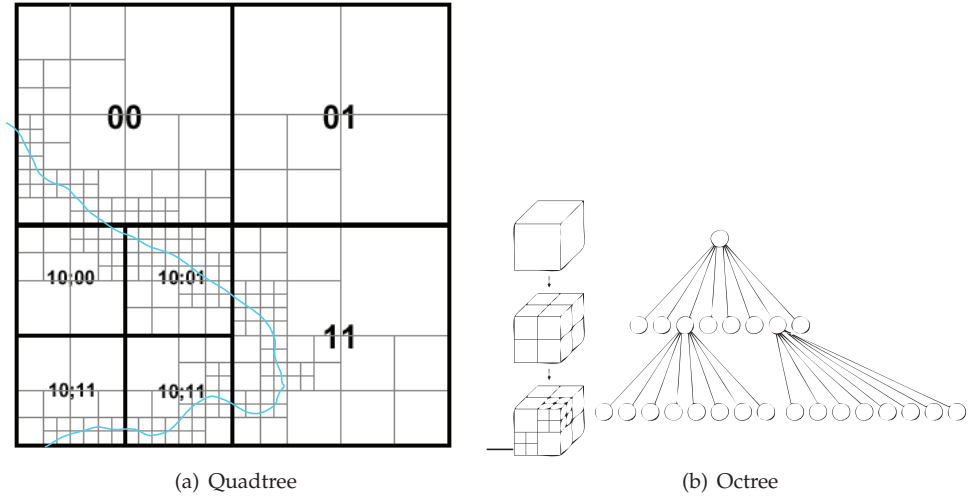


Figure C.1: kd-tree grid representations

neighbors, being virtual nodes on the edges and faces of the grid cells. Hence, the spatial derivative required in the level set equation is obtained by a weighted central difference, to account for the difference in distance to the neighbor nodes. The derivative is approximated by[36]

$$\frac{\partial \varphi}{\partial x} = \frac{h_1^2 \varphi(x_{i+1}) - (h_1^2 - h_2^2) \varphi(x_i) - h_2^2 \varphi(x_{i-1})}{h_1 h_2 (h_1 + h_2)} \quad (\text{C.1})$$

where h_1 defines the distance to the left neighbor x_{i-1} , and h_2 the distance to the right neighbor x_{i+1} . This derivative approximation has first order accuracy in x .

C.3 Adaptive kd-tree CIR-scheme

The CIR-scheme for the semi-Lagrangian level set solution method is defined by the algorithm:

The algorithm has been implemented as a toolbox in the C++ programming language. The implementation keeps track of the grid nodes and grid boxes. Each grid boxes contains references to its parent box, and to its vertex nodes. After each modification of the grid, the new neighbor nodes of the grid nodes are found to speed up the calculation of the approximated spatial derivative.

Using the toolbox, implementation of reachability problems is very straightforward. The user has to supply the dynamics with the optimal inputs based on the co-state, and the initial or target set. After compilation of the code, the calculations can

Algorithm 3: CIR-scheme for semi-Lagrangian level set evolution.

```

begin
  initialize the grid boxes and their nodes with the initial/target condition
   $t = t_0$ 
  repeat
    for each grid node do
      evaluate the spatial derivative  $\frac{\partial \phi}{\partial x}$ 
      determine the optimal control inputs
      evaluate the velocity  $F(x, t_n)$  for the grid node
      move  $x$  backwards with velocity  $-F(x, t_n)$  to get to
       $s = x + \delta t F(x, t_n)$ 
      interpolate  $\phi(x, t_n)$  to the point  $s$  to obtain  $\phi(x, t_{n+1}) = \phi(s, t_n)$ 
    end
    for each grid box do
      if any grid node  $<$  scale  $2^{\text{level}}$  then
        split box and mark grid nodes of neighboring boxes for
        re-evaluation
      end
      if all child-boxes' grid nodes level set value  $>$  scale  $2^{\text{level}+1}$  then
        merge child boxes
      end
    end
    process the marked and new nodes
    Re-normalize the grid such that difference in grid-level between
    adjacent box is maximally one
     $t = t + \Delta t$ 
  until  $t = t_{\text{final}}$ 
end

```

be run from the command-line and MATLAB readable results are stored together with a log file.

BIBLIOGRAPHY

- [1] M. J. Abzug and E. E. Larrabee. *Airplane Stability and Control - A History of the Technologies That Made Aviation Possible*. Ed. by M. J. Rycroft. Cambridge University Press, 1997.
- [2] H. Alwi, C. Edwards, O. Stroosma, and J. A. Mulder. "Fault Tolerant Sliding Mode Control Design with Piloted Simulator Evaluation". In: *Journal of Guidance, Control, and Dynamics* 31.5 (2008), pp. 1186–1201.
- [3] N. Ananthkrishnan and N. K. Sinha. "Level Flight Trim and Stability Analysis Using Extended Bifurcation and Continuation Procedure". In: *Journal of Guidance, Control, and Dynamics* 24.6 (2001), pp. 1225–1228.
- [4] Z. Artstein. "Stabilization with relaxed controls". In: *Nonlinear Analysis* 7.11 (1983), pp. 1163–1173.
- [5] K. J. Åström and B. Wittenmark. *Adaptive Control*. Addison Wesley Longman, 1995.
- [6] H. Backström. *Report on the usage of the Generic Aerodata Model*. Tech. rep. Saab Aircraft AB, 1997.
- [7] B. J. Bacon and I. M. Gregory. "General Equations of Motion for a Damaged Asymmetric Aircraft". In: *Proceedings of the AIAA Atmospheric Flight Mechanics Conference and Exhibit*. 2007-6306. AIAA. Hilton Head, South Carolina, USA, Aug. 2007.
- [8] D. L. Balough. "Determination of X-36 Stability Margins Using Real-Time Frequency Response Techniques". In: *Proceedings of the AIAA Atmospheric Flight Mechanics Conference and Exhibit*. AIAA 1998-4154. Boston, MA, USA, 1998.
- [9] A. R. Barron. "Self-organizing Methods in Modeling". In: ed. by S. J. Farlow. New York, NY, USA: Marcel Dekker, Inc, 1984. Chap. Predicted Squared Error: A Criterion for Automatic Model Selection, pp. 87–104.
- [10] A. M. Bayen, I. M. Mitchell, M. M. K. Oishi, and C. J. Tomlin. "Aircraft Autolander Safety Analysis Through Optimal Control-Based Reach Set Computation". In: *Journal of Guidance, Control, and Dynamics* 30.1 (2007), pp. 68–77.

- [11] R. E. Bellman. *Dynamic Programming*. Princeton, NJ: Princeton University Press, 1957.
- [12] S. A. Billings, M. J. Korenberg, and S. Chen. "Identification of nonlinear output-affine systems using an orthogonal least squares algorithm". In: *International Journal of Systems Science* 19 (1988), pp. 1559–1568.
- [13] M. Blanke, M. Satorswiecki, and N. E. Wu. "Concepts and Methods in Fault-Tolerant Control". In: *Proceedings of the 2001 American Control Conference*. June 2001, pp. 2606–2620.
- [14] M. Bodson. "Evaluation of Optimization Methods for Control Allocation". In: *Journal of Guidance, Control, and Dynamics* 25.4 (2002), pp. 703–711.
- [15] Boeing Company. *Statistical Summary of Commercial Jet Airplane Accidents: Worldwide Operations since 1959*. Tech. rep. Boeing Commercial Airplanes, 2009.
- [16] J. A. Boudreau and H. I. Berman. *Dispersed and Reconfigurable Digital Flight Control Systems*. Tech. rep. Grumman Aerospace Corporation, 1979.
- [17] J. S. Brinker and K. A. Wise. "Flight Testing of Reconfigurable Control Law on the X-36 Tailless Aircraft". In: *Journal of Guidance, Control, and Dynamics* 24 (May 2001), pp. 903–909.
- [18] J. Buffington, G. Tallant, V. Crum, et al. "Validation and Verification of Intelligent and Adaptive Control Systems". In: *Proceedings of the Second AIAA Unmanned Unlimited Conference*. AIAA-2003-6603. 2003.
- [19] J. M. Buffington, D. F. Enns, and A. R. Teel. "Control Allocation and Zero Dynamics". In: *Journal of Guidance, Control, and Dynamics* 21.3 (1998), pp. 458–464.
- [20] R. C. *F-15 loses wing in mid-air collision - lands safely*. Accessed 2010-08-19. Aug. 19, 2010. URL: <http://www.strangemilitary.com/content/item/110099.html>.
- [21] A. Calise, S. Lee, and M. Sharma. "Development of a Reconfigurable Flight Control Law for the X-36 Tailless Aircraft". In: *Journal of Guidance, Control and Dynamics* 24.5 (2001), pp. 896–902.
- [22] C. Cao and N. Hovakimyan. "Vision-Based Aerial Tracking using Intelligent Excitation". In: *American Control Conference, 2005. Proceedings of the*. Vol. 7. June 2005, pp. 5091–5096.
- [23] C. Cao, N. Hovakimyan, and J. Wang. "Intelligent Excitation for Adaptive Control With Unknown Parameters in Reference Input". In: *Automatic Control, IEEE Transactions on* 52.8 (Aug. 2007), pp. 1525–1532.
- [24] J. V. Carroll and R. K. Mehra. "Bifurcation analysis of nonlinear aircraft dynamics". In: *Journal of Guidance, Control, and Dynamics* 5.5 (1982), pp. 529–536.

- [25] J. Chen, R. J. Patton, and Z. Chen. "An LMI Approach to Fault-Tolerant Control of Uncertain Systems". In: *Proceedings of the 1998 IEEE/CIRA/ISAS Conference*. 1998, pp. 175–180.
- [26] S. Chen, S. A. Billings, and W. Luo. "Orthogonal Least Squares Methods and their Applications to Non-linear System Identification". In: *International Journal of Control* 50.5 (1989), pp. 1873–1896.
- [27] R. Courant, K. Friedrichs, and H. Lewy. "Über die partiellen Differenzgleichungen der mathematischen Physik". In: *Mathematische Annalen* 100.1 (1928), pp. 32–74.
- [28] R. Courant, E. Isaacson, and M. Rees. "On the solution of nonlinear hyperbolic differential equations by finite differences". In: *Communications on Pure and Applied Mathematics* 5 (1952), pp. 243–255.
- [29] M. G. Crandall, L. C. Evans, and P. L. Lions. "Some properties of viscosity solutions of Hamilton-Jacobi equations". In: *Transactions of the American Mathematical Society* 282.2 (1984), pp. 487–502.
- [30] M. G. Crandall and P-L. Lions. "Viscosity solutions of Hamilton-Jacobi equations". In: *Transactions of the American Mathematical Society* 277.1 (1983), pp. 1–42.
- [31] P. A. Cummings. *Continuation Method for Qualitative Analysis of Aircraft Dynamics*. Tech. rep. CR-2004-213035. NASA Langley Research Center, July 2004.
- [32] C. G. Darwin and A. R. Wallace. "On the tendency of species to form varieties; and on the perpetuation of varieties and species by natural means of selection". In: *Journal of the Proceedings of the Linnean Society of London. Zoology* 3 (1858), pp. 45–62.
- [33] M. de Berg, O. Cheong, M. van Kreveld, and M. Overmars. *Computational Geometry - Algorithms and Applications*. 3rd ed. Springer-Verlag, 2008.
- [34] C. de Boor. "A Practical Guide to Splines". In: Springer-Verlag, 1978, pp. 87, 109.
- [35] J. G. de Gooijer, B. Abraham, A. Gould, and L. Robinson. "Methods for Determining the Order of an Autoregressive-Moving Average Process: A Survey". In: *International Statistical Review* 53.3 (1985), pp. 301–329.
- [36] E. K. de Rivas. "On the Use of Nonuniform Grids in Finite-Difference Equations". In: *Journal of Computational Physics* 10 (1972), pp. 202–210.
- [37] C. C. de Visser, Q. P. Chu, and J. A. Mulder. "A new approach to linear regression with multivariate splines". In: *Automatica* 45.12 (Dec. 2009), pp. 2903–2909.

- [38] J. Dehaene, M. Moonen, and J. Vandewalle. "Continuous-Time Recursive Least-Squares Estimation, Adaptive Neural Networks and Systolic Arrays". In: *IEEE Transactions on Circuits and Systems I: Fundamental Theory and Applications* 42.2 (1995), pp. 116–119.
- [39] B. Djeridane and J. Lygeros. "Neural approximation of PDE solutions: An application to reachability computations". In: *Decision and Control, 2006 45th IEEE Conference on*. Dec. 2006, pp. 3034–3039.
- [40] N. Draper and H. Smith. *Applied Regression Analysis*. John Wiley & Sons, Inc., 1981.
- [41] E. L. Duke, R. F. Antoniewicz, and K. D. Krambeer. *Derivation and Definition of a Linear Aircraft Model*. Tech. rep. RP-1207. NASA Ames Research Center Dryden Flight Research Facility, 1988.
- [42] B. Dunbar. *NASA - NASA Dryden Fact Sheet - Intelligent Flight Control System*. Apr. 28, 2010. URL: <http://www.nasa.gov/centers/dryden/news/FactSheets/FS-076-DFRC.html> (visited on 12/2009).
- [43] W. C. Durham. "Constrained Control Allocation". In: *Journal of Guidance, Control, and Dynamics* 16.4 (1993), pp. 717–725.
- [44] W. C. Durham, F. H. Lutze, and W. Mason. "Kinematics and aerodynamics of the velocity vector roll". In: *Journal of Guidance, Control, and Dynamics* 17.6 (1994), pp. 1228–1233.
- [45] C. Edwards, T. J. J. Lombaerts, and H. Smaili, eds. *Fault Tolerant Flight Control - A Benchmark Challenge*. 1st ed. Lecture Notes in Control and Information Sciences 399. Springer, 2010.
- [46] C. Edwards and S. Spurgeon. *Sliding Mode Control: Theory and Applications*. Washington, D.C.: Taylor and Francis, 1998, pp. 31–34, 65.
- [47] L. Egbert and I. Halley. "Stabilator Reconfiguration Flight Testing on the F/A-18E/F". In: *Proceedings of the SAE Control and Guidance Meeting*. Mar. 2001.
- [48] D. F. Enns. "Control Allocation Approaches". In: *Proceedings of the AIAA Guidance, Navigation, and Control Conference and Exhibit*. Boston MA, USA, 1998, pp. 98–108.
- [49] D. Enright, F. Losasso, and R. Fedkiw. "A Fast and Accurate Semi-Lagrangian Particle Level Set Method". In: *Computers & Structures* 83.6-7 (Feb. 2005), pp. 479–490.
- [50] R. Eslinger and P. Chandler. "Self-repairing flight control system program overview". In: *Proceedings of the IEEE 1988 National Aerospace and Electronics Conference*. Vol. 2. May 1988, pp. 504–511.

- [51] J. S. Eterno, J. L. Weiss, D. P. Looze, and A. S. Willsky. "Design issues for fault tolerant-restructurable aircraft control". In: *Proceedings of the 24th IEEE Conference on Decision and Control*. Dec. 1985, pp. 900–905.
- [52] B. Etkin and L. D. Reid. *Dynamics of Flight: Stability and Control*. 3rd. John Wiley & Sons, 1996.
- [53] L. C. Evans and P. E. Souganidis. "Differential games and representation formulas for solutions of Hamilton-Jacobi-Isaacs equations". In: *Indiana University Mathematics Journal* 33.5 (1984), pp. 773–797.
- [54] W. Falkena, C. Borst, and J. A. Mulder. "Investigation of Practical Flight Envelope Protection Systems for Small Aircraft". In: *Proceedings of the AIAA Guidance, Navigation, and Control Conference*. 2010-7701. AIAA. Toronto, Ontario, Canada, Aug. 2010.
- [55] J. Farrell, M. Polycarpou, and M. Sharma. "Adaptive Backstepping with Magnitude, Rate, and Bandwidth Constraints: Aircraft Longitude Control". In: *American Control Conference*. Denver, CO, June 2003, pp. 3898–3903.
- [56] J. A. Farrell, M. Polycarpou, M. Sharma, and W. Dong. "Command Filtered Backstepping". In: *Automatic Control, IEEE Transactions on* 54.6 (June 2009), pp. 1391–1395.
- [57] J. A. Farrell, M. Sharma, and M. Polycarpou. "Backstepping Based Flight Control with Adaptive Function Approximation". In: *Journal of Guidance, Control and Dynamics* 28.6 (Jan. 2005), pp. 1089–1102.
- [58] J. Farrell, M. Sharma, and M. Polycarpou. "On-line Approximation Based Aircraft Longitudinal Control". In: *American Control Conference, Denver, CO*. Denver, CO, June 2003, pp. 1011–1015.
- [59] J. A. Farrell and M. M. Polycarpou. *Adaptive Approximation Based Control, Unifying Neural, Fuzzy and Traditional Adaptive Approximation Approaches*. John Wiley & Sons, Inc., 2006.
- [60] L. Forssell and U. Nillsson. *ADMIRE The Aero-Data Model in a Research Environment Version 4.0, Model Description*. Tech. rep. FOI-R-1624-SE. FOI - Swedish Defence Research Agency, 2005.
- [61] R. A. Freeman, M. Krstić, and P. V. Kokotović. "Robustness of Adaptive Nonlinear Control to Bounded Uncertainties". In: *Automatica* 34 (1998), pp. 1227–1230.
- [62] M. G. Goman and A. V. Khramtsovsky. "Computational framework for investigation of aircraft nonlinear dynamics". In: *Advances in Engineering Software* 39 (2008), pp. 167–177.
- [63] M. G. Goman, G. I. Zagaynov, and A. V. Khramtsovsky. "Application of Bifurcation Theory to Nonlinear Flight Dynamcis Problems". In: *Progress in Aerospace Sciences* 33.9 (1997), pp. 539–586.

- [64] G. Goodwin and D. Mayne. "A Parameter Estimation Perspective of Continuous Time Model Reference Adaptive Control". In: *Automatica* 23 (1987), pp. 55–70.
- [65] K. D. Graham, T. B. Cunningham, and C. Shure. *Airfract Flight Control Survivability Through use of Computational Techniques*. Tech. rep. 77028-30. Naval Air Development Center, 1980.
- [66] O. Hachicho and B. Tibken. "Estimating Domains of Attraction of a Class of Nonlinear Dynamical Systems with LMI Methods Based on Theory of Moments". In: *Proceedings of the IEEE Conference on Decision and Control*. 2002, pp. 3150–3155.
- [67] T. Hacker and C. Oprisiu. "A Discussion of the Roll-Coupling Problem". In: *Progress in Aerospace Sciences* 15 (1974), pp. 151–180.
- [68] O. Härkegård. "Backstepping and Control Allocation with Applications to Flight Control". PhD thesis. Linköping, Sweden: Linköping University, 2003.
- [69] D. M. Hawkins and W. J. R. Eplett. "The Cholesky Factorization of the Inverse Correlation or Covariance Matrix in Multiple Regression". In: *Technometrics* 24.3 (1982), pp. 191–198.
- [70] W. H. Herbst. "Dynamics of Air Combat". In: *Journal of Aircraft* 20.7 (1983), pp. 594–598.
- [71] S. E. Hieber and P. Koumoutsakos. "A Lagrangian Particle Level Set Method". In: *Journal of Computational Physics* 210 (2005), pp. 342–367.
- [72] J. F. Horn, A. J. Calise, and J. V. R. Prasad. "Flight Envelope Cueing on a Tilt-Rotor Aircraft Using Neural Network Limit Prediction". In: *Journal of the American Helicopter Society* 46.1 (Jan. 2001), pp. 23–31.
- [73] J. F. Horn, A. J. Calise, and J. V. R. Prasad. "Flight Envelope Limit Detection and Avoidance for Rotorcraft". In: *Journal of the American Helicopter Society* 47.4 (Oct. 2002), pp. 253–262.
- [74] R. A. Hull, D. Schumacher, and Z. Qu. "Design and Evaluation of Robust Nonlinear Missile Autopilots from a Performance Perspective". In: *Proc. of the American Control Conference, Washington*. June 1995.
- [75] I. Hwang, D. M. Stipanović, and C. J. Tomlin. "Applications of Polytopic Approximations of Reachable Sets to Linear Dynamic Games and a Class of Nonlinear Systems". In: *American Control Conference. Proceedings of the 2003*. Vol. 6. 2003, pp. 4613–4619.
- [76] R. A. Hyde and K. Glover. "The application of scheduled \mathcal{H}_∞ controllers to a VSTOL aircraft". In: *Automatic Control, IEEE Transactions on* 38.7 (1993), pp. 1021–1039.
- [77] *In-Flight Separation of Vertical Stabilizer American Airlines Flight 587*. Tech. rep. NTSB/AAR-04/04. National Transportation Safety Board, 2001.

- [78] A. Isidori. *Nonlinear Control Systems*. 3rd ed. Springer, 1995.
- [79] T. A. Johansen, T. I. Fossen, and S. P. Berge. "Constrained Nonlinear Control Allocation with Singularity Avoidance using Sequential Quadratic Programming". In: *Control Systems Technology, IEEE Transactions on* 12.1 (2004), pp. 211–216.
- [80] T. A. Johansen, T. I. Fossen, and P. Tøndel. "Efficient Optimal Constrained Control Allocation via Multi-parametric Programming". In: *Journal of Guidance, Control, and Dynamics* 28.3 (2005), pp. 506–515.
- [81] E. Johnson and S. Kannan. "Adaptive Trajectory Control for Autonomous Helicopters". In: *Journal of Guidance, Control, and Dynamics* 28.3 (2005), pp. 524–538.
- [82] E. N. Johnson, A. J. Calise, and M. A. Turbe. "Fault Tolerance Through Direct Adaptive Control Using Neural Networks". In: *Proceedings of the AIAA Guidance, Navigation, and Control Conference, San Francis*. 2006.
- [83] H. K. Khalil. *Nonlinear Systems*. 3rd ed. Prentice Hall, 2002.
- [84] S. H. Kim, Y. S. Kim, and C. Song. "A Robust Adaptive Nonlinear Control Approach to Missile Autopilot Design". In: *Control Engineering Practice* 12.2 (2004), pp. 149–154.
- [85] V. Klein and E. A. Morelli. *Aircraft System Identification: Theory and Practice*. Education Series. AIAA, 2006.
- [86] M. J. Korenberg, S. A. Billings, Y. P. Liu, and P. J. McIlroy. "Orthogonal parameter estimation algorithm for nonl-linear stochastic systems". In: *International Journal of Control* 48 (1988), pp. 193–210.
- [87] M. Krstić, I. Kanellakopoulos, and P. V. Kokotović. "Adaptive Nonlinear Control without Overparameterization". In: *Systems and Control Letters* 19 (1992), pp. 177–185.
- [88] M. Krstić, I. Kanellakopoulos, and P. V. Kokotović. *Nonlinear and Adaptive Control Design*. John Wiley and Sons, 1995.
- [89] A. B. Kurzhanski and P. Varaiya. "Dynamic Optimization for Reachability Problems". In: *Journal of Optimization Theory and Applications* 108.2 (Feb. 2001), pp. 227–251.
- [90] H. G. Kwatny, J.-E. T. Dongmo, R. C. Allen, B. Chang, and G. Bajpai. "Loss-of-Control: Perspectives on Flight Dynamics and Control of Impaired Aircraft". In: *Proceedings of the AIAA Guidance, Navigation, and Control Conference*. 2010-8005. AIAA. Toronto, Ontario, Canada, Aug. 2010.
- [91] A. A. Lambregts, G. Nesemeier, J. E. Wilborn, and R. L. Newman. "Airplane Upsets: Old Problems, New Issues". In: *AIAA Modeling and Simulation Technologies Conference and Exhibit*. AIAA-2008-6867. Honolulu, Hawaii, Aug. 2008.

- [92] I. D. Landau. *Adaptive control: the model reference approach*. Ed. by M. Dekker. Dekker, New York, 1979.
- [93] I. D. Landau and B. Courtiol. "Design of multivariable adaptive model following control systems". In: *Automatica* 10.5 (1974), pp. 483–494.
- [94] M. D. Lichter, A. J. Bateman, and G. J. Balas. "Flight Test Evaluation of a Run-time Stability Margin Estimation Tool". In: *Proceedings of the AIAA Guidance, Navigation, and Control Conference*. AIAA 2009-6257. Chicago, IL, USA, 2009.
- [95] C. Livadas, J. Lygeros, and N. Lynch. "High-level modeling and analysis of the traffic alert and collision avoidance system (TCAS)". In: *Proceedings of the IEEE* 88.7 (July 2000), pp. 926–948.
- [96] T. J. J. Lombaerts. "Fault Tolerant Flight Control, A Physical Model Approach". PhD thesis. Delft University of Technology, Faculty of Aerospace Engineering, 2010.
- [97] T. J. J. Lombaerts, H. O. Huisman, Q. P. Chu, J. A. Mulder, and D. A. Joosten. "Nonlinear Reconfiguring Flight Control Based on Online Physical Model Identificatin". In: *Journal of Guidance, Control, and Dynamics* 32.3 (2009), pp. 727–748.
- [98] T. J. J. Lombaerts, E. R. van Oort, Q. P. Chu, and J. A. Mulder. "On-line Aerodynamic Model Strucutre Selection and Parameter Estimation for Fault Tolerant Control". In: *AIAA Guidance, Navigation, and Control Conference*. AIAA-2009-5725. Chicago, Illinois, Aug. 2009.
- [99] T. J. J. Lombaerts, E. R. van Oort, Q. P. Chu, J. A. Mulder, and D. A. Joosten. "Online Aerodynamic Model Structure Selection and Parameter Estimation for Fault Tolerant Control". In: *Journal of Guidance, Control, and Dynamics* 33.3 (2010), pp. 707–723.
- [100] D. Looze, J. Weiss, J. Eterno, and N. Barrett. "An automatic redesign approach for restructurable control systems". In: *Control Systems Magazine, IEEE* 5.2 (May 1985), pp. 16–22.
- [101] F. Losasso, J. O. Talton, N. Kwatra, and R. Fedkiw. "Two-way coupled SPH and Particle Level Set Fluid Simulation". In: *IEEE Transactions on Visualization & Computer Graphics* 14.4 (2008), pp. 797–804.
- [102] F. Losasso, F. Gibou, and R. Fedkiw. "Simulating water and smoke with an octree data structure". In: *SIGGRAPH '04: ACM SIGGRAPH 2004 Papers*. Los Angeles, California: ACM, 2004, pp. 457–462.
- [103] M. Lowenberg. "Bifurcation and Continuation Method". In: ed. by C. Fielding, A. Varga, S. Bennani, and M. Selier. Vol. 283. *Advanced Techniques for Clearance of Flight Control Laws, Lecture Notes in Control and Information Sciences*. Springer-Verlag, 2002. Chap. 6, pp. 89–106.

- [104] W. Luo and S. A. Billings. "Adaptive model selection and estimation for nonlinear systems using a sliding data window". In: *Signal Processing* 46.2 (1995), pp. 179–202.
- [105] Y. Luo, A. Serrani, S. Yurkovich, D. Doman, and M. Oppenheimer. "Dynamic Control Allocation with Asymptotic Tracking of Time-varying Control Input Commands". In: *Proceedings of the American Control Conference*. Portland, OR, USA, 2005, pp. 2098–2103.
- [106] Y. Luo, A. Serrani, S. Yurkovich, D. Doman, and M. Oppenheimer. "Model Predictive Dynamic Control Allocation with Actuator Dynamics". In: *Proceedings of the American Control Conference*. Vol. 2. Boston, MA, USA, 2004, pp. 1695–1700.
- [107] A. M. Lyapunov. *The general problem of the stability of motion*. Ed. by A. T. Fuller. Taylor and Francis Ltd., 1992.
- [108] J. Lygeros. "On reachability and minimum cost optimal control". In: *Automatica* 40.6 (2004), pp. 917–927.
- [109] J. C. Maxwell. "On Governors". In: *Proceedings of the Royal Society of London* 16 (1867), pp. 270–283.
- [110] M. B. McFarland and A. J. Calise. "Multilayer neural networks and adaptive nonlinear control of agile anti-air missiles". In: *Proceedings of the AIAA Guidance, Navigation, and Control Conference*. AIAA. Reston, VA, Aug. 1997, pp. 401–410.
- [111] D. McRuer, I. Ashkenas, and D. Graham. *Aircraft Dynamics and Automatic Control*. Princeton University Press, 1973.
- [112] A. Melikyan, A. Akhmetzhanov, and N. Hovakimyan. "On Initial Value and Terminal Value Problems for Hamilton-Jacobi Equations". In: *System & Control Letters* 56 (2007), pp. 714–721.
- [113] E. M. A. M. Mendes and S. A. Billings. "An Alternative Solution to the Model Structure Selection Problem". In: *IEEE Transactions on Systems, Man, and Cybernetics* 31.6 (2001), pp. 597–608.
- [114] A. W. Merz. "The game of two identical cars". In: *Journal of Optimization Theory and Applications* 9.5 (1972), pp. 324–343.
- [115] I. M. Mitchell. *A Toolbox of Level Set Methods*. Tech. rep. TR-2007-11. UBC Department of Computer Science, June 2007.
- [116] I. M. Mitchell. "Application of Level Set Methods to Control and Reachability Problems in Continuous and Hybrid Systems". PhD thesis. Stanford University, 2002.
- [117] I. M. Mitchell. *Games of two Identical Vehicles*. Tech. rep. 740. Stanford University Department of Aeronautics and Astronautics, 2001.

- [118] J. F. Monaco, D. G. Ward, R. L. Barron, and R. A. Bird. "Implementation and Flight Test Assessment of an Adaptive, Reconfigurable Flight Control System". In: *Proceedings of the AIAA Guidance, Navigation, and Control Conference, New Orleans, Louisiana*. Aug. 1997, pp. 1443–1454.
- [119] J. F. Monaco, D. G. Ward, and A. J. Bateman. "A Retrofit Architecture for Model-Based Adaptive Flight Control". In: *Proceedings of the AIAA First Intelligent Systems Conference*. 2004.
- [120] R. V. Monopoli. "Model reference adaptive control with an augmented error signal". In: *Automatic Control, IEEE Transactions on* 19.5 (1974), pp. 474–484.
- [121] E. A. Morelli. "Global nonlinear aerodynamic modeling using multivariate orthogonal functions". In: *Journal of Aircraft* 32 (1995), pp. 270–277.
- [122] J. A. Mulder. "Design and evaluation of dynamic flight test manoeuvres". PhD thesis. Delft University of Technology, Faculty of Aerospace Engineering, 1986.
- [123] C. H. Murphy. "Symmetric Missile Dynamic Instabilities". In: *Journal of Guidance, Control, and Dynamics* 4.5 (1981), pp. 464–471.
- [124] J. Nakanishi, J. A. Farrell, and S. Schaal. "Composite adaptive control with locally weighted statistical learning". In: *Neural Networks* 18 (2005), pp. 71–90.
- [125] J. C. Neidhoefer, J. Ryan, K. Al-Ali, A. Ishihara, and N. Kulkarni. "Experimental Validation of Metrics-Driven Enhanced-Safety (ME) Adaptive Control". In: *Proceedings of the AIAA Guidance, Navigation, and Control Conference and Exhibit*. AIAA 2008-6984. 2008.
- [126] L. T. Nguyen, M. E. Ogburn, W. P. Gilbert, et al. *Simulator Study of Stall/Post-stall Characteristics of a Fighter Airplane with Relaxed Longitudinal Static Stability*. Tech. rep. 1538. NASA Langley Research Center, 1979.
- [127] N. Nguyen, K. Krishnakumar, J. Kaneshige, and P. Nespeca. "Flight Dynamics and Hybrid Adaptive Control of Damaged Aircraft". In: *Journal of Guidance, Control, and Dynamics* 31.3 (2008), pp. 751–764.
- [128] R. A. Nichols, R. T. Reichert, and W. J. Rugh. "Gain scheduling for \mathcal{H}_∞ controllers: a flight control example". In: *Control Systems Technology, IEEE Transactions on* 1 (1993), pp. 69–75.
- [129] J. Nocedal and S. J. Wright. "Numerical Optimization". In: 2nd ed. Springer, 2006. Chap. 12, pp. 304–351.
- [130] J. Oliveira, Q. P. Chu, J. A. Mulder, H. M. N. K. Balini, and W. M. Vos. "Output Error Method and Two Step Method for Aerodynamic Model Identification". In: *Proceedings of the AIAA Guidance, Navigation and Control Conference and Exhibit*. San Francisco, California, USA, Aug. 2005.

- [131] M. Oppenheimer and D. Doman. "A Method for Including Control Effector Interactions in the Control Allocation Problem". In: *Proceedings of the AIAA Guidance, Navigation and Control Conference and Exhibit*. AIAA-2007-6418. Hilton Head, SC, USA, 2007.
- [132] S. Osher and R. Fedkiw. *Level Set Methods and Dynamic Implicit Surfaces*. Springer-Verlag, 2003.
- [133] A. B. Page and M. L. Steinberg. "Effects of Control Allocation Algorithms on a Nonlinear Adaptive Design". In: *Proceedings of the AIAA Guidance, Navigation, and Control Conference and Exhibit, Portland, OR*. Aug. 1999.
- [134] R. Pandita, A. Chakraborty, P. Seiler, and G. Balas. "Reachability and Region of Attraction Analysis Applied to GTM Dynamic Flight Envelope Assessment". In: *AIAA Guidance, Navigation, and Control Conference*. 2009.
- [135] I. Panella. "Flight Clearance Metrics for Autonomous UAVs". In: *Proceedings of the AIAA Guidance, Navigation, and Control Conference and Exhibit*. AIAA 2005-6412. San Francisco, CA, USA, 2005.
- [136] A. Paranjape, N. K. Sinha, and N. Ananthkrishnan. "Use of Bifurcation and Continuation Methods for Aircraft Trim and Stability Analysis - A state-of-the-art". In: *45th AIAA Aerospace Sciences Meeting and Exhibit, 8-11 January 2007, Reno, Nevada*. AIAA 2007-1051. AIAA. 2007.
- [137] A. A. Pashilkar, N. Sundararajan, and P. Saratchandran. "Adaptive Nonlinear Neural Controller for Aircraft Under Actuator Failures". In: *Journal of Guidance, Control, and Dynamics* 30 (2007), pp. 835–847.
- [138] R. J. Patton. "Fault-Tolerant Control: The 1997 situation". In: *Proceedings of the 3rd IFAC Symposium on Fault Detection, Supervision and Safety for Technical Processes*. Aug. 1997, pp. 1033–1055.
- [139] W. H. Phillips. *Effect of steady rolling on longitudinal and directional stability*. Tech. rep. TN 1627. NACA, 1948.
- [140] M. M. Polycarpou, J. A. Farrell, and M. Sharma. "Robust On-line Approximation Control of Uncertain Nonlinear Systems Subject to Constraints". In: *9th IEEE International Conference on Engineering of Complex Computer Systems*. 2004, pp. 66–74.
- [141] M. M. Polycarpou and P. A. Ioannou. "A Robust Adaptive Nonlinear Control Design". In: *Automatica* 32.3 (1996), pp. 423–427.
- [142] V. Poonamallee, S. Yurkovich, A. Serrani, and D. Doman. "A Nonlinear Programming Approach for Control Allocation". In: *Proceedings of the American Control Conference*. Vol. 2. Boston, MA, USA, 2004, pp. 1689–1694.
- [143] L. Praly, G. Bastin, J. B. Promet, and Z. Jiang. *Foundations of Adaptive Control*. Berlin: Springer-Verlag, 1991. Chap. Adaptive Stabilization of Nonlinear Systems, pp. 347–434.

- [144] J. A. Primbs, V. Nevistić, and J. C. Doyle. "Nonlinear Optimal Control: A Control Lyapunov Function and Receding Horizon Perspective". In: *Asian Journal of Control* 1.1 (Mar. 1999), pp. 14–24.
- [145] H. Ranter. *Airliner Accident Statistics 2006*. Tech. rep. Aviation Safety Network, 2007.
- [146] S. Rigal. *Guidage d'un Véhicule Sous Marin de Type Glider par des Méthodes de Viabilité*. Tech. rep. Nantes, France: Ecole Centrale de Nantes, 2001.
- [147] G. J. J. Ruijgrok. *Elements of Airplane Performance*. Delft University Press, 1996.
- [148] J. Shamma and M. Athans. "Analysis of gain scheduled control for nonlinear plants". In: *Automatic Control, IEEE Transactions on* 35.8 (Aug. 1990), pp. 898–907.
- [149] J. Shamma and M. Athans. "Gain scheduling: potential hazards and possible remedies". In: *Control Systems Magazine, IEEE* 12.3 (June 1992), pp. 101–107.
- [150] M. Sharma and D. G. Ward. "Flight-path angle control via neuro-adaptive backstepping". In: *Proceedings of the AIAA Guidance, Navigation, and Control Conference and Exhibit*. Monterey, California, USA, Aug. 2002.
- [151] D. H. Shin and Y. Kim. "Nonlinear Discrete-Time Reconfigurable Flight Control Law Using Neural Networks". In: *Control Systems Technology, IEEE Transaction on* 14.3 (May 2006), pp. 408–422.
- [152] J. Shin. *Analysis of Linear Parameter Varying System Model Based on Reachable Sets*. Tech. rep. CR-2001-211231. NASA Langley Research Center, Oct. 2001.
- [153] Y. Shin, A. J. Calise, and M. D. Johnson. "Adaptive Control of Advanced Fighter Aircraft in Nonlinear Flight Regimes". In: *Journal of Guidance, Control, and Dynamics* 31.5 (2008), pp. 1464–1477.
- [154] Y. B. Shtessel and J. Buffington. "Multiple Time Scale Flight Control Using Reconfigurable Sliding Modes". In: *Journal on Guidance, Control and Dynamics* 22.6 (1999), pp. 873–883.
- [155] A. T. Simmons and A. S. Hodel. "Control Allocation for the X-33 using Existing and Novel Quadratic Programming Techniques". In: *Proceedings of the 2004 American Control Conference*. Boston, Massachusetts, USA, 2004.
- [156] S. N. Singh and M. Steinberg. "Adaptive Control of Feedback Linearizable Nonlinear Systems With Application To Flight Control". In: *Proceedings of the AIAA Guidance, Navigation and Control Conference*. July 1996.
- [157] N. K. Sinha. "Application of Bifurcation Methods to Nonlinear Aircraft Dynamics". In: *Journal of the Aeronautical Society of India* 53.4 (2001), pp. 253–270.
- [158] R. Skjetne. "The Maneuvering Problem". PhD thesis. Trondheim, Norway: Norwegian University of Science, Technology, Faculty of Information Technology, Mathematics, and Electrical Engineering, 2005.

- [159] J. J. E. Slotine and W. Li. *Applied Nonlinear Control*. Prentice Hall, 1991.
- [160] J. J. E. Slotine and W. Li. "Composite Adaptive Control of Robot Manipulators". In: *Automatica* 25 (1989), pp. 509–519.
- [161] M. H. Smaili and J. A. Mulder. "Flight data reconstruction and simulation of El Al Flight 1862". In: *AIAA Modeling and Simulation Technologies Conference and Exhibit*. AIAA-2000-4586. Washington, DC, 2000.
- [162] L. Smith. *Falcon Flight Model Evolution*. Tech. rep. SimHQ, 2004.
- [163] L. Sonneveldt. "Adaptive Backstepping Control for Modern Fighter Aircraft". PhD thesis. Delft University of Technology, Faculty of Aerospace Engineering, July 2010.
- [164] L. Sonneveldt, Q. P. Chu, and J. A. Mulder. "Nonlinear Flight Control Design using Constrained Adaptive Backstepping". In: *Journal of Guidance, Navigation, and Dynamics* 30.2 (2007), pp. 322–336.
- [165] L. Sonneveldt, E. R. van Oort, Q. P. Chu, and J. A. Mulder. "Comparison of Inverse Optimal and Tuning Functions Designs for Adaptive Missile Control". In: *Proceedings of the AIAA Guidance, Navigation, and Control Conference and Exhibit*. 2007.
- [166] L. Sonneveldt, E. R. van Oort, Q. P. Chu, and J. A. Mulder. "Immersion and Invariance Based Nonlinear Adaptive Flight Control". In: *Proceedings of the AIAA Guidance, Navigation, and Control Conference*. 2010-7690. AIAA. Toronto, Ontario, Canada, 2010.
- [167] E. D. Sontag. "Smooth stabilization implies coprime factorization". In: *IEEE Transactions on Automatic Control* 34 (1989), pp. 435–443.
- [168] E. D. Sontag and Y. Wang. "On Characterizations of Input-to-State Stability with Respect to Compact Sets". In: *Proceedings of the IFAC Non-linear Control Systems Design Symposium*. Tahoe City, CA, USA, 1995, pp. 226–231.
- [169] O. J. Sjørdalen. "Optimal Thrust Allocation for Marine Vessels". In: *Control Engineering Practice* 5.9 (1997), pp. 1223–1231.
- [170] J. Stark. "Adaptive Model Selection Using Orthogonal Least Squares Methods". In: *Proceedings: Mathematical, Physical and Engineering Sciences* 453.1956 (1997), pp. 21–42.
- [171] G. Stein. "Applications of Adaptive Control". In: ed. by K. S. Narendra and R. V. Monopoli. Academic Press, New York, 1980. Chap. Adaptive flight control - a pragmatic view.
- [172] G. Stein, G. Hartmann, and R. Hendrick. "Adaptive Control Laws for F-8 Flight Test". In: *Automatic Control, IEEE Transactions on* 22 (1977), pp. 758–767.
- [173] M. Steinberg. "Historical Overview of Research in Reconfigurable Flight Control". In: *Proceedings of the Institution of Mechanical Engineers, Part G: Journal of Aerospace Engineering* 219.4 (2005), pp. 263–275.

- [174] R. F. Stengel. "Intelligent Failure-Tolerant Control". In: *IEEE Control Systems Magazine* 11.4 (1991), pp. 14–23.
- [175] V. Stepanyan and N. Hovakimyan. "Adaptive Disturbance Rejection Controller for Visual Tracking of a Maneuvering Target". In: *Journal of Guidance, Control, and Dynamics* 30.4 (2007), pp. 1090–1106.
- [176] B. L. Stevens and F. L. Lewis. *Aircraft Control and Simulation*. 2nd ed. Wiley Interscience, New York, 2003.
- [177] J. Strain. "Semi-Lagrangian Methods for Level Set Equations". In: *Journal of Computational Physics* 151 (1999), pp. 498–533.
- [178] O. Stroosma, M. H. Smaili, T. J. J. Lombaerts, and J. A. Mulder. "Piloted Simulator Evaluation of New Fault-Tolerant Flight Control Algorithms for Reconstructed Accident Scenarios". In: *AIAA Modeling and Simulation Technologies Conference and Exhibit, Honolulu, Hawaii, Aug 18 - 21*. AIAA 2008-6534. 2008.
- [179] S. Suresh, S. N. Omkar, and V. Mani. "Direct Adaptive Neural Flight Controller for F-8 Fighter Aircraft". In: *Journal of Guidance, Control, and Dynamics* 29.2 (2006), pp. 454–464.
- [180] W. Tan. "Nonlinear Control Analysis and Synthesis using Sum-of-Squares Programming". PhD thesis. Berkeley, California, USA: University of California, 2006.
- [181] L. Tang, M. Roemer, J. Ge, et al. "Methodologies for Adaptive Flight Envelope Estimation and Protection". In: *AIAA Guidance, Navigation, and Control Conference*. AIAA 2009-6260. Chicago, IL, 2009.
- [182] R. Teo, J. S. Jang, and C. J. Tomlin. "Flight Demonstration of Provably Safe Closely Spaced Parallel Approaches". In: *Proceedings of the AIAA Guidance, Navigation, and Control Conference and Exhibit*. 2005-6197. AIAA. San Francisco, California, USA, Aug. 2005.
- [183] R. Teo and C. J. Tomlin. "Computing Danger Zones for Provably Safe Closely Spaced Parallel Approaches". In: *Journal of Guidance, Control, and Dynamics* 26.3 (2003), pp. 434–442.
- [184] J. Thunberg and J. W. C. Robinson. "Block Backstepping, NDI, and Related Cascade Designs for Efficient Development of Nonlinear Flight Control Laws". In: *Proceedings of the AIAA Guidance, Navigation, and Control Conference and Exhibit*. AIAA 2008-6960. AIAA. Honolulu, HI, USA, 2008.
- [185] B. Tibken and Y. Fan. "Computing the Domain of Attraction for Polynomial Systems via BMI Optimization Methods". In: *Proceedings of the American Control Conference*. 2006, pp. 117–122.
- [186] J. Tjønnås. "Nonlinear and Adaptive Dynamic Control Allocation". PhD thesis. Trondheim, Norway: Norwegian University of Science, Technology, Faculty of Information Technology, Mathematics, and Electrical Engineering, 2008.

- [187] J. Tjønnås and T. A. Johansen. "Optimizing Nonlinear Adaptive Control Allocation". In: *Proceedings of the 16th IFAC World Congress*. Prague, Czech Republic, 2005.
- [188] U. Topcu, A. Packard, and P. Seiler. "Local Stability Analysis using Simulations and Sum-of-Squares Programming". In: *Automatica* 44.10 (2008), pp. 2669–2675.
- [189] E. van Kampen, Q. P. Chu, J. A. Mulder, and M. H. van Emden. "Nonlinear Aircraft Trim using Interval Analysis". In: *Proceedings of the AIAA Guidance, Navigation and Control Conference and Exhibit*. Hilton Head, South Carolina, USA, 2007.
- [190] E. R. van Oort, Q. P. Chu, and J. A. Mulder. "Adaptive Dynamic Control Allocation and Backstepping Design". In: *Proceedings of the AIAA Guidance, Navigation, and Control Conference*. Under review. 2011.
- [191] E. R. van Oort, Q. P. Chu, and J. A. Mulder. "Maneuver Envelope Determination through Reachability Analysis". In: *Proceedings of the CEAS EURO GNC 2011 conference*. Accepted, to be presented. 2011.
- [192] E. R. van Oort, Q. P. Chu, and J. A. Mulder. "Safe Dynamic Flight Envelope Determination with Application to an F-16 Model". In: *Journal of Guidance, Control, and Dynamics* (2011). Under review.
- [193] E. R. van Oort, Q. P. Chu, and J. A. Mulder. "Safe Flight Envelope Determination by Reachability Analysis". In: *Proceedings of the ICNPAA 2010 World Congress: 8th International Conference on Mathematical Problems in Engineering, Aerospace and Sciences*. São José dos Campos, Brazil, 2010.
- [194] E. R. van Oort, L. Sonneveldt, Q. P. Chu, and J. A. Mulder. "A Comparison of Adaptive Nonlinear Control Designs for an Over-actuated Fighter Aircraft Model". In: *AIAA Guidance, Navigation, and Control Conference and Exhibit*. Honolulu, Hawaii, USA, Aug. 2008.
- [195] E. R. van Oort, L. Sonneveldt, Q. P. Chu, and J. A. Mulder. "Adaptive Dynamic Control Allocation and Backstepping Design". In: *Journal of Guidance, Control, and Dynamics* (2011). To be submitted.
- [196] E. R. van Oort, L. Sonneveldt, Q. P. Chu, and J. A. Mulder. "Full Envelope Modular Adaptive Control of a Fighter Aircraft using Orthogonal Least Squares". In: *Proceedings of the AIAA Guidance, Navigation, and Control Conference*. 2010-7857. AIAA. Toronto, Ontario, Canada, Aug. 2010.
- [197] E. R. van Oort, L. Sonneveldt, Q. P. Chu, and J. A. Mulder. "Full Envelope Modular Adaptive Control of a Fighter Aircraft using Orthogonal Least Squares". In: *Journal of Guidance, Navigation and Dynamics* 33.5 (2010), pp. 1461–1472.

- [198] E. R. van Oort, L. Sonneveldt, Q. P. Chu, and J. A. Mulder. "Modular Adaptive Input-to-state Stable Backstepping of a Nonlinear Missile Model". In: *AIAA Guidance, Navigation, and Control Conference and Exhibit*. Hilton Head, South Carolina, USA, Aug. 2007.
- [199] J. A. M. M. Wedershoven. "Analysis of Nonlinear Dynamic Inversion based Control Law Designs". MA thesis. Delft University of Technology, Faculty of Aerospace Engineering, June 2010.
- [200] K. H. Well. "Aircraft Control Laws for Envelope Protection". In: *Proceedings of the AIAA Guidance, Navigation, and Control Conference and Exhibit*. 2006-6055. AIAA. Keystone, Colorado, USA, Aug. 2006.
- [201] N. Wiener. *Cybernetics or Control and Communication in the Animal and the Machine*. New York: Wiley & Sons, Inc., 1948.
- [202] J. E. Wilborn and J. V. Foster. "Defining Commercial Aircraft Loss-of-Control: A Quantative Approach". In: *Proceedings of the AIAA Atmospheric Flight Mechanics Conference and Exhibit*. 2004-4811. AIAA. Providence, Rhode Island, USA, Aug. 2004.
- [203] K. A. Wise and J. L. Sedwick. "Stability Analysis of Reconfigurable and Gain Scheduled Flight Control Systems using LMIs". In: *Proceedings of the AIAA Guidance, Navigation, and Control Conference*. 1998, pp. 118–126.
- [204] J. M. Wohletz. "Retrofit Systems for Reconfiguration in Civil Aviation". PhD thesis. Massachusetts Institute of Technology, Cambridge, Massachusetts, 2000.
- [205] I. Yavrucuk, J. V. R. Prasad, and S. Unnikrishnan. "Envelope Protection for Autonomous Unmanned Aerial Vehicles". In: *Jornal of Guidance, Control, and Dynamics* 32 (2009), pp. 248–261.
- [206] P.-C. P. Yip. "Robust and Adaptive Nonlinear Control using Dynamic Surface Controller with Applications to Intelligent Vehicle Highway Systems". PhD thesis. University of California, 1997.
- [207] P.-C. P. Yip and J. K. Hedrick. "Adaptive dynamic surface control: a simplified algorithm form adaptive backstepping control of nonlinear systems". In: *International Journal of Control* 71.5 (1998), pp. 959–979.
- [208] L. A. Zadeh. "From Circuit Theory to System Theory". In: *Proceedings of the IRE*. Vol. 50. 5. May 1962, pp. 856–865.
- [209] G. I. Zagaynov and M. G. Goman. "Bifurcation analysis of critical aircraft flight regimes". In: *Proceedings of the 14th congress of ICAS*. 84-4.2.1. Toulouse, France, 1984.
- [210] Y. Zhang and J. Jiang. "Bibliographical review on reconfigurable fault-tolerant control systems". In: *Annual Reviews in Control* 32.2 (Dec. 2008), pp. 229–252.

NOMENCLATURE

Acronyms

AIC	Akaike's Information Criterion
AOCLF	Adaptive Optimizing Control Lyapunov Function
CA	Control Allocation
CABS	Constrained Adaptive Backstepping
CFL	Courant-Friedrichs-Lewy
CIR	Cholesky Inverse Root
CLF	Control Lyapunov Function
ENO	Essentially non-oscillatory
FBL	Feedback Linearization
FBW	Fly-By Wire
FDD	Fault Detection and Diagnosis
FDIE	Fault Detection Isolation and Estimation
FTCS	Fault Tolerant Control System
FTFC	Fault Tolerant Flight Control
GAM	Generic Aerodata Model
GUAS	Globally Uniformly Asymptotically Stable
ISS	Input-to-State Stable
LOC	Loss of Control
LPV	Linear Parameter Varying
MRAC	Model Reference Adaptive Control
NDI	Nonlinear Dynamic Inversion
NN	Neural Network
OCLF	Optimizing Control Lyapunov Function
ODE	Ordinary Differential Equation

OLS	Orthogonal least squares
PSE	Predicted square error
QP	Quadratic Programming
RFC	Reconfigurable Flight Control
RLS	Recursive Least Squares
RMS	Root Mean Square
ROA	Region of Attraction
SSPE	Structure Selection and Parameter Estimation
SVD	Singular Value Decomposition
TSS	Time-Scale Separation
TVD	Total Variation Diminishing
UA	Uniformly Attractive
UAS	Uniform Asymptotic Stability
US	Uniformly Stable
VSC	Variable Structure Control

Greek Letters

α	Angle of attack	rad
β	Sideslip angle	rad
Δ	Uncertainty	
δ_*	Control surface deflection	rad
ϵ	Estimation error	
Γ	Update gain matrix	
κ, μ	Nonlinear damping gain matrix > 0	
λ	Forgetting factor	
λ	Lagrange multiplier	
ω_*	Angular velocity in the $*$ coordinate system	rad/s
Φ	Data matrix	
ϕ	Level set function	
Ψ	Composite update law weight matrix	
σ	Leakage gain > 0	
φ	Regressor function	
ξ, Ξ	Filter state	
θ	Unknown parameter	

$\hat{\theta}$	Estimated parameter
$\tilde{\theta}$	Parameter error

Latin Letters

\bar{c}	Reference chord length	m
\bar{q}	Dynamic pressure	N/m ²
\bar{X}	Force in x_B direction	N
\bar{Y}	Force in y_B direction	N
\bar{Z}	Force in z_B direction	N
b	Reference span length	m
C	Tracking error gain matrix > 0	
J	Inertia tensor	kgm ²
K	Integral gain matrix	
L	Roll moment	Nm
M	Pitch moment	Nm
N	Yaw moment	Nm
p_*	Roll rate in $*$ coordinate system	rad/s
p_{static}	Static pressure	N/m ²
q_*	Pitch rate in $*$ coordinate system	rad/s
R	Cholesky factor	
r_*	Yaw rate in $*$ coordinate system	rad/s
S	Inverse Cholesky factor	
S	Total wingarea	m ²
$T_{A \rightarrow B}$	Transformation matrix from A to B coordinates	
V_T	Total airspeed	m/s

Notation

$\langle x, y \rangle$	$\int_0^t \exp^{\lambda(\tau-t)} x(\tau)y(\tau)^T d\tau$
\otimes	Kronecker product
a_{\times}	Cross-product matrix

Superscripts

0 Unfiltered

Subscripts

B Body Fixed Coordinate System
b Backwards
c Commanded
d Desired
E Earth Fixed Coordinate System
f Forwards
r Reference
S Stability-Axis Coordinate System
W Wind-Axis Coordinate System

SAMENVATTING

Adaptieve Backstepping Besturing en Veiligheidsanalyse van Moderne Jachtvliegtuigen

Er bestaan vele voorbeelden van incidenten met vliegtuigen waar het de piloten gelukt is om met behulp van de overgebleven besturingsmogelijkheden het vliegtuig, de passagiers en vracht te redden uit een schijnbaar hopeloze situatie. Helaas is het omgekeerde ook waar. Verschillende ongelukken zijn gebeurd waarin de bemanning niet in staat was het vliegtuig te redden, hoewel analyse na de vlucht uitwees dat met gebruik van alternatieve, misschien onconventionele, besturing dit wel tot de mogelijkheden behoorde. Deze ongelukken tonen aan dat er een mogelijk nut bestaat voor fout-tolerante vliegtuigbesturingssystemen (FTFC) die veranderingen in de vliegtuigdynamica door schade en actuator falen kunnen opvangen. Sommige ongelukken hadden voorkomen kunnen worden door middel van dergelijke FTFC technieken vanuit een luchtvaarttechnisch oogpunt.

Algemeen gezegd, kunnen FTFC methoden ingedeeld worden in twee types: *actief* en *passief*. De passieve ontwerpen zijn robuust tegen een verzameling van vooraf aangenomen fouten. Echter, een regelaar met genoeg robuustheid om alle mogelijk foutsituaties te bevatten is waarschijnlijk onnodig conservatief in veel gevallen. Er bestaat ook geen garantie dat onvoorziene en meerdere gelijktijdige fouten, noch dat een dergelijke regelaar zelfs bestaat. In tegenstelling tot de passieve methoden, reageren actieve methoden actief door de stuuracties te reconfigureren zodat stabiliteit en acceptable prestaties van het systeem behouden blijven, zelfs na het optreden van schade en fouten.

De huidige staat van de techniek toont aan dat er nog openstaande problemen en beperkingen zijn aan FTFC. De passieve methoden zijn gelimiteerd tot en om die reden heeft een actieve benadering meer potentieel wanneer onvoorziene fouten en combinaties van fouten kunnen optreden. Slechts een handvol methoden zijn toepasbaar over het hele vliegdomein, en met name de schatting van de dynamica gebeurt alleen op of om de huidige vliegconditie. Er wordt geen volledig model opgebouwd door deze methoden, en de geschatte modellen worden niet opgeslagen voor hergebruik wanneer op dezelfde vliegconditie gevlogen wordt. Directe adaptieve methoden passen de parameters van de regelaar aan zodat de gewenste

prestaties worden behaald, en schatten geen model van het systeem. Op neurale netwerken gebaseerde methoden hebben last van convergentie problemen, en zijn gebaseerd op *black-box* structuren die de transparantie van de geschatte modellen reduceren. In dit onderzoek is gekozen voor een benadering gebaseerd op kennis van vliegtuigdynamica, wat leidt tot transparante modellen en ook kunnen deze modellen gebruikt worden voor foutdiagnose en reconfiguratie.

Incidenten door verlies van controle (LOC) gebeuren niet alleen met beschadigde vliegtuigen. Sommige rapporten claimen dat LOC de grootste factor in fatale vliegtuigongelukken van de laatste tien jaar. Op dit moment heeft de industrie nog geen volledige LOC preventie toegepast. Het limiteren van het vliegdomein is een eerste en nodige stap gemaakt door vliegtuig bouwers. Kennis van het veilige vliegdomein is zeer belangrijk om LOC ongelukken te kunnen voorkomen, en tegelijkertijd het opereren van vliegtuig aan de grenzen van hun kunnen mogelijk te maken. In vliegcondities met schade of fouten zou men willen weten welk gebied van het vliegdomein nog steeds veilig is, om zo de missie voort te zetten en een veilige (crash) landing mogelijk te maken. Dit onderzoeksgebied heeft nog niet veel aandacht gehad binnen de luchtvaartgemeenschap, zelfs niet voor vliegtuigen zonder schade en fouten.

Het onderzoek beschreven in deze dissertatie heeft daarom de volgende doelen:

- Het ontwikkelen van een regelaar met gewenste prestatie karakteristieken over het gehele vliegdomein van het vliegtuig, zelfs in aanwezigheid van fouten en schade.
- Omdat moderne vliegtuigen zijn uitgerust met vele, redundante, besturingsmogelijkheden, moet het gewenste stureffect verdeeld worden over de beschikbare stuurvlakken. Deze verdeling kan optimaal gedaan worden ten opzichte van een kostfunctie, en neemt de eigenschappen van de individuele stuurvlakken in beschouwing. Stabiliteit van de regelaar gecombineerd met de *control allocation* kan bewezen worden.
- Fouten en schade aan het vliegtuig beïnvloeden de dynamica van het systeem, de verandering moet geïdentificeerd worden om reconfiguratie van de besturing mogelijk te maken, en besturingsprestaties te herstellen. Hevige fouten leiden tot grote veranderingen in modelstructuur nodig om het systeem te modelleren, asymmetrische schade leidt bijvoorbeeld tot het opnemen van vele gekoppelde longitudinale en latera voorspellende variabelen. Als de model structuur en geschatte model parameters overeenkomen met de onderliggende fysica van het systeem, kan het model gebruikt worden voor fout diagnose en het veilige vliegdomein. Ontwikkeling van online structuur selectie methoden en efficiënte opslag van het geschatte model is benodigd.
- Met name voor wendbare vliegtuigen en vliegtuigen met fouten en schade, worden beperkingen opgelegd aan het veilige vliegdomein door de dyna-

mica. Kennis van het vliegdomein voor vliegtuigen met schade kan het verschil betekenen tussen een onafwendbaar ongeluk of een veilige landing. Om die reden, moet er een methode ontwikkeld worden waarmee het veilige vliegdomein bepaald kan worden, gebaseerd op het beschikbare model van het vliegtuig, rekening houdend met *input* limieten en mogelijke verstoringen.

Adaptive backstepping is een recursieve, op Lyapunov-theorie gebaseerde, niet-lineaire ontwerpmethodede die gebruik maakt van *update laws* voor model parameters om te compenseren voor parametrische onzekerheid in het systeem. Het basis idee van *backstepping* is om de regelaar recursief te definiëren door toestandsvariabelen als virtuele stuur *input* te beschouwen en daarvoor een virtuele regelaar te ontwerpen. Het *backstepping* ontwerp kan uitgebreid worden met *command filters* om het toe te kunnen passen op niet-feedback lineariseerbare systemen, en tegelijkertijd wordt het ontwerp versimpeld doordat de analytische afgeleiden van de virtuele stuur *inputs* niet meer nodig zijn.

Verscheidende *update laws* voor de model parameters kunnen gebruikt worden wat leidt tot geïntegreerde, modulaire en samengestelde ontwerpen. De geïntegreerde ontwerpen maken gebruik van een op Lyapunov gebaseerde *update law*, de modulaire benadering maakt het gebruik van de recursieve kleinste kwadratenmethode mogelijk. Echter, om de scheiding tussen regelaar en modelschatter mogelijk te maken zijn niet-lineaire dempingstermen nodig in het ontwerp. De samengestelde *update law* combineert de geïntegreerde en modulaire ontwerpen en heeft de beste convergentie eigenschappen.

In een vergelijking tussen de geïntegreerde en modulaire benaderingen resulteerden beide tot een verbetering van prestaties voor beschadigde vliegtuigen in vergelijking met een niet adaptief ontwerp. De prestaties en parameter schattingen van het modulaire ontwerp waren beter dan van het geïntegreerde ontwerp.

Control allocation kan geïntegreerd worden in het *backstepping* framework door *update laws* voor de gewenste stuursignalen te ontwerpen vanuit een Lyapunov perspectief. In dit ontwerp convergeren deze signalen continu naar de optimale oplossing in plaats van het expliciet oplossen van het *control allocation* probleem op elk tijdstip.

Het probleem van volledig vliegdomein model schatting is benaderd door het opdelen van het domein in kleinere regio's genaamd *hyperboxes*. In elke *hyperbox* wordt een lokaal geldig lineair in de parameters model geïdentificeerd. De *output* van deze modellen wordt geïnterpoleerd door middel van B-splines om de *output* te verkrijgen voor het volledige domein. Omdat B-splines lokale ondersteuning hebben, is slecht een beperkt aantal lokale modellen actief op elk punt in het vliegdomein.

De structuur benodigd om aërodynamische fouten te modeleren is niet op voorhand bekend, het meenemen van teveel voorspellende variabelen leidt tot *overfitting* en vermindert extrapolatie eigenschappen. Een on-line structuur selectie methode is ontwikkeld gebaseerd op orthogonale kleinste kwadraten welke ge-

bruikt kan worden in combinatie met het *adaptive backstepping* ontwerp. Tijdens het selecteren van de structuur wordt recursief de voorspellende variabele geselecteerd die de grootste vermindering van het foutresidu geeft totdat er aan een criterium wordt voldaan.

De *adaptive backstepping* methode met *control allocation*, vliegdomein partitionering en model structuur selectie is getest op het over-bestuurde, niet-lineaire ADMIRE vliegtuig model. Het voorgestelde ontwerp laat uitstekende prestaties zien voor verscheidene fout en schade scenario's, van een simpele verandering in de aërodynamische coëfficiënten, tot stuurvlak fouten en verschuivingen van het zwaartepunt. Als de fout binnen het bereik van de verzameling van beschikbare voorspellende variabelen valt, kunnen de correcte structuur en parameter waarden geïdentificeerd worden wanneer er aan een *persistency of excitation* voorwaarde voldaan wordt. Zelfs wanneer de fout niet compleet gemodelleerd kan worden binnen de beschikbare voorspellende variabelen kan de besturingsprestatie goed zijn, zolang het model fout residu maar klein is.

De toepassing van adaptieve regelmethoden voor vliegbesturing laat zien dat het wellicht mogelijk is om een vliegtuig te stabiliseren voor een verscheidenheid van fouten en schade, maar dat het nog steeds onduidelijk is in hoeverre de prestaties van het vliegtuig achteruit zijn gegaan door deze fouten en schade.

Verder onderzoek of het gebied van FTFC zou realistische aërodynamische foutmodellen en testvluchten met UAV en onderzoeksvliegtuigen moeten omvatten. De interactie tussen adaptieve regelsystemen en de piloten moet onderzocht worden. Voordat toepassing van FTFC in productie vliegtuigen mogelijk is, zouden richtlijnen en voorschriften voor de validatie en verificatie van dergelijke systemen ontwikkeld worden.

Het veilige vliegdomein is gedefinieerd als de regio in de toestandsruimte waarin veilige opereren van het vliegtuig, en veiligheid van de vracht en passagiers kan worden gegarandeerd, en tegelijkertijd extern opgelegde restricties in acht worden genomen. Deze regio in de toestandsruimte is beschreven door de overlap tussen de dynamische, structurele en omgevings- domeinen. Het veilige dynamische domein kan bepaald worden door middel van de voorwaarts en achterwaarts bereikbare verzamelingen voor een gegeven verzameling van veilige toestanden, bijvoorbeeld een verzameling van evenwichtstoestanden. Deze bereikbare verzamelingen, of sets, kunnen bepaald worden door evolutie van de initiële of doel verzameling in de tijd gebruikmakend van de *level-set* methode. Gebaseerd op de toepassing op simpele voorbeeldsystemen, laat de *semi-Lagrangian* methode het grootste potentieel zien voor bepaling van het veilige vliegdomein. De voorgestelde methode is toegepast op de longitudinale dynamica van een F-16 vliegtuig model. De vorm van de voor- en achteruit bereikbare sets komt overeen met de verwachtingen vanuit de vliegdynamica. Op grotere hoogte wordt het vliegtuig minder wendbaar voor dezelfde vliegsnelheid wat aan de vermindering van luchtdichtheid geweten kan worden. Als het zwaartepunt naar achter wordt verschoven in lengterichting, wordt het vliegtuig onstabiel wat resulteert in grotere wendbaarheid maar het

ook moeilijker maakt om het vliegtuig terug in evenwicht te krijgen. In het geval van verlies van hydraulische druk, resulterend in kleinere mogelijke uitslagen van het horizontale stuurvlak, gaat de wendbaarheid drastisch omlaag voor lage snelheden.

Vervolgonderzoek op dit gebied is noodzakelijk, bijvoorbeeld door het splitsen van het probleem in langzame en snelle dynamica door middel van *time-scale-separation* argumenten. Als de snelheid waarmee de oplossing wordt berekend verbetert, behoort online toepassing tot de mogelijkheden.

ACKNOWLEDGMENTS

This dissertation is the result of four years of research conducted within the Aerospace Software and Technologies Institute (ASTI) at the Delft University of Technology. During this period, many people have contributed in different ways to the realization of this work. I am very grateful to all of these people, but would like to mention some *dramatis personae* in particular.

First of all, I would like to thank my daily supervisor dr. Ping Chu, my direct colleague Lars Sonneveldt and promotor prof. Bob Mulder. Ping talked me into pursuing a Ph.D. degree at the Delft University of Technology, and his door was always open for a chat and discussion on a wide variety of subjects. I would like to thank Lars for his cooperation, the inspiring discussions on many different subjects, and the gaming sessions. Our research was part of the same project, and as a result we could directly compare both of our approaches. The integrated adaptive backstepping designs can mainly be attributed to Lars. Furthermore I cherish the memories I have of all the exotic conference locations we were able to visit to present our work. I am very grateful to Bob for his scientific support, expert advice and for being my promotor. Bob's extensive knowledge in the field of aerospace control, dynamics and identification always provided a new perspective on my work.

The research would not have been initiated without the efforts of prof. lt. gen. (ret.) Ben Droste, former commander of the Royal Netherlands Air Force and former dean of the faculty of Aerospace Engineering, and support of the National Aerospace Laboratory (NLR). I would like to thank the people at the NLR, especially Jan Breeman, for their scientific input and support. I would like to express my gratitude to the people at Lockheed Martin Aeronautics and the Royal Netherlands Air Force, as well as to the reviewers that read the journal and conference papers containing parts of the research, for providing me scientific input and practical expertise. Naturally, I am very grateful to the committee members for taking time to read this book, and making the trip to Delft.

I would also like to thank my former colleagues both at ASTI and Control & Simulation for their friendship, good times, enduring the ranting about the woes of doing

research, not to forget the *vrijmibo* and other social events in Delft and abroad. In no particular order, Erik-Jan, Elwin, Joost, Coen, Thomas, Jan, Paul, Daan, Joost, Olaf, Wouter, Clark, Herman, and Rita: thank you! A big thanks to Meine, Vera and Bertine for their support on the project management and administrative parts of a promotion project.

Last, but most definitely not least, I am very grateful to my parents, brother Roald, and Bella for their love, encouragement and support.

*Delft,
March 2011*

Eddy van Oort

CURRICULUM VITAE

Eduard Richard van Oort was born in Bilthoven, The Netherlands on May 31, 1983. From 1994 to 2000 he attended College Blaucapel in Utrecht, obtaining the Gymnasium certificate.

In September 2000 he started his studies at the Delft University of Technology, Faculty of Aerospace Engineering. After obtaining his B.Sc. in Aerospace Engineering in 2004, he completed an internship at the Universidad de Concepción, Concepción, Chile, where he worked on modeling and model verification of small UAV aircraft. After returning to Delft he did masters program at the Control and Simulation Division, specializing in flight control. In May 2006 he finished and defended his M.Sc. thesis on robust model predictive control of an F-16 aircraft model, and received his M.Sc. degree with honors in September 2006.

In October 2006 he started as a Ph.D. student at the Delft University of Technology within the Aerospace Software and Technologies Institute (ASTI). His Ph.D. research was conducted in cooperation with the National Aerospace Laboratory (NLR) in Amsterdam, and under supervision of the Control and Simulation Division at the Faculty of Aerospace Engineering.